Beyond stomatal closure : mechanisms of water loss in leaves during severe drought and implication for plant survival

Guillaume Forget

université de BORDEAUX

THÈSE PRÉSENTÉE

POUR OBTENIR LE GRADE DE

DOCTEUR DE

L'UNIVERSITÉ DE BORDEAUX

ÉCOLE DOCTORALE : SVS

SPÉCIALITÉ : SCIENCES AGRONOMIQUES

Par Guillaume FORGET

Quels mécanismes physiologiques entrent en jeu après la fermeture stomatique ? Etudes des pertes d'eau résiduelles des feuilles lors de sécheresses sévères et implications pour la survie des plantes

Beyond stomatal closure: mechanisms of water loss in leaves during severe drought and implication for plant survival

Sous la direction de : Jérôme JOUBES et Sylvain DELZON

Soutenue le mercredi 10 décembre 2025

Membres du jury :

Mme SCOFFONI Christine	Associate professor, CAL State University, Los Angeles	Rapportrice
M. LE THIEC Didier	Directeur de recherche, INRAE, Université de Nancy	Rapporteur Président du jury
Mme TIXIER Aude	Chargée de recherche, INRAE, Université de Dijon	Examinatrice
M. JOUBES Jérôme	Professeur des universités, CNRS, Université de Bordeaux	Directeur de thèse
M. DELZON Sylvain	Directeur de recherche, INRAE, Université de Bordeaux	Co-directeur de thèse

Invités:

Mme BAYER Emmanuelle	Directrice de recherche, CNRS, Université de Bordeaux
M. MARTIN ST PAUL Nicolas	Chargé de recherche, INRAE, Université d'Avignon

Résumés en français et en anglais

Quels mécanismes physiologiques entrent en jeu après la fermeture stomatique ? Etudes des pertes d'eau résiduelles des feuilles lors de sécheresses sévères et implications pour la survie des plantes

Le changement climatique accentue la fréquence et l'intensité des extrêmes climatiques exerçant une pression croissante sur la végétation. Parmi eux, la sécheresse perturbe le fonctionnement vasculaire des plantes, compromettant leur croissance, leur rendement et même leur survie. Les avancées récentes dans le domaine de l'hydraulique végétale ont révélé un lien étroit entre la mortalité liée à la sécheresse et la résistance du xylème à l'embolie. Toutefois, il reste difficile de prédire le temps de survie d'une plante soumise à une sécheresse prolongée, l'amenant à une rupture hydraulique de l'appareil vasculaire. En effet, la plupart des études se sont concentrées sur le rôle des stomates dans la régulation de la transpiration en début de sécheresse, négligeant les pertes résiduelles qui persistent, après fermeture stomatique, lors de sécheresses prolongées et/ou sévères. Or, ces pertes d'eau paraissent essentielles pour prédire la survie : elles définissent la transpiration résiduelle ainsi que le trait associé, la conductance minimale foliaire. Dans ce contexte, cette thèse s'attache à explorer les mécanismes de perte d'eau résiduelle au niveau de la feuille lors de stress hydriques sévères sur une espèce cultivée, le tournesol (*Helianthus annuus*), et un arbre, le tulipier de Virginie (*Liriodendron tulipifera*). Ce travail s'articule autour de trois axes visant à mieux comprendre les déterminants de la conductance foliaire minimale et leur impact sur la survie des végétaux : (i) l'analyse de la fuite stomatique en fonction de l'intensité du stress hydrique, (ii) l'exploration de la coordination spatiale des stomates, de son rôle dans l'équilibre entre transpiration et assimilation du carbone, et (iii) l'étude des principaux constituants de la cuticule et leurs impacts sur la perte en eau résiduelle. Nous avons pu mettre en évidence, à l'aide de techniques complémentaires et indépendantes, la présence de fuites stomatiques dès la fermeture des stomates (correspondant à la perte de turgescence) et jusqu'à des niveaux de stress hydrique important (Ψ_{P50}) influençant durablement la conductance résiduelle foliaire. Nos résultats montrent qu'une fermeture hétérogène des stomates (i.e. "stomatal patchiness") est également une réponse spécifique à la sécheresse. En particulier entre la perte de turgescence (Ψ_{tlp}) et le début de l'embolie du xylème (Ψ_{P12}), ce phénomène joue le rôle de tampon permettant de prolonger les fonctions physiologiques de la feuille face au stress hydrique. De plus, en l'analysant suivant deux échelles temporelles, nous montrons qu'il existe une hiérarchie spatiale dans le patchiness avec des patchs unitaires pouvant s'agréger en patchs plus vastes, affinant la réponse foliaire aux variations environnementales dont le stress hydrique. Parallèlement aux stomates, l'analyse de différentes couches cuticulaires lors d'un stress hydrique révèle qu'elles n'exercent pas la même influence sur la limitation des pertes en eau durant la sécheresse. Si la quantité de cutine et de cires augmente avec l'intensité du stress hydrique, seule la cutine contribue réellement à limiter ces pertes en eau retardant le début de l'embolie vasculaire et la rupture hydraulique. En conclusion, ces résultats soulignent l'importance des mécanismes stomatiques et cuticulaires, dans la régulation des pertes en eau lors de sécheresses sévères. Il est primordial de les prendre en compte dans les modèles prédisant la survie des végétaux dans le cadre du changement climatique. La combinaison d'une réponse spatiale hétérogène des stomates et de la contribution différenciée des couches cuticulaires illustre comment la feuille limite les pertes en eau. Ce couplage entre flexibilité stomatique et cuticulaire traduit une stratégie adaptative efficace, visant à préserver les fonctions physiologiques tout en minimisant les pertes hydriques.

Mots clés : Sécheresse, stomates, fuite stomatique, cuticule, cutine et cires, hétérogénéité stomatique.

Beyond stomatal closure: mechanisms of water loss in leaves during severe drought and implication for plant survival

Climate change is increasing the frequency and intensity of extreme weather events, exerting increasing pressure on vegetation. Among these, drought disrupts the plant hydraulic system, thereby compromising growth, productivity and even survival. Recent advances in plant hydraulics have revealed a close relationship between drought-induced mortality and xylem resistance to embolism. However, it remains difficult to predict the survival time of a plant subjected to prolonged drought that could lead to fatal hydraulic failure. Indeed, most studies have focused on the role of stomata in regulating water loss during drought, neglecting the residual water losses that persist after stomatal closure during prolonged and/or severe droughts. Yet, these water losses appear crucial for predicting survival, as they define the residual transpiration and the associated trait, the minimal leaf conductance. In this context, this thesis explores the mechanisms of residual water loss in leaves under severe water stress in a crop, sunflower (*Helianthus annuus*), and a tree species, tulip poplar (*Liriodendron tulipifera*). This work is structured around three main axes and aimed at better understanding the determinants of minimal leaf conductance and their impact on plant survival : (i) analysis of stomatal leakiness, (ii) the significance of spatial stomatal coordination and its role in balancing transpiration and carbon assimilation and (iii) the study of the main constituents of the cuticle and their impact on residual water loss. Using complementary and independent techniques, we demonstrated the occurrence of stomatal leakage from the stomatal closure (corresponding to turgor loss) to high levels of water stress (Ψ_{P50}), which strongly influences residual leaf conductance and thus survival. Our results highlight that the heterogeneous closure of stomata (i.e. stomatal patchiness) is a leaf's response to drought. In particular, between turgor loss (Ψ_{tlp}) and the onset of xylem embolism (Ψ_{P12}), this phenomenom acts as a buffering mechanism that prolongs leaf physiological activity under water stress. Furthermore, by analysing it across two temporal scales, we reveal a spatial hierarchy in patchiness, with small patches aggregating into larger ones revealing a spatial hierarchy that improves the leaf's response to environmental cues such as water stress. In parallel with stomata, analysis of different cuticular layers during water stress reveals that they do not have the same influence on limiting water loss during drought. While the amounts of cutin and waxes both increase with drought intensity, only cutin effectively contributes to reducing water loss, delaying the onset of vascular embolism and hydraulic rupture. In conclusion, these results highlight the importance of both stomatal and cuticular mechanisms in regulating water loss during severe drought. It is essential to take them into account in models predicting plant survival in the context of climate change. The combination of spatially heterogeneous stomatal responses and the differentiated contributions of cuticular layers illustrates how leaves attempt to conserve water. This coupling between stomatal and cuticular flexibility reflects an efficient adaptive strategy aimed at maintaining physiological functions while minimising water loss.

Keywords: Drought, stomata, stomatal leakiness, cuticle, cutin and waxes, stomatal patchiness

Unité de recherche : Laboratoire de biogenèse membranaire, UMR 5200, CNRS, Université de Bordeaux, Campus INRAE Bordeaux Aquitaine ; Biodiversité Gènes et Communautés, UMR 1202, Université de Bordeaux

Table of contents

Avant-propos

Ce manuscrit est rédigé sous forme de thèse sur publication dont la plupart des chapitres ont été soumis ou bien sont en cours de soumission dans des journaux scientifiques internationaux. Cette thèse a été financée pour une durée de trois ans par le programme "Investments for the Future" GPR Bordeaux Plant Sciences de l'Université de Bordeaux. Ce travail s'est déroulé au sein de l'UMR 1202 Biodiversité, Gènes et Communautés (BioGeCo – INRAE, Université de Bordeaux) et de l'UMR 5200 Laboratoire de Biologie Membranaire (LBM – CNRS, Université de Bordeaux). Au cours de cette thèse, un séjour de cinq mois a été effectué à l'Université de l'Essex (Colchester, Angleterre) dans l'équipe du Professeur Tracy Lawson.

Remerciements

Tout d'abord, je tiens à exprimer ma profonde gratitude à mes deux directeurs de thèse, Jérôme Joubès et Sylvain Delzon, pour la confiance qu'ils m'ont accordée et pour leur soutien indéfectible tout au long de ces trois années. Sans vous, je n'aurais pas eu l'opportunité de mener à bien ce travail. Vous m'avez offert une grande liberté, me permettant d'explorer et d'expérimenter différentes idées. Trois années ne suffisent pas pour faire le tour d'un tel sujet, mais elles marquent, je l'espère, le début d'une collaboration durable entre nous et vos laboratoires.

Je souhaite également remercier sincèrement les rapporteurs Christine Scoffoni et Didier Le Thiec pour le temps et l'attention qu'ils ont consacrés à l'évaluation de ce manuscrit. Ma gratitude va aussi à Emmanuelle Bayer, Aude Tixier et Nicolas Martin Saint-Paul pour avoir accepté de faire partie de mon jury, ainsi qu'aux membres de mon comité de thèse, Hervé Cochard, Gregory Gambetta et Eric Gomes, pour nos discussions toujours stimulantes et riches d'enseignements.

Un grand merci à mes collègues des laboratoires BioGeCo et LBM, qui m'ont accompagné et soutenu durant ces trois années. Je pense en particulier à Déborah, ma voisine de bureau : merci beaucoup pour nos échanges parfois éloignés du monde scientifique, mais toujours enrichissants. Merci aussi à Gaëlle, Juliette, Max, Camille et Thomas pour nos discussions conviviales entre autres autour d'un café et pour m'avoir conseillé quand j'en avais besoin. Daniela, un petit mot particulier pour toi afin de te remercier de m'avoir aidé avec cette chambre climatisée mais pas seulement : c'est toujours un plaisir de discuter avec toi. Je remercie également l'ensemble des doctorants de BioGeCo pour ce lien qui nous lie et qui permet d'avancer ensemble.
Je remercie chaleureusement les membres du LBM de m'avoir accueilli dans un environnement qui m'était nouveau et de m'avoir aidé avec bienveillance à chaque fois que je venais dans vos locaux. Ma reconnaissance va tout particulièrement à la Wax team bien sûr (Fred, Stéphanie, Didier, François, Sarah et plus spécifiquement Erwan) pour ces réunions où je me suis souvent retrouvé totalement à la rue. Un grand merci à Terezinha, Claire, Stéphanie, Sarah, Fred, Jérôme et Matthieu pour votre aide lors de

cette manip cuticule qui va de l'accompagnement à la serre pour arroser, à l'extraction des cires, en passant par la préparation des échantillons et des images au MET.
Lors de la première année, j'ai eu la chance d'encadrer Eva lors de son stage de M1. C'est une rencontre qui compte pour moi et j'espère que nous aurons l'occasion de retravailler ensemble. Merci à toi pour toutes nos discussions, elles me sont précieuses.

Je remercie l'Université de Bordeaux de m'avoir donné l'opportunité de vivre une expérience à l'étranger, qui a été remarquable tant sur le plan personnel que professionnel. Je suis très reconnaissant envers Tracy Lawson et l'ensemble de son laboratoire pour leur accueil et leur aide durant ces cinq mois. Un merci tout particulier à Showkat Ganie, Phil Davey et, bien sûr, à Tracy Lawson.

Ce travail n'aurait pas été possible sans deux personnes qui comptent énormément pour moi : Régis et Santiago. Je ne sais pas comment vous remercier pour tout ce que vous avez fait pour moi durant ces trois années. Je ne compte plus nos discussions, vos messages et votre soutien constant, qui m'ont permis d'avancer. Je vous ai beaucoup, parfois trop, sollicités et vous ne m'avez jamais lâché. Rien que pour cela, je vous en suis reconnaissant. J'ai énormément appris, et je continue d'apprendre à vos côtés. Certaines rencontres marquent une vie : vous en faites partie.

Une autre rencontre essentielle, datant de la fin de mes études, est celle de Patrick, que je considère comme mon mentor. Tu as toujours été présent pour me pousser à aller plus loin, à viser plus haut. Des séchoirs à poissons aux séchoirs à fromages, jusqu'à la conductance des feuilles… il n'y a finalement qu'un pas !

Je souhaite enfin remercier chaleureusement ma famille, ma belle-famille et mes plus proches amis pour leur soutien constant et leurs précieux conseils au cours de ces trois années. Et pour terminer, je voudrais adresser mes remerciements les plus profonds à ma compagne Sophie, qui a partagé au quotidien les bons et les moins bons moments de cette aventure. Merci pour ton soutien, pour ton écoute et pour ta présence indéfectible, non seulement durant cette thèse, mais aussi au fil des quatorze dernières années.

CHAPTER 1

General introduction

Chapter 1 General introduction

1. The role of stomata and the cuticle in the success of terrestrial vascular plants

1.1. Challenges faced by early land plants

The colonisation of terrestrial environments by plants was one of the most important events in Earth's biological and geochemical history. Embryophytes, or land plants, are thought to have evolved from freshwater Charophyte algae, with the closest extant relatives being filamentous Zygnematales (Harris *et al.* 2020). This transition (Figure 1.1), occurring in the mid-Cambrian to Early Ordovician period, approximately 515–470 million years ago (Ma), presented substantial challenges due to the fundamentally different nature of the terrestrial environment. Unlike their aquatic ancestors, early land plants were exposed to biotic and abiotic stresses including desiccation, ultraviolet radiation, mechanical damage, and novel pathogen attack (Kong *et al.* 2020; Donoghue *et al.* 2021). Challenges imposed by terrestrial life such as desiccation required the development of structural and biochemical adaptations to reduce water loss and maintain physiological homeostasis.

The four major land plant lineages (liverworts, mosses, hornworts, and tracheophytes) had already diverged by the late Silurian (Figure 1.1), around 420 Ma, and vascular plants (tracheophytes) are estimated to have emerged in the Late Ordovician to Silurian, roughly 450–420 Ma. Among the most significant innovations that enabled their success were the development of a waxy cuticle to protect the entire tissues to harsh environmental cues, stomata for the exchange of gases with the environment, and vascular tissues for efficient water and nutrient transport. These innovations were acquired relatively fast after the initial colonisation of land and provided the physiological and structural foundations necessary for plants to thrive outside aquatic habitats. The establishment of land plants with the fungi symbiosis fundamentally transformed the Earth's atmosphere (carbon and oxygen cycles) and soil geochemistry (weathering). This led to a reduction in atmospheric carbon dioxide and a rise in oxygen levels, which in turn influenced global climate and enabled the diversification of terrestrial life.

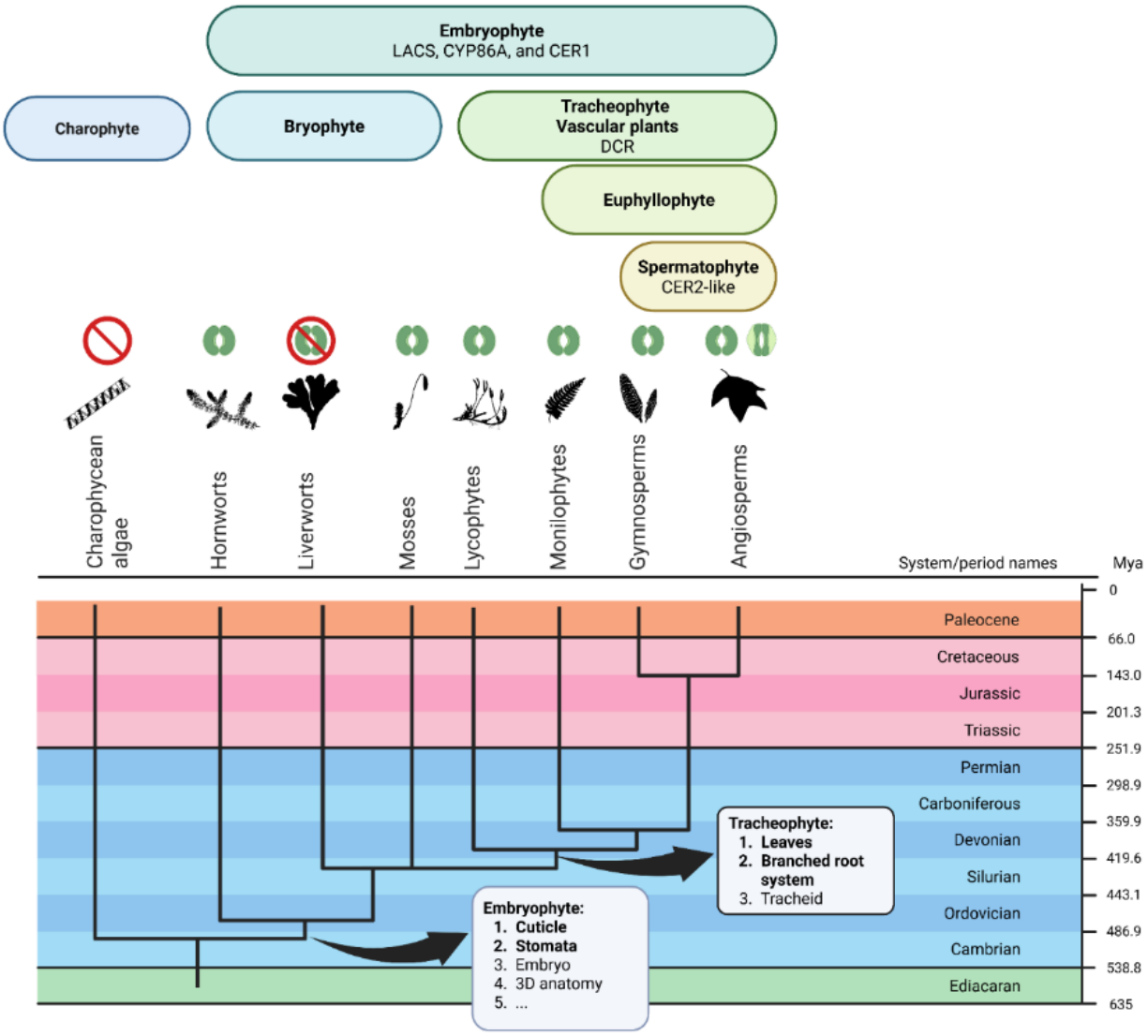

FIGURE 1.1:Phylogenetic tree of embryophytes.
This summary timescale of embryophyte phylogeny is based on the dated 'monophyletic bryophytes' phylogeny of Morris and colleagues (adapted from Chater *et al.* 2017; Kong *et al.* 2020; Donoghue *et al.* 2021)). Presence of stomata is represented by kidney-shaped stomata icons whereas the loss of this organ is represented by the stomata icon crossed out (Liverworth). The angiosperms have two kinds of stomata: the kidney-shaped and the dumbbell-shaped. The charophytes didn't have this organ. Below the lineage name the main genes for cuticle evolution are indicated. Icons are from Phylopic.org and created in BioRender.com.

1.2. Evolution of the cuticle as a protective barrier

Among the earliest and most vital innovations facilitating terrestrial adaptation was the plant cuticle, a hydrophobic lipidic extracellular layer deposited on the outer epidermal walls of aerial tissues of land plants. The cuticle serves as a barrier to control water loss, as well as a defense against pathogens and UV damage (Seale 2020; Donoghue *et al.* 2021). Kong *et al.* (2020) present a comprehensive study showing the evolutionary origins and diversification of the cuticle biosynthetic machinery in land plants from charophyte

algae to angiosperms. The authors demonstrate that the genetic foundation for cuticle biosynthesis originated in the last common ancestor of embryophytes approximately 500 Ma. They identify orthologs of 32 cuticle-related genes, such as LACS, CYP86A, GPAT, and CER1 (Figure 1.1), across all land plant groups, with partial or absent representation in algal lineages. Crucially, they show that gene family expansions, particularly in seed plants, are linked to increased cuticle complexity and functional enhancements. For instance, CER2-like genes, which are involved in wax elongation, and DCR, a key enzyme in cutin polymerization, emerged in vascular plants such as lycophytes and were further kept and diversified in seed plants (spermatophyte). These genes likely contributed to the enhanced structural and chemical diversity of the cuticle. Seed plants, in particular, exhibit higher accumulation of cutin monomer and very-long-chain fatty acids or waxes, along with improved hydrophobicity and moisture retention. The study also reveals conserved coexpression networks and regulatory mechanisms, involving transcription factors like MYB, which regulate expression of cuticle biosynthetic genes across land plants. Physiological assays confirm that these biochemical and genetic innovations have functional consequences, enabling seed plants to thrive in arid and UV-exposed environments. Together, the findings underscore the cuticle's pivotal role in terrestrial adaptation (Seale 2020).

1.3. Appearance of stomata in early non-vascular land plants and diversification in vascular plants

Stomata, microvalves composed by two guard cells (dedicated cells responding to biotic and abiotic cues), represent one of the most important evolutionary innovations that enabled terrestrial colonisation. Stomata typically regulate gaseous exchange in plants, but in some mosses, they also serve a reproductive function by promoting water loss from the sporophyte capsule, thereby facilitating its drying and the maturation necessary for spore release (Sussmilch *et al.* 2019; Clark *et al.* 2022). Fossil and molecular evidence places the origin of stomata in the common ancestor of land plants, prior to the divergence of bryophytes (mosses) and tracheophytes (vascular plant) between 495-515 Ma (Morris *et al.* 2018; Donoghue *et al.* 2021; Clark *et al.* 2022).

Despite morphological and functional divergence (liverworts exhibiting a loss of stomata), genetic data support the homology of stomata across land plants. Key transcription factors, which regulate stomatal development, trace back to the

embryophyte ancestor (Harris *et al.* 2020). Stomatal evolution reflects feedback with atmospheric CO_2 concentrations. Early stomata likely facilitated optimisation of carbon gain relative to water loss (Clark *et al.* 2022). Functional genes related to the phytohormone abscisic acid (ABA) sensitivity and hydroactive stomatal movement also predate the bryophyte-tracheophyte divergence (Harris *et al.* 2020; Clark *et al.* 2022). Seed plants evolved the capacity to optimise water-use efficiency (WUE) by hydroactive movement through stomatal responses to environmental cues such as light, CO_2, and vapour pressure deficit (VPD; describe the air dryness) and soil water scarcity (McAdam & Brodribb 2012; Yang, Brodribb & Bi 2021). In contrast, ferns and lycophytes exhibit more limited responsiveness, often lacking feedback regulation between photosynthesis and stomatal aperture (Brodribb, McAdam & Field 2009; McAdam & Brodribb 2012). This physiological divergence is thought to underlie the evolutionary success of seed plants, particularly under fluctuating light and water conditions (Yang *et al.* 2021). A recent review made by Clark *et al.* in 2022 and presented in Figure 1.2, challenge the hypothesis that hydroactive stomatal regulation (especially ABA and CO_2 responsiveness) evolved only with gymnosperms and angiosperms, instead supporting the view that such responsiveness was present in the earliest land plants. Humidity-driven (hydropassive) responses are also widespread, but the presence of hydroactive mechanisms across the phylogeny underscores the deep evolutionary roots of sophisticated stomatal control.

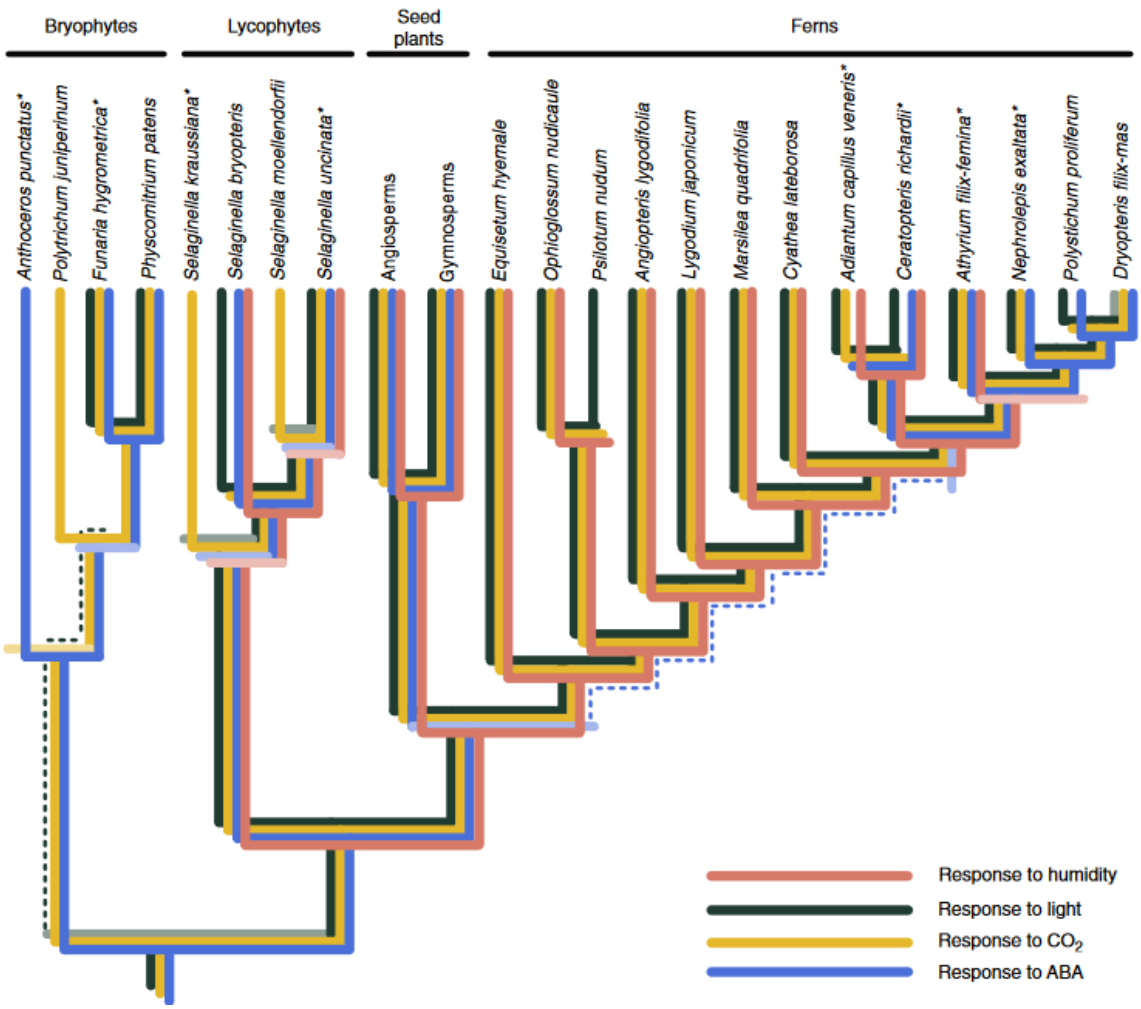

FIGURE 1.2:The diversity of stomatal responses among land plants (from Clark *et al.* 2022). Experimental evidence for stomatal responses to humidity, light, CO_2 and ABA are mapped onto the land plant phylogeny for species selected to represent a diversity of stomatal responses to various cues. This shows the possibility that stomatal responses to environmental cues are widely distributed among and possibly ancestral to land plants. Note that in many cases, the absence of a response does not indicate loss, but that the response has not been determined. The dotted lines represent a part of the tree where the evolution of the ABA response in ferns and light response in bryophytes remains uncertain.

The evolution of the cuticle and stomata in land plants not only facilitated terrestrial colonisation but also had crucial consequences for Earth's atmospheric composition and climate. Early land plants have been implicated as geoengineers of the global carbon cycle (Donoghue *et al.* 2021). Their spread across the continents enhanced silicate weathering, leading to CO_2 drawdown and contributing to Palaeozoic glaciations, including the end-Ordovician event (Donoghue *et al.* 2021).

2. Cuticle composition and structure

The cuticle consists primarily of a cutin matrix and waxes, two lipid-based components that confer a barrier against biotic and abiotic stresses. The cuticle is closely associated with the outer epidermal cell wall (OEW), which can be viewed as a cutinised cell wall (Domínguez *et al.* 2011). Rather than forming a uniform, well-defined layer, the cuticle exhibits a compositional gradient throughout its structure (Figure 1.3). Polysaccharides derived from the cell wall are present within the cuticle but decrease in abundance with increasing distance from the cell wall. Conversely, waxes show the opposite pattern: they are most concentrated at the outer surface as epicuticular waxes, and their abundance gradually decreases inward as they diffuse into the cutin matrix, forming the intracuticular wax layer (Domínguez *et al.* 2011). Although the biochemical composition and thickness of the cuticle vary across plant species, organs and developmental stages, a core set of primary compounds is ubiquitously present.

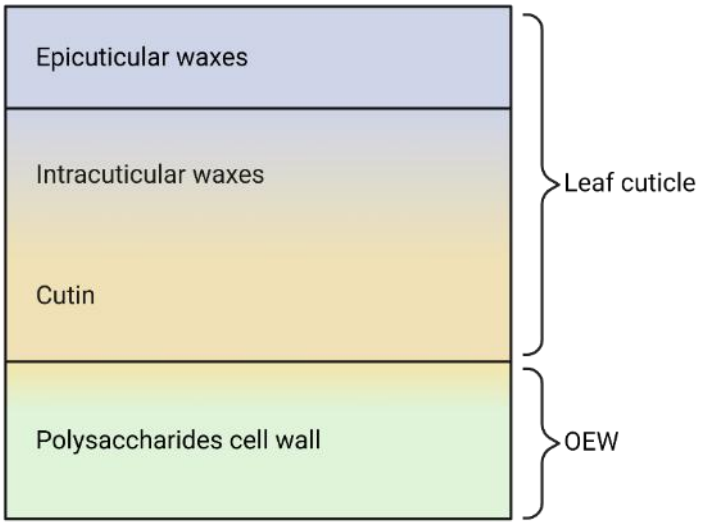

FIGURE 1.3: Scheme of a transverse section of the cuticle representing the different components and main structural features.
(adapted from Domínguez *et al.* 2011; Yeats & Rose 2013). Abbreviation: OEW; Outer epidermal cell wall. Created in BioRender.com.

2.1. Cutin biosynthesis

Cutin is the primary structural polymer of the cuticle. It is composed mainly of inter-esterified ω-hydroxy, polyhydroxy and epoxy long chain fatty acids (predominantly C16 and C18), cross-linked to form a three-dimensional polyester matrix. The biosynthesis of cutin begins with de novo fatty acid synthesis in the plastid of epidermal cells (Figure 1.6).

The C16:0, C18:0 or C18:1 fatty acids, produced in plastids, are then transferred to the cytosolic acyl-coenzyme A (CoA) pool. The next steps occur in the endoplasmic reticulum (ER) where fatty acids are oxidised before being transferred to glycerol to form sn-2 mono(oxygenated)acyl-glycerol molecules (2MAG; Yeats *et al.* 2014) which constitute the fundamental building blocks of the cutin polymer (Figure 1.6). This matrix provides the main mechanical strength of the cuticle and forms the foundational "cuticle proper" when embedded with intracuticular waxes (Joubès & Domergue 2020; Batsale *et al.* 2021). Cutin is typically poor in very-long-chain fatty acids (VLCFAs with more than 20 carbons), distinguishing it chemically and structurally from the wax layer (Batsale *et al.* 2021). While there is considerable diversity in the structure of cutin monomers (Figure 1.4), the major cutin monomers, include ω-hydroxy fatty acids, mid-chain hydroxy fatty acids like 10,16 dihydroxyhexadecanoic acid, 16-hydroxyhexadecanoic acid, 9,10-epoxyoctadecanoic acid, 9,10,18-trihydroxy octadecanoic acid, and octadeca-cis-6,cis-9-diene-1, 18-dioate (Figure 1.4).

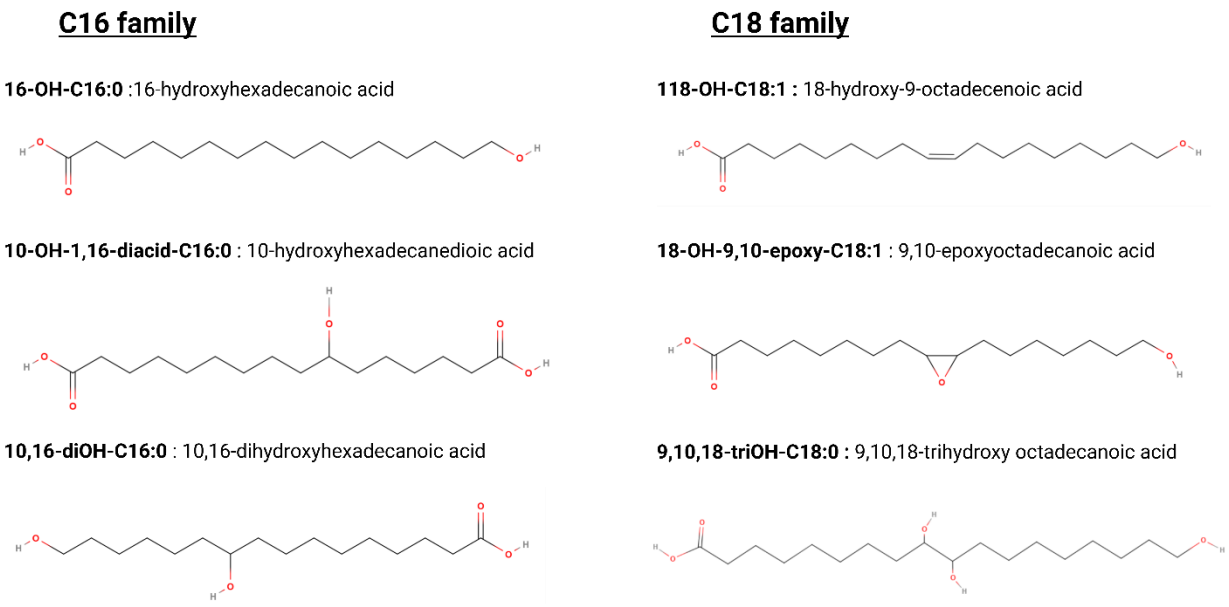

FIGURE 1.4: Typical cutin monomers found in the cuticle.
(Example taken with *Helianthus annuus* cutin monomer (see chapter 5)). Created in BioRender.com and MolView.

2.2. Cuticular waxes biosynthesis

Cuticular waxes consist of a complex mixture of very-long-chain (VLC) aliphatic compounds (C20–C38). The biosynthesis begins with de novo C16 or C18 fatty acid

biosynthesis in the plastid of epidermal cells (Figure 1.6) (Yeats & Rose 2013). These long-chain fatty acid compounds are converted to CoA thioesters by a long-chain acyl-coenzyme A synthase (LACS) isozyme and are ultimately transferred to the endoplasmic reticulum (ER). Located in the endoplasmic reticulum, the FAE complex catalyses the sequential addition of two-carbon units to acyl-CoA substrates, extending chain length up to C38. At this step, two pathways are possible. First, the alcohol-forming pathway, producing even-numbered molecules (Figure 1.5) where VLCFAs are reduced by FAR (fatty acyl-CoA reductase) to primary alcohols, which can be further esterified to acyl-CoA by WS (wax synthase) to form alkyl esters. The second is the alkane-forming (Figure 1.5) pathway producing odd-numbered molecules where VLCFAs are first converted to aldehydes, then to alkanes by the alkane synthase. Alkanes can be further oxidized by MAH1 (midchain alkane hydroxylase) to secondary alcohols and ketones.

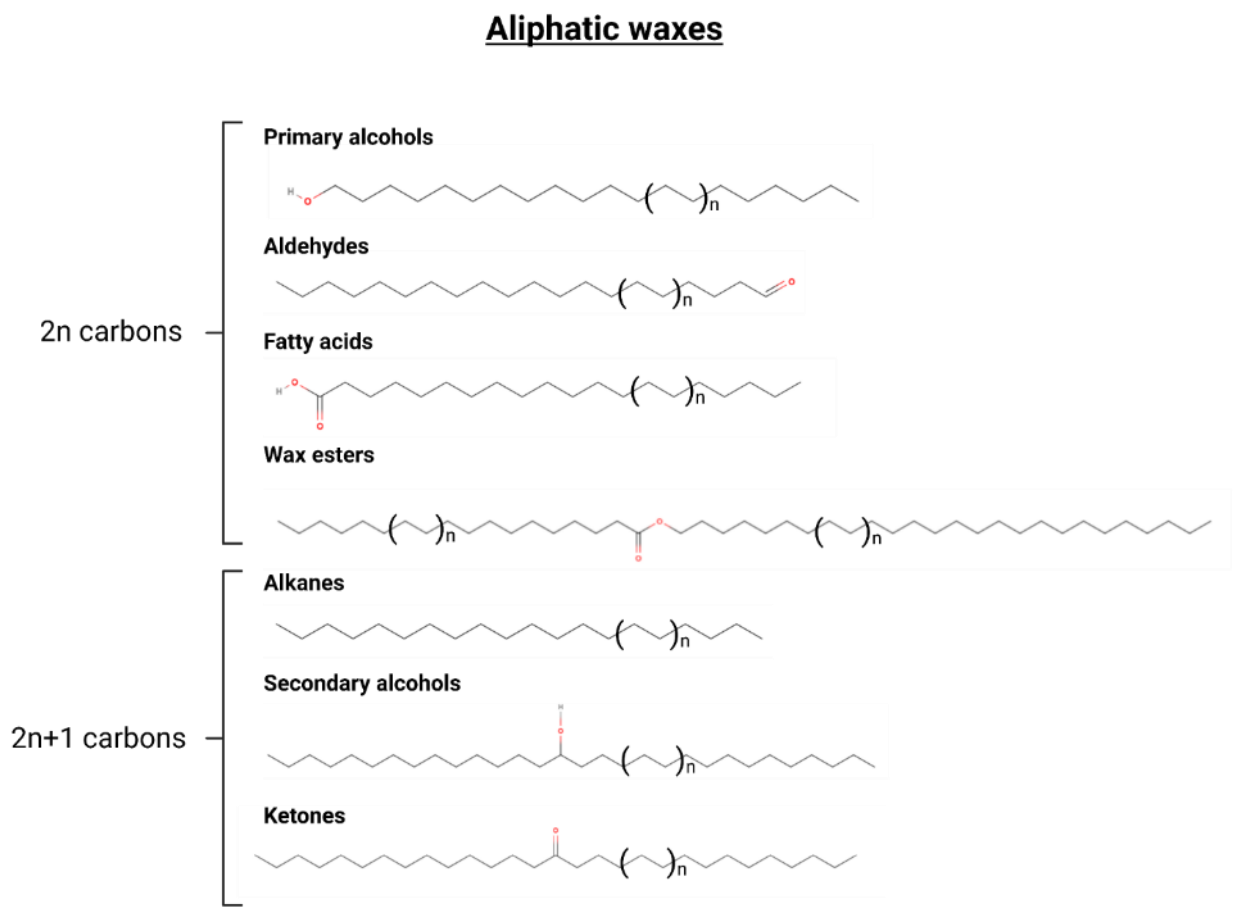

FIGURE 1.5: Cuticular wax compounds.
In the case of the *Helianthus annuus*, main waxes are the primary alcohols, fatty acids, alkanes and secondary alcohols (see chapter 5). Created in MolView.

The export of cutin monomers and wax compounds involves a coordinated series of intracellular and extracellular transport processes. These hydrophobic molecules synthesised within the endoplasmic reticulum (ER) are then transported in a directional manner through the Golgi apparatus and trans-Golgi network (TGN) to reach the plasma membrane before being secreted to cover the cell wall of epidermal cells facing the external environment (Yeats & Rose 2013). To cross the plasma membrane, ATP-binding cassette (ABC) transporters, are crucial for exporting cutin monomers and waxes (Figure 1.6).

For the cutin monomer, the final step is the incorporation of the cutin polymer. The key enzyme is the cutin synthase (CD) which catalyzes the polymerization of the cutin monomers into the cutin polyester.

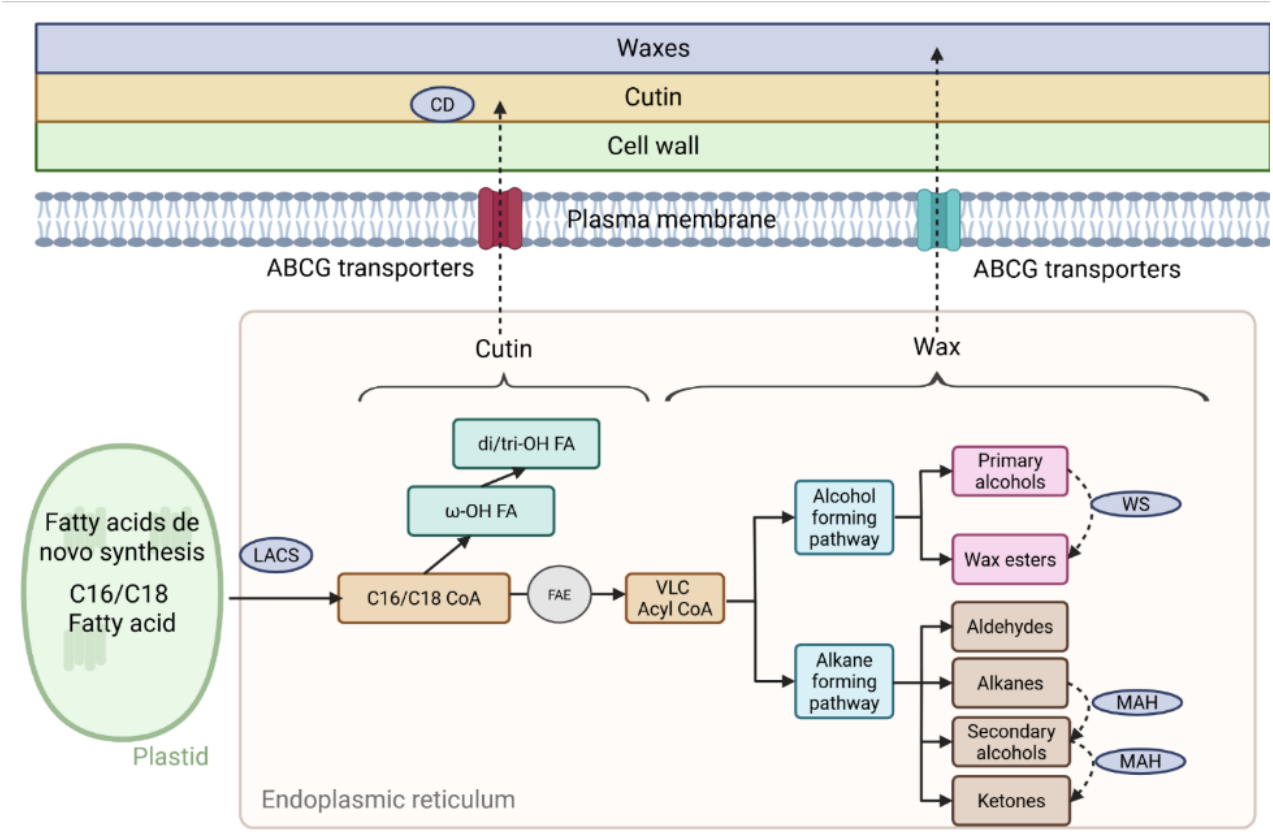

FIGURE 1.6: Biosynthesis and export of cutin and wax monomers in plant epidermal cells (adapted from Yeats & Rose 2013; Bhanot *et al.* 2021).
Abbreviations: LACS: long chain acyl-CoA synthetases, FAE: fatty acid elongase, CD: cutin synthase, MAH: midchain alkane hydroxylase, ABCG transporter: ATP binding cassette transporter, WS: Wax synthase, FA: Fatty acid, ω-OH FA: ω-hydroxy fatty acid, di/triOH FA: di- and tri-hydroxy fatty acid. Created in BioRender.com.

2.3. Role of the cuticle during abiotic and biotic stresses

The plant cuticle plays a central role in interactions with the environment serving as a barrier against abiotic (water stress, UV radiation) and biotic stresses (pathogens) (Shepherd & Griffiths 2006).

2.3.1. Abiotic Stress incidences on water permeability

Water transport through the plant cuticle can be explained via three distinct pathways: the cellulose (or polysaccharide), the lipophilic (hydrophobic matrix), and the aqueous pore pathway (Tredenick & Farquhar 2021). The cellulose pathway, highly humidity dependent, involves the movement of water (polar molecule) along with polar polysaccharides via diffusion or absorption, such as cellulose fibers, which are embedded within the cuticle structure. The lipophilic pathway, in contrast, refers to the movement of water through the hydrophobic matrix of the cuticle, which is composed mainly of cutin and waxes. Although water is a polar molecule, it can still diffuse through this non-polar environment due to its small size, but this diffusive process is generally less efficient than movement through polar pathways (Tredenick & Farquhar 2021). The rate of water transport via the lipophilic pathway is highly sensitive to temperature and te structural properties of the cuticular waxes. The third pathway, known as the aqueous pathway (Schreiber 2005), consists of dynamic aqueous pores within the cuticle (Fernández *et al.* 2017). The aqueous pathway is considered the primary route for hydrophilic molecules, including water, especially when environmental humidity is high. The relative contribution of each pathway to total water transport depends on factors such as plant species, cuticle structure, and environmental conditions but we have the repartition of 67% to polysaccharides, 32% to cutin and 1% to waxes (Chamel *et al.* 1991). Environmental cues such as drought, high light intensity, UV radiation, and salinity induce changes in cuticle composition (Liu, Wang & Chang 2022). For example, drought and ABA treatments upregulate wax biosynthesis genes, including several KCS genes, KCR1, and CER10 (Batsale *et al.* 2021). The MYB96 and MYB94 transcription factor directly activates expression of different genes under drought conditions, enhancing wax deposition and improving stress tolerance (Lee & Suh 2022). Interestingly, in Arabidopsis wax biosynthesis is generally induced by water deficit, ABA and osmotic stress while cutin biosynthesis responds primarily to water deficit and may not by ABA or osmotic stress (Kosma *et al.* 2009). During stress such as drought, physicochemical properties of the cuticle change: increasing cutin and wax content can modulate its thermal properties,

enhancing heat resistance and modifying the cuticle's glass transition temperature to better withstand high temperatures (Heredia-Guerrero *et al.* 2018).

2.3.2. Biotic Stress

From a microorganism's point of view, cuticular waxes form an important physical barrier that limits direct contact between pathogens such as fungi and bacteria and the epidermal cell wall, thereby impeding pathogen entry and colonisation (Lewandowska *et al.* 2020). The composition and structure of the wax layer can inhibit pathogen development, pathogen spore germination and the development of a specialised infection structure called appressorium (a flattened structure creating pressure on the surface and facilitating penetration via a peg). However, some pathogens have evolved strategies to overcome this barrier by secreting enzymes like cutinases that degrade waxes and cutin (Arya *et al.* 2021). The breakdown products of these compounds can act as signals, sometimes triggering plant defense responses or, in other cases, facilitating pathogen infection. Plants can dynamically modify wax composition and increase wax deposition in response to pathogen attack as part of their inducible defense mechanisms (Lewandowska *et al.* 2020).

In terms of interactions with insects, cuticular waxes serve as a physical dissuasive barrier reducing insect attachment, feeding, and oviposition by altering the surface composition or crystal structure thereby affecting insect mobility and adhesion. Plants may respond to insect herbivory by altering their wax profiles, increasing the production of compounds that are less profitable to insects. The effectiveness of wax-based defenses varies widely depending on the plant and insect species involved, as well as environmental conditions (Lewandowska *et al.* 2020).

3. Stomatal regulation and its pivotal role in the life cycle of plants

Stomata serve as dynamic microvalves that regulate gaseous exchange between the leaf and the atmosphere (CO_2 uptake and water vapor release through evapotranspiration) (Lawson & Matthews 2020a). The ability of plants to regulate stomatal aperture in response to internal status and external environmental cues is critical for maintaining optimal photosynthetic rates, cooling efficiency, and resisting pathogen invasion (Buckley 2019; Ye *et al.* 2022).

3.1. Guard cell morphology and function

Guard cells, derived from the epidermis cells, exhibit two main morphologies across plant taxa: kidney-shaped, typical of most dicots, and dumbbell-shaped, found predominantly in monocots (Lawson & Matthews 2020a; Ye *et al.* 2022). This morphological divergence has critical functional implications. Dumbbell-shaped guard cells are associated with faster stomatal kinetics compared to their kidney-shaped counterparts due to their increased surface area-to-volume ratio (Lawson & Matthews 2020a). Another critical component of the stomatal complex is the subsidiary cell, which is morphologically distinct and assists guard cell movement. Solutes like potassium (K^+) and chloride (Cl^-) are transferred from subsidiary to guard cells to drive osmotic changes, enabling stomatal movement (Lawson & Matthews 2020a). Recent 3D imaging has revealed that vacuolar restructuring within guard cells is central to stomatal opening. Specifically, the vacuole expands significantly to occupy a major portion of the guard cell volume, while the nucleus-cytosolic compartment remains constant (Mirasole *et al.* 2023). This shift underlines the vacuole's critical role in turgor modulation and the elastic deformation of guard cells during pore opening and closure.

3.2. Stomatal kinetics and photosynthesis coupling

Stomatal conductance (g_s) corresponds to the rate of gaz exchange (carbon uptake and water loss) through the leaf and depends on both the anatomical stomatal features (size, shape, and density) and their dynamic behavior (aperture changes in response to environmental and internal cues) (Ochoa *et al.* 2024) (Figure 1.7). Stomatal density and size are inversely correlated (Franks & Beerling 2009), and density is a primary determinant of maximum conductance (Ochoa *et al.* 2024). The speed of stomatal responses is also crucial, with faster stomatal kinetics improving CO_2 uptake and water use efficiency (Drake *et al.* 2013; Vialet-Chabrand *et al.* 2017). Smaller, more numerous stomata generally respond more rapidly to environmental changes). The shape of guard cells also matters: dumbbell-shaped guard cells (in grasses) enable faster and more efficient stomatal movements compared to kidney-shaped ones, due to their geometry and mechanical coupling with subsidiary cells (Lawson & Matthews 2020a).

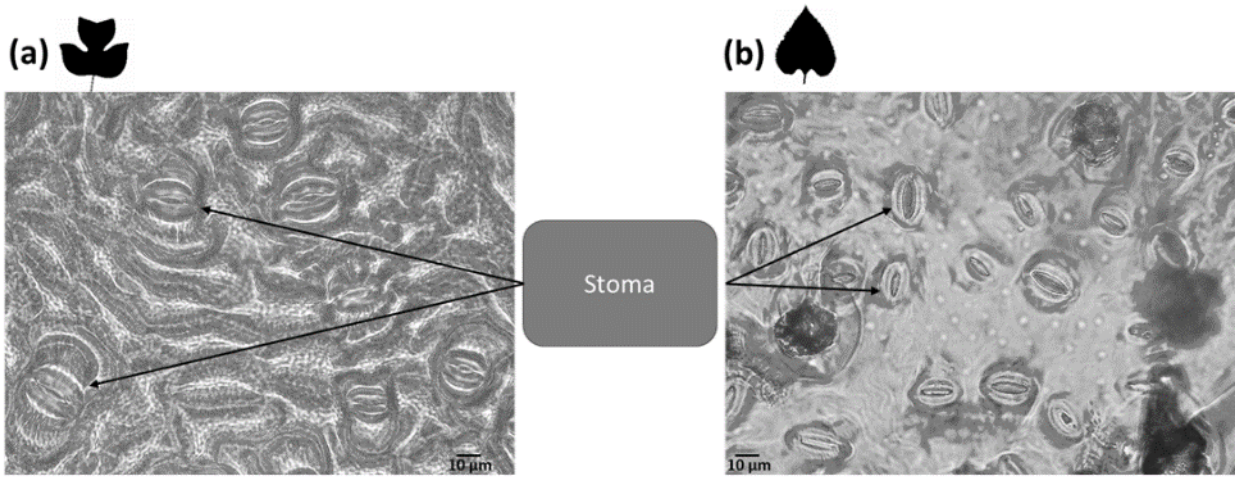

FIGURE 1.7:Nail polish imprint images from (a) *Liriodendron tulipifera* and (b) *Helianthus annuus*. Viewed at 40x under a microscope. Each arrow shows a stoma which is a pore (or ostiole) delimited by two guard cells. More informations about stomatal anatomy properties for the adaxial and abaxial surfaces are available in chapter 3.

3.3. Photosynthesis and response to drought

The most active photosynthetic tissue in higher plants is the leaf mesophyll. Mesophyll cells have chloroplasts, which contain the specialised light-absorbing green pigments, the chlorophylls. Photosynthesis process is closely linked to plant hydraulic function, as water transport through the xylem maintains leaf turgor and stomatal opening, thereby sustaining CO_2 uptake and metabolic activity (Brodribb 2009). During drought and soil salinity stresses for example, photosynthesis is constrained by both diffusive and metabolic limitations (Chaves *et al.* 2009; Pinheiro & Chaves 2011). The diffusive rate is constrained by stomatal closure restricting CO_2 uptake while alterations in mesophyll metabolism such as reduced enzymatic activity compromise carbon fixation efficiency (Chaves *et al.* 2009; Pinheiro & Chaves 2011).

Light energy absorbed by chlorophyll excites electrons in the reaction centers, triggering electron transfer through carriers in the thylakoid membrane (Figure 1.8). The light reactions involve two photosystems working in sequence: the photosystem II (PSII) and the photosystem I (PSI). PSII is responsible for the photolysis of water, splitting H_2O molecules to release oxygen (O_2), protons, and electrons. These electrons move through the electron transport chain via plastoquinone (PQ), the cytochrome b_6f complex, and plastocyanin (PC) to PSI (P700), where they are re-energized and used to reduce $NADP^+$ to NADPH through ferredoxin. As electrons flow, protons are pumped into the thylakoid

lumen, creating a gradient that drives ATP synthesis by the enzyme ATP synthase through photophosphorylation.

Thus, the light reactions convert solar energy into the chemical energy carriers ATP and NADPH, which are subsequently used in the Calvin cycle for carbon fixation. The Calvin–Benson cycle, which occurs in the chloroplast stroma, is the main pathway for carbon fixation in plants. It consists of three phases: carboxylation, reduction, and regeneration. First, the enzyme Rubisco fixes CO_2 to ribulose-1,5-bisphosphate (RuBP), forming 3-phosphoglycerate (3-PGA). In the reduction phase, ATP and NADPH from the light reactions convert 3-PGA into glyceraldehyde-3-phosphate (GAP). Some GAP is used to produce carbohydrates such as sucrose and starch, while the rest regenerates RuBP using ATP, allowing the cycle to continue.

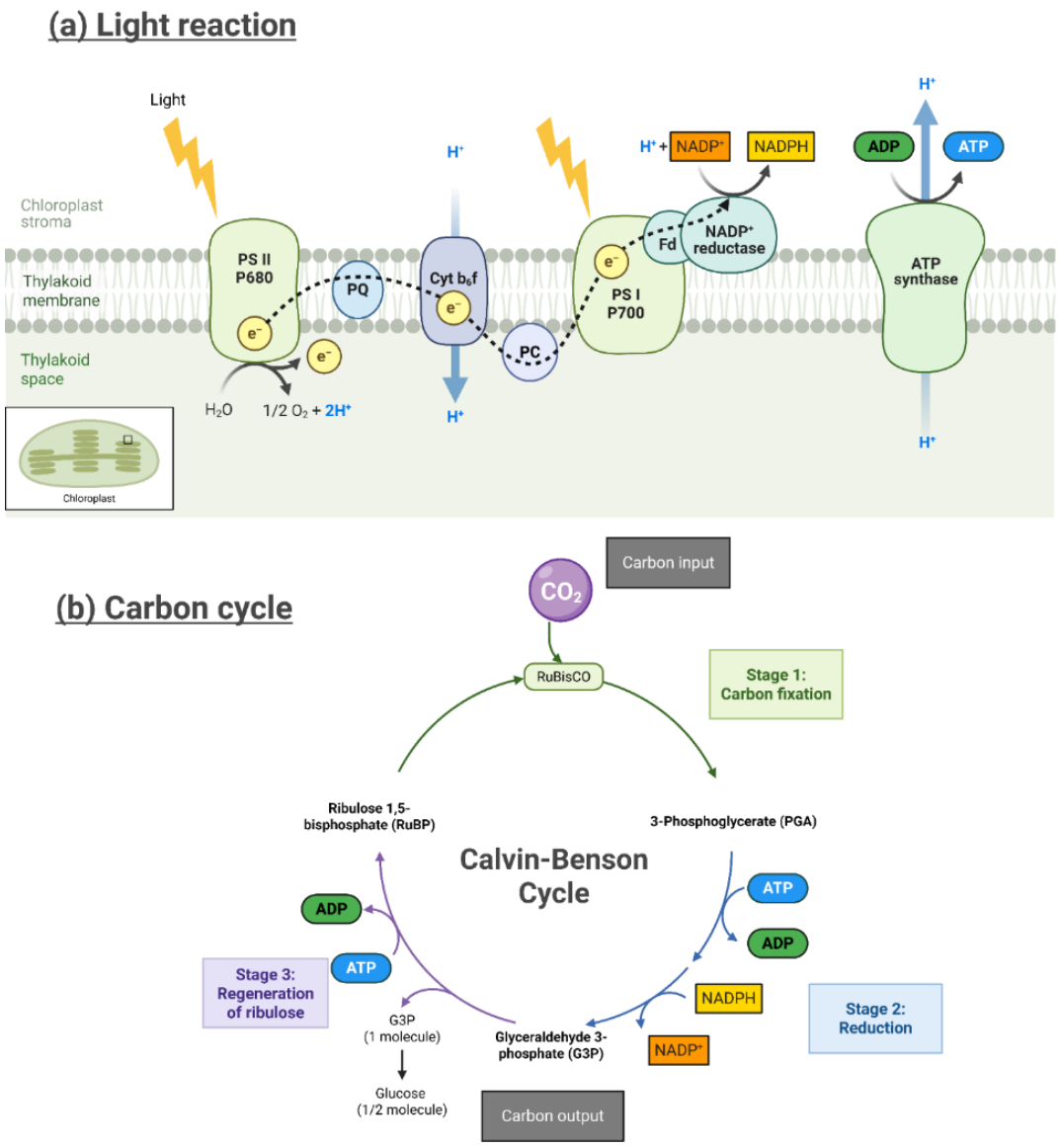

FIGURE 1.8: Light cycle and the Calvin-Benson cycle
(a) Light cycle: transfer of electrons and protons in the thylakoid membrane. Water is oxidized and protons are released in the lumen by PSII. PSI reduces NADP+ to NADPH in the stroma, via the action of ferredoxin (Fd) and NADP+ reductase. Protons are also transported into the lumen by the action of the cytochrome b6f complex and contribute to the electrochemical proton gradient. These protons must then diffuse to the ATP synthase enzyme, where their diffusion down the electrochemical potential gradient is used to synthesize ATP in the stroma. The dashed lines represent electron transfer; solid lines represent proton movement. (b) The Calvin–Benson cycle proceeds in three phases: (1) carboxylation; (2) reduction and (3) regeneration (adapted from Taiz *et al.* 2015). Created in BioRender.com.

During drought, both the light and carbon cycles are affected (Flexas *et al.* 1999; Medrano 2002; Golding & Johnson 2004; Flexas 2009; Chaves *et al.* 2009). Due to stomatal closure, CO_2 availability decreases, reducing CO_2 assimilation (*A*; µmol m^{-2} s^{-1}). The CO_2/O_2 ratio increases thereby increasing photorespiration (Wingler *et al.* 1999). Under conditions where the Calvin cycle is limited, electron transport is down-regulated

to minimise electron flow to O_2. Thermal dissipation in the antenna becomes progressively more important and the non-photochemical quenching (NPQ) corresponding to heat dissipation increases to protect photosystems (Medrano 2002; Golding & Johnson 2004) (Figure 1.9).

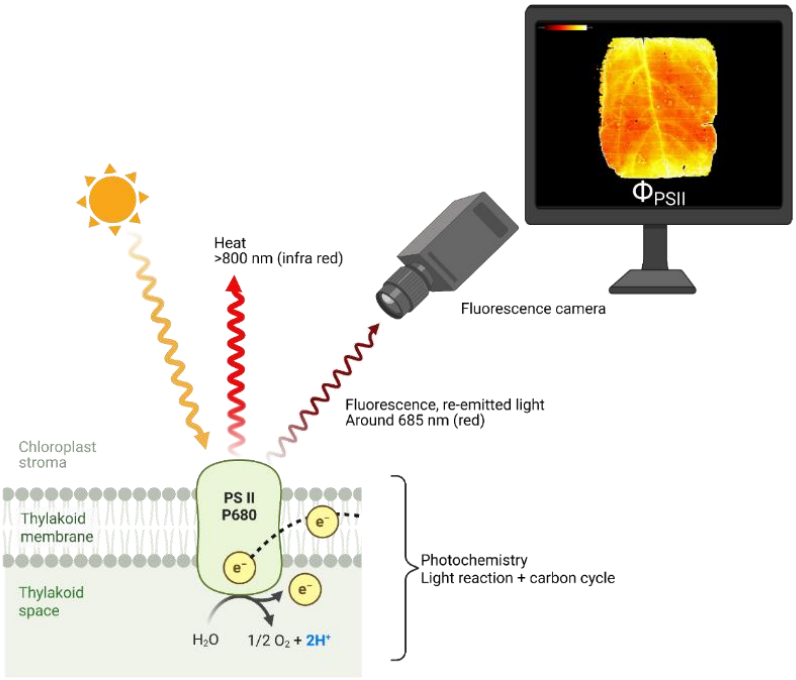

FIGURE 1.9: Scheme of PSII during light induction leading to emission of a photon captured by the fluorescence camera.
Light energy absorbed by chlorophyll molecules can: (i) drive photosynthesis (photochemistry), (ii) be re-emitted as heat and (iii) be re-emitted as light (fluorescence). The camera connected to the computer detects the fluorescence emission; software is used to convert the information into fluorescence parameters in the form of a 2D matrix. Created in BioRender.com.

3.4. Water Use Efficiency

Water use efficiency (WUE), a concept introduced a century ago, describes how a plant effectively converts carbon into biomass per unit of water loss. Defined as the ratio of the photosynthetic rate (net CO_2 uptake, accounting for both absorption during photosynthesis and loss via respiration) to transpiration, WUE highlights the trade-off between biomass production and water conservation. While stomatal conductance (g_s) often correlates with photosynthetic assimilation rate (A), the kinetics of stomatal opening and closing are typically slower than photosynthetic responses, especially under fluctuating light (Vialet-Chabrand *et al.* 2017; Lawson & Vialet-Chabrand 2019). This temporal disconnect can limit carbon gain and reduce crop productivity (Hatfield & Dold

2019). Guard cell traits such as size, influence the speed and magnitude of stomatal movement (Lawson & Matthews 2020a). Both, water use efficiency (WUE=*A*/E) and "intrinsic" water use efficiency (*i*WUE=*A*/g_s) are constrained by stomatal behavior and plant water use strategies (Figure 1.10) (Liang *et al.* 2023a). Plants with rapid stomatal responses have faster kinetics (Drake *et al.* 2013b) and are better able to optimise on brief periods of high light (sunflecks) and minimise unnecessary water loss during low light or darkness (Lawson & Vialet-Chabrand 2019). This dynamic regulation is particularly important for crop species grown in dense canopies or under field conditions, where light fluctuations are frequent and unpredictable (Lawson & Vialet-Chabrand 2019). Species from habitats with highly variable light or frequent drought tend to have faster stomatal kinetics, reflecting natural selection for efficient water use and rapid photosynthetic adjustment. Conversely, species from more stable environments may have slower, less responsive stomata (Lawson & Vialet-Chabrand 2019).

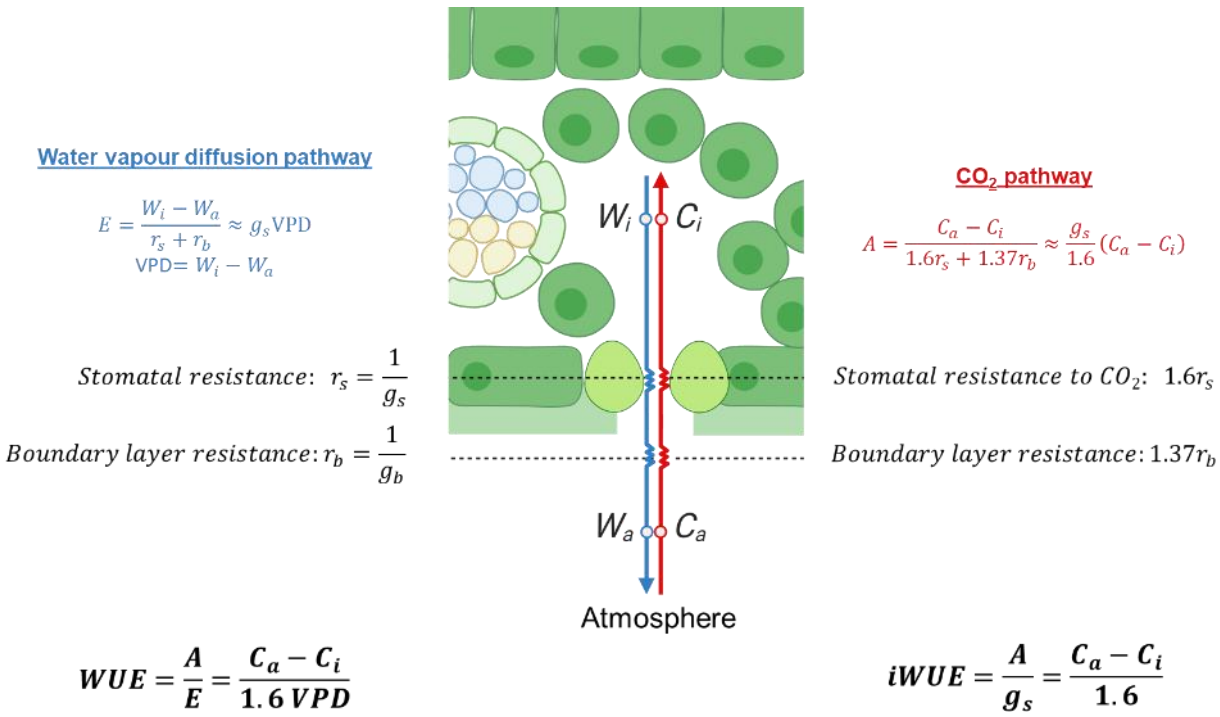

FIGURE 1.10: Water use efficiency and "intrinsic" water use efficiency.
WUE and *i*WUE definition and relationship with carbon assimilation (*A*) and water loss (transpiration, E and stomatal conductance, g_s). VPD: the vapour pressure deficit; C_i and C_a the intercellular and ambient CO_2 concentration, respectively; W_i and W_a the intercellular and ambient water concentration, respectively. Created in BioRender.com.

3.5. Leaf energy budget dynamics

The leaf energy budget describes the balance of energy inflows and outflows at the leaf surface, which determines leaf temperature and influences physiological processes such as photosynthesis and transpiration. The energy budget is a balance between absorbed radiation and energy losses through multiple pathways (Figure 1.11):

- Energy inputs: Mostly solar (shortwave) and thermal (longwave) radiation absorbed by the leaf.
- Energy outputs: Consist of sensible heat flux (H) through the convection (natural and forced) by air speed, latent heat flux (L) through evaporation/transpiration, thermal radiation loss, and minor components like energy stored in the leaf and used in photosynthesis.

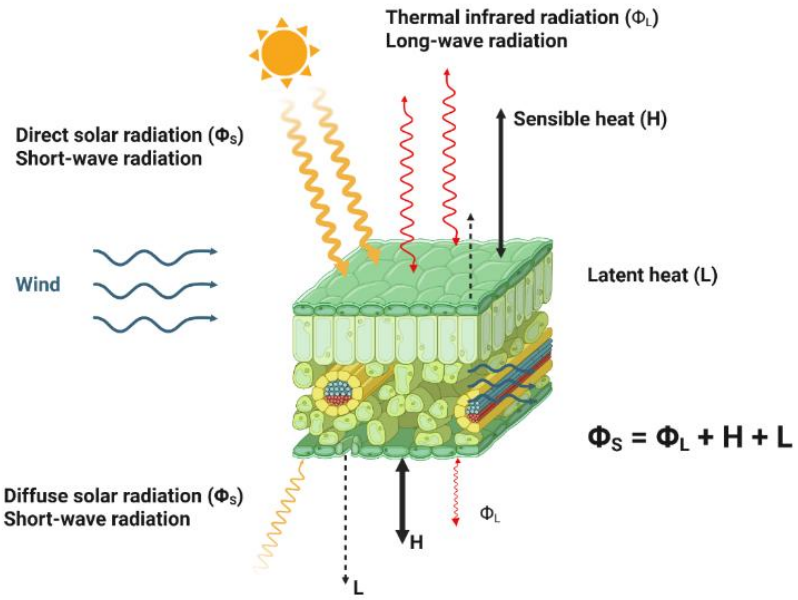

FIGURE 1.11: Simplified leaf energy budged.
It's an equilibrium between the incoming thermal short-wave radiation from the sun (Φ_S) and the thermal long-wave radiation re-emitted (Φ_L) with the thermal losses by sensible heat (H) and latent heat (L). Storage is not represented. Created in BioRender.com.

Leaf cooling results from a combination of sensible heat loss (H), latent heat loss (L) and thermal radiation (Φ_L). Sensible heat flux is heat transferred to the air through convection, dependent on the aerodynamic resistance of the leaf boundary layer, wind speed, and leaf characteristics like size and shape. Latent heat flux arises from water evaporation via stomata, which consumes energy and cools the leaf surface. Leaf traits

such as size, shape and orientation affect how much radiation is intercepted and how effectively heat is lost. For example, small leaves tend to have thinner boundary layers, promoting more efficient sensible heat loss, while leaf stomatal conductance influences latent heat loss. Environmental factors (sunlight, air temperature, wind speed, and humidity) also modulate these heat transfer processes.

Leaf energy budgets explain plant adaptations like smaller leaf size in warm, dry environments to minimise overheating by enhancing convective cooling, and larger leaves in shaded or cooler environments to optimize photosynthesis despite a thicker boundary layer. Under well-wathered conditions, leaf cooling is mainly due to remeted energy (61%) followed by sensible heat (24%) and latent heat (13%) (Muller 2023).

During drought conditions, water availability is reduced and leads to stomatal closure, limiting latent heat flux (evaporative cooling). Under such conditions, the leaf energy budget shifts towards sensible heat loss to maintain leaf temperature if the ratio of emitted waves is the same. As the stomata close to limit water loss and prolong plant's survival, the cuticle, whose thickness and composition might change during drought, can play a role in survival by limiting water loss, but also by avoiding heating the leaves, by reflecting short and long waves. Indeed, the leaf reflectance increases as the relative water content (leaf drought-related trait) decreases (Fabre *et al.* 2011).

3.6. Diurnal and environmental responsiveness

Guard cells integrate multiple environmental and internal signals to control stomatal aperture. Key external stimuli include light (blue and red light), humidity, CO_2 concentration, and pathogens, while endogenous signals involve phytohormones such as abscisic acid (ABA), reactive oxygen species (ROS), and various metabolic cues.

3.6.1. Light Response

Light is a primary regulator of stomatal behavior, with distinct red and blue light signaling pathways. Red light, acting via the mesophyll, is tightly coupled to photosynthetic electron transport often considered to be the link between carbon assimilation (A) and stomatal conductance (g_s) (Lawson & Matthews 2020a). In contrast, blue light is directly targeted by guard cells through specific photoreceptors and can open stomata independently of mesophyll photosynthesis (Lawson & Matthews 2020a). Blue light is approximately 20 times more efficient per photon in inducing stomatal opening

than red light, although this often results in excessive water loss due to uncoupling from photosynthetic demand.

3.6.2. Circadian and Nocturnal Regulation

Nocturnal stomatal conductance (g_{dark}) has been observed in several species (Resco *et al.* 2016; Resco *et al.* 2019) especially in *Helianthus annuus* and *Liriodendron tulipifera*, with implications for nighttime water loss without carbon gain (Lawson & Matthews 2020a). Although that function seems counter-intuitive, several hypotheses have been made including facilitating nutrient transport, O_2 supply for respiration or CO_2 excess removal. A meta-analysis by Resco De Dios et la. (2019) challenges these hypotheses, suggesting instead that g_{dark} may be relative to growth rates and suggest that circadian-driven nocturnal conductance enhances predawn stomatal conductance, priming stomata for photosynthesis early in the light period. Recent study by Wang *et al.* (2021) proposes that plants regulate nighttime stomatal conductance to balance the potential benefits and costs of nocturnal water loss. They found that nighttime stomatal conductance decreases with drier soil (see appendix A3), higher atmospheric CO_2, wetter air, lower leaf temperature, and lower leaf respiration rates. The model also suggests that the gradual decline in nighttime stomatal conductance after sunset is linked to decreasing leaf respiration.

3.6.3. CO_2 and ABA Signaling

Recent research has significantly advanced our understanding of how stomatal functioning is regulated by both CO_2 and abscisic acid (ABA) signaling, with important implications for plant adaptation to changing environmental conditions. Stomata close in response to elevated CO_2 (Liang *et al.* 2023b) and open at low CO_2 (Foyer *et al.* 2025), optimising water loss and carbon gain. Both guard cells and mesophyll tissues contribute to CO_2 sensing (Engineer *et al.* 2016). This rapid CO_2-induced closure is further amplified and sustained by ABA accumulating under drought and osmotic stress. ABA not only enhances the magnitude of the stomatal closure response to CO_2 but is also crucial for maintaining low stomatal conductance over longer periods. Internal CO_2 concentration (C_i) was formerly considered the main link between photosynthesis and stomatal opening. However, recent studies show that stomata still respond to red light even when C_i remains constant, suggesting the involvement of specific signals from the mesophyll (Lawson & Matthews 2020a). ABA is central to stomatal closure under drought conditions.

3.6.4. Stomatal response to VPD and soil water status

Stomatal responses to vapor pressure deficit (VPD) and plant water status are central to the regulation of plant water loss and carbon gain and recent research has clarified the mechanisms underpinning these responses.

As VPD rises, meaning the air becomes drier, stomata typically close to limit excessive transpiration and prevent dehydration (Oren *et al.* 1999; McAdam & Brodribb 2015; McDowell & Allen 2015; Grossiord *et al.* 2020). Buckley (2005, 2019) describes that stomatal closure under high VPD is not solely a passive hydraulic response to water loss, but involves active signaling mechanisms, including the rapid generation of abscisic acid (ABA) in leaves in response to declining leaf turgor or humidity at the leaf surface.

Stomatal closure due to soil water limitation is a regulated process that allows plants to minimise water loss and prevent hydraulic failure as drought progresses. It results from the integration of hydraulic signals such as declining leaf and guard cell turgor and chemical signals, particularly the accumulation of ABA, which promotes ion efflux from guard cells and loss of turgor pressure. This coordinated response reflects a balance between conserving water and maintaining photosynthetic carbon uptake, ensuring plant survival under conditions of limited soil water availability (Tombesi *et al.* 2015; Buckley 2019). As drought progress, reductions in leaf hydraulic conductance and vulnerability to xylem embolism further amplify the water supply limitation to guard cells, reinforcing stomatal closure (Wang *et al.* 2018). Moreover, dynamic resistance in the soil-plant continuum can modulate the timing and sensitivity of stomatal closure (Manandhar *et al.* 2024).

Thus, stomatal behavior in response to VPD and soil water status reflects a complex interplay between passive hydraulic effects, active hormonal signaling, and environmental sensing, allowing plants to dynamically balance photosynthetic carbon gain with water conservation under fluctuating environmental conditions. Altogether, stomatal behavior results from a complex integration of anatomical, physiological, and biochemical components to optimise gas exchange in changing environments (Figure 1.12).

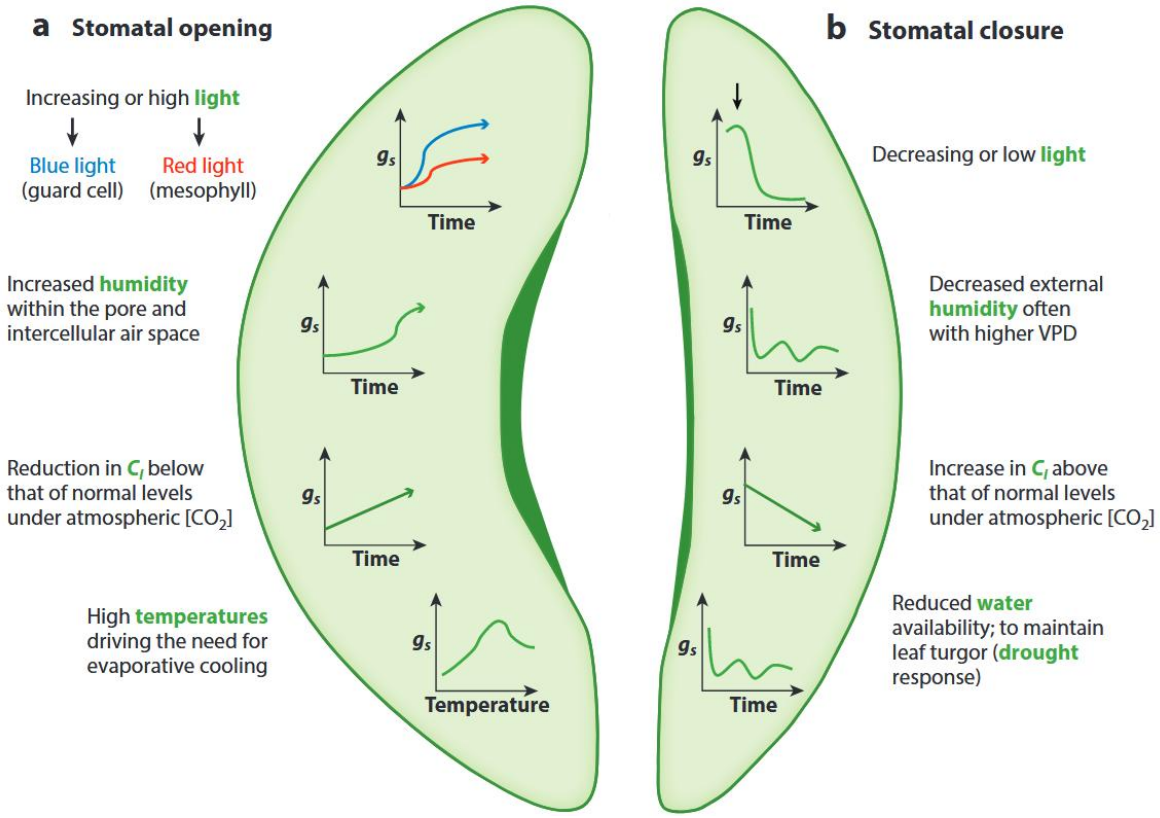

FIGURE 1.12: Stomatal response to environmental cues.
(a) Environmental factors contributing to stomatal opening (a) and closure (b), including but not limited to light, humidity, CO_2 concentration, and temperature. g_s corresponds to the stomatal conductance and C_i, the internal CO_2 concentration. The kidney-shaped green form represents guard cells. On the left, turgid and on the right, flaccid, indicating that the stomata are open or closed. (adapted from Lawson & Matthews 2020b)

3.6.5. Stomatal patchiness

Stomatal response to environmental cues described above show an individual mechanism of opening/closure in response to those changing factors. Stomata must compose with internal (water status) and external cues to optimise their pore aperture. Opening/closing stomatal pore is not a discrete evolution but a continuous variation between the maximal and minimal aperture. Stomatal pore aperture oscillation is a natural phenomenon because it's physically impossible to maintain a steady state continuously (Cardon *et al.* 1994). At stomata level, the equilibrium is never reached. Stomata are numerous over a leaf, for example it's close to 400 per mm² for *Helianthus annuus*. At this scale, individual response could not be optimal due to the number of different individual behaviours. In order to have an optimal response, stomata can have a grouped or a collective response (Beyschlag *et al.* 1992; Mott *et al.* 1993; Buckley, Farquhar & Mott 1997; Mott & Buckley 2000). Called stomatal patchiness (Figure 1.13, chapter 3 and 4), it can be defined as the difference in stomatal pore aperture between adjacent stomata

leading to spatial heterogeneity in responses to internal and external cues (Lawson *et al.*1998; Mott & Buckley 2000; Peak *et al.* 2004; Peak *et al.* 2023; Marenco *et al.* 2006; Mott & Peak 2007; Kamakura *et al.* 2011; Kamakura *et al.* 2012a; Kamakura *et al.* 2012b, 2015). Usually those studies focused on the direct effects of environmental cues such as vapor pressure deficit (VPD), temperature, wind and light intensity (Mott & Buckley 1998; Beyschlag & Eckstein 2001) but dynamics of stomatal patchiness under a progressive drought remain insufficiently understood. As soil water scarcity intensifies, local variation in water potential within the leaf (Jain *et al.* 2023, 2024) also increases and can cause a heterogeneous stomatal response. This spatial heterogenous stomatal response to drought prolonged locally transpiration and carbon uptake. This spatial heterogeneity could be considered as an independent leaf response to drought in order to prlong gas exchange. Studying stomatal patchiness along a drought sequence could reveal a significant gap in our understanding of leaf response during drought.

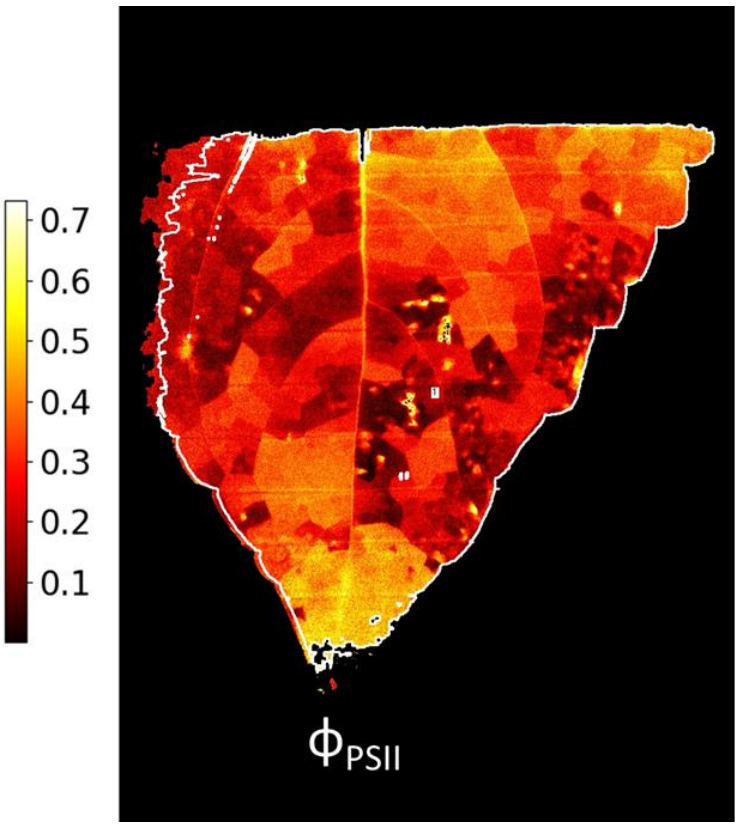

FIGURE 1.13: Stomatal patchiness represented here by the quantum efficiency of photsystem II (Φ_{PSII}) under low oxygen concentration.

4. Global impact of droughts on ecosystems and agriculture

4.1. Type of drought

Drought is a multifaceted phenomenon that can be classified into meteorological, hydrological, agricultural, and ecological types, each reflecting a unique aspect of water scarcity and its impacts (IPCC 2023). Meteorological drought refers to prolonged periods of precipitation deficits, while hydrological drought is based on reduced water availability within surface and subsurface reservoirs and streamflows such as lakes, rivers, and groundwater sources. Agricultural and ecological droughts link closely with soil moisture deficits, while agricultural drought inhibits crop growth or reduces yields, ecological drought manifests primarily as plant water stress, which can induce tree mortality and shifts in ecosystem composition (IPCC 2023). These types of drought can overlap, propagate from one domain to another, or occur asynchronously, influenced by both climatic drivers and land-atmosphere feedbacks (Figure 1.14).

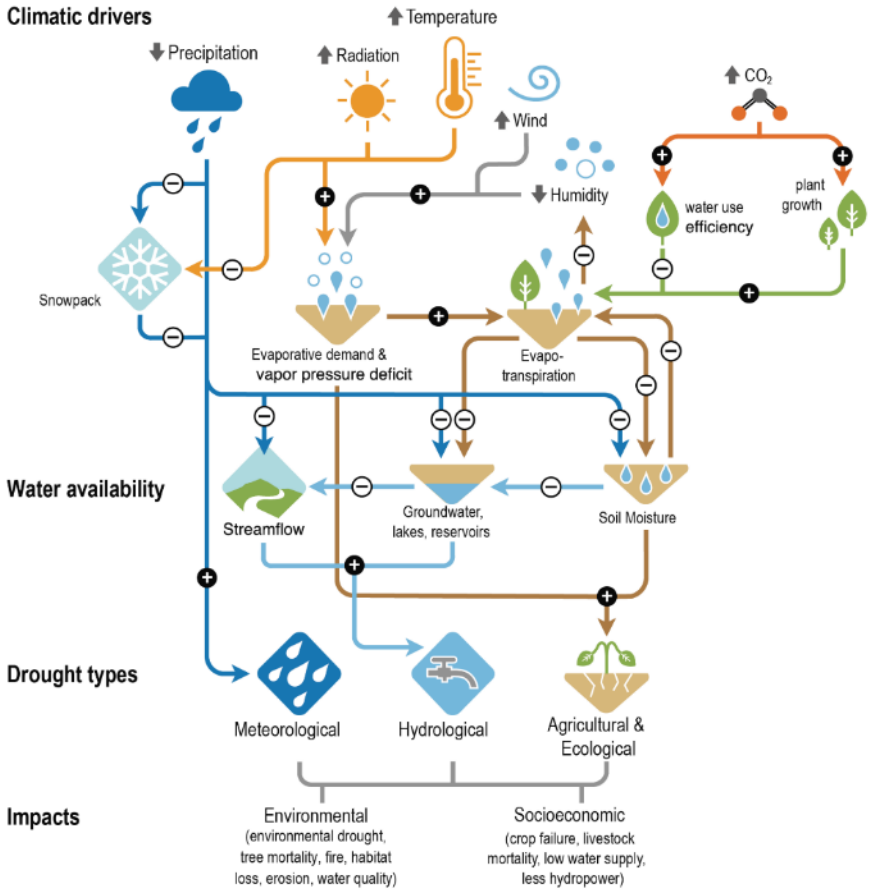

FIGURE 1.14: Climatic drivers of drought, effects on water availability, and impacts.
Plus, and minus signs denote the direction of change that drivers have on factors such as snowpack, evapotranspiration, soil moisture, and water storage. The four main types of drought are listed: meteorological, hydrological, agricultural and ecological (IPCC 2023).

4.2. Flash drought

A subtype of drought is the flash drought, which develops rapidly over days to weeks, in contrast to the slow onset of traditional droughts. These events are characterised by an abrupt decline in soil moisture often accompanied by high evapotranspiration and temperatures (Otkin *et al.* 2018; Qing *et al.* 2023; Christian *et al.* 2024). According to Christian *et al.* (2021), flash droughts have occurred globally across diverse climate zones, and their frequency has increased in recent decades, largely due to rising temperatures and shifting atmospheric circulations. Their rapid onset causes particular challenges for ecosystems and agricultural systems, which have limited time to respond and adapt to the sudden water stress. Recent findings by Gu *et al.* (2025) reveal that flash droughts are especially damaging when accompanied by extreme heat due to the elevated atmospheric evaporative demand (AED) (modulated by extreme temperature, wind, and solar radiation), as the combined stressors intensify plant physiological responses and reduce carbon uptake. Their study shows that the coupling of flash drought with heatwaves has drastically increased the impact of these events on ecosystems productivity, particularly in croplands threatening global food security.

4.3. Drought impact on ecosystem and food production

The effects of drought on natural ecosystems and agriculture are multifactorial and complex. Increased atmospheric evaporative demand has compounded plant stress beyond the effects of reduced precipitation alone. High AED and vapor pressure deficit (VPD) disrupt plant physiological processes, disrupting plant hydraulic continuum such as stomatal and xylem conductance, often culminating in severe carbon starvation and following plant mortality (IPCC 2023). Soil moisture availability is crucial for sustaining plant function and carbon uptake; prolonged deficits have been tied to widespread xylem embolism, the major physiological cause of drought-induced tree mortality and to declines in gross primary productivity (Anderegg *et al.* 2016; Adams *et al.* 2017; Arend *et al.* 2021; Hammond *et al.* 2022; Allen, Breshears & McDowell 2015).

Climate-induced tree mortality under hotter drought conditions has been increasing since field measurements began in the mid-1960s (McDowell 2022; Hammond *et al.* 2022). This tree mortality is present across all biomes from the tropic to the boreal, from the sea level to 3500 m (Hammond *et al.* 2022) (Figure 1.15). Tree mortality will continue to increase due to the exacerbation of extreme weather events (McDowell 2022)

and this high mortality involves diverse disturbance processes that amplify forest die-off such as insects and pathogens attack, wind exposure and wildfire (Seidl *et al.* 2017).

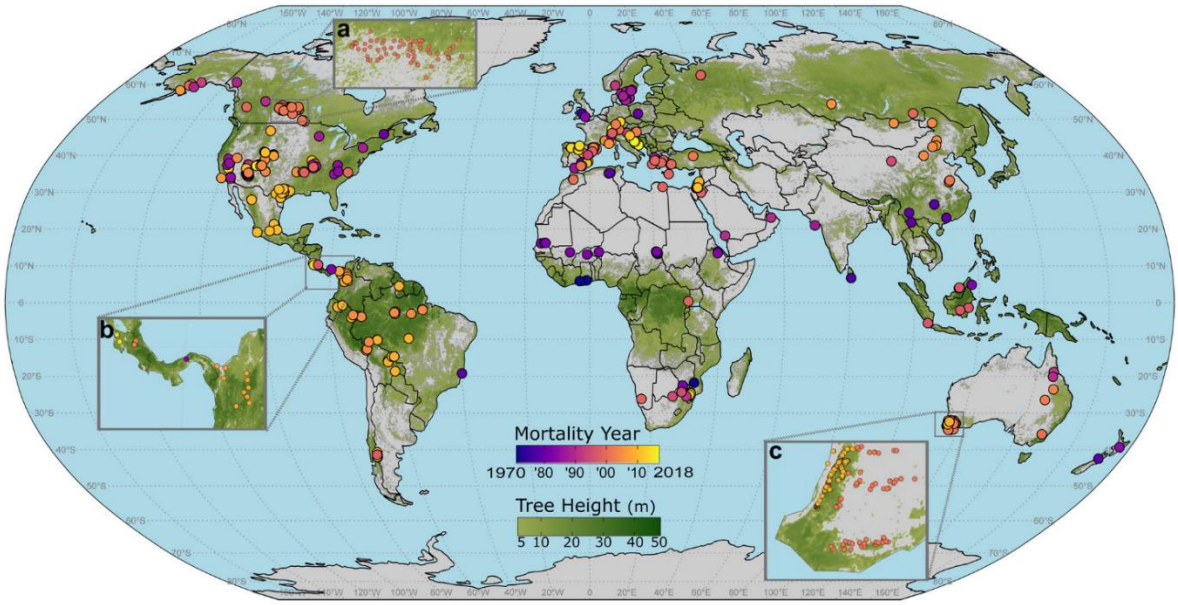

FIGURE 1.15: Global distribution of hotter-drought tree mortality plots (Hammond *et al.* 2022). Dots are color coded according to the year of mortality. Insets show examples of dense plot networks in Canada, Central America, and Southwest Australia.

In agriculture, not only soil moisture deficits disrupt crop growth, but increased AED under warming climates amplifies irrigation demands, further stressing local and downstream water resources (IPCC 2023). All types of droughts but especially agricultural and ecological droughts have struck major agricultural regions worldwide not equally (Freedman *et al.* 2025) with increasing frequency and severity, including the Amazon, southwestern North America, Australia, and the Mediterranean, contributing to significant crop yield losses and threatening food security (IPCC 2023) (Figure 1.16). The decline in yields linked to droughts for all different cropping systems is a major challenge for food security. This global decline, affecting major cereal crops such as wheat, maize, and soybean with notable regional differences is expected to persist. To counteract its impact, it is crucial to develop drought-resistant crop varieties and implement adaptive agricultural practices to mitigate the adverse effects of climate change on crop production. Although little documented, it has become crucial to examine the link between yield and drought resistance in annual crops. A recent study on soybeans demonstrated this close link by showing that cultivars with higher leaf embolism resistance maintained higher

yields in the field (Schell *et al.* 2025). It is therefore important to consider embolism resistance and the hydraulic traits of major crops in breeding programmes (Schell *et al.* 2025) and not only focus on water use efficiency. In breeding programmes, genetics is an important area of research for improving yield and resistance to biotic and abiotic stresses. A major study on wheat yields in France showed that, since 1990, climate change has partially offset genetic progress, leading to stagnating yields (Brisson *et al.* 2010). Despite ongoing efforts to improve yields through genetic advances and changes in agricultural practices, yields are stagnating. This is particularly true in French regions with intensive agriculture and high yield potential. Effects of climate change are mainly due to a general warming and more frequent droughts in winter and spring thus impacting the development and the physiology of crops as well as on their water and nitrogen nutrition (Brisson *et al.* 2010).

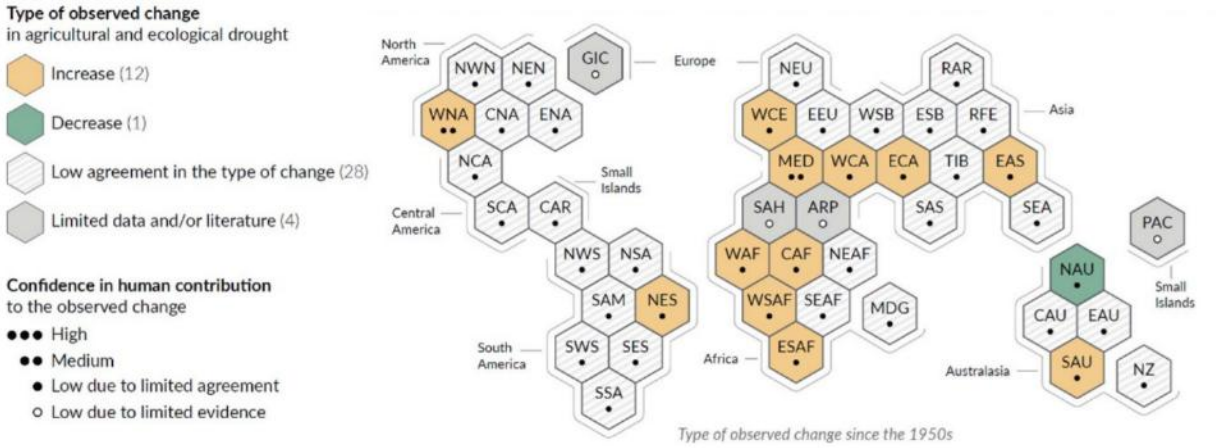

FIGURE 1.16: Synthesis of assessment of observed change in agricultural and ecological drought and confidence in human contribution to the observed changes in the AR6 land-regions, excluding Antarctica (IPCC 2023).

4.4. Projection in a context of climate change

Under current and projected climate change, drought dynamics are evolving rapidly (Cook *et al.* 2018). Recent studies (IPCC 2023; Gebrechorkos *et al.* 2025) show that AED has risen over recent decades across most continents, enhancing evapotranspiration and exacerbating water stress, particularly during dry seasons. While meteorological drought trends remain regionally variable, observational evidence indicates intensifying agricultural and ecological droughts in many areas due to increased AED and changing precipitation patterns (IPCC 2023). Climate models project that with

each increment of global mean surface temperature (GMST), more regions will experience severe and persistent droughts; at 2°C of warming, the risk of substantial agricultural and ecological droughts becomes even more pronounced (IPCC 2023) leading to a collapse of the food production in some regions. A recent study from Hultgren *et al.* (2025) estimates that for every 1 °C increase in global mean surface temperature, global food production declines by approximately 5.5×10^{14} kcal per year, corresponding to a reduction of 120 kcal per person per day (4.4% of the recommended daily intake). Although increased atmospheric CO_2 can improve plant water-use efficiency (IPCC 2023), this effect is unlikely to fully offset the more severe water limitations imposed by higher temperatures and enhanced AED, particularly when soil moisture becomes critically low. Furthermore, repeated droughts and the associated ecosystem stresses pose significant risks to the global land carbon sink, undermining its ability to sequester carbon and thus further amplifying climate change (IPCC 2023). There is an important and urgent need to better understand which both climates zones and species are the most vulnerable to anticipate the degree to which the future climatic changes will affect forests' structure and function (Mantova *et al.* 2022) but also food production.

5. Contextualising drought stress on plant

Drought exerts a profound impact on plant physiology, particularly affecting water transport (Torres-Ruiz *et al.* 2024). Under drought conditions, the availability of soil water declines, and plants must rely on their hydraulic architecture to limit water loss while maintaining essential physiological functions such as photosynthesis. When soil water availability declines, water transport is impacted, leading to a cascade of hydraulic and physiological failure if the stress exceeds the plant's thresholds for xylem embolim. As drought intensifies, global plant performance and production collapse, increasing the risk of pest infestation and fatal hydraulic failure leading to death (Figure 1.17).

Recent advances in plant hydraulics have revealed a close link between plant hydraulics and the mechanisms and processes related to plant growth, survival and production, as well as biotic attacks (Torres-Ruiz *et al.* 2024) especially the link between drought-related mortality and xylem resistance to embolism. Most studies have focused especially on the role of stomatal closing during drought in limiting water loss (left part of Figure 1.17), neglecting residual water losses persisting after stomatal closure. My research will focus on what happens after stomatal closure in terms of water loss

impacting survival and leading to death (right part of the Figure 1.17). These water losses, although negligible in terms of percentage of maximum stomatal function (less than 5%), become significant if the drought persists.

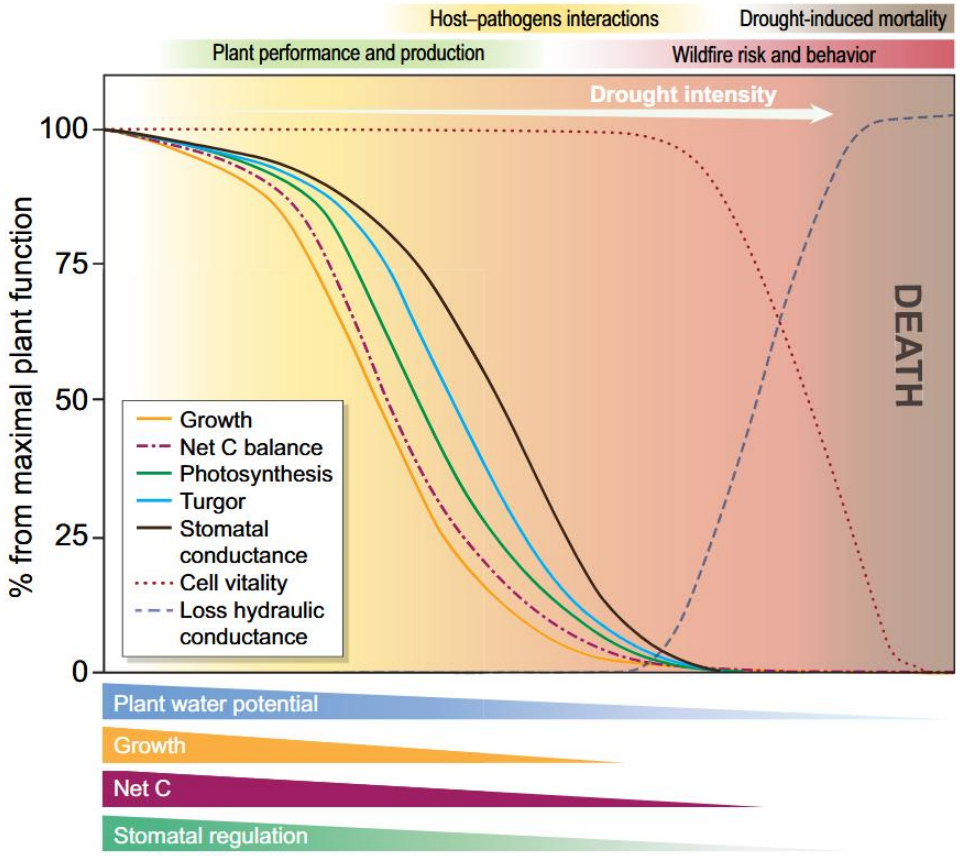

FIGURE 1.17: Conceptual graph illustrating the relative variations in the main physiological functions associated with plant hydraulic traits as plants are exposed to increasing levels of water stress.
The panel at the bottom shows the negative effects of stress intensity on the different physiological functions (Torres-Ruiz *et al.* 2024).

5.1. Plant hydraulic

5.1.1. Soil-plant-atmosphere plant continuum

The soil-plant-atmosphere continuum (SPAC) describes the continuous movement of water from the soil, through the plant and into the atmosphere (Figure 1.18). Water moves from regions of higher to lower water potential, beginning in the soil where water potential is relatively high (close to 0 MPa at saturation), passing through the root and xylem tissues of the plant, and finally evaporating from the leaf surfaces into the atmosphere (close to -100 MPa). The water potential (ψ; MPa) consists of the sum of

potentials (corresponding to the free energy of free water in a given state): pressure ($\psi_{pressure}$), represents the effect of hydrostatic pressure; osmosis ($\psi_{osmotic}$), represents solutes' dilution and gravimetric ($\psi_{gravitational}$), represents the force of gravity and depends on the height of the plant. Both osmotic and gravitational water potential are negligible in plants. Water uptake at the root-soil interface is driven by differences in water potential between soil water and root cells, while within the plant, water moves through the xylem by negative pressures created by transpiration. The driving force throughout the SPAC is the gradient of water potential (ψ) where $\psi_{soil} > \psi_{root} > \psi_{stem} > \psi_{leaf} > \psi_{atmosphere}$.

Water diffuses from internal leaf tissues into the atmosphere through stomatal openings in vapor form. The steepest drop in water potential occurs at the leaf-air interface, due to the lower humidity of the atmosphere than inside the leaf, which sustains transpiration and effectively "pulls" water through the plant. To maintain this flow, plant hydraulic structures including root, xylem vessels, and stomata regulate water loss and mitigate the risk of cavitation (air bubble formation) that disrupts water transport (Taiz *et al.* 2015).

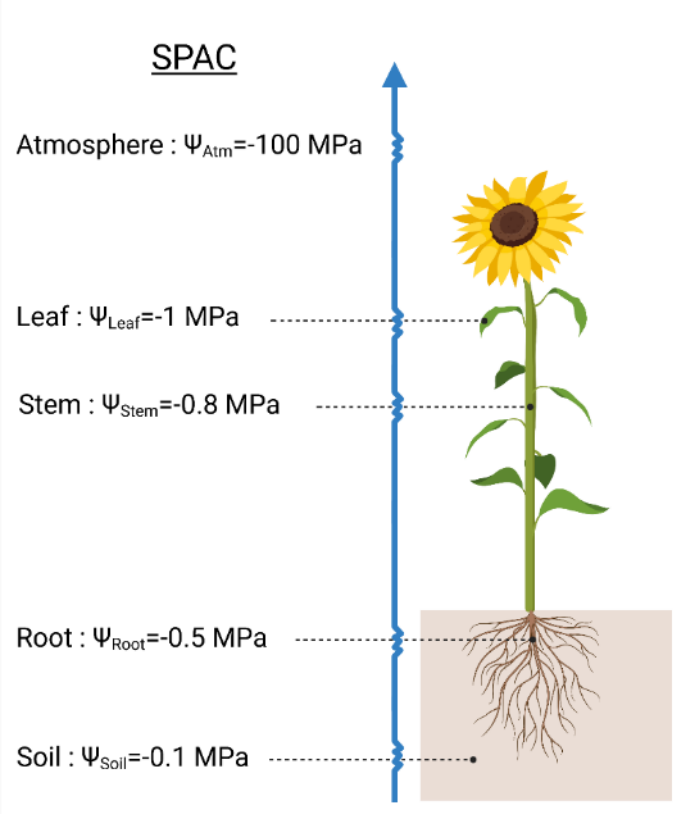

FIGURE 1.18: Soil-plant-atmosphere continuum (SAPC).
The solid blue line represents the water flow. Resistance corresponds to the hydraulics resistance at each stage. Ψ_X corresponds to the water potential (MPa) at each stage (soil, root, stem, leaf and atmosphere). Created in BioRender.com.

This entire process depends on the continuous hydraulic connection in the SPAC and on the ability of plants to regulate water transport and loss in response to environmental conditions.

5.1.2. Cohesion-tension theory

Within the plant, water transport relies on the cohesion-tension mechanism developed by Boehm (1893) and Dixon and Joly (1894), where water molecules are pulled upward under tension generated by transpiration at the leaves (Taiz *et al.* 2015). This mechanism relies on two properties of water: cohesion, which is the attraction between water molecules due to hydrogen bonding, and tension, which is the negative pressure generated by the transpiration from leaf surfaces. As water evaporates from the stomata in leaves, it creates a negative pressure that pulls more water upward through the plant's vascular system. The continuous column of water in the xylem is maintained by cohesive forces between water molecules and adhesive forces that bind water to the xylem walls, preventing the column from breaking even under considerable tension.

5.2. Plant response to drought

Plants respond to drought through a complex set of physiological and hydraulic adjustments that aim to maintain water balance while minimising the risk of catastrophic failure in water transport systems (Choat *et al.* 2012; Torres-Ruiz *et al.* 2024).

5.2.1. Hydraulic trait and vulnerability

Hydraulic traits, such as xylem vulnerability to embolism and the capacity to buffer internal water deficits, are central to a plant's drought response (Mantova *et al.* 2022). Vulnerability curves (which show the decline in hydraulic conductivity with decreasing water potential) allow quantification of key parameters like Ψ_{P12}, Ψ_{P50}, Ψ_{P88}, the water potential at which 12%, 50% and 88% respectively of xylem conductivity is lost due to air embolism (Choat *et al.* 2012). Ψ_{P12} is considered as the beginning of xylem embolism and Ψ_{P50} for conifers or Ψ_{P88} for angiosperms are considered as a fatal threshold for plant survival. Species with more negative Ψ_{P50} values are considered more resistant to drought-induced hydraulic failure, as they can withstand lower water potentials before catastrophic loss of hydraulic conductivity occurs (Choat *et al.* 2012). However, global analyses reveal that xylem vulnerability is remarkably convergent among forest species, typically indicating that most trees are at risk of losing critical hydraulic function under severe drought, regardless of their ecosystem of origin (Torres-Ruiz *et al.* 2024). As a drought progresses, sustained water deficits first lead to a drop-in plant water potential, and if the plant's hydraulic system cannot maintain sufficient conductivity, water transport collapses, resulting in tissue desiccation and death (Choat *et al.* 2012; Torres-Ruiz *et al.* 2024).

5.2.2. Stomatal closure and safety margin

Stomatal conductance is a primary regulator of water loss during drought along with the cuticular conductance. At the turgor loss point (Ψ_{tlp}), stomata are closed, reducing transpiration helping to maintain leaf and stem water potentials above dangerous thresholds. The stomatal safety margin describes the buffer between the water potential at which stomata are fully closed (Ψ_{gs90} or Ψ_{P12}) and the water potential at which xylem embolism occurs (Ψ_{P50} or Ψ_{P88}) (Figure 1.19). The safety margin quantifies the degree of conservatism in a plant’s hydraulic strategy (Choat *et al.* 2012). Species with a wider

safety margin close their stomata sooner, or have a greater embolism resistance or both like the highly drought-resistant species (Choat *et al.* 2012; Petek-Petrik *et al.* 2023). Coordination between stomatal closure and xylem vulnerability is critical. If stomata do not close before water potentials approach xylem vulnerability thresholds, plants are at high risk of hydraulic failure (Meinzer *et al.* 2009; Choat *et al.* 2018).

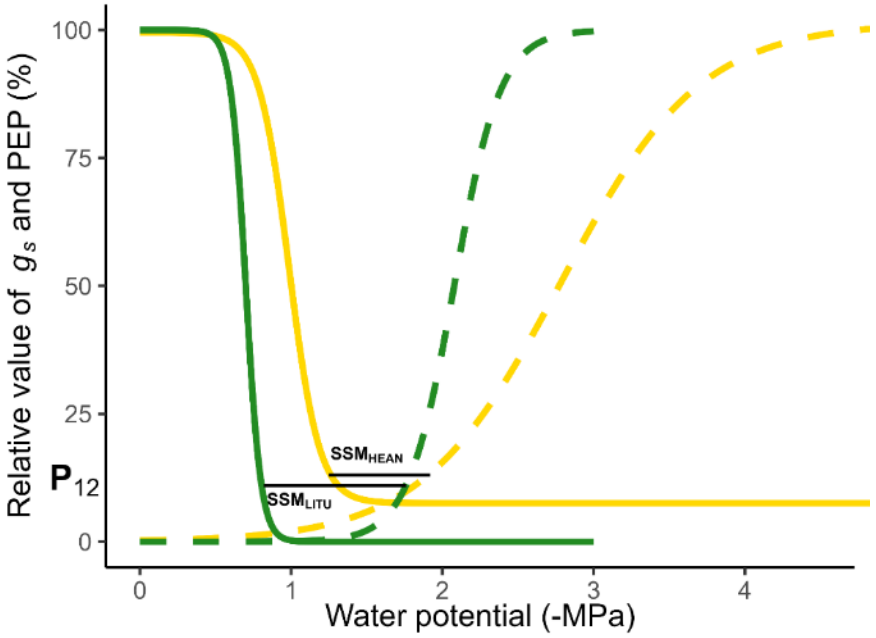

FIGURE 1.19: Stomata safety margin (SSM) for *Liriodendron tulipifera* (green) and *Helianthus annuus* (yellow).
Solid line corresponds to the relative stomatal conductance whereas the dotted line corresponds to the xylem vulnerability to cavitation curves. P_{12} corresponds to the water potential at which 12% of xylem conductivity is lost. Xylem vulnerability to cavitation curves. was assessed using the Cavitron technique in 2022 (Cochard 2002; Burlett *et al.* 2022) at the platform for hydraulic traits (Caviplace, Phenobois platform, University of Bordeaux, Pessac, France). Relative stomatal conductance ($g_{s,rel}$) came from the paper "*Deciphering the impact of stomatal leakiness and its spatial variability within the leaf on residual water loss during severe drought*".

5.2.3. Minimum leaf conductance (g_{min})

During drought, water loss from leaves continues even after stomatal closure, and it's called the minimum leaf conductance (g_{min}). The residual pathway for water vapor diffusion includes both cuticular transpiration and stomatal leakiness from incompletely closed stomata (Duursma *et al.* 2019) (Figure 1.20). While g_{min} typically accounts for less than 5% of maximum stomatal conductance (1.4% for *L. tulipifera* and 2.2% for *H. annuus*, see chapter 3), its physiological significance during drought is crucial. The margin defined by the SSM is a hydraulic margin that does not consider residual water loss after

stomata closure. However, over time if drought conditions persist, these persistent water losses will consume this safety margin leading to xylem embolism leading to a fatal hydraulic failure (Figure 1.20). Define as the ratio between the stomatal safety margin and the g_{min} (SMRIΨ_{P50}), the safety margin retention index is a key parameter to evaluate the speed taken by the plant to cross the stomatal safety margin (Petek-Petrik *et al.* 2023). Consequently, g_{min} is a pivotal parameter which dominates water loss (Figure 1.20) after stomatal closure and can decide the plant's future if drought conditions persist. Recent studies emphasise that the g_{min}, as a hydraulic trait, is crucial for the time to hydraulics failure leading to the death of the plant (Burlett *et al.* 2025) predicted in mechanistic soil-plant-atmosphere models such as SurEau (Cochard *et al.* 2020; Ruffault *et al.* 2022).

As the stomata close, the cuticle becomes increasingly important in limiting water loss and its permeability is governed by changes in the chemistry of cutin and waxes during drought. Moreover, incomplete stomatal closure, named as stomatal leakiness, can have a significant impact on g_{min}.

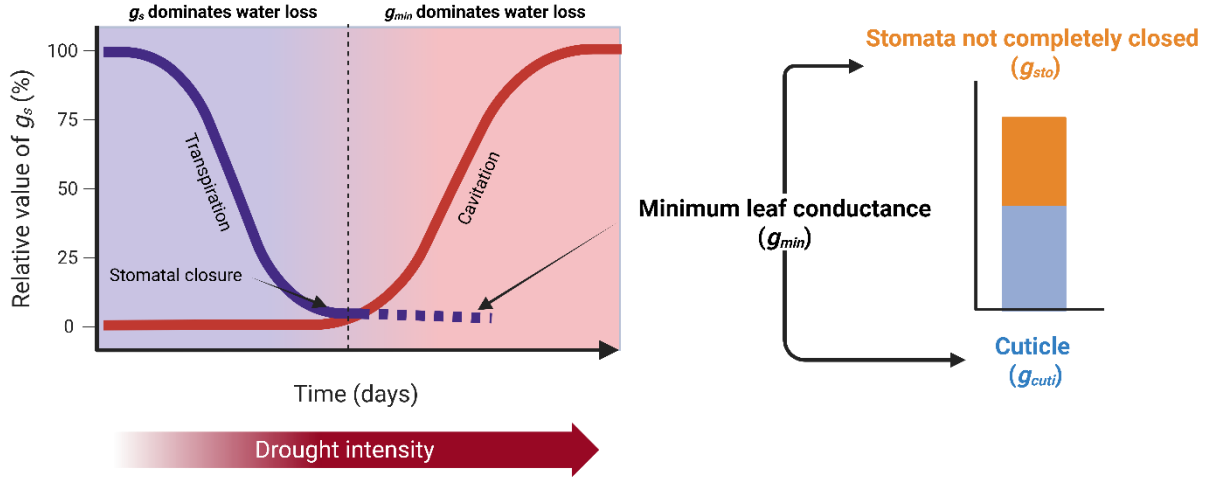

FIGURE 1.20: Conceptual diagram of stomatal closure and cavitation under drought.
g_s corresponds to the stomatal conductance. The minimum leaf conductance (g_{min}) corresponds to the sum of cuticular conductance (g_{cuti}) and stomatal leakiness (g_{sto}).

Due to its crucial role, the minimum leaf conductance has long been studied using both ecophysiological and biochemical approaches. However, no unified, common method has been developed to determine this trait, partly due to the difference in focus between studies, with some focusing on overall losses (cuticular and stomatal) and others focusing only on the cuticular part. Detached leaf mass loss (DLML) method, application

of ABA, vaseline coating on the stomatous side, and cuticular permeance measurements from isolated astomatous cuticles are commonly used approaches to estimate minimum leaf conductance. Reviews (Kerstiens 2006; Duursma *et al.* 2019) have reported a wide range of g_{min} values across species, clades, and climates since the 1930s. Recent studies conclude that the minimum leaf conductance varies significantly and depends on environmental cues, using water loss measurement from detached leaves (Bueno *et al.* 2019; Machado *et al.* 2021; Slot *et al.* 2021; Boisseaux *et al.* 2025). Nevertheless, two meta-analyses (221 and 160 species respectively) conclude that g_{min} variability (Duursma *et al.* 2019) and cuticular water permeability (Schuster *et al.* 2017) were not clearly related to species groups.

Using a standardised method to evaluate the minimum leaf conductance using the detached leaf mass loss (DLML) method and hydraulic trait, Burlett *et al.* 2025 highlighted the variability of that trait (chapter 2). To go further and using the same protocol, Trueba et al, 2025 (in revision), estimate the g_{min} on 101 species on a wide phylogenetic and ecological diversities and conclude that g_{min} is significantly variable across species with a weak phylogenetic signal (Figure 1.21).

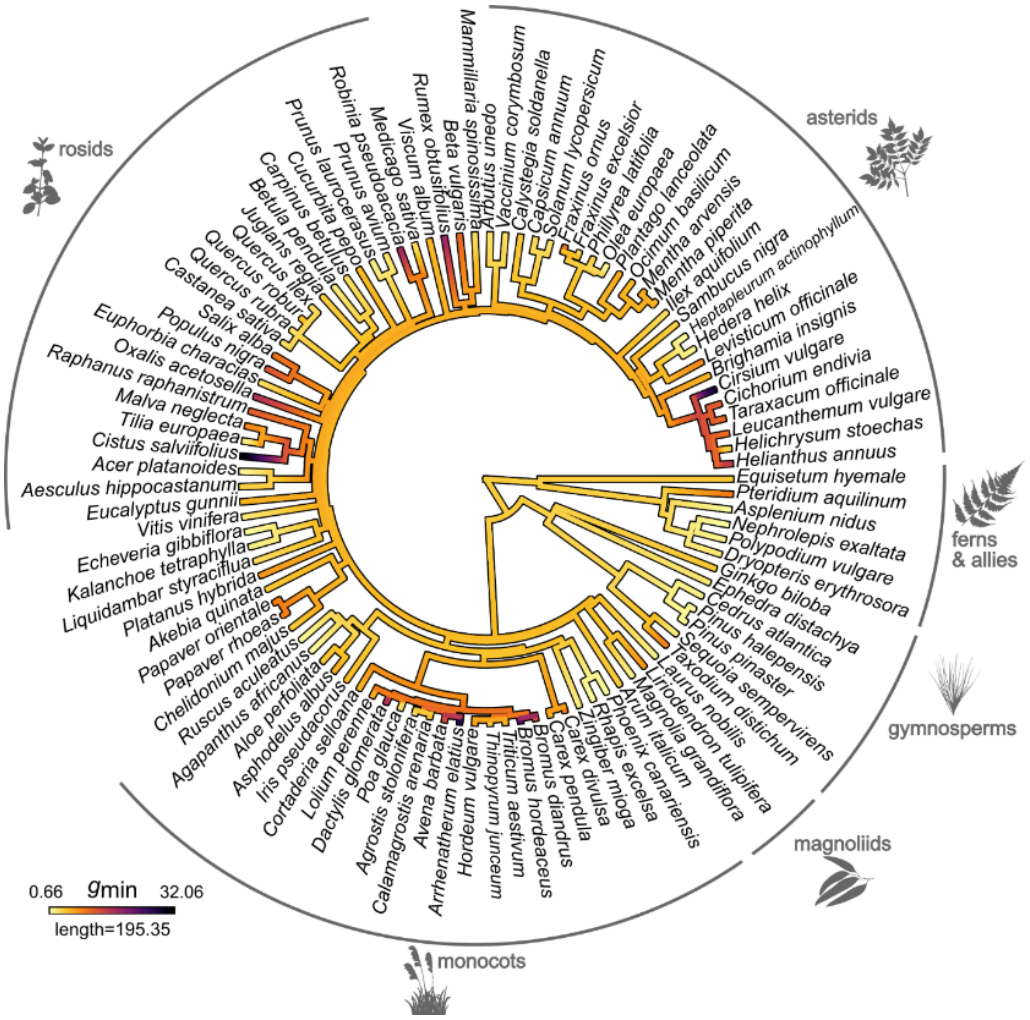

FIGURE 1.21: Minimum conductance to water vapor after stomatal closure (g_{min}) across vascular plant species.
Conductance is mapped on a phylogenetic tree of 101 species. The color gradient along the branches of the tree indicates lower (light) and higher (dark) values of g_{min}. A scale bar (in My) is included. Major clades of sampled vascular plants are indicated. The species not included in any group are all eudicot angiosperms, which also includes the ensemble of asterids + rosids (from Trueba et al, 2025, in revision).

6. Thesis aims and outline

Drought affects plant physiology in many ways, leading to reduced growth and productivity, thereby contributing to plant mortality. Therefore, it is of utmost importance to investigate drought resilience of plants from roots to leaves. As plant leaves can be exposed to various stresses with different types and intensities, they are frequently the first organs directly affected by stresses. Mechanisms associated with the resistance and potential recovery of leaves remain poorly understood. While stomatal behavior has been extensively studied in response to both vapor pressure deficit and soil water stress, the mechanisms of water loss after drought-induced stomatal closure are still unclear in terms of components and dynamics. Referred as to the minimum leaf conductance, it consists of stomatal not completely closed and cuticular transpiration. We hypothesise that under prolonged and severe drought conditions, these components play a decisive role in the time to reach hydraulic failure.

By integrating independent methodologies within an interdisciplinary context, this present work aims to clarify and to quantify the components of minimal leaf conductance and to evaluate their roles in plant survival under severe drought. Specifically, the objectives of this study are to: (i) examine the dynamics of water loss following stomatal closure (Chapter 2), (ii) determine the contribution of stomatal leakiness to minimal leaf conductance (Chapter 3), (iii) underline the physiological significance of stomatal patchiness during drought (Chapter 4), and (iv) investigate the drought-induced responses of the leaf cuticle and their effects on water loss (Chapter 5).

This thesis follows an article-based format. Each chapter aims to examine specific aspects and part of the minimum leaf conductance as follows:

- Chapter 2 describes the variability of the minimum leaf conductance estimating at different water potential thresholds from the residual leaf conductance. As water stress level increases, the g_{min} decreases impacting greatly the time to hydraulic failure making it necessary to take this variability into account in mortality prediction models.
- Chapter 3 goes further by focusing on the stomatal component of minimum leaf conductance with the stomatal leakiness. This chapter aims to demonstrate the presence of stomatal leakiness, its role in the minimum leaf conductance, and the impact on plant survival. This chapter investigates stomatal leakiness using spatial

methods, questioning the need to consider the spatial heterogeneity of stomatal closure in stomatal conductance models.

- Chapter 4 also focuses on the role of stomata to highlight the impact of stomatal patchiness, mainly at the onset of water stress. The spatial nature of patchiness allows for a local response extending gas exchange. Beyond the spatial aspect, stomatal patchiness is a hierarchical spatio-temporal process that enables a rapid, localised and appropriate response to water stress.
- Chapter 5 focuses on the second component of minimum leaf conductance, the cuticle. By studying the composition of the cutin polyester and the epicuticular waxes independently, the aim of this chapter is to examine the response of each cuticle component along a stress gradient and their impact on water loss.
- The chapter ‘Conclusion and prospects’ summarises the main findings of this thesis, highlights the importance of transdisciplinary research, and opens up the possibility of taking multistress factors into account in studies.

CHAPTER 2

Minimum leaf conductance (g_{min}) is not constant along drought gradient

Chapter 2 Minimum leaf conductance (g_{min}) is not constant along drought gradient

This chapter is presented in the form of a summary of Burlett et al, published in 2025 to New Phythologist, entitled: Minimum leaf conductance during drought: unravelling its variability and impact on plant survival. by R. Burlett, S. Trueba, X. Bouteiller, G. Forget, JM. Torres-Ruiz, N. Martin-StPaul, C. Parise, H. Cochard and S. Delzon.

My contribution to this work included the development of the R function g_residual and available on this repository: https://gitub.u-bordeaux.fr/phenobois/g_residual. This function is explained in detail in appendix A1 and calculates residual leaf conductance as the slope of mass data over time using the detached leaf mass loss method (DLML) and, in parallel, the corresponding RWC, water potential and VPD.

1. Short introduction

The role of minimum leaf conductance (g_{min}) in plant survival under severe drought is crucial. Until now, the dynamics of minimum leaf conductance have remained largely unexplored, and the lack of a standardised estimation method means that it's difficult to compare studies. Burlett *et al.* (2025) proposed a standardised and an open-source methodology for measuring g_{min} with a comparative analysis across nine species of trees to quantify its variability and functional significance. By linking dynamic changes in residual water loss to time-to-hydraulic-failure predictions, we highlight that g_{min} as a critical trait in drought-mortality models.

2. Minimum leaf conductance during drought: unravelling its variability and impact on plant survival

Water loss after stomatal closure is an essential characteristic of plants, particularly in the event of prolonged drought. It is therefore essential to study its dynamics over time using a reliable and accurate standardised method. Burlett *et al.* (2025) present a comprehensive study on the significance and dynamics of residual leaf conductance (g_{res}) as a dynamic water loss during dehydration after stomatal closure, and the minimum leaf conductance (g_{min}) as a trait bounded by physiology boundaries or hydraulics traits during a severe drought. This study addresses a crucial gap in plant ecophysiology by clarifying the difference between g_{res} and g_{min}. The study used nine woody angiosperm species (five deciduous and four evergreens) including *Liriodendron tulipifera* that span a wide spectrum of drought resistance (see Table 1 of the study in appendix A5). By employing a method that simulates a severe drought on several detached leaves (Billon *et al.* 2020; Burlett *et al.* 2025), it's possible to record the water loss of each individual leaf in a controlled environment. During drought, leaf shrinkage is one of the primary effects with turgor loss playing a role in hydraulic decline and estimation of hydraulics traits (Scoffoni *et al.* 2014). Additionally, water potential decline during leaf dehydration can slightly influence the water vapor pressure (w_i) inside the leaf and therefore modifying the driving force, i.e. the VPD for transpiration between the leaf and the atmosphere (Nobel 2009). Considering the shrinkage and the impact of water potential on VPD we can accurately estimate the residual leaf conductance and thus the minimal leaf conductance at different hydraulic thresholds.

2.1. Residual conductance varies during dehydration

The residual leaf conductance, g_{res}, decreases progressively during the dehydration and this decline varies across species. g_{res} is mainly due to the mass loss per unit of time whereas the correction effect of the shrinkage and the VPD slightly increased the residual leaf conductance estimations. After stomata stomatal closure, leaves continue to lose water by incompletely close stomata and cuticle, with a slowdown over time due to the availability of water inside the leaf impacting negatively the water potential and the RWC. For all species, residual leaf conductance dynamics is the same with a higher leaf minimum conductance at turgor loss point (g_{min_tlp}) than this measured between 50% and 80% of RWC ($g_{min\_RWC80\text{-}50}$). Given the decline in g_{res} over time, g_{min} values thresholded at water status inducing Ψ_{P12}, Ψ_{P50}, and Ψ_{P88} declined sequentially

across all species. This variability during the dehydration sequence could be the result of stomatal closure dynamics and by stomata not being fully closed (stomatal leakiness) as well as the response of the cuticle through changes in composition and accumulation of cuticular waxes. Although cuticle responses during drought are well documented, there is still a lack of convergence in studies on the impact of cuticle responses on water loss during drought.

2.2. Impact of the variation in minimum conductance estimates on time-to-death prediction

This variability has pronounced ecological and modeling implications. Indeed, the time to hydraulic failure defined as the time required by a plant to reach a fatal threshold corresponding to a loss of 88% of hydraulic conductance (for angiosperms) and the stomatal margin retention index ($SMRI_{\Psi 50}$) which reflects the time required to cross the stomatal safety margin (SSM) (Petek-Petrik *et al.* 2023) are related to the residual leaf conductance and used as parameter the minimum leaf conductance. Over- or underestimating g_{min} can misrepresent water loss under drought and lead to large errors in predicting time to hydraulic failure using mechanistic models such as SurEau (Cochard *et al.* 2020). The time to hydraulic failure estimated from a fixed g_{min} value tends to show greater dispersion than estimates based on a variable g_{min} value, reinforcing the variable nature of this trait during a drought sequence.

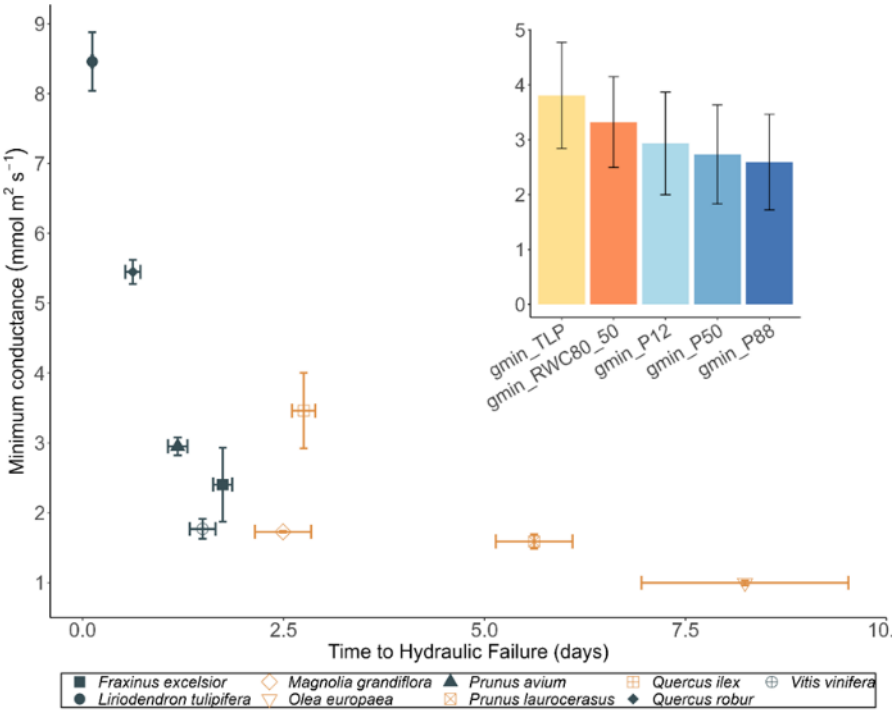

FIGURE 2.1: Relationship between measured time to hydraulic failure (THF) and leaf minimum conductance (g_{min}) corrected for shrinkage and vapor pressure deficit variation.
For each sample, g_{min} is computed for a relative water content between 50% and 80%. Error bars represent SE. Deciduous species are represented by blue symbols and evergreen species by yellow symbols. Inset represents averaged g_{min} values computed at different thresholds (from Burlett *et al.* (2025)).

2.3. Toward a standardized methodology to estimate g_{min}

The open-source tools introduce a methodology for continuously assessing residual and minimum leaf conductance, incorporating adjustments for leaf and VPD changes during dehydration. This approach improves the reproducibility and analysis of g_{min} measurements between studies. The adoption of physiological thresholds (such as 80-50% relative water content) further improves comparability by anchoring measurements between common, biologically significant reference points. The dynamic nature of g_{res} and the associated trait g_{min} underscores that plant water loss is mediated not only by how quickly stomata close or leakiness, but also by the cuticular part as well as on physical changes in the leaves and environmental conditions. Species differ in how g_{min} evolves during severe dehydration. Drought-resistant species, for example, may not simply have a lower starting g_{min}, but might be characterised by a more responsive or resilient pattern of decline as their water status declines. Such differences must be accounted for to predict which species or communities are most at risk during future droughts. The paper thus emphasises that accurate characterisation of g_{min} is pivotal for

both physiological research and for large-scale modeling such as predicting drought-induced tree mortality under climate change scenarios.

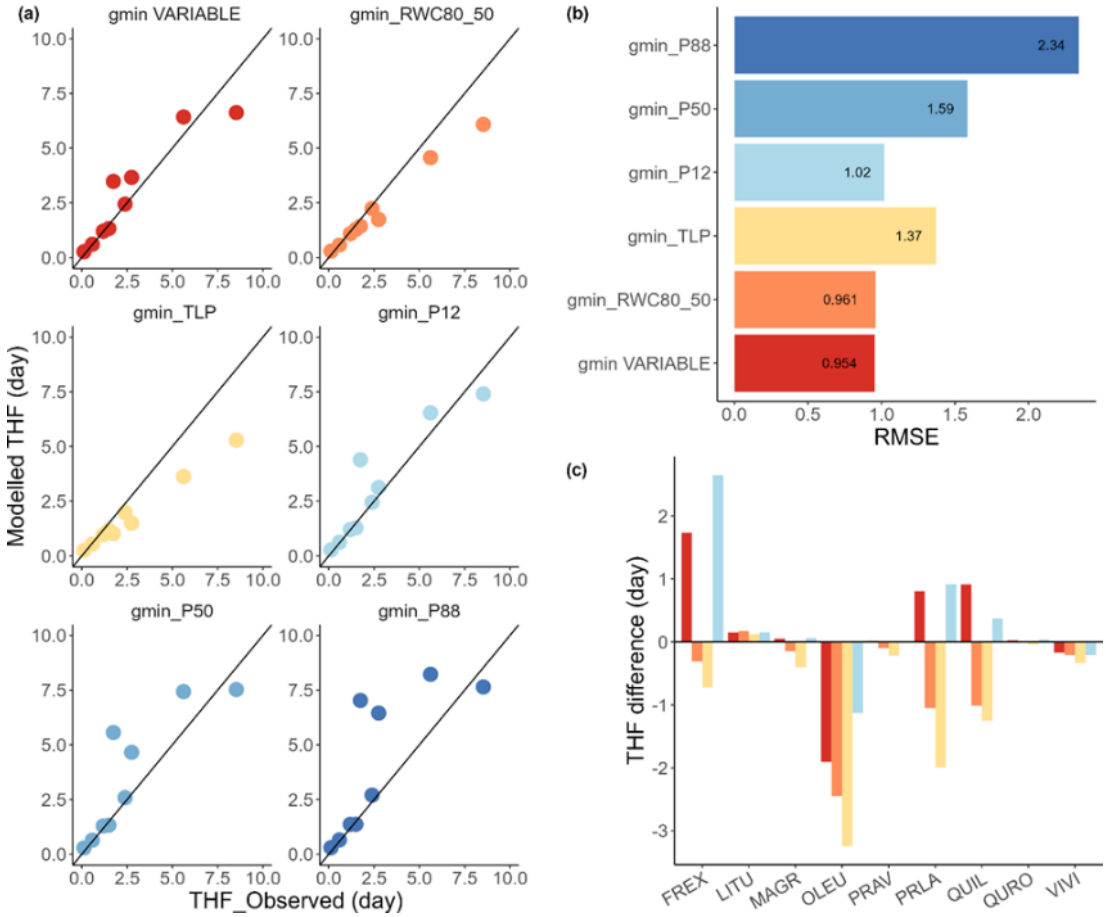

FIGURE 2.2: Relationship between modelled and observed time to hydraulic failure using different computations of g_{min}.
(a) Comparison between modeled and measured time to hydraulic failure (THF) across different g_{min} estimations. THF is defined as the time to reach P88. Each point corresponds to the average of THF for each of the studied species. Black lines indicate a 1:1 relationship. (b) Root mean square error (RMSE) comparing the performance of the models using different g_{min} values. (c) Difference between modelled and observed THF for each species, and color codes, corresponding to different g_{min} values, are the same as in panel b. Species abbreviation codes: FREX: Fraxinus excelsior; LITU: Liriodendron tulipifera; MAGR: Magnolia grandiflora; OLEU: Olea europaea; PRAV: Prunus avium: PRLA: Prunus laurocerasus; QUIL: Quercus ilex; QURO: Quercus robur; VIVI: Vitis vinifera.

CHAPTER 3

Stomatal leakiness under drought: a key driver of residual conductance in leaves

Chapter 3 Stomatal leakiness under drought: a key driver of residual conductance in leaves

This chapter is presented in the form of a paper recently submitted to Plant, Cell & Environment, entitled: Deciphering the impact of stomatal leakiness and its spatial variability within the leaf on residual water loss during severe drought. by G. Forget, R. Burlett, S. Trueba, T. Lawson, J. Joubès and S. Delzon.
The dual imaging experiment was performed during a five-month international mobility at the University of Essex, England. The detached leaf mass loss (DLML) method was conducted at BioGeCo, University of Bordeaux.

1. Short introduction

For decades, studies on stomata have focused on their closure during stress in response to increased VPD or soil dryness. In contrast, few results have been obtained on closure capacity or potential leaks after this closure point, even though we know that residual transpiration is an important trait for plant survival in drought conditions. Understanding stomatal behaviour beyond stomatal closure is crucial for explaining plant mortality under drought.

In this chapter, stomatal leakiness and spatial heterogeneity have been analysed in two contrasting species, *Liriodendron tulipifera* and *Helianthus annuus* with regard to residual leaf conductance. Using independent but nonetheless complementary methods, our results will show that incomplete stomatal closure or leaky stomata is present and consistent along the drought sequence contributing significantly to the residual leaf conductance. Concomitant with this water leakage, spatial heterogeneity appears to be a collective local response of stomata allowing physiological functions to be prolonged.

2. Deciphering the impact of stomatal leakiness and its spatial variability within the leaf on residual water loss during severe drought

2.1. Abstract

During drought, plants can continue to lose substantial amounts of water even after reaching the turgor loss point and experiencing a marked decline in stomatal conductance. This residual water loss occurs through both cuticle and incompletely closed stomata (also known as stomatal leakiness). However, the dynamics of these two processes during drought, and the thresholds at which they remain significant, are still poorly understood. We estimated minimum leaf conductance (g_{min}) in *Liriodendron tulipifera* and *Helianthus annuus* using the detached leaf mass loss (DLML) method, while independently quantifying stomatal leakiness using newly developed techniques. Our comparative analysis reveals that stomatal leakiness is present in both species studied, even under severe drought conditions. Additionally, spatial heterogeneity in stomatal closure, known as stomatal patchiness, emerges as a critical feature for leaf water fluxes, influencing g_{min} and extending carbon assimilation during prolonged drought. Incorporating both stomatal leakiness and patchiness into mechanistic models of plant hydraulics will improve predictions of time to hydraulic failure and drought-induced damages. This study highlights the importance of considering post-closure stomatal dynamics in our understanding of plant drought resistance and identifies stomatal leakiness as a key contributor to residual water loss under water scarcity.

Keywords

Drought stress, infiltration, leaky stomata, patchiness, residual leaf conductance, cuticular conductance, water potential, stomatal closure.

2.2. Introduction

Drought episodes are increasing in frequency and intensity across all biomes (Pörtner & Roberts 2022) disrupting local water cycles, impairing plant physiological processes and, in severe cases, threatening plant survival (Anderegg *et al.* 2015; Adams *et al.* 2017). In this context, maintaining plant water status is crucial for plant function,

particularly for gas exchange (H_2O and CO_2) between the leaf and the atmosphere. This exchange takes place through the stomatal pores and is essential for photosynthesis and atmospheric carbon capture (Flexas 2002; Lawson 2010; Lawson & Blatt 2014). Furthermore, water loss through transpiration provides evaporative cooling that helps maintain optimal leaf surface temperature, thereby preventing thermal stress (Drake *et al.* 2018). Plants have evolved various adaptive mechanisms to cope with drought stress. Among these mechanisms, two major types of mechanistic traits contribute to plant responses and adaptation to drought: xylem traits that ensure maintenance of the hydraulic function, such as resistance to embolism (Choat *et al.* 2012), and foliar traits that regulate water loss through stomatal aperture, which is governed by the turgor of guard cells (Yi *et al.* 2022; Mirasole *et al.* 2023). In addition to stomatal control of water loss, the leaf cuticle also plays a major role in water retention under drought conditions (Kerstiens 1996; Burghardt 2003). A recent theoretical study analysing data from 200 species highlighted the contributions of both these pathways in regulating water loss (Ochoa *et al.* 2024). Among stomatal traits influencing water loss, stomatal density and aperture are key determinants (Franks & Beerling 2009; Dow *et al.* 2014; Sack & Buckley 2016; Ochoa *et al.* 2024). Stomatal density is established early during leaf development, varies among species and is influenced by environmental conditions, thus adjusting over longer timescales (Lawson & Matthews 2020). In contrast, stomatal aperture is a dynamic process that occurs on shorter timescales (minutes to hours), balancing the mesophyll demands for CO_2, with water loss, in response to external cues (Lawson 2010; Lawson *et al.* 2014). Stomatal aperture, which fluctuates through oscillations (Marenco *et al.* 2006), is a time-dependent variable. Additionally, stomatal conductance can also exhibit temporal variability due to patchy stomatal behaviour, in which some areas of the leaf have stomata with lower aperture than others (Mott & Buckley 1998). By contrast, water loss through the cuticle is a passive process driven by the diffusion due to humidity gradient between the interior of the leaf and the environment (Tredenick & Farquhar 2021). Cuticular conductance represents a relatively minor flux compared to the flux associated with stomatal conductance (Schreiber & Riederer 1996; Riederer & Schreiber 2001; Stinziano *et al.* 2020) and is often neglected when calculating water flux in well-hydrated leaves or plants. Commercially available devices, such as infrared gas analysers and porometers, although account for cuticular conductance when measuring leaf gas exchange, they do not separate this from stomatal conductance. Both, stomatal and cuticular fluxes, commonly aggregated under a single variable i.e. stomatal

conductance (g_s, in mmol m^{-2} s^{-1}) are known to vary in response to biotic and abiotic factors (Lawson & Matthews, 2009).

During ecological and agricultural severe drought, characterised by prolonged soil moisture deficit (IPCC 2023) and inducing xylem embolism leading to plant death (Urli *et al.* 2013), water continues to escape from the leaf through a flux known as residual leaf conductance (g_{res}, in mmol m^{-2} s^{-1}). This flux is defined as the water loss that occurs after stomatal closure through both imperfectly closed stomata and the leaf cuticle (Duursma *et al.* 2019) and determines how long a plant can cope with restricted water availability before reaching fatal hydraulic failure (Choat *et al.* 2018; Burlett *et al.* 2025). As stomata close during drought, cuticular water loss becomes increasingly dominant. However, stomatal dynamics during closure, particularly incomplete closure and persistent leakiness, remain significant contributors to residual conductance (Šantrůček *et al.* 2004; Brodribb *et al.* 2014; Kane *et al.* 2020; Machado *et al.* 2021). Therefore, understanding the impact of stomata on residual leaf conductance remains imperative. In this context, it is essential to investigate the extent to which stomata can completely shut off leaf water loss under severe drought conditions, by quantifying the contribution of leaky stomata to g_{res} along a sequence of drought-related hydraulic traits.

To date, no method can precisely measure stomatal leakiness across both temporal and spatial scales. Here, we propose the combination of several methodological approaches to study this phenomenon at both scales. Leaf infiltration represents one of these approaches, providing a spatial visualisation of stomatal closure. Previous studies have demonstrated that infiltrating a leaf with water at a known pressure, reveals the proportion of stomata with apertures above a specific threshold (Alvim & Havis 1954; Lawson *et al.* 1998a,b; Mott & Buckley 1998). The second approach, combining thermography (Jones *et al.* 2009; Vialet-Chabrand & Lawson 2019, 2020) with chlorophyll fluorescence (Murchie & Lawson 2013) provides a novel approach to investigate the spatial biological implications of stomatal kinetics on photosynthetic performance (McAusland et al, 2014). To monitor the leaf water loss during drought, we combined both approaches with the detached leaf mass loss (DLML) method to quantify the residual leaf conductance (g_{res}). The DLML method is commonly used to estimate leaf residual conductance by measuring mass loss over time, simulating severe drought conditions where water supply to the leaf has ceased (Kerstiens 1996; Duursma *et al.* 2019; Billon *et al.* 2020; Burlett *et al.* 2025).

Using these independent methodologies, we aimed to quantify the relative contribution of foliar traits to residual water loss in drought conditions. (i) First, we investigated whether stomatal leakage significantly contributes to residual water loss along a dehydration process using the detached leaf mass loss (DLML) method and leaf infiltration. We hypothesised that stomata do not fully close during the dehydration process and validated this hypothesis using micro-CT imaging. (ii) Next, we explored the physiological significance of spatio-temporal heterogeneity in stomatal closure using complementary approaches, including combined thermal and chlorophyll fluorescence imaging, leaf infiltration and modelling. We hypothesised that spatially partial stomatal closure i.e. stomatal patchiness, results in heterogeneous stomatal leakiness and leads to an overestimation of leaf conductance when calculated with the standard equation for g_{leaf}.

2.3. Materials and Methods

2.3.1. Plant material

Two species with contrasted growth forms, habits and stomatal features were used in this study: a woody deciduous hypostomatous tree (*Liriodendron tulipifera*) and an annual amphistomatous forb (*Helianthus annuus*). *Helianthus annuus* seeds were sown into 3 litres pots containing compost whereas *Liriodendron tulipifera* seedlings were purchased from a local nursery. DLML, infiltration and micro-CT experiments were carried out on plants grown in a 9 m² climatic chamber (Strader, France) at the University of Bordeaux where the climatic and light parameters were set to 25°C; 80% RH; Photon Flux Density c. 700 µmol m^{-2} s^{-1}. An acclimation phase of 10 days was used for *L. tulipifera* individuals, while *H. annuus* were grown for 45 days before any measurements on fully expanded leaves. After the acclimation and growth, plants were subjected to drought stress by stopping watering with groups of four individual plants per species. For the dual imaging experiments, *Helianthus annuus* seeds were sown in plastic trays containing compost and germinated in a growth cabinet (Reftech BV, Sassenheim, the Netherlands). After germination, seedlings (one per pot) were transplanted into 1.5 litres pots containing compost and transferred to a temperature-controlled glasshouse at the University of Essex (average temperature was maintained at 21.8 ± 0.9 °C with RH between 40% and 55% depending on biomass in the glasshouse), supplementary sodium vapour lights

(8am until 8pm) provided a light environment of 400 µmol s^{-1} m^{-2} at the plant height. A similar growth phase of 45 days was respected before any measurements with *H. annuus* individuals.

2.3.2. Hydraulic and anatomical trait measurements

2.3.2.1. Water status and pressure-volume curve estimations

Pressure-volume curves were performed using a method adapted from Sack *et al.*, (2011) on eight leaves of *H. annuus*, and five leaves of *L. tulipifera*. Pressure-volume curves were used to determine leaf physiological traits such as the water potential (Ψ_{tlp}, MPa) and relative water content (RWC_{tlp}, %) at turgor loss point along with the elasticity modulus (ε) and osmotic potential at full turgor (π_0) (Table 3.1). Using ε and π_0 we estimated the water potential at any RWC during the DLML experiment based on the relative water content. We also measured the leaf water potential (Ψ_{leaf}, MPa) with a pressure chamber (DG Meca, Gradigan, France) directly on paired leaves for the infiltration experiment and with a psychrometer (PSY1, ICT International, Armidale, NSW, Australia) for the dual imaging experiment.

TABLE 3.1: Leaf hydraulics and photosynthetic variables used in this study. Mean and standard errors for each variable are provided.

Definition	Abbreviation	Unit	*L. tulipifera*	*H. annuus*
Relative water content	RWC	%	-	-
Relative water content at turgor loss point	RWC_{tlp}	%	90.03 ± 0.74	77.98 ± 3.10
Water potential at turgor loss point	Ψ_{tlp}	MPa	-1.64 ± 0.10	-0.98 ± 0.05
Water potentials inducing 12% losses of conductance in the stem	Ψ_{P12}	MPa	-1.66 ± 0.06	-1.77 ± 0.15
Water potentials inducing 50% losses of conductance in the stem	Ψ_{P50}	MPa	-1.86 ± 0.06	-2.78 ± 0.18
Elasticity modulus	E	MPa	10.45 ± 1.35	2.03 ± 0.31
Osmotic potential at full turgor	π_0	MPa	-1.05 ± 0.08	-0.74 ± 0.06

Quantum efficiency	Φ_{PSII}	-	-	-

To facilitate analysis, leaves were categorised by water potential values and divided into three classes using Ψ_{tlp} and Ψ_{P50} as boundaries to establish three classes. There were well-hydrated leaves considered with no stress [0; Ψ_{tlp}], with mild stress [Ψ_{tlp}; Ψ_{P50}] and with a severe stress [Ψ_{P50}; -Inf].

2.3.2.2. Relative water content

Relative water content is a mass-derived important parameter that we used in the DLML for the determination of the water potential. Turgid weight (TW, g) of each individual leaf was measured before the water loss measurements in the climatic chamber. Weight measurements were performed with a 4-digit balance (Pioneer, Ohaus, USA). At the end of the measurement, leaves were put in an oven at 65°C for 72h and dry weight (DW, g) was measured. The relative water content (RWC, %) was then computed for each mass value (fresh mass; FW, g) during the dehydration process using equation 3.1:

$$RWC = 100 * \frac{FW - DW}{TW - DW} \quad (3.1)$$

2.3.2.3. Stem embolism vulnerability

Stem vulnerability to xylem embolism was assessed on five replicates per species using the Cavitron technique (Cochard 2002; Burlett *et al.* 2022). Measurements were carried out at the platform for hydraulic traits (Caviplace, Phenobois platform, University of Bordeaux, Pessac, France). For each species a percentage loss of conductance or PLC curve was obtained and embolism vulnerability determined at thresholds Ψ_{P12}, Ψ_{P50} and Ψ_{P88} (MPa), which correspond to the xylem pressure/water potential inducing 12%, 50% and 88% losses of hydraulic conductivity, respectively.

2.3.2.4. Stomatal conductance measurements

Stomatal conductance (g_s, mmol m^{-2} s^{-1}), which can be defined as the conductance at a time t as a function of the local climatic conditions and water level of the plant (Lawson & Blatt 2014; McElwain et la. 2016), was measured using a porometer (LI-600; LICOR, USA). g_s measurements were taken daily (45 days for *L. tulipifera* and 15 days for *H. annuus*) between 9:00 and 12:00 on seven leaves of *L. tulipifera* and three leaves of *H. annuus*. Leaves were tagged to ensure daily measurements on the same

location (upper right quadrant of the leaf blade) of each leaf. $g_{s,mean}$ is then calculated as the average value for each every day. $g_{s,max}$ and $g_{s,min}$ is the maximum and minimum average value for each plant across the experiment. g_s is then expressed here as a relative stomatal conductance ($g_s/g_{s,max}$, $g_{s,rel}$) in order to facilitate the study of stomatal dynamics during drought.

2.3.2.5. Anatomical properties

Epidermal impressions were collected on three leaves for both species using a transparent nail polish applied to the abaxial and adaxial surfaces and allowed to dry for c. 15 minutes. After drying, nail polish was covered by a transparent tape and transferred to a microscope slide. Slides were observed with a light microscope (Leica DM2500, Leica Microsystems, Germany) with a connected digital camera (Leica MC190 HD, Leica Microsystems, Germany) and photographed at ×20 magnification for *H. annuus* and x10 for *L. tulipifera* to calculate stomatal density, and at ×40 magnification for the measurements of stomatal size. Along with stomatal size and density, we also assessed stomatal length for both species (Table 3.2). Measurements were carried out using ImageJ v.1.53q (Schneider *et al.* 2012).

TABLE 3.2: Stomatal anatomy properties for the adaxial and abaxial surfaces of leaves. Mean and standard errors for each trait are provided; NA = not available.

Definition		Abbreviation	Unit	*L. tulipifera*	*H. annuus*
Stomatal density	Abaxial	d_L	N mm^{-2}	116 ± 6.11	410.66 ± 66.82
	Adaxial	d_U		NA	234.66 ± 41.65
Stomatal area	Abaxial	s_L	µm²	374.70 ± 39.00	118.47 ± 11.65
	Adaxial	s_U		NA	103.97 ± 9.34
Stomatal length	Abaxial	p_L	µm	27.22 ± 1.39	18.90 ± 1.09
	Adaxial	p_U		NA	17.48 ± 0.76

2.3.3. Residual leaf conductance (g_{res}) and estimation of residual leaf conductance at different hydraulic thresholds (g_{min})

Residual leaf conductance (g_{res}) using the detached leaf mass loss (DLML) method was measured on 12 and 16 well-watered leaves of *H. annuus* and *L. tulipifera* respectively. Leaves were cut with a razor blade and the petiole sealed with paraffin to avoid water loss. Each leaf was weighed with a 4-digit balance (Pioneer, Ohaus, USA)

and scanned (v850 pro, Epson, Japan) to estimate the projected leaf area (A_{leaf}, m²). Leaves were then clipped to load cells inside a climatic chamber to simulate drought through desiccation (Billon *et al.*, 2020). Conditions inside the chamber were kept stable at 25°C and 60% of relative humidity, with a vapour pressure deficit (VPD) of c. 1.26 kPa. We assume the leaf temperature equals the surrounding air temperature; the small temperature difference is neglected when computing the VPD. Micro load cells by Wheastone bridge board (1046_OB, Phidgets Inc., Canada) were used to record the mass every five minutes in the chamber. During measurements, samples were placed in the dark to avoid light impacting stomatal kinetics. A detailed description of the system and setup is provided in (Burlett *et al.* 2025). A custom function in R was developed for the parameterisation and treatment of raw data (*g_residual*, PHENOBOIS, University of Bordeaux; https://gitub.u-bordeaux.fr/phenobois). The main function, g_residual, calculates the residual leaf conductance as the slope of the mass data over time (eq. 3.2) using the Savitsky-Golay filter to smooth the data and calculate derivatives on noisy data. The same function computes the corresponding RWC, water potential and VPD for each time step. Residual leaf conductance g_{res} (mmol m^{-2} s^{-1}) was computed for each leaf as the water evaporation rate divided by its driving force (VPD) using equation 3.2:

$$g_{res} = \frac{dw/dt}{M_{H2O}\, A_{leaf}} \times \frac{Patm}{VPD} \qquad (3.2)$$

, where dw/dt is the slope of the mass (g s^{-1}), M_{H2O} is the molecular weight of water (18.01 g mol^{-1}), P_{atm} is the atmospheric pressure in the chamber (*c*. 101.9 kPa) and VPD is the measured vapour pressure deficit of the air inside the chamber (kPa) calculated at each time step. Leaf water potential decreases during drought, and crosses different hydraulics thresholds such as turgor loss point (Ψ_{tlp}), which coincides with stomatal closure (Brodribb *et al.*, 2003), along with Ψ_{P12}, Ψ_{P50} and Ψ_{P88}, corresponding to the water potentials inducing 12%, 50% and 88% losses of conductance, respectively. Recent research has described the variability of g_{res} across leaf dehydration processes, hence promoting the use of water potential thresholds to measure minimum (g_{min}) leaf conductance (Burlett *et al.* 2025). We estimated g_{min} at each relevant threshold described above, to establish a hydraulic trait that could facilitate interpretation and comparison between species. We assume that the physico-chemical properties of the cuticle remain unchanged during measurements, as the short time scale and use of detached leaves do not allow for the biosynthetic changes typically observed during drought. Such changes in wax coverage,

thickness, or composition have been reported to occur in-vivo only after 1 to 15 days following drought initiation (Chen *et al.* 2020). In this context, we assume a constant epidermal and cuticular conductance estimated at Ψ_{P88} in order to have a minimal impact of stomata.

2.3.4. Theoretical leaf conductance model

We used equation (3.3), based on (Ochoa *et al.* 2024), to estimate the theoretical leaf conductance using anatomical properties (Table 3.2).

$$g_{th\ leaf}(\alpha) = \frac{D_{wa}\pi\alpha^2\mu^2 d_U s_U}{V_{ma}(4j + \pi\sqrt{\alpha})(\chi' + \alpha\mu\sqrt{s_U})} + \frac{D_{wa}\pi\alpha^2\mu^2 d_L s_L}{V_{ma}(4j + \pi\sqrt{\alpha})(\chi' + \alpha\mu\sqrt{s_L})} + \left(1 - \frac{\pi}{4}\alpha\mu^2 d_U s_U\right) g_{ec} + \left(1 - \frac{\pi}{4}\alpha\mu^2 d_L s_L\right) g_{ec} \quad (3.3)$$

, where α is the stomatal aperture relative to maximum (circular pore) (unitless), d_U and d_L are stomatal densities (pores m^{-2}), s_U and s_L are stomatal areas (m^{-2}) for adaxial and abaxial surfaces, respectively. χ' is the mean free path in air (the mean distance a gas molecule travels before colliding with another) (m), D_{wa} is the binary diffusivity of water vapour in air ($m^{-2}\ s^{-1}$), V_{ma} is the molar volume of air ($m^3\ mol^{-1}$), μ and j are the dimensionless scaling factors (Table S3.8), g_{ec} is the conductance of the non-stomatal leaf surface area, i.e. of the cuticle conductance (mmol $m^{-2}\ s^{-1}$) estimated using the DLML method at Ψ_{P88} for each species, as it provided g_{min} values with the minimum stomatal impact.

Based on previously formulated assumptions linking the influence of stomatal anatomy on water vapor conductance (Franks & Beerling 2009; Dow *et al.* 2014; Sack & Buckley 2016), this equation allows for variation in stomatal opening, decomposition of conductance between the abaxial and adaxial surfaces, and inclusion of the non-stomatal component in conductance. In order to compare values measured with a porometer, which measures only one surface at a time, we applied the calculation exclusively of the

abaxial surface using equation 3.4. Isolating the lower surface in the calculations was particularly pertinent for *H. annuus* due to its amphistomatous leaves.

$$g_{th\ leaf\ abaxial}(\alpha) = \frac{D_{wa}\pi\alpha^2\mu^{'2}d_L s_L}{V_{ma}(4\,j + \pi\sqrt{\alpha})(\chi' + \alpha\mu\sqrt{s_L})} + \left(1 - \frac{\pi}{4}\alpha\mu^{'2}d_L s_L\right) g_{ec} \qquad (3.4)$$

2.3.5. Assessments of stomatal leakiness using the infiltration method

Stomatal leakiness was assessed on 16 plants of *L. tulipifera* and 15 plants of *H. annuus*. For daily monitoring throughout the experiment, a set of leaves on each plant (seven leaves for *L. tulipifera* and three leaves for *H. annuus*) were marked with a coloured tag on the petiole.

2.3.5.1. Leaf infiltration technique

For each plant, a set of two contiguous leaves with the closest possible characteristics such as age, surface area and at an equivalent dehydration rate, were collected. One leaf was used for the infiltration experiment and the second leaf was used to assess water potential using a pressure chamber. Our system consists of a hermetically sealed cylindrical vacuum chamber containing 5 litres of distilled water. Prior to measurements, water was degassed using a vacuum pump and a magnetic stir plate. The stomatal conductance of the leaf was measured before excision then the leaf was excised using a razor blade, scanned, weighed and and then placed into the water filled vacuum chamber. The infiltration process takes place in three phases (Ranjbaran & Datta 2019). Phase one: pressure reduction from atmospheric pressure to the pump's minimum vacuum (c. -0.8 bars). This creates air bubbles on the surface of the leaf partly from the air in the sub-stomatal cavities. The pressure is reduced linearly for 90 s until at least 90% of the vacuum limit is reached. Phase two: the pressure continues to drop, but at a much slower rate and air continues to escape from the leaves. The aim is to achieve maximum depressurization of the cavities. Phase two lasts 60 s and 98% of the vacuum limit is reached. Phase three: rapid re-pressurization to atmospheric pressure. Leaf cavities that are free of gas and water at a lower pressure are filled with water. Re-pressurization takes place almost instantaneously. Leaf infiltration is determined by the stomata opening, the minimum pressure reached, the contact angle between the liquid and the gas, the surface

tension and the viscosity of the liquid (Schönherr & Bukovac 1972). The Laplace-Young law allows these parameters to be linked (Fry & Walker 1967):

$$\Delta P = \gamma \left(\frac{1}{R_1} + \frac{1}{R_2}\right) 10^{-3} \quad (3.5)$$

, where ΔP is the pressure differential (bar), γ the surface tension of water (dyne cm^{-1}), R_1 and R_2 the radii of curvature of the stomata (cm).

As the stomata geometry can be reduced to an ellipse, the Laplace-young equation can be re-written (Schönherr & Bukovac 1972; Hack 1974):

$$\Delta P = 2\gamma \left(\frac{sin\,(\theta + \xi)}{r}\right) 10^{-3}\ with\ r = \frac{2 * r_1 r_2}{r_1 + r_2} \quad (3.6)$$

, where r_1 and r_2 are the semi minor axis and the semi major axis, θ the contact angle between the fluid and the cell wall (same value for both species fixed at 88°) and ξ the wall angle between the horizontal and the cell wall (estimated from Micro-CT images, with 53° for *L. tulipifera* and 60° for *H. annuus*).

Once the infiltration process was completed, water was removed from the leaves surface before scanning and weighing. Image acquisition was performed using the transmission mode with a bed scanner (V800, Epson, Japan). Image analyses were done with ImageJ (Schneider *et al.* 2012) to estimate the total leaf area (cm^2). The percentage of infiltrated area, relative to the total leaf area, was estimated using a colour thresholding function (Figure S3.1) of the HSB type, followed by a noise reduction function and finally the particle analysis function calculating the infiltrated area (Figure S3.1). The result of an infiltration is a binary classification of leaf area in which the stomata are open or closed (Takanashi *et al.* 2006).

The capability of the system to infiltrate the leaf is verified by equation 3.6 and by the anatomical properties of stomata. r_1 is the semi minor axis and it's the pore aperture (a, m) divided by 2 whereas the major axis r_2 is the length pore *p* (p_U and p_L for the length pore for the upper (adaxial) and lower (abaxial) surface) divided by 2. The maximum area

(m²) corresponds to a circle when $a_{max} = p$. With equation 3.6 we estimated for a specific pressure difference ΔP the minimal percentage pore aperture ($\alpha_{min} = a_{min}/a_{max}$) for adaxial and abaxial surface a_{min} knowing the pore length. Below this value, infiltration is not possible, whereas above it is.

Using the minimal percentage aperture (α_{min}) estimated with equation 3.6 we calculated the theoretical minimum leaf conductance for infiltration.

Theoretical leaf conductance estimated by equations 3.3 and 3.4 assume that stomata over the entire leaf have the same aperture, indicated with the parameter α (percentage aperture to a circular pore). In previous studies, leaf conductance measured locally using infrared gas analyser (IRGA) can vary due to the variation in stomatal aperture and density (Mott & Buckley 1998, 2000). To consider this heterogeneity, we introduced into equation 3.4 a new parameter β, corresponding to the percentage of stomata using the same α:

$$g_{th\ leaf\ abaxial}(\alpha,\beta) = \left(\frac{D_{wa}\pi\alpha^2\mu^{'2}d_L s_L}{V_{ma}(4j+\pi\sqrt{\alpha})(\chi'+\alpha\mu\sqrt{s_L})} + (1-\frac{\pi}{4}\alpha\mu^{'2}d_L s_L)g_{ec}\right)\beta + \left(1-\frac{\pi}{4}\alpha\mu^{'2}d_L s_L\right)g_{ec}(1-\beta) \quad (3.7)$$

In order to estimate all possible values for the theoretical leaf conductance, $g_{th\ leaf\ abaxial}$, we developed a model using equation 3.7 with two nested loops to systematically vary the parameters α and β within the range 0 to 1. Additionally, we evaluate the global stomatal aperture (α) for different measured conditions during drought-induced stomatal closure. To determine this value, we inverted equation 3.7, knowing the $g_{th\ leaf\ abaxial}$ measure via the porometer and the infiltrated area using the infiltrated area as a proxy of β parameter.

2.3.5.2. Assessment of infiltrated areas using Micro CT

X-ray micro-Computed Tomography of *H. annuus* leaves were performed at the PSICHE beamline (King *et al.* 2016) of the SOLEIL synchrotron (Saclay, France) to evaluate if the infiltrated water inside the leaf is only due to open stomata and not by wounds or cracks in the cuticle. Just before the infiltration for each leaf, we measured the

stomatal conductance (g_s) with a porometer (LI-600; LICOR, USA). Infiltrated leaves were preserved between filter paper and tape in order to avoid desiccation during image acquisition. Samples were then placed in an aluminium holder and mounted on the sample stage. We moved the sample on the x-axis several times to obtain a continuum and to visualise a large section of the leaf. We calculated the percentage of infiltrated area on microCT images by using a segmentation method on the 2D images using imageJ and compared it with the g_s before the infiltration.

2.3.6. Dual chlorophyll fluorescence and thermal imaging

Dynamic responses of stomatal conductance (g_s) and quantum efficiency of photosystem II $\left(\Phi_{PSII} = \frac{Fq'}{Fm'}\right)$ at low VPD, corresponding to high relative humidity levels (between 70% and 99%), were assessed using a modified system developed at the University of Essex (McAusland *et al.* 2013). We used the same system configuration and open-top chamber as described in Faralli *et al.* (2024). Throughout the experiment and during each analysis, ambient CO_2 concentration (C_a) was maintained close to 400 $\mu mol_{CO2}\ mol^{-1}$ while the photosynthetic photon flux density (PPFD) was maintained at 500 $\mu mol\ m^{-2}\ s^{-1}$ inside the open-top chamber. The ambient temperature was maintained close to 25°C and was recorded using a temperature sensor. The relative humidity (RH) was regulated by a controlled evaporating mixer unit and measured with an infrared gas analyser (IRGA) (Li- 840, LI-COR, NE, USA). Change in vapour pressure deficit (VPD) was performed by changing the relative humidity into the chamber. A leaf connected to the rest of the plant was placed in the open-top chamber and a paired image (thermal and chlorophyll a fluorescence) was recorded every minute during 10 minutes at low VPD. To visualise the impact of stomatal kinetics on photosynthetic performance, we inhibited photorespiration as a sink for the end product of electron transport by reducing the oxygen concentration to 2% (Murchie & Lawson 2013) (Figure S3.5).

The evaporative cooling effect of transpiration can be used for the estimation of stomatal conductance (g_s). For this reason, gs was estimated following the equations proposed by Leinonen *et al.*, (2006) and Jones *et al.*, (2009) using a dry temperature reference with equation 3.8:

$$\frac{1}{g_s} = r_s = -\frac{\rho c_p r_{HR}[s(T_l - T_a) + D]}{\gamma \rho c_p (T_l - T_{dry})} - r_{aW} \quad (3.8)$$

, where T_l, T_a and T_{dry} were the leaf, air and dry temperature (°C), respectively. T_{dry} corresponded to leaf temperature apex covered with grease. r_{aW} (r_{aW}=0.92.r_H, Jones *et al.*, 2009) was the boundary layer resistance to water vapour (s m^{-1}). r_H is the sensible resistance estimated in our system at 15.38 s m^{-1} (g_H= 0.065 m s^{-1}) and can be assimilated to the boundary layer resistance. ρ was the density of air (kg m^{-3}), c_p was the specific heat capacity of air (J kg^{-1} K^{-1}), s was the slope of the curve relating saturating water vapour pressure to temperature (Pa $°C^{-1}$), γ was the psychrometric constant (Pa K^{-1}), D was the air vapour pressure deficit (Pa) and r_{HR} is the parallel resistance to heat and radiative transfer (s m^{-1}) as calculated with equation 3.9:

$$r_{HR} = \frac{r_H r_R}{r_H + r_R} \text{ and } r_R = \frac{\rho c_p}{4\varepsilon\sigma(T_a + 27.15)^3} \quad (3.9)$$

, where ε is the emissivity (fixed at 0.965) and σ is the Stefan-Boltzmann constant ($5.6703.10^{-8}$ W m^{-2} K^{-4}). Although emissivity changes during leaf dehydration, for convenience we have chosen to use a constant value. g_s is converted in mmol m^{-2} s^{-1} using the perfect gas equation from equation 3.10:

$$\frac{g_s(\,molm^{-2}s^{-1})}{g_s(ms^{-1})} = \frac{P_{atm}}{8.314 * (T_l + 273.15)} \quad (3.10)$$

2.3.7. Data processing and analysis

All data processing and analysis were carried out using RStudio 2022.12.0+353 (R Core Team 2020). To compare data between the different drought classes, a one-way ANOVA with Tukey HSD post hoc test was performed after checking for normality and homogeneity of variance. Non-parametric tests were used, when normality was not reached. Data are expressed as mean ± se. Coefficient of variation is expressed as the ratio of standard deviation to the mean $\left(cv = \frac{sd}{mean}\right)$.

2.4. Results

2.4.1. Dynamics of stomatal conductance (g_s) and minimum leaf conductance (g_{min}) during drought

Maximum stomatal conductance ($g_{s,max}$) of well-watered leaves (before the turgor loss point), was 362.01 ± 52.32 mmol m^{-2} s^{-1} for *Liriodendron tulipifera* and 732.97 ± 51.12 mmol m^{-2} s^{-1} for *Helianthus annuus* (Figure S3.4). After a sharp decline, minimum stomatal conductance ($g_{s,min}$) occurred at water potentials beyond Ψ_{P50}, reaching minimal values. These values correspond to less than 1% of the maximum stomatal conductance ($g_{s,max}$), expressed as relative stomatal conductance ($g_{s,rel}$, %) for the respective species (Figure S3.4).

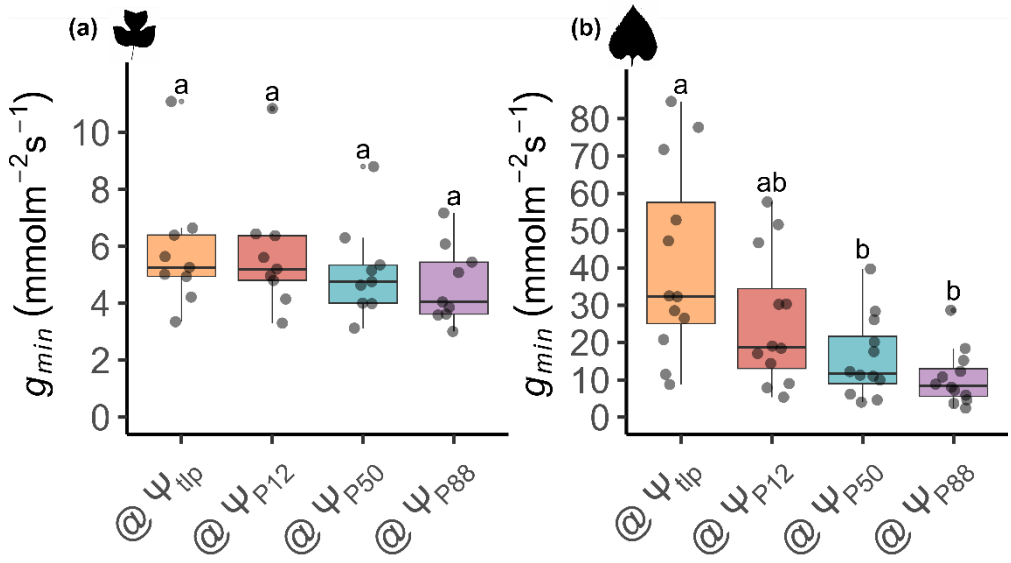

FIGURE 3.1: Minimal leaf conductance at different drought-induced physiological thresholds in *Liriodendron tulipifera* (a) and *Helianthus annuus* (b).
Ψ_{tlp}, Ψ_{12}, Ψ_{50}, Ψ_{88} are the water potentials at turgor loss point, 12%, 50% and 88% losses of stem hydraulic conductance, respectively. Horizontal lines, boxes and bars show the median, quartiles and extreme values, respectively. Grey dots are individual leaves, data points and letters indicate significant differences across different thresholds as indicated with a one-way ANOVA with Tukey HSD post hoc test. Sample size is 9 and 14 for *L. tulipifera* and *H. annuus*, respectively.

For both species, minimum leaf conductance (g_{min}, g_{res} estimated at Ψ_{tlp}, Ψ_{P12}, Ψ_{P50} and Ψ_{P88}) decreased with increasing water stress but no significant differences were observed between the different hydraulic thresholds for *L. tulipifera* (Figure 3.1a). In contrast *H. annuus* (Figure 3.1b), had a significant decrease of g_{min} over the dehydration period, with the lowest g_{min} values found at Ψ_{P88} (Table 3.3). Significant differences in minimum leaf conductance were observed between species during dehydration and for all hydraulic thresholds, with *H. annuus* exhibiting 7-fold higher values at Ψ_{tlp} and 3-fold higher values at Ψ_{P50} compared to *L. tulipifera* (Figure 3.1 and Table 3.3).

TABLE 3.3: Average and standard error of minimum leaf conductance (g_{min}) and coefficient of variation at different drought-induced hydraulic dysfunction thresholds.
Letters indicate significant differences across different thresholds as indicated with a one-way ANOVA with Tukey HSD post hoc test.

	Liriodendron tulipifera		*Helianthus annuus*	
	Mean ± se	Coefficient of variation	Mean ± se	Coefficient of variation
Unit	mmol m^{-2} s^{-1}	-	mmol m^{-2} s^{-1}	-
$g_{min\ @\ tlp}$	5.84 ± 0.74^{a}	0.38	41.3 ± 7.39^{a}	0.62
$g_{min\ @\ P12}$	5.74 ± 0.72^{a}	0.37	25.7 ± 5.14^{ab}	0.70
$g_{min\ @\ P50}$	5.13 ± 0.55^{a}	0.32	15.9 ± 3.15^{b}	0.68
$g_{min\ @\ P88}$	4.66 ± 0.46^{a}	0.29	10.5 ± 2.14^{b}	0.70

2.4.2. Relative contribution of stomatal conductance to g_{min}

Cuticular conductance, estimated using the DLML at Ψ_{P88}, to ensure minimal stomatal impact was 4.66 ± 0.46 mmol m^{-2} s^{-1} for *L. tulipifera* and 10.50 ± 2.14 mmol m^{-2} s^{-1} for *H. annuus.* Assuming a constant cuticular conductance throughout the dehydration process, the stomatal relative contribution ranged from 20.21% at Ψ_{tlp} to 9.16% at Ψ_{P50} for *L. tulipifera*. In contrast, for *H. annuus*, the stomatal relative contribution ranged from 74.58% at Ψ_{tlp} to 33.96% at Ψ_{P50}. At Ψ_{P50}, therefore, the stomatal relative contribution to minimum leaf conductance was 3-fold higher in *H. annuus* than in *L. tulipifera*.

2.4.3. Dynamics of leaf infiltration during drought

We observed similar trends in water infiltration dynamics for both species, characterised by a decrease in the infiltrated area with decreasing Ψ_{leaf} (Figures 3.2; 3.3). The total leaf infiltrated area observed is in reality the sum of unitary infiltrated areas formed by the Bundle Sheath Extension (BSE) network, confirming the heterobaric leaf structure of *Liriodendron tulipifera* and *Helianthus annuus* (Figure S3.2). The relationship between infiltration area and water status followed a four-parameter logistic model (Figure S3.4), with a sharp decrease in infiltration area before Ψ_{tlp} for *L. tulipifera* (Figure 3.3a) with a significant difference between leaves with Ψ_{leaf} higher than Ψ_{tlp} and others classes (inset Figure 3.3a). For *H. annuus* (Figure 3.3b), a sharp decrease in infiltration area occurred close to Ψ_{tlp} with a statistical difference between drought classes (inset Figure 3.3b). The lowest infiltration area was reached before the turgor loss point in *L. tulipifera* (Figure 3.3a) and between Ψ_{tlp} and Ψ_{P12} in *H. annuus* (Figure 3.3b). Under severe dehydration, below Ψ_{P50}, the average total infiltrated area was similar for both species, 9.1 ± 2.3 % in *L. tulipifera* (Figure 3a) and 9.2 ± 2.9 % in *H. annuus* (Figure 3.3b). While post-Ψ_{P50} infiltration areas were equivalent in both species (c. 9%), we observed the highest variability in infiltration surfaces between Ψ_{tlp} and Ψ_{P50} for *H. annuus* (Figure 3.3b).

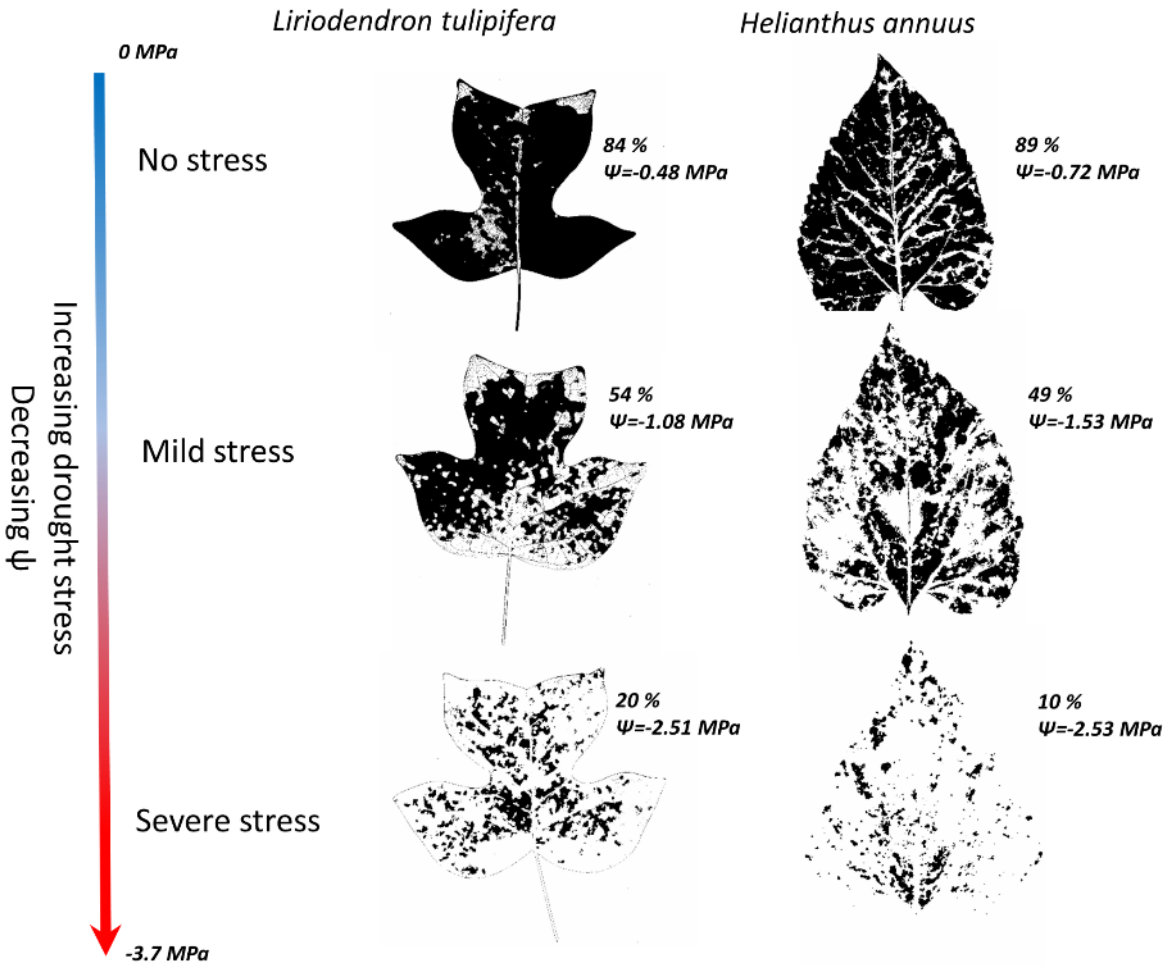

FIGURE 3.2:Infiltrated area along a water stress gradient in *Liriodendron tulipifera* and *Helianthus annuus*. Black areas correspond to the infiltrated area. Percentages indicate the proportion of infiltrated area relative to the total leaf area.

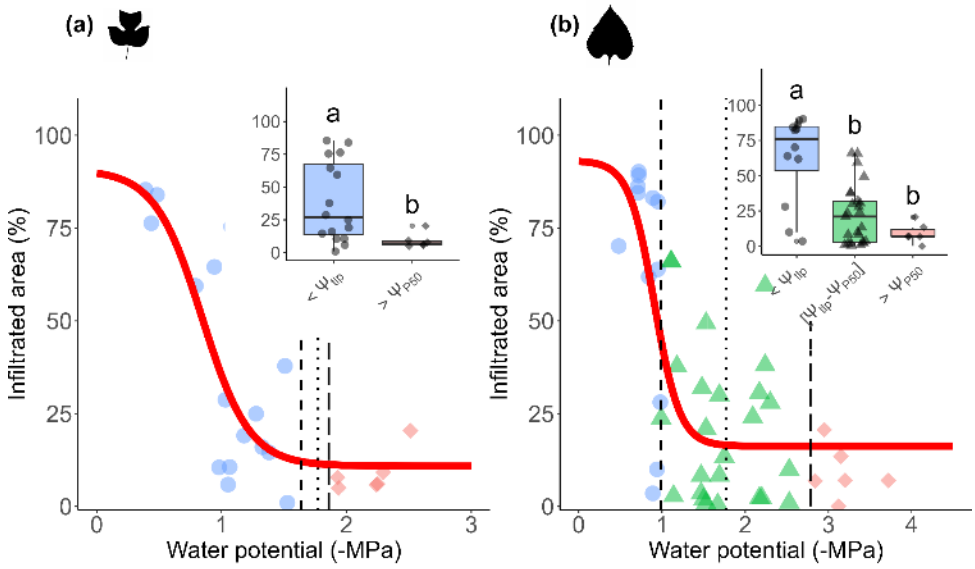

FIGURE 3.3: Leaf infiltration in *Liriodendron tulipifera* (a) and *Helianthus annuus* (b) as a function of water potential.
Dots represent individual leaves. Solid red regression corresponds to the fit according to a logistic model The result fo the fit (solid red line) are available in the TABLE S 3.2. Dashed lines represent Ψ_{tlp} (water potential at tugor loss point) dotted line represent Ψ_{P12} (Water potentials inducing 12% losses of conductance in the stem) and long-dashed lines represent Ψ_{P50} (Water potentials inducing 50% losses of conductance in the stem). Insets: boxplot representations of leaf infiltration by drought stress class. Horizontal lines, boxes and bars show the median, quartiles and extreme values, respectively. letters indicate significant differences across different thresholds as indicated with a one-way ANOVA with Tukey HSD post hoc test. Dots represent individual infiltrated leaves, shapes and colours represent drought stress classes (No stress [0, Ψ_{tlp}]: blue circle; Mild stress [Ψ_{tlp}, Ψ_{P50}]: green triangles and Severe stress [Ψ_{P50}, -Inf]: red diamonds).

Using microCT, we imaged water infiltration inside the mesophyll of four *H. annuus* leaves (Figure 3.4a). A comparison of the percentage of intercellular air spaces between leaves with low (below 50 mmol m^{-2} s^{-1}) and high (above 280 mmol m^{-2} s^{-1}) g_s, measured before infiltration, showed significant differences between both groups (Figure 3.4b). Leaves with low g_s had an average intercellular air area of 24.5 ± 3.3% whereas leaves with high g_s showed an average intercellular air area of 16.2 ± 7.4%, indicating a higher degree of water infiltration. Water infiltrated mainly into air spaces within the spongy mesophyll but importantly zones of the palisade mesophyll were also infiltrated in leaves with high g_s (Figure 3.4a). These observations suggest that leaf infiltration occurs through open stomata and that water infiltrates the mesophyll intercellular air spaces and not only the substomatal cavity (Figure 3.4).

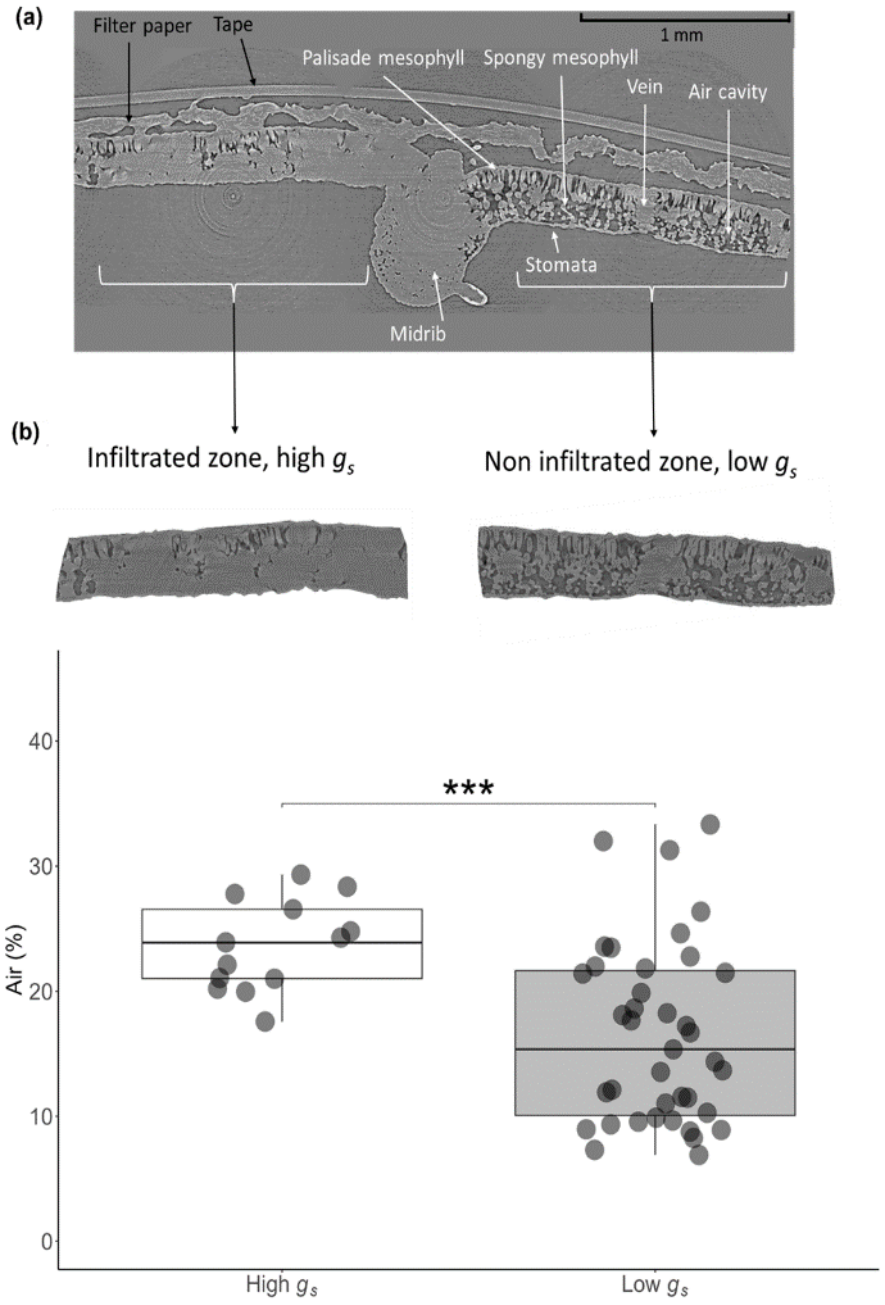

FIGURE 3.4: Water infiltration within *Helianthus annuus* leaf.
(a) micro-CT image showing the full thickness of the leaf after infiltration illustrating a leaf with low and high infiltration in different zones of the leaf. (b) comparison of the intercellular air space after infiltration for different leaves with high and low stomatal conductance. Horizontal lines, boxes and bars show the median, quartiles and extreme values, respectively. The grey dots come from different parts of scans from four different leaves. Significance of Wilcoxon test: ***, *p-value* ≤ 0.001.

2.4.4. Relationship between residual leaf conductance and infiltration area

We found significant positive correlations between residual leaf conductance calculated with the DLML method and infiltration area in both species (Figure 3.5) (r = 0.94; $p < 0.05$ for *L. tulipifera* and $r = 0.97$; $p < 0.0001$ for *H. annuus*). For *L. tulipifera*

(Figure 3.5a), leaves under moderate water stress (water potentials ranging between -2 and -2.5 MPa), with the minimum infiltrated area (7.0 ± 1.1%) had the lowest residual leaf conductance values (4.0 ± 0.2 mmol m^{-2} s^{-1}). We observed an increase of the residual leaf conductance to a maximum value of 9.6 ± 1.4 mmol m^{-2} s^{-1} on well-watered leaves (water potentials ranging between 0 and -0.5 MPa), corresponding to the maximum of infiltration (81.8 ± 2.8%). Moreover, g_{min} values estimated at different hydraulic thresholds on the residual leaf conductance response curve correspond to an area infiltration of less than 20%.

For *H. annuus* (Figure 3.5b), leaves under severe water stress (water potentials ranging between -3.5 and -4 MPa), inducing a minimal value for the residual leaf conductance (6.1 ± 0.9 mmol m^{-2} s^{-1}), showed a minimum infiltrated area of 6.97%. The dynamic of the g_{res} values as a function of the infiltration area is more linear for *H. annuus* with a positive increase to a maximum of 34.6 ± 15.3 mmol m^{-2} s^{-1}, corresponding to a maximum of infiltration area of 70.2% and well-watered leaves (water potentials ranging between 0 and -0.5 MPa). Due to the large range of g_{min} values along the hydraulic thresholds, such g_{min} values are reached at infiltrated area levels ranging from 80% to 20% (Figure 3.5).

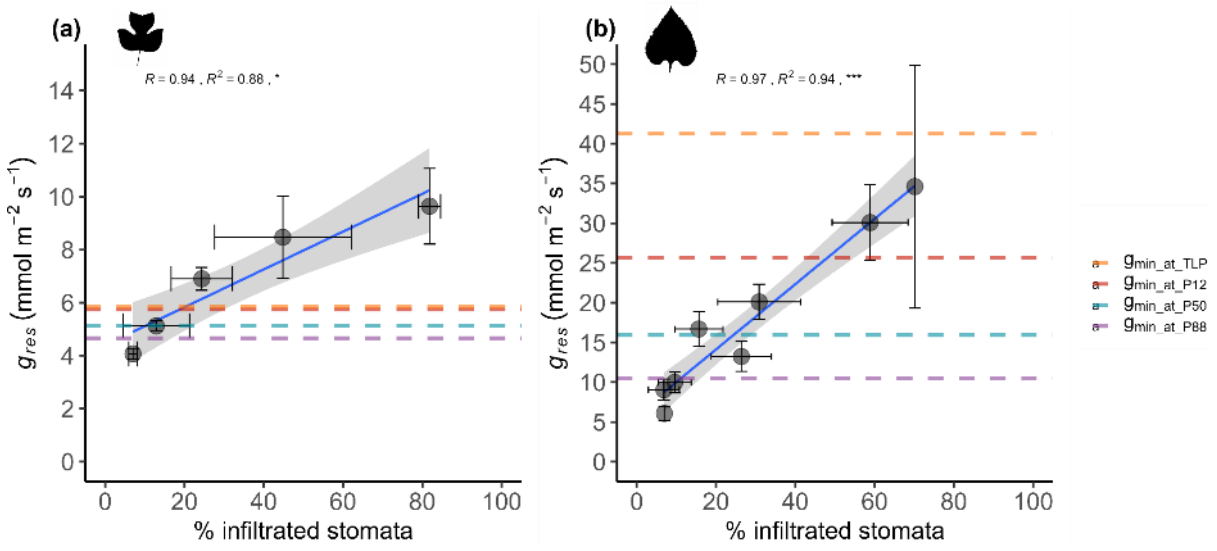

FIGURE 3.5: Residual leaf conductance as a function of percentage of infiltrated leaf area for *L. tulipifera* (a) and *H. annuus* (b).
Dotted lines represent the minimal leaf conductance g_{min} calculated at different hydraulic thresholds. Pearson's correlation for *L. tulipifera* (a): R=0.94; p-value < 0.05 and for *H. annuus* (b): R=0.97; p-value < 0.0001. Error bars for each dot represent the standard error.

2.4.5. Quantification of stomatal closure by thermal and fluorescence imaging

To visualise the impact of stomatal closure in *H. annuus* under varying water conditions the quantum efficiency of photosystem II (Φ_{PSII}) was measured under non-photorespiratory conditions, which was achieved by reducing the surrounding oxygen concentration to 2% (demonstrated in Figure S3.6). During the drought sequence, a spatial decline in Φ_{PSII} was observed, accompanied by the appearance of distinct patches with lower Φ_{PSII} values after the turgor loss point (Figure 3.6a). As water stress progressed beyond the turgor loss point, Φ_{PSII} continued to decline significantly, eventually reaching a plateau after Ψ_{P12} (Figures 3.6b and 3.6c). As the severity of drought increase, up to the Ψ_{P50} threshold, Φ_{PSII} decreased and the size of the patches became smaller and more uniform over the leaf. Additionally, the standard error of Φ_{PSII} (Figure 3.6b) remained low before Ψ_{tlp} but increased significantly between Ψ_{tlp} and Ψ_{P12}, indicating strong variation in Φ_{PSII} between turgor loss and hydraulic dysfunction. Φ_{PSII} increased non-linearly with increasing stomatal conductance (Figure 3.6d), reaching its maximum value at g_s around 245 mmol m^{-2} s^{-1}. At higher g_s, Φ_{PSII} stabilised around 0.52 (Figure 3.6d).

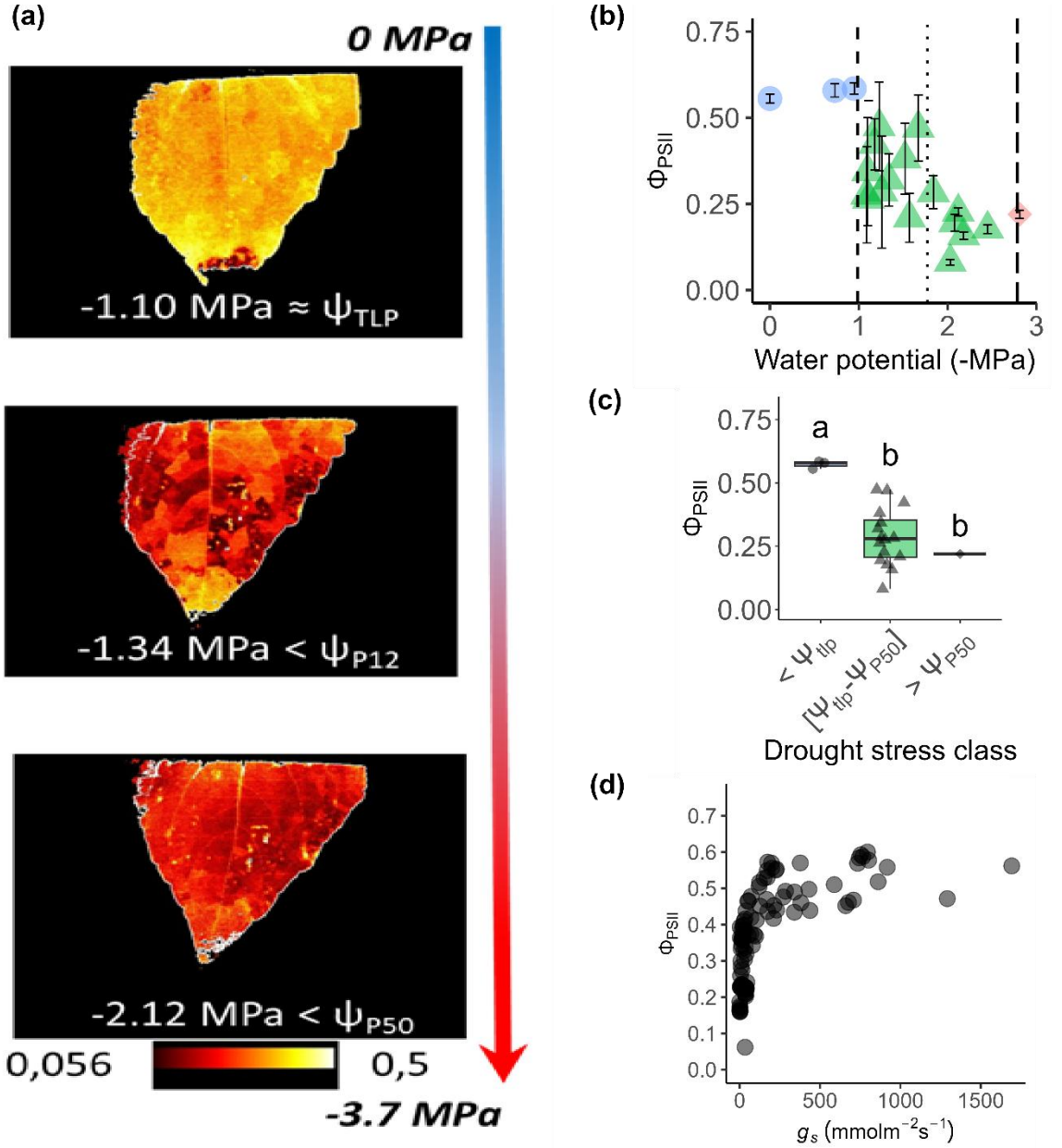

FIGURE 3.6: Quantum efficiency of the photosystem II (Φ_{PSII}) under drought stress in *H. annuus*. Φ_{PSII} images at different water potentials (a).
Φ_{PSII} as a function of water potential (b). Dots represent the mean value of Φ_{PSII} for average leaves and errors bars the standard deviation. The water potential thresholds inducing Ψ_{tlp} (dashed line), Ψ_{12} (dotted line) and Ψ_{P50} (long dashed line) are indicated. Boxplot representation of Φ_{PSII} in different drought stress classes (c). Horizontal lines, boxes and bars show the median, quartiles and extreme values, respectively. Letters indicate significant differences across different thresholds as indicated with a one-way ANOVA with Tukey HSD post hoc test. Dots represent individual leaves, shapes and colours represent drought stress classes (No stress [0, Ψ_{tlp}]: blue circle; Mild stress [Ψ_{tlp}, Ψ_{P50}]: green triangle and Severe stress [Ψ_{P50}, -Inf]: red diamonds). Relationships of quantum efficiency (Φ_{PSII}) and stomatal conductance (g_s) (d).

2.4.6. Leaf theoretical conductance and infiltration

The minimal stomatal pore aperture (α_{min}) required for infiltration is strongly influenced by pressure differentials (around 0.8 bar) and the anatomical characteristics

specific to each species. In our study, α_{min} for *L. tulipifera* was 0.09 (9%) for the abaxial surface only, whereas for *H. annuus,* it was equal to 0.10 (10%) and 0.11 (11%) for the abaxial and the adaxial surfaces, respectively. These minimal pore percentage apertures, applied to equation 3.3, allows us to determine three different minimal leaf theoretical conductance estimations for *H. annuus*, where $g_{th\ leaf,min}$ is the sum of $g_{th\ leaf\ abaxial,min}$ and $g_{th\ leaf\ adaxial,min}$ (Table 3.4). The resulting theoretical $g_{th\ leaf,min}$values at minimal stomatal aperture for infiltration α_{min} were high for both species, indicating that, below this theoretical value, infiltration is not possible.

TABLE 3.4: Theoretical minimum leaf conductance for the abaxial and adaxial surfaces in *H. annuus* and *L. tulipifera* at minimum stomatal aperture for infiltration.

	Liriodendron tulipifera	*Helianthus annuus*
$g_{th\ leaf,min}$ (mmol m^{-2} s^{-1})†	153.72	528.12
$g_{th\ leaf\ abaxial,min}$ (mmol m^{-2} s^{-1})†	149.07	341.40
$g_{th\ leaf\ adaxial,min}$ (mmol m^{-2} s^{-1})†	4.65	186.72

†*Theoretical values were calculated with stomatal anatomical features using equation 3.3.*

We also observed a large difference in both species for $g_{th\ leaf\ abaxial,max}$with *H. annuus* showing a value 2-fold higher than *L. tulipifera* (1011.29 mmol m^{-2} s^{-1} and 2001.72 mmol m^{-2} s^{-1} for *L. tulipifera* and *H. annuus,* respectively), when the parameter α (i.e. the stomatal aperture relative to maximum) is set equal to 1 (Figures 3.7a and 3.7b). These theoretical values are 2.79-fold higher for *L. tulipifera* and 2.73-fold higher for *H. annuus* than $g_{s,max}$, the maximum stomatal conductance measured with a porometer.

Our results show that as α and β increase, the curvature for the same $g_{th\ leaf\ abaxial}$ value decreases. At low $g_{th\ leaf\ adaxial}$ value (close to 100 mmol m^{-2} s^{-1} or below), the interdependence between α and β means that a large number (β >60%) of open stomata with a low aperture (α <20%) can give the same conductance as a smaller number (β <10%) of widely open stomata (α>70%).

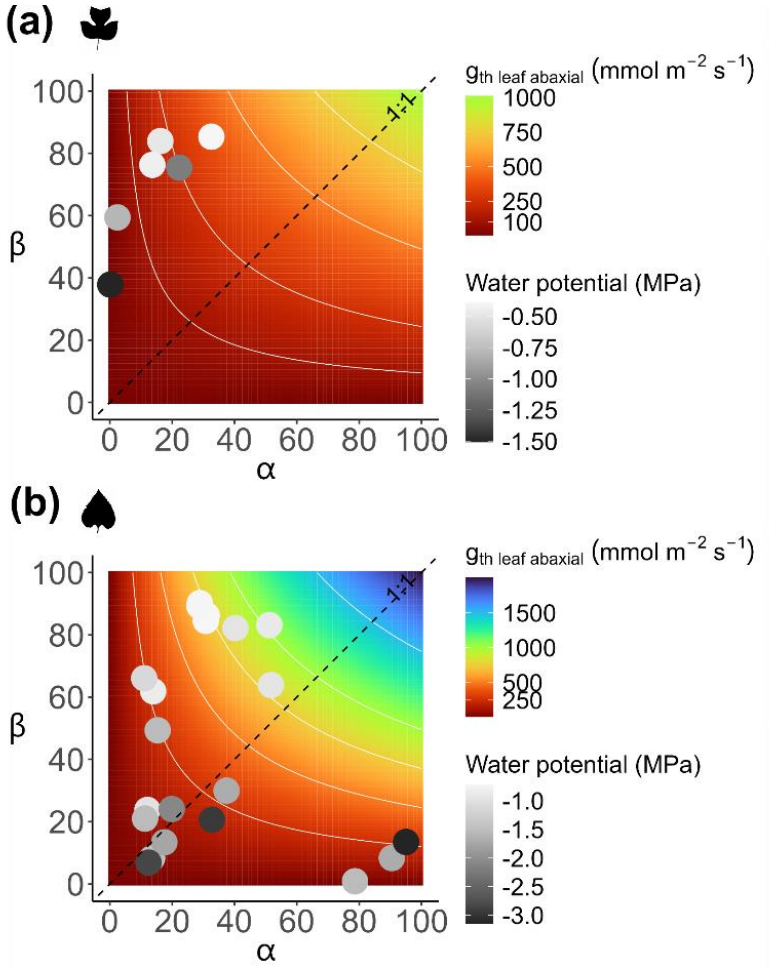

FIGURE 3.7: Theoretical leaf abaxial conductance for multiple combinations of stomatal pore aperture (α) and infiltrated area (β) for *L. tulipifera* (a) and *H. annuus* (b).
Colour map represent constant $g_{th\ leaf,abaxial}$ for various combinations of α and β. White curves represent isolines for theoretical conductance. Dots correspond to individual leaf values from the inversion of equation 3.7 using measured stomatal conductance associated with the infiltrated area to determine the percentage of pore aperture, α. Grey-scale gradient corresponds to the water potential of each of these leaves.

Maximal values of stomatal conductance before infiltration represented by dots (Figures 3.7a and 3.7b) correspond to a large area (β above 60% for both species) with moderate pore apertures for both species (α between 20% and 60%). However, a high pore aperture (α above 70%) is associated with a minimal infiltrated area for *H. annuus* (β below 20%) (Figure 3.7b). We observed a decrease in both surface and stomatal aperture according to the water potential for both species but with a higher variability for *H. annuus* (grey gradient for both species, Figures 3.7a and 3.7b).

2.5. Discussion

Studying stomatal behaviour beyond the turgor loss point is essential for predicting plant responses to extreme drought. Using the detached leaf mass loss (DLML) method and leaf infiltration, our study reveals that stomatal leakiness occurs in both species examined, but not with the same temporal dynamics. Notably, stomatal leakiness was still observed under severe drought conditions (ca. Ψ_{P50}), contributing significantly to residual leaf conductance. An increase in spatial heterogeneity of stomatal closure, particularly beyond the turgor loss point in *H. annuus* and until severe drought conditions (ca. Ψ_{P50}), suggests localised regulation of water loss under stress. Spatial heterogeneity in stomatal aperture was demonstrated by two independent methods, dual-imaging and leaf infiltration, reflecting a spatiotemporal response and a local collective behaviour of stomata. Incorporating heterogeneity in stomatal closure, based on the proportion of infiltrated leaf area, into stomatal conductance models highlights the importance of accounting for both stomatal patchiness and leakiness to improve plant productivity and estimation of plant survival under drought.

2.5.1. Assessing the role of stomatal leakiness in residual water loss during leaf dehydration

2.5.1.1. Minimum leaf conductance along a drought gradient

Like stomatal conductance, minimum leaf conductance (g_{min}) does not remain constant and decreases during dehydration. Across the drought sequence, two contrasting patterns emerged: *L. tulipifera* exhibits rapid stomatal closure immediately after reaching the turgor loss point, followed by stabilisation of minimum leaf conductance (g_{min}). In contrast, *H. annuus* displays a gradual and continuous decline in minimum leaf conductance, indicative of slower stomatal closure. Our findings corroborate recent findings (Burlett *et al.* 2025) highlighting the dynamics of minimal leaf conductance (g_{min}) between a long-lived tree species and an annual crop. Variability in minimum leaf conductance observed at specific hydraulic thresholds, particularly for *H. annuus*, may stem from the wide range of pre-drought initial stomatal conductance values. This phenomenon is especially pronounced in amphistomatous species such as *H. annuus* where high stomatal density increases the potential for conductance variability (Earley *et al.* 2024). Conductance variability at low water potentials could be attributed to changes in osmotic pressure. Indeed, *H. annuus* possesses the capability of an important osmotic adjustment, thereby altering osmotic pressure and providing high plasticity in this species

(Cardoso *et al.* 2018, 2020), whereas in L. tulipifera osmotic adjustment is low (Abrams & Kubiske 1993).

2.5.1.2. Contribution of stomatal leakiness to the residual leaf conductance along a drought gradient

The influence of stomatal leakiness on residual leaf conductance is evident throughout the drought sequence. Under low water potential conditions, a part of this residual conductance can be attributed to incomplete stomatal closure, which contributes to plant dehydration alongside cuticular water loss. Quantifying the magnitude of this leakage is complex due to the small water fluxes involved (Márquez *et al.* 2025). For instance, minimum leaf conductance (g_{min}; accounting both stomatal and cuticular fractions) at Ψ_{P50} represented 1.4% for *L. tulipifera* and 2.2% for *H. annuus* of maximal stomatal conductance. However, despite these low values, our study based on leaf infiltration, indicate that stomata were not fully closed even at water potentials below Ψ_{P50}. Although inherently destructive, the leaf infiltration method proves simple and effective for revealing spatial and temporal stomata contribution to water loss particularly when commercial instruments lack the sensitivity to detect such small water fluxes. However, the leaf infiltration method only reveals whether stomata are open or closed at a specific infiltration pressure, providing a binary result (Lawson *et al.* 1998b). This limits its ability to interpret the degree of stomatal aperture and, by extension, restricts accurate interpretation of stomatal conductance (Lawson *et al.* 1998b; Takanashi *et al.* 2006). Micro-CT imaging confirmed that infiltrated water enters through the stomata, not through cracks or wounds, and reaches beyond the sub-stomatal cavity into the air spaces between mesophyll cells, thus validating the leaf infiltration method. This shows that stomata connect directly to internal mesophyll air spaces, which is key for gas exchange (Baillie & Fleming 2020; Whitewoods 2021). Even at critical low water potentials below Ψ_{P50}, a small proportion of stomata (α_{min} closed to 10 %) remained sufficiently open to allow infiltration. In *L. tulipifera*, cuticular conductance dominates as a major mechanism of water loss during leaf dehydration, consistent with rapid stomatal closure (Figures 3.1 and 3.5). However, this did not eliminate stomatal leakiness, which remained low but persistent throughout the drought sequence. In contrast, in *H. annuus*, stomatal leakiness remained important and consistent throughout dehydration, highlighting a more persistent contribution of stomatal leakiness in residual leaf conductance.

Leaky stomata seem to be widespread across diverse plant clades, as shown in recent studies (Brodribb *et al.* 2016; Machado *et al.* 2021). Leakiness, particularly during drought, may result from the interaction of opposing signals, potentially preventing complete closure of the stomata and leading to leakage. Alternatively, passive dynamic closure controlled exclusively by local water status is also possible but so far this feature is only present in species with highly embolism-resistant xylem (Mercado-Reyes *et al.* 2024), which is not the case for the species investigated in this study. Further mechanisms of incomplete stomatal closure may also be linked to stomatal anatomy as the inability of full closure has been evidenced in Arabidopsis thaliana, another species with kidney-shaped guard cells (Woolfenden *et al.* 2017; Yi *et al.* 2022).

2.5.1.3. The potential of stomatal leakage inclusion into models of drought-induced mortality

Stomatal leakiness constitutes a significant component of minimum leaf conductance. Due to the spatial heterogeneity revealed by leaf infiltration patterns, stomatal leakiness influences the overall water loss dynamics during the dehydration process. This variability at each hydraulic threshold and along the drought sequence should be included into mechanistic soil-plant-atmosphere models such as SurEau (Cochard *et al.* 2020; Ruffault *et al.* 2022) to improve predictions of fatal hydraulic failure risk under extreme drought. This would enable more accurate estimation of the time to hydraulic failure defined as the interval between the turgor loss point and 88% loss of conductance (Urli *et al.* 2013; Li *et al.* 2016) and allow a better estimation of the stomatal margin retention index ($SMRI_{\Psi 50}$) (Petek-Petrik *et al.* 2023) which quantifies the time required to cross the stomatal safety margin (SSM) defined as the difference between water potential at 90% stomatal closure (Ψ_{gs90}) and Ψ_{P12}, Ψ_{P50} and Ψ_{P88} (Creek *et al.* 2020). To improve modelling accuracy, minimum leaf conductance values with standard error estimated at various hydraulic thresholds or residual leaf conductance during dehydration with confidence intervals can be incorporated as functions of time-dependent variables such as water potential, or relative water content (RWC). Using a constant value for the minimum leaf conductance throughout the dehydration process could introduce a significant error such as predicting an early or later time of hydraulic failure (Burlett *et al.* 2025).

2.5.2. Exploring the physiological significance of spatiotemporal heterogeneity in stomatal closure through imaging and modelling

2.5.2.1. Shedding light on stomatal patchiness during drought

Our results highlight that spatial variation in stomatal conductance is strongly influenced by both stomatal pore size and density. This is evident in the heterogeneous distribution of infiltrated surfaces observed at the onset of stress and beyond in both species (Figures 3.2 and 3.6a). These findings suggest that stomatal closure does not occur uniformly but rather in distinct regions, a phenomenon known as stomatal patchiness (Beyschlag *et al.* 1992; Mott *et al.* 1993; Weyers & Lawson 1997; Lawson *et al.* 1998b; Mott & Buckley 1998; Lawson & Weyers 1999; Mott & Peak 2007). These independent patches of closure underline the complex and localised regulation of stomata under stress conditions. Such heterogeneity is clearly captured by both infiltration (Figure 3.2) and quantum efficiency of photosystem II (Φ_{PSII}) at 2% O_2 (Figure 3.7a) (Hofmann *et al.* 2025), shown by the formation of patches of varying sizes at different drought levels. As water stress increases, patch area decreases, resulting in numerous small, irregularly distributed conductive areas/areoles across the leaf surface.

2.5.2.2. Influence of stomatal patchiness and leakiness on leaf water loss during drought

Dual fluorescence and thermal imaging provided complementary insight into stomatal closure dynamics during drought, linking water loss with CO_2 assimilation. Spatial images show heterogeneity in both quantum efficiency of photosystem II (Φ_{PSII}) and transpiration (measured as leaf temperature) across the leaf surface. Notably, Φ_{PSII} offered higher spatial resolution than thermal imaging due to camera resolution. This advantage arises from limitations in thermal imaging precision of the thermal camera and the thermal spread caused by the boundary layer. Moreover, Φ_{PSII}, has been validated as a reliable proxy for detecting stomatal patchiness (Mott *et al.* 1993; Lawson 2009; Kamakura *et al.* 2012; Vialet-Chabrand *et al.* 2024). The observed variability in Φ_{PSII} (Figure 3.6) suggests an inherent trade-off between transpiration (water loss) and CO_2 assimilation (carbon gain), driven by localised differences in stomatal closure. This spatial heterogeneity arises from the physiological phenomenon of stomatal patchiness, where distinct leaf regions exhibit different stomatal apertures; some remain open or leaky to permit minimal CO_2 uptake with water loss, while others remain closed, restricting both

fluxes. Low Φ_{PSII} is due to stomatal closure and rapid consumption of CO_2 with limited vertical and horizontal gas fluxes diffusion (Morison *et al.* 2005; Lawson & Morison 2006).

Patchiness observed on the surface is related to heterogeneous water potential within the leaf (Mott & Buckley 2000). During prolonged drought, this internal water potential heterogeneity becomes more severe, amplifying patchiness. Even after apparent stomatal closure, the persistence of leaky stomata points to a localised trade-off between carbon uptake and water loss through minimum leaf conductance (Machado *et al.* 2021). Higher minimum leaf conductance characterised by smaller and numerous stomata allows a greater assimilation rate and a higher *i*WUE $\left(iWUE = \frac{A}{g_s}\right)$ (Drake *et al.* 2013; Lawson & Vialet-Chabrand 2019) but, especially during prolonged drought, has a negative impact on plant survival (Machado *et al.* 2021). Moreover, this spatiotemporal organisation of stomatal activity along a drought sequence likely plays a crucial role in optimising carbon gain relative to water loss. Gas-exchange measurements especially during drought, can be affected by heterogeneous stomatal behaviour (i.e. stomatal patchiness) across the leaf surface leading to an overestimation of intercellular CO_2 concentration (C_i) which is based on stomatal conductance (g_s) (Mott 1995; Boyer 2015). Indeed, in the Stomatal Network Model (Peak *et al.* 2023) stomatal patchiness is highly correlated to the water use efficiency where patchiness can increase intrinsic water-use efficiency in the short term by concentrating transpiration in open stomatal regions, reducing overall water loss per unit carbon fixed. The variation in stomatal patchiness due to stomatal pore opening over time increases the difficulty of estimating an accurate *i*WUE for the whole leaf. New technologies such as the use of non-destructive hydrogel nanoreporters within the leaf (Jain *et al.* 2021) recently highlighted the significant spatial variability of water potential and its implication within the same leaf (Jain *et al.* 2023).

Stomatal aperture is related to turgor pressure of the guard cells and epidermal cells in a non-linear manner (Franks *et al.* 1998). Depending on the species, epidermal cells play an important role in the relationship and can lead, in some species, to a minimal stomatal aperture above zero, creating water vapor leaks (Franks *et al.* 1998; Franks & Farquhar 2007). We can hypothesise that during drought, a reduction in turgor pressure within epidermal cells diminishes their mechanical influence or back pressure on stomatal closure, leading to stomatal leakage (Buckley 2019). Further studies linking water potential variability within a leaf with Φ_{PSII} at low oxygen level coupled with thermal

imaging would be helpful to better understand the trade-off between water loss and CO_2 assimilation (Hofmann *et al.* 2025).

2.5.2.3. Modelling the spatiality of theoretical leaf conductance

Implementing stomatal patchy behaviour into models is possible using statistical approaches (Takanashi *et al.*, 2006) or using a spatially explicit approach (Haefner *et al.*, 1997). Models based on spatially connected networks (Mott & Peak 2007) and cellular automata suggest an emergent phenomenon (Peak *et al.* 2023) and explore new ways to understand how stomatal coordination influences gas exchange and water use efficiency. Although leaf infiltration highlights spatial heterogeneity and stomatal patchiness, its binary nature and high variability complicate both interpretation and quantification, making it difficult to incorporate reliably into leaf-scale modelling frameworks. Chlorophyll fluorescence imaging, on the other hand, is a more precise method, providing the same kind of pattern but with a gradient rather than a binary result (Figure 3.2 and 3.6). A recent model (Ochoa *et al.* 2024) for estimating theoretical leaf conductance considers variation in pore opening but not their spatial repartition. In fact, the theoretical minimum leaf conductance for infiltration, estimated using a_{min} in equation 3.3, is expected to allow infiltration only above this threshold. However, our measurements showed that infiltration can occur even at stomatal conductance values lower than the one predicted by the model (cf. a_{min} in equation 3.3). Since infiltration occurs at stomatal conductance levels lower than those predicted by theoretical minimum leaf conductance, theoretical values are overestimated due to the omission of spatial heterogeneity in stomatal aperture. Chlorophyll fluorescence imaging in contrast to infiltration provides a promising venue for visualising spatial variability and represents a step toward developing models that explicitly incorporate stomatal heterogeneity.

2.6. Conclusion

Located at the interface between plant and atmosphere, stomata are key regulators of gas exchange under both optimal and drought conditions. Our study demonstrates that stomatal leakiness plays a pivotal role in determining minimum leaf conductance. Our results provide clear evidence of both the presence and persistence of leaky stomata throughout the drought sequence, even beyond Ψ_{P50}, for both species underscoring the critical influence of stomatal closure on minimum leaf conductance. By

combining spatial techniques such as leaf infiltration, chlorophyll fluorescence and thermal imaging, we gain valuable insight into the spatial heterogeneity of stomatal closure. These approaches reveal patchy stomatal patterns that evolve with drought stress intensity. Incorporating spatial heterogeneity and leakiness into mechanistic models might significantly improve the accuracy of predicting the time to hydraulic failure. Finally, our findings not only highlight the physiological relevance of stomatal leakiness during drought but also emphasise the need to account for these dynamics to better understand plant adaptation in the context of increasingly frequent and intense drought conditions driven by climate change.

Author contributions

GF, RB and ST, contributed to the design of the infiltration experiment; GF, TL, RB contributed to the design of the dual imaging experiment; GF performed data collection, analysis and the interpretation of the results; GF wrote the manuscript with help from all authors.

Conflict of interest

The authors declare no conflict of interest.

Funding

This study received financial support from the French government in the framework of the IdEX Bordeaux University "Investments for the Future" program / GPR Bordeaux Plant Sciences. TL acknowledges the following BBSRC funding BB/T0042741/1; BB/S005080/1; BB/Y000722/1 T.L. was supported by a Royal Society Leverhulme Trusts Senior Research Fellowship (SF/R1/231041).

Acknowledgements

We would like to thank the Phenobois platform team and particularly Gaëlle Capdeville who conducted xylem embolism resistance experiments and Daniela NDo for her help in the anatomical measurements. We thank Dr Phil Davey for the technical assistance for the dual imaging experiment at the university of Essex. We thank Dr Andrew King for assistance during measurements at the PSICHÉ beamline of the SOLEIL synchrotron.

2.7. References

Abrams M.D. & Kubiske M.E. (1993) Synchronous changes in tissue water parameters of mature foliage from well-watered and periodically droughted tree seedlings.

Adams H.D., Zeppel M.J.B., Anderegg W.R.L., Hartmann H., Landhäusser S.M., Tissue D.T., … McDowell N.G. (2017) A multi-species synthesis of physiological mechanisms in drought-induced tree mortality. *Nature Ecology & Evolution* 1, 1285–1291.

Alvim P.D.T. & Havis J.R. (1954) An Improved Infiltration Series for Studying Stomatal Opening as Illustrated with Coffee. *Plant Physiology* 29, 97–98.

Anderegg W.R.L., Hicke J.A., Fisher R.A., Allen C.D., Aukema J., Bentz B., … Zeppel M. (2015) Tree mortality from drought, insects, and their interactions in a changing climate. *New Phytologist* 208, 674–683.

Baillie A.L. & Fleming A.J. (2020) The developmental relationship between stomata and mesophyll airspace. *New Phytologist* 225, 1120–1126.

Beyschlag W., Pfanz H. & Ryel RonaldJ. (1992) Stomatal patchiness in Mediterranean evergreen sclerophylls: Phenomenology and consequences for the interpretation of the midday depression in photosynthesis and transpiration. *Planta* 187.

Billon L.M., Blackman C.J., Cochard H., Badel E., Hitmi A., Cartailler J., … Torres-Ruiz J.M. (2020) The DroughtBox: A new tool for phenotyping residual branch conductance and its temperature dependence during drought. *Plant, Cell & Environment* 43, 1584–1594.

Boyer J.S. (2015) Impact of cuticle on calculations of the CO2 concentration inside leaves. *Planta* 242, 1405–1412.

Brodribb T.J., Bienaimé D. & Marmottant P. (2016) Revealing catastrophic failure of leaf networks under stress. *Proceedings of the National Academy of Sciences* 113, 4865–4869.

Brodribb T.J. & Holbrook N.M. (2003) Stomatal Closure during Leaf Dehydration, Correlation with Other Leaf Physiological Traits. *Plant Physiology* 132, 2166–2173.

Brodribb T.J., McAdam S.A.M., Jordan G.J. & Martins S.C.V. (2014) Conifer species adapt to low-rainfall climates by following one of two divergent pathways. *Proceedings of the National Academy of Sciences* 111, 14489–14493.

Buckley T.N. (2019) How do stomata respond to water status? *New Phytologist* 224, 21–36.

Burghardt M. (2003) Ecophysiological relevance of cuticular transpiration of deciduous and evergreen plants in relation to stomatal closure and leaf water potential. *Journal of Experimental Botany* 54, 1941–1949.

Burlett R., Parise C., Capdeville G., Cochard H., Lamarque L.J., King A. & Delzon S. (2022) Measuring xylem hydraulic vulnerability for long-vessel species: an improved methodology with the flow centrifugation technique. *Annals of Forest Science* 79, 5.

Burlett R., Trueba S., Bouteiller X.P., Forget G., Torres-Ruiz M., Martin-StPaul N.K., … Delzon S. (2025) Minimum leaf conductance during drought: unravelling its variability and impact on plant survival. *New Phytologist*.

Cardoso A.A., Brodribb T.J., Kane C.N., DaMatta F.M. & McAdam S.A.M. (2020) Osmotic adjustment and hormonal regulation of stomatal responses to vapour pressure deficit in sunflower. *AoB PLANTS* 12, plaa025.

Cardoso A.A., Brodribb T.J., Lucani C.J., DaMatta F.M. & McAdam S.A.M. (2018) Coordinated plasticity maintains hydraulic safety in sunflower leaves. *Plant, Cell & Environment* 41, 2567–2576.

Chen M., Zhu X., Zhang Y., Du Z., Chen X., Kong X., … Chen C. (2020) Drought stress

modify cuticle of tender tea leaf and mature leaf for transpiration barrier enhancement through common and distinct modes. *Scientific Reports* 10, 6696.

Choat B., Brodribb T.J., Brodersen C.R., Duursma R.A., López R. & Medlyn B.E. (2018) Triggers of tree mortality under drought. *Nature* 558, 531–539.

Choat B., Jansen S., Brodribb T.J., Cochard H., Delzon S., Bhaskar R., … Zanne A.E. (2012) Global convergence in the vulnerability of forests to drought. *Nature* 491, 752–755.

Cochard H. (2002) A technique for measuring xylem hydraulic conductance under high negative pressures. *Plant, Cell & Environment* 25, 815–819.

Cochard H., Pimont F., Ruffault J. & Martin-StPaul N. (2020) SurEau *.c : a mechanistic model of plant water relations under extreme drought*. Plant Biology.

Creek D., Lamarque L.J., Torres-Ruiz J.M., Parise C., Burlett R., Tissue D.T. & Delzon S. (2020) Xylem embolism in leaves does not occur with open stomata: evidence from direct observations using the optical visualization technique. *Journal of Experimental Botany* 71, 1151–1159.

Dow G.J., Bergmann D.C. & Berry J.A. (2014) An integrated model of stomatal development and leaf physiology. *New Phytologist* 201, 1218–1226.

Drake J.E., Tjoelker M.G., Vårhammar A., Medlyn B.E., Reich P.B., Leigh A., … Barton C.V.M. (2018) Trees tolerate an extreme heatwave via sustained transpirational cooling and increased leaf thermal tolerance. *Global Change Biology* 24, 2390–2402.

Drake P.L., Froend R.H. & Franks P.J. (2013) Smaller, faster stomata: scaling of stomatal size, rate of response, and stomatal conductance. *Journal of Experimental Botany* 64, 495–505.

Duursma R.A., Blackman C.J., Lopéz R., Martin-StPaul N.K., Cochard H. & Medlyn B.E. (2019) On the minimum leaf conductance: its role in models of plant water use, and ecological and environmental controls. *New Phytologist* 221, 693–705.

Earley A.M., Nolting K.M., Donovan L.A. & Burke J.M. (2024) Trait variation and performance across varying levels of drought stress in cultivated sunflower (*Helianthus annuus* L.). *AoB PLANTS* 16, plae031.

Faralli M., Mellers G., Wall S., Vialet-Chabrand S., Forget G., Galle A., … Lawson T. (2024) Exploring natural genetic diversity in a bread wheat multi-founder population: Dual imaging of photosynthesis and stomatal kinetics. *Journal of Experimental Botany*, erae233.

Flexas J. (2002) Drought-inhibition of Photosynthesis in C3 Plants: Stomatal and Non-stomatal Limitations Revisited. *Annals of Botany* 89, 183–189.

Franks P.J. & Beerling D.J. (2009) Maximum leaf conductance driven by CO_2 effects on stomatal size and density over geologic time. *Proceedings of the National Academy of Sciences* 106, 10343–10347.

Franks P.J., Cowan 1 2 I. R. & Farquhar G.D. (1998) A study of stomatal mechanics using the cell pressure probe. *Plant, Cell and Environment* 21, 94–100.

Franks P.J. & Farquhar G.D. (2007) The Mechanical Diversity of Stomata and Its Significance in Gas-Exchange Control. *Plant Physiology* 143, 78–87.

Fry K.E. & Walker R.B. (1967) A Pressure-Infiltration Method for Estimating Stomatal opening in Conifers. *Ecology* 48, 155–157.

Hack H.R.B. (1974) The Selection of an Infiltration Technique for Estimating the Degree of Stomatal Opening in Leaves of Field Crops in the Sudan and a Discussion of the Mechanism which Controls the Entry of Test Liquids. *Annals of Botany* 38, 93–114.

Haefner J.W., Buckley T.N. & Mott K.A. (1997) A spatially explicit model of patchy stomatal responses to humidity. *Plant, Cell and Environment* 20, 1087–1097.

Hofmann T.A., Atkinson W., Fan M., Simkin A.J., Jindal P. & Lawson T. (2025) Impact of climate-driven changes in temperature on stomatal anatomy and physiology. *Philosophical Transactions of the Royal Society B: Biological Sciences* 380.

IPCC (2023) *Climate Change 2021 – The Physical Science Basis: Working Group I Contribution to the Sixth Assessment Report of the Intergovernmental Panel on Climate Change*, 1st ed. Cambridge University Press.

Jain P., Huber A.E., Rockwell F.E., Sen S., Holbrook N.M. & Stroock A.D. (2023) Localized measurements of water potential reveal large loss of conductance in living tissues of maize leaves.

Jain P., Liu W., Zhu S., Chang C.Y.-Y., Melkonian J., Rockwell F.E., … Stroock A.D. (2021) A minimally disruptive method for measuring water potential in planta using hydrogel nanoreporters. *Proceedings of the National Academy of Sciences* 118, e2008276118.

Jones H.G., Serraj R., Loveys B.R., Xiong L., Wheaton A. & Price A.H. (2009) Thermal infrared imaging of crop canopies for the remote diagnosis and quantification of plant responses to water stress in the field. *Functional Plant Biology* 36, 978.

Kamakura M., Kosugi Y., Takanashi S., Tobita H., Uemura A. & Utsugi H. (2012) Observation of the scale of patchy stomatal behavior in leaves of Quercus crispula using an Imaging-PAM chlorophyll fluorometer. *Tree Physiology* 32, 839–846.

Kane C.N., Jordan G.J., Jansen S. & McAdam S.A.M. (2020) A Permeable Cuticle, Not Open Stomata, Is the Primary Source of Water Loss From Expanding Leaves. *Frontiers in Plant Science* 11, 774.

Kerstiens G. (1996) Cuticular water permeability and its physiological significance. *Journal of Experimental Botany* 47, 1813–1832.

King A., Guignot N., Zerbino P., Boulard E., Desjardins K., Bordessoule M., … Itié J.-P. (2016) Tomography and imaging at the PSICHE beam line of the SOLEIL synchrotron. *Review of Scientific Instruments* 87, 093704.

Lawson T. (2009) Guard cell photosynthesis and stomatal function. *New Phytologist* 181, 13–34.

Lawson T. & Blatt M.R. (2014) Stomatal Size, Speed, and Responsiveness Impact on Photosynthesis and Water Use Efficiency. *Plant Physiology* 164, 1556–1570.

Lawson T., James W. & Weyers J. (1998a) A surrogate measure of stomatal aperture. *Journal of Experimental Botany* 49, 1397–1403.

Lawson T. & Matthews J. (2020) Guard Cell Metabolism and Stomatal Function. *Annual Review of Plant Biology* 71, 273–302.

Lawson T. & Morison J. (2006) Visualising patterns of CO_2 diffusion in leaves. *New Phytologist* 169, 641–643.

Lawson T., Simkin A.J., Kelly G. & Granot D. (2014) Mesophyll photosynthesis and guard cell metabolism impacts on stomatal behaviour. *New Phytologist* 203, 1064–1081.

Lawson T. & Vialet-Chabrand S. (2019) Speedy stomata, photosynthesis and plant water use efficiency. *New Phytologist* 221, 93–98.

Lawson T. & Weyers J. (1999) Spatial and temporal variation in gas exchange over the lower surface of Phaseolus vulgaris L. primary leaves. *Journal of Experimental Botany* 50, 1381–1391.

Lawson T., Weyers J. & A'Brook R. (1998b) The nature of heterogeneity in the stomatal behaviour of Phaseolus vulgaris L. primary leaves. 9.

Leinonen I., Grant O.M., Tagliavia C.P.P., Chaves M.M. & Jones H.G. (2006) Estimating stomatal conductance with thermal imagery. *Plant, Cell and Environment* 29, 1508–1518.

Li S., Feifel M., Karimi Z., Schuldt B., Choat B. & Jansen S. (2016) Leaf gas exchange performance and the lethal water potential of five European species during

drought. *Tree Physiology*, tpv117.
Machado R., Loram-Lourenço L., Farnese F.S., Alves R.D.F.B., Sousa L.F., Silva F.G., … Menezes-Silva P.E. (2021) Where do leaf water leaks come from? Trade-offs underlying the variability in minimum conductance across tropical savanna species with contrasting growth strategies. *New Phytologist* 229, 1415–1430.
Marenco R.A., Siebke K., Farquhar G.D. & Ball M.C. (2006) Hydraulically based stomatal oscillations and stomatal patchiness in Gossypium hirsutum. *Functional Plant Biology* 33, 1103.
Márquez D.A., Gardner, Anna & Busch, Florian (2025) Navigating Challenges in Interpreting Plant Physiology Responses through Gas Exchange Results in Stressed Plants.
McAusland L., Davey P.A., Kanwal N., Baker N.R. & Lawson T. (2013) A novel system for spatial and temporal imaging of intrinsic plant water use efficiency. *Journal of Experimental Botany* 64, 4993–5007.
McElwain J.C., Yiotis C. & Lawson T. (2016) Using modern plant trait relationships between observed and theoretical maximum stomatal conductance and vein density to examine patterns of plant macroevolution. *New Phytologist* 209, 94–103.
Mercado-Reyes J.A., Pereira T.S., Manandhar A., Rimer I.M. & McAdam S.A.M. (2024) Extreme drought can deactivate ABA biosynthesis in embolism-resistant species. *Plant, Cell & Environment* 47, 497–510.
Mirasole F.M., Nastasi S.P., Cubero-Font P. & De Angeli A. (2023) Vacuolar control of stomatal opening revealed by 3D imaging of the guard cells. *Scientific Reports* 13, 7647.
Morison J.I.L., Gallouët E., Lawson T., Cornic G., Herbin R. & Baker N.R. (2005) Lateral Diffusion of CO2 in Leaves Is Not Sufficient to Support Photosynthesis. *Plant Physiology* 139, 254–266.
Mott K.A. (1995) Effects of patchy stomatal closure on gas exchange measurements following abscisic acid treatment. *Plant, Cell & Environment* 18, 1291–1300.
Mott K.A. & Buckley T.N. (1998) Stomatal heterogeneity. *Journal of Experimental Botany* 49, 407–417.
Mott K.A. & Buckley T.N. (2000) Patchy stomatal conductance: emergent collective behaviour of stomata. *Trends in Plant Science* 5, 258–262.
Mott K.A., Cardon Z.G. & Berry J.A. (1993) Asymmetric patchy stomatal closure for the two surfaces of *Xanthium strumarium* L. leaves at low humidity. *Plant, Cell & Environment* 16, 25–34.
Mott K.A. & Peak D. (2007) Stomatal Patchiness and Task-performing Networks. *Annals of Botany* 99, 219–226.
Murchie E.H. & Lawson T. (2013) Chlorophyll fluorescence analysis: a guide to good practice and understanding some new applications. *Journal of Experimental Botany* 64, 3983–3998.
Ochoa M.E., Henry C., John G.P., Medeiros C.D., Pan R., Scoffoni C., … Sack L. (2024) Pinpointing the causal influences of stomatal anatomy and behavior on minimum, operational, and maximum leaf surface conductance. *Plant Physiology*, kiae292.
Peak D., Hogan M.T. & Mott K.A. (2023) Stomatal patchiness and cellular computing. *Proceedings of the National Academy of Sciences* 120, e2220270120.
Petek-Petrik A., Petrík P., Lamarque L.J., Cochard H., Burlett R. & Delzon S. (2023) Drought survival in conifer species is related to the time required to cross the stomatal safety margin. *Journal of Experimental Botany* 74, 6847–6859.
Photosynthesis and Stomatal Behaviour (2010) *Progress in Botany*, 265–304.
Pörtner H.-O. & Roberts D.C. (2022) Climate Change 2022: Impacts, Adaptation and

Vulnerability. 3068.
R Core Team (2020) R Core Team (2020) R: A Language and Environment for Statistical Computing. R Foundation for Statistical Computing, Vienna, Austria. https://www.r-project.org/.
Ranjbaran M. & Datta A.K. (2019) Pressure-driven infiltration of water and bacteria into plant leaves during vacuum cooling: A mechanistic model. *Journal of Food Engineering* 246, 209–223.
Riederer M. & Schreiber L. (2001) Protecting against water loss: analysis of the barrier properties of plant cuticles. *Journal of Experimental Botany* 52, 2023–2032.
Ruffault J., Pimont F., Cochard H., Dupuy J.-L. & Martin-StPaul N. (2022) SurEau-Ecos v2.0: a trait-based plant hydraulics model for simulations of plant water status and drought-induced mortality at the ecosystem level. *Geoscientific Model Development* 15, 5593–5626.
Sack L. & Buckley T.N. (2016) The Developmental Basis of Stomatal Density and Flux. *Plant Physiology* 171, 2358–2363.
Sack, Pasquet-Kok & Megan Bartlett (2011) Leaf pressure-volume curve parameters.
Šantrůček J., Šimáňová E., Karbulková J., Šimková M. & Schreiber L. (2004) A new technique for measurement of water permeability of stomatous cuticular membranes isolated from Hedera helix leaves. *Journal of Experimental Botany* 55, 1411–1422.
Schneider C.A., Rasband W.S. & Eliceiri K.W. (2012) NIH Image to ImageJ: 25 years of image analysis. *Nature Methods* 9, 671–675.
Schönherr J. & Bukovac M.J. (1972) Penetration of Stomata by Liquids: Dependence on Surface Tension, Wettability, and Stomatal Morphology. *Plant Physiology* 49, 813–819.
Schreiber L. & Riederer M. (1996) Ecophysiology of cuticular transpiration: comparative investigation of cuticular water permeability of plant species from different habitats. *Oecologia* 107, 426–432.
Stinziano J.R., Tominaga J & Hanson DT (2020) Where in the leaf is intercellular CO2 (Ci)? Considerations and recommendations 1 for assessing gaseous diffusion in leaves.
Takanashi S., Kosugi Y., Matsuo N., Tani M. & Ohte N. (2006) Patchy stomatal behavior in broad-leaved trees grown in different habitats. *Tree Physiology* 26, 1565–1578.
Tredenick E.C. & Farquhar G.D. (2021) Publisher Correction: Dynamics of moisture diffusion and adsorption in plant cuticles including the role of cellulose. *Nature Communications* 12, 5830.
Urli M., Porte A.J., Cochard H., Guengant Y., Burlett R. & Delzon S. (2013) Xylem embolism threshold for catastrophic hydraulic failure in angiosperm trees. *Tree Physiology* 33, 672–683.
Vialet-Chabrand S. & Lawson T. (2019) Dynamic leaf energy balance: deriving stomatal conductance from thermal imaging in a dynamic environment. *Journal of Experimental Botany* 70, 2839–2855.
Vialet-Chabrand S. & Lawson T. (2020) Thermography methods to assess stomatal behaviour in a dynamic environment. *Journal of Experimental Botany* 71, 2329–2338.
Vialet-Chabrand S., Matsubara S. & Lawson T. (2024) Editorial: Dynamic photosynthesis under non-steady conditions. *Frontiers in Plant Science* 15.
Weyers J.D.B. & Lawson T. (1997) Heterogeneity in Stomatal Characteristics. In *Advances in Botanical Research*. pp. 317–352. Elsevier.
Whitewoods C.D. (2021) Riddled with holes: Understanding air space formation in plant leaves. *PLOS Biology* 19, e3001475.

Woolfenden H.C., Bourdais G., Kopischke M., Miedes E., Molina A., Robatzek S. & Morris R.J. (2017) A computational approach for inferring the cell wall properties that govern guard cell dynamics. *The Plant Journal* 92, 5–18.

Yi H., Chen Y. & Anderson C.T. (2022) Turgor pressure change in stomatal guard cells arises from interactions between water influx and mechanical responses of their cell walls. *Quantitative Plant Biology* 3, e12.

2.8. Supporting information

The following Supporting Information is available for this article:

FIGURE S3.1: Sequence to estimate infiltrated area using ImageJ

FIGURE S3.2: Infiltration pattern

FIGURE S3.3: Relationships of infiltrated area (Φ_{PSII}) and stomatal conductance (g_s)

FIGURE S3.4: Relative value of leaf infiltration and stomatal conductance as a function of water potential

FIGURE S3.5: Same leaf under the same environmental conditions except oxygen concentration in the air flow with (a) 21% and (b) 2%.

TABLE S3.6: Two-parameter model results for *L. tulipifera* and *H. annuus*

TABLE S3.7: For-parameter logistic model results for *L. tulipifera* and *H. annuus*

TABLE S3.8: Constant used for the theoretical leaf conductance for both species

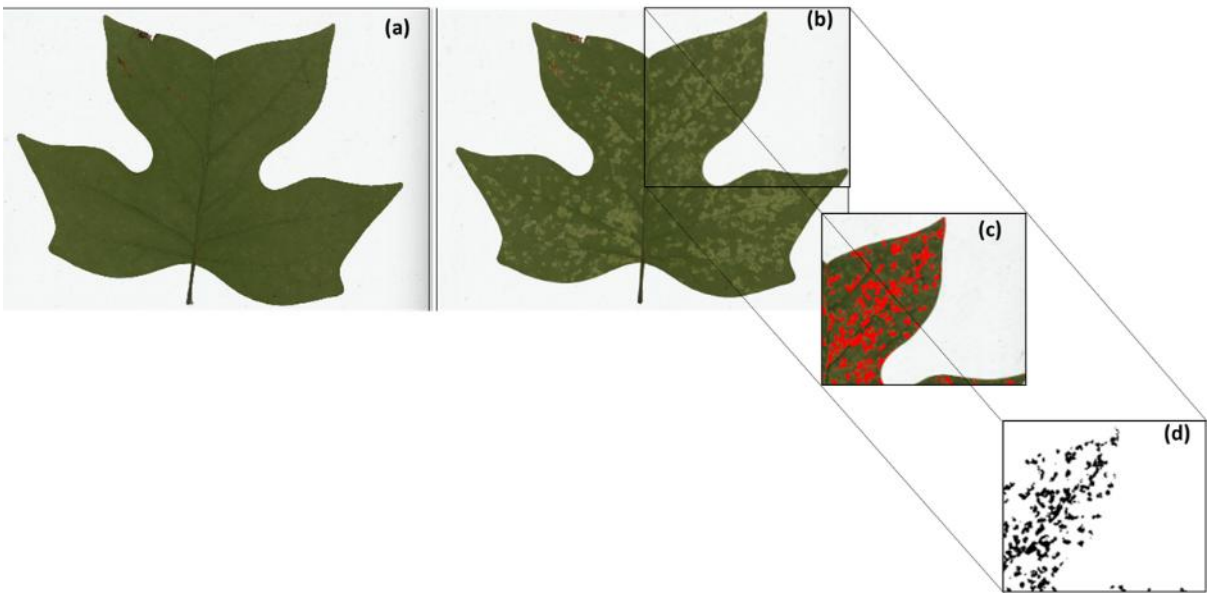

FIGURE S 3.1: Sequence to estimate infiltrated area using ImageJ (example on Tulip tree's leaf.
(a) is non-infiltrated leaf, (b) is the infiltrated leaf, (c) is the thresholding with only infiltrated area (shown only here in the part of the leaf) and (d) is a binary image from thresholding used with the particle analysis function in ImageJ to estimate the relative infiltrated area.

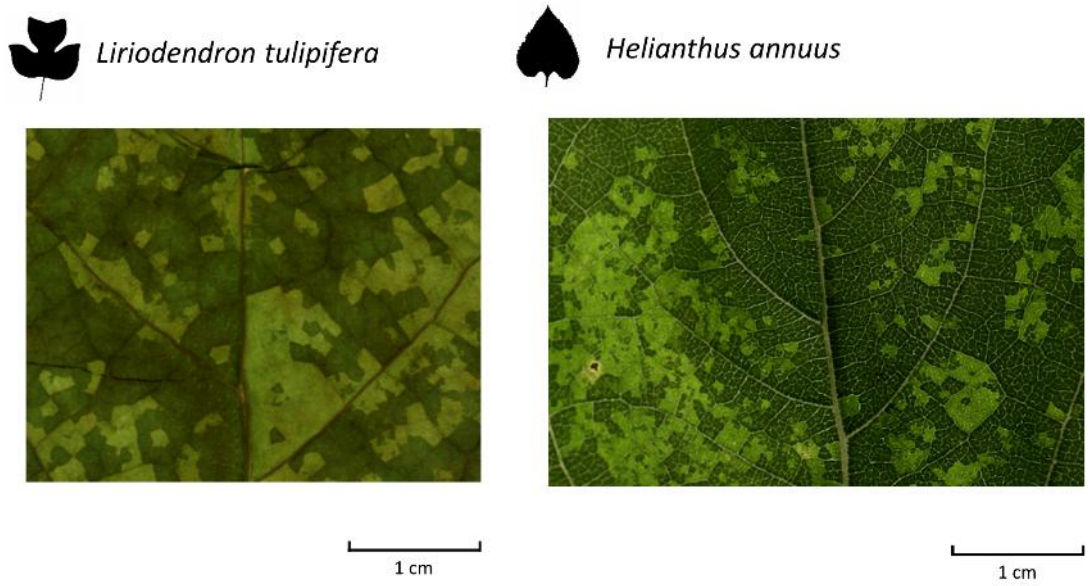

FIGURE S 3.2: Infiltration pattern for *L. tulipifera* (leaf) and *H. annuus* (right). Light green represents the infiltrated zone.

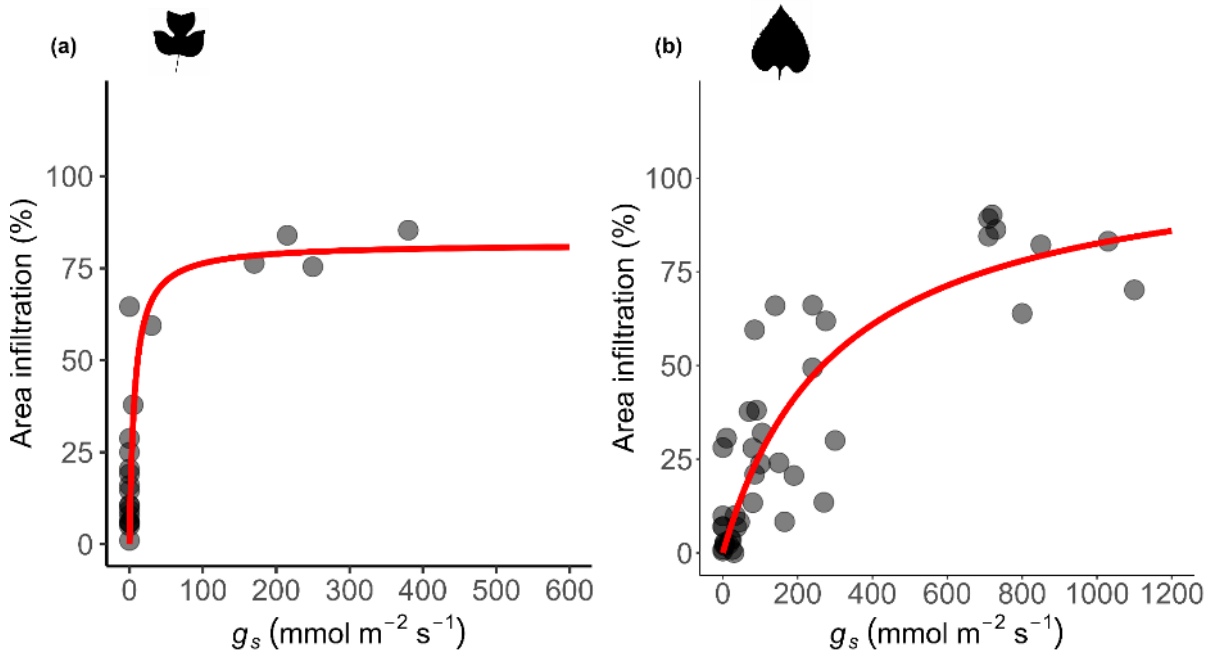

FIGURE S 3.3: Relationships of infiltrated area (Φ_{PSII}) and stomatal conductance (g_s) for *Liriodendron tulipifera* (a) and *Helianthus annuus* (b).
Dots represent individual leaves. Solid red regression corresponds to the fit according to a logistic model.

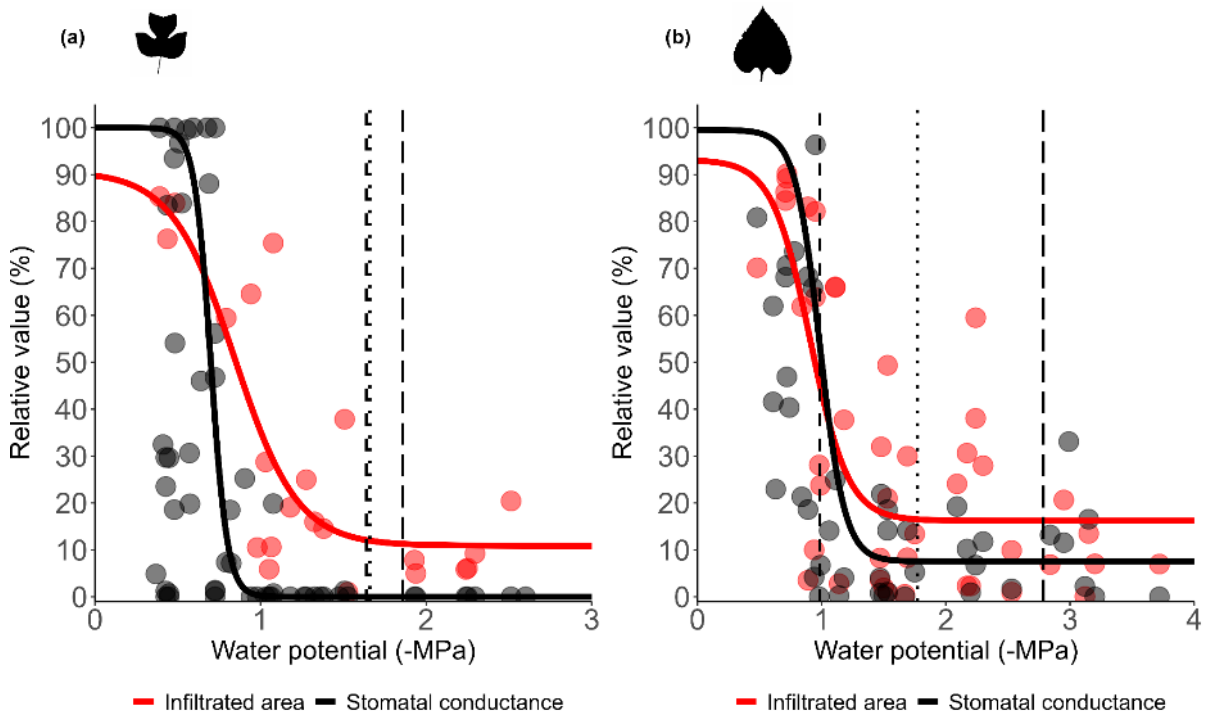

FIGURE S 3.4: Relative value of leaf infiltration and stomatal conductance as a function of water potential in *Liriodendron tulipifera* (a) and *Helianthus annuus* (b).
Black dots represent the relative stomatal conductance ($g_{s,rel}$), red dots represent individual infiltrated leaves. Solid black and red regressions correspond to the fit according to a logistic model. The water potential thresholds inducing Ψ_{tlp} (dashed line), Ψ_{12} (dotted line) and Ψ_{P50} (long dashed line) are indicated.

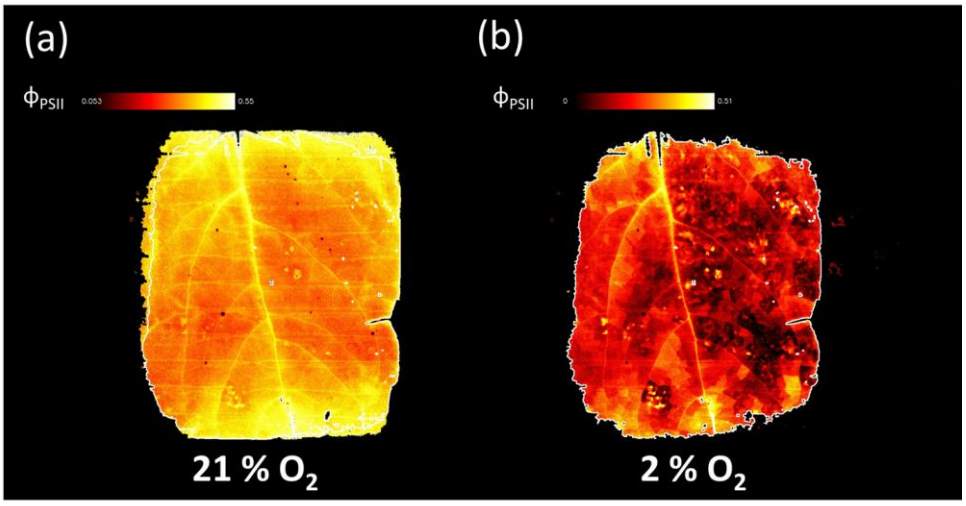

FIGURE S 3.5: Same leaf under the same environmental conditions except oxygen concentration in the air flow with (a) 21% and (b) 2%.

TABLE S 3.1: Two-parameter model results for *L. tulipifera* and *H. annuus*

Liriodendron tulipifera fit results Figure S3.3a

Formula: Infiltrated area ~ (A * g_s)/(B + g_s)

Estimate	Std.	Error	t value	Pr(>|t|)	
A	81.706	10.681	7.649	2.31E-07	***
B	7.086	6.763	1.048	0.307	

Residual standard error: 19.36 on 20 degrees of freedom

Helianthus annuus fit results Figure S3.3b

Formula: Infiltrated area ~ (A * g_s)/(B + g_s)

Estimate	Std.	Error	t value	Pr(>|t|)	
A	108.04	14.82	7.29	6.44E-09	***
B	309.16	100.16	3.087	0.00362	**

Residual standard error: 15.42 on 41 degrees of freedom

TABLE S 3.2: For-parameter logistic model results for *L. tulipifera* and *H. annuus*

Liriodendron tulipifera fit results Figure 3.3a and Fig S3.4a

Formula: Infiltrated area ~ C + A/(1 + exp((Xo - Water potential)/B))

Estimate	Std.	Error	t value	Pr(>|t|)	
A	79.8277	30.8111	2.591	0.01845	*
B	0.1902	0.1499	1.269	0.220506	
Xo	-0.8441	0.2132	-3.96	9.18E-04	***
C	10.8878	6.8025	1.601	0.126876	

Residual standard error: 17.49 on 18 degrees of freedom

Helianthus annuus fit results Figure 3.3b and Figure S3.4b

Formula: Infiltrated area ~ C + A/(1 + exp((Xo - Water potential)/B))

Estimate	Std. Error	t value	Pr(>|t|)	
A	76.9451	30.973	2.484	0.01738	*
B	0.1531	0.1066	1.435	0.15913	
Xo	-0.9087	0.149	-6.098	3.78E-07	***
C	16.230	4.5871	3.538	0.00106	**

Residual standard error: 21.34 on 39 degrees of freedom

TABLE S 3.3: Constant used for the theoretical leaf conductance for both species

Definition	Abbreviation	Value	Unit
Mean free path in air	χ'	$6.67.10^{-8}$	M
Binary diffusivity of water vapour in air.	D_{wa}	$2.55.10^{-5}$	$m^{-2}\ s^{-1}$
Molar volume of air	V_{ma}	$2.44.10^{-2}$	$m^3\ mol^{-1}$
Ratio of pore depth to pore length	j	0.5	unitless
Ratio of pore length to stomatal length to the square root of j	μ	$1/\sqrt{2}$	unitless

CHAPTER 4

Beyond individual stomata: the importance of collective behaviour during drought

Chapter 4 Beyond individual stomata: the importance of collective behaviour during drought

This chapter is presented in the form of a paper entitled: Revealing stomatal patchiness under drought in sunflower plants. *by G. Forget, R. Burlett, J. Joubès, S. Delzon and T. Lawson.*
The dual imaging experiment was performed during a five-month international mobility at the University of Essex, England. A set of Python functions have been developed, explained in detail in appendix A2 and available on this repository https://gitub.u-bordeaux.fr/guforget/thermal-and-fluorescence-images-analysis

1. Short introduction

The previous chapter highlighted the role of stomatal leakiness in contributing to residual water loss and introduced the spatial heterogeneity arising from the collective behaviour of stomata. This collective behaviour, known as stomatal patchiness, has been the subject of numerous researches focusing on the impact on gas exchange, yet its dynamics under progressive drought conditions remain poorly understood. In this chapter, we study stomatal spatial response at two distinct but closely related time scales. The first represents a long-term progressive water stress, driven by declining soil water availability. The second reflects a short-term response occurring within minutes. By combining thermal and chlorophyll fluorescence imaging, we will emphasise that stomatal patchiness emerges as a spatiotemporal response to drought. This spatial behaviour can persist until advanced levels of water stress, maintaining localised regulation of gas exchange.

2. Revealing stomatal patchiness under drought in sunflower plants

2.1. Abstract

Stomatal patchiness, a spatial and temporal stomatal behaviour is a well-known stomatal response to environmental fluctuations such as changes in light intensity or vapour pressure deficit. However, what is its contribution as an adaptive strategy for gas exchange and photosynthesis during a progressive drought? Using thermal and chlorophyll fluorescence imaging under low oxygen concentration during drought, we highlighted that stomatal patchiness is a one of the leaf-level drought responses in *Helianthus annuus*. The maximum spatial variability in stomatal closure occurs between the bulk water potential at turgor loss point (Ψtlp) and the onset of embolism (ΨP12), an interval that functions as a spatial buffer enabling local optimisation of gas exchange. This spatial heterogeneity allows specific leaf regions to maintain photosynthetic activity while others limit water loss, thereby delaying hydraulic failure and metabolic decline. Despite reductions in ΦPSII, the structural photochemical capacity remains intact until severe drought level (ΨP50), indicating that declines in ΦPSII are driven by stomatal limitations rather than photodamage. Moreover, we reveal a hierarchical spatial organisation of stomatal patchiness from micro- (vein-level), meso- (local), and macro- (whole-leaf) scales, underscoring a multiscale coordination in drought and environmental cues responses. Incorporating this spatiotemporal complexity into models of leaf conductance could improve our understanding of the mechanisms underlying stomatal coordination and its impact on whole-leaf gas exchange during water stress.

Keywords

Drought, stomatal patchiness, spatiotemporal, heterogeneity, thermal and chlorophyll fluorescence imaging, transpiration, photosynthesis, scaling.

2.2. Introduction

Drought events are increasing in frequency due to climate change and pose significant threat to plants survival and productivity (Pörtner & Roberts 2022; Gebrechorkos *et al.* 2025; Hultgren *et al.* 2025). Under conditions of reduced soil water availability, stomatal closure represents the fastest (Drake *et al.* 2013; Adams *et al.* 2017)

and most efficient (Buckley 2019) physiological response to maintain overall plant water status. However, this water-conserving strategy comes at the cost of reduced CO_2 uptake for photosynthesis, highlighting the permanent trade-off that plants must maintain between conserving water and carbon assimilation for growth and survival (Mott & Buckley 2000; Machado *et al.* 2021). The rates of carbon and water vapour flux between the plant and the atmosphere occur at the leaf surface by the stomatal density and aperture (Franks & Beerling 2009; Dow *et al.* 2014; Sack & Buckley 2016; Ochoa *et al.* 2024). Interestingly, stomata do not function solely as isolated unit; they can operate in coordinated groups, leading to a heterogeneous spatial distribution of stomatal apertures across the leaf surface (Weyers & Lawson 1997; Lawson *et al.* 1998; Peak *et al.* 2004; Marenco *et al.* 2006), a phenomenon known as stomatal patchiness. First highlighted in 1993 (Mott *et al.* 1993), this mosaic-like pattern of non-uniform stomatal conductance across the leaf lamina has been observed in many species, particularly among angiosperms (Lawson *et al.* 1998; Marenco *et al.* 2006; Kamakura *et al.* 2011; Kamakura *et al.* 2012a,b, Kamakura *et al.* 2015). Stomatal patchiness can be defined as the difference in stomatal pore aperture between adjacent stomata leading to spatial heterogeneity in responses to internal and external cues (Lawson *et al.* 1998; Mott & Buckley 2000; Peak *et al.* 2004; Peak, Hogan & Mott 2023; Marenco *et al.* 2006; Mott & Peak 2007; Kamakura *et al.* 2011, 2012a b, 2015). This phenomenon may arise due to local variation in water potential within the leaf (Jain *et al.* 2023, 2024) as well as rapid changes in VPD (Kamakura *et al.* 2021). Stomatal patchiness can be both spatial and temporal, therefore, advances in imaging techniques including as thermal (Jones *et al.* 2009) and chlorophyll fluorescence imaging (Morison *et al.* 2005; McAusland *et al.* 2013; Lawson & Morison 2006; Hofmann *et al.* 2025) have emerged as powerful and complementary tools for visualising and quantifying the extent and impact of heterogeneous stomatal behaviour on plant performance (Mott & Buckley 1998; Šantrůček *et al.* 2003; Peak *et al.* 2004; Takanashi *et al.* 2006; Mott & Peak 2007).

Due to significant implications for the calculation of C_i (intercellular CO_2 concentration) from gas exchange measurements and the impact this has on photosynthetic responses (Buckley *et al.* 1997a), as well as the implications for scaling up gas exchange measurements (Weyers & Lawson 1997; Lawson *et al.* 1998) it is essential to quantify and include stomatal heterogeneity into existing gas exchange models, using statistical approaches (Takanashi 2006). For instance, spatially explicit models, such as those developed by Haefner *et al.* (1997) have been central to the

analysis of spatial patterns and interactions within systems. More recent models, based on connected spatial networks and cellular automata (Mott & Peak 2007), have shown promise in capturing emergent behaviour, as demonstrated by (Peak *et al.* 2023).

Most research on stomatal patchiness has focused on direct effects of environmental cues such as vapor pressure deficit (VPD), temperature, wind and light intensity (Mott & Buckley 1998; Beyschlag & Eckstein 2001). Nevertheless, dynamics of stomatal patchiness under prolonged drought conditions remain insufficiently understood, highlighting a critical gap in our knowledge of its functional significance during water stress.

This study aims to address this gap by investigating stomatal collective behaviour responses to drought across two distinct temporal scales. The first is a long-term response driven by progressive drought reflecting changes in soil water status in nature that leads to changes in leaf water potential. The second is a short-term response occurring over several minutes at a given leaf water potential, capturing quasi instantaneous stomatal responses driven by light and uncontrolled air flow dynamic leading to a steady state.

Using thermal and chlorophyll fluorescence imaging to monitor stomatal closure, we aim to investigate how under progressive water stress, spatial stomatal dynamics, contribute to the trade-off between water loss and carbon uptake. Specifically, our objectives are to: (i) highlight the occurrence of stomatal patchiness during water stress, (ii) determine the range of hydraulics thresholds at which stomatal patchiness becomes biologically significant and (iii) characterise the hierarchical organisation of stomatal patchiness at different spatial scales. We hypothesise that stomatal patchiness represents a key spatiotemporal leaf's response during drought, that persists after the turgor loss point and beyond. This response allows plants to avoid a uniform, rigid response to soil water stress and instead maintain localised spatial regulation that sustains and prolongs gas exchange.

2.3. Materials and Methods

2.3.1. Plant material

Helianthus annuus seeds were sown in plastic trays containing compost and germinated in a growth cabinet (Reftech BV, Sassenheim, the Netherlands). After germination, seedlings (one per pot) were transplanted into 1.5 litres pots containing compost and transferred to a temperature-controlled glasshouse at the University of Essex (average temperature was maintained at 21.8 ± 0.9 °C with RH between 40% and 55% depending on biomass in the glasshouse), supplementary sodium vapour lights (8am until 8pm) provided 400 (µmol s^{-1} m^{-2}) at the plant height. Plants were grown for 45 days before measurements were taken on the youngest fully expanded leaf on individual *H. annuus* plants. After the plants reached leaf maturity but before flowering, groups of four individuals were put under water stress by stopping watering. This procedure was repeated four times, creating sets of plants with different levels of stress.

2.3.2. Hydraulic trait measurements: Pressure-volume curve and stem embolism vulnerability

Pressure-volume curves were performed using a method adapted from Sack *et al.*, (2011) on eight leaves of *H. annuus*. Pressure-volume curves were used to determine leaf physiological traits such as the water potential (Ψ_{tlp}, MPa) at turgor loss point along with the elasticity modulus (ε) and osmotic potential at full turgor (π_0) (Table 4.1). Using ε and π_0 we estimated the water potential at any RWC during the DLML experiment based on the relative water content. Leaf water potential (Ψ_{leaf}, MPa) was measured with a psychrometer (PSY1, ICT International, Armidale, NSW, Australia) before each measurement.

Stem vulnerability to xylem embolism was assessed on five *H. annuus* stems using the Cavitron technique (Cochard 2002; Burlett *et al.* 2022). Measurements were carried out at the platform for hydraulic traits (Caviplace, Phenobois platform, University of Bordeaux, Pessac, France). A percentage loss of conductance or PLC curve was obtained and embolism vulnerability determined at thresholds Ψ_{P12}, Ψ_{P50} and Ψ_{P88} (MPa), which correspond to the xylem pressure/water potential inducing 12%, 50% and 88% losses of hydraulic conductivity, respectively.

TABLE 4.1: Leaf hydraulics variables used in this study. Mean and standard errors for each variable are provided.

Definition	Abbreviation	Unit	*H. annuus*
Water potentials at turgor loss point	Ψ_{tlp}	MPa	-0.98 ± 0.05
Water potentials inducing 12% losses of conductance in the stem	Ψ_{P12}	MPa	-1.77 ± 0.15
Water potentials inducing 50% losses of conductance in the stem	Ψ_{P50}	MPa	-2.78 ± 0.18
Elasticity modulus	ε	MPa	2.03 ± 0.31
Osmotic potential at full turgor	π_0	MPa	-0.74 ± 0.06

To facilitate analysis, leaves were categorised and divided into three classes using: the water potential at 0 MPa, corresponding to a fully hydrated state in equilibrium with pure water and used as the reference point; the water potential at turgor loss point (Ψ_{tlp}) and embolism vulnerability threshold at 12% losses of hydraulic conductivity (Ψ_{P12}). The three groups were non-stress well-hydrated leaves [0; Ψ_{tlp}], with mild stress [Ψ_{tlp}; Ψ_{P12}] and with a medium to severe stress [Ψ_{P12}; -Inf].

2.3.3. Dual thermal and chlorophyll fluorescence imaging

Stomatal dynamics using thermal and chlorophyll fluorescence imaging were assessed using a modified in-house system developed at the University of Essex (McAusland *et al.* 2013) (Figure S4.5). We used the same system configuration and open-top chamber as described in Faralli *et al.* (2024).Throughout the experiment and during each analysis, ambient CO_2 concentration (C_a) was maintained close to 400 μmol_{CO2} mol^{-1} while the photosynthetic photon flux density (PPFD), was maintained at 500 µmol m^{-2} s^{-1} inside the open-top chamber. The relative humidity (RH) and ambient temperature, maintained close to 25°C, were continuously recorded using a probe (HygroClip2, HC2A-S, Rotronic, Bassersdorf, Switzerland) connected to an Arduino. Vapor vapor concentration was regulated by a mass flow controlled evaporating mixer unit (CEM Evaporator W-202A, Bronkhorst, Newmarket, UK). Both CO_2 and H_2O vapour concentrations were measured with an infrared gas analyzer (IRGA) (Li- 840, LI-COR, NE, USA). Changes in vapour pressure deficit (VPD) was performed by altering the relative humidity going into the chamber. A leaf connected to the rest of the plant was placed in the open-top chamber and a paired image (thermal and chlorophyll a

fluorescence) recorded every minute for 10 minutes at low VPD (between 70% and 99% of relative humidity).

To visualise the impact of stomatal closure on photosynthetic performance, we inhibited photorespiration (which is a sink for the end product of electron transport) by reducing the oxygen concentration to 2% (Murchie & Lawson 2013; Hofmann *et al.* 2025) (Figure S4.6).

2.3.3.1. Estimation of stomatal conductance from leaf temperature

The evaporative cooling effect of transpiration can be used to estimate stomatal conductance (g_s) using the following equations proposed by Leinonen *et al.*, (2006) and Jones *et al.* (2009) along with a dry temperature reference with equation 4.1:

$$\frac{1}{g_s} = r_s = -\frac{\rho c_p r_{HR}[s(T_l - T_a) + D]}{\gamma \rho c_p (T_l - T_{dry})} - r_{aW} \qquad (4.1)$$

, where T_l is the leaf temperature (°C), T_a is the air temperature (°C) and T_{dry} is the dry reference temperature (°C) (a point on the leaf apex covered with grease), r_{aW} (r_{aW}=0.92.r_H, Jones *et al.*, 2009) is the boundary layer resistance to water vapour (s m^{-1}). r_H is the sensible resistance estimated in our system at 15.38 s m^{-1} (g_H= 0.065 m s^{-1}) and can be assimilated to the boundary layer resistance. ρ is the density of air (kg m^{-3}), c_p is the specific heat capacity of air (J $kg^{-1}K^{-1}$), s is the slope of the curve relating saturating water vapour pressure to temperature (Pa $°C^{-1}$) (Leinonen *et al.* 2006; Monteith & Unsworth 2013), γ is the psychrometric constant (Pa K^{-1}), D is the air vapour pressure deficit (Pa), and r_{HR} is the parallel resistance to heat and radiative transfer (s m^{-1}) as calculated with equation 4.2:

$$r_{HR} = \frac{r_H r_R}{r_H + r_R} \text{ and } r_R = \frac{\rho c_p}{4\varepsilon\sigma(T_a + 27.15)^3} \qquad (4.2)$$

, where ε is the emissivity (fixed at 0.965) and σ is the Stefan-Boltzmann constant ($5.6703.10^{-8}$ W m^{-2} K^{-4}). Although emissivity changes during leaf dehydration, for

convenience we have chosen to use a fixed value. g_s was converted to mmol m^{-2} s^{-1} using the perfect gas equation from equation 4.3:

$$\frac{g_s(\,mol\,m^{-2}s^{-1})}{g_s(m\,s^{-1})} = \frac{P_{atm}}{8.314 * (T_l + 273.15)} \qquad (4.3)$$

The temperature difference between the leaf surface and air temperature, $\Delta T = T_l - T_a$, used to estimate the stomatal conductance (g_s) in equation 4.1 was also used as a proxy of the stomatal dynamics. In equation 4.1, the main driver of the g_s was the temperature difference due to the effective evaporative cooling.

2.3.3.2. *Estimation of chlorophyll fluorescence parameter*

Chlorophyll a fluorescence imaging (CF, Technologica, Essex, UK) was used to capture the following parameters F_o, F_m, F' and F'_m (see Table 4.2). F_o minimal fluorescence in the dark-adapted state was measured using a weak measuring beam of 0.1 µmol m^{-2} s^{-1}, insufficient to drive photosynthesis. Application of a saturating pulse to the dark-adapted leaf induced maximum fluorescence, F_m. After which actinic light was applied at a value of 500 µmol m^{-2} s^{-1} and steady-state fluorescence measuring in the light termed F'. A saturating pulse applied under actinic light during 800 ms providing a measure of maximum chlorophyll a fluorescence in the light termed F'_m (Baker 2008; Murchie & Lawson 2013). Using these parameters, it was possible to calculate the photosystem II photosynthetic efficiency, Φ_{PSII} (or F_q'/F_m', unitless), which is a measure of the proportion of absorbed light used in photosystem II photochemistry (Genty *et al.*, 1992) and was defined by equation 4.4:

$$\frac{F'_q}{F'_m} = \frac{F'_m - F'}{F'_m} \qquad (4.4)$$

Φ_{PSII}, (F_q'/F_m'), was broken down into two products (Murchie & Lawson 2013):

$$\frac{F_q'}{F_m'} = \frac{F_q'}{F_v'} * \frac{F_v'}{F_m'} \tag{4.5}$$

(ii) the maximum efficiency of photosystem II photochemistry in the light, if all centres were open, F_v'/F_m' , defined by equation 4.6:

$$\frac{F_v'}{F_m'} = \frac{F_m' - F_o'}{F_m'} \tag{4.6}$$

and (iii) the level of photochemical quenching of photosystem II, F_q'/F_v' , defined by equation 4.7:

$$\frac{F_q'}{F_v'} = \frac{F_m' - F'}{F_m' - F_o'} \tag{4.7}$$

Where,

$$F_o' = \frac{F_o}{\left(\frac{F_m - F_o}{F_m}\right) + \left(\frac{F_o}{F_m'}\right)} \tag{4.8}$$

TABLE 4.2: Common primary parameters measured by the chlorophyll fluorescence camera

Definition	Abbreviation
Maximal chlorophyll fluorescence in the dark-adapted state	F_m
Maximal chlorophyll fluorescence in the light-adapted state	F_m'
Minimum value for chlorophyll fluorescence	F_o
Steady-state level of chlorophyll fluorescence in the light	F'
Photosystem II operating efficiency	$\Phi_{PSII} = F_q'/F_m'$
Maximum efficiency of photosystem II	F_v'/F_m'
Level of photochemical quenching of photosystem II	F_q'/F_v'

2.3.4. Image processing

Images from the chlorophyll a fluorescence and thermal cameras were recorded as a 2D matrix using the internally developed instrument software (FluorImager V2, University of Essex), where each pixel corresponded to either a chlorophyll a fluorescence parameter value or temperature value. Environmental data including air temperature and relative humidity was also included in the files with the 2D matrix containing raw temperature from the camera and a timestamp, whilst a second file contained matrices of the four primary chlorophyll a fluorescence parameters (F_o, F_m, F' and F'_m). Using a Python script and equations 4.4, 4.5, 4.6 and 4.7, three new matrices (Φ_{PSII}, F'_v/F'_m and F'_q/F'_v) were generated based on the five primary chlorophyll fluorescence parameters (F_o, F_m, F' and F'_m). The raw temperature matrix represented a global view of the entire environment captured by the thermal camera, not only the leaf. As the chlorophyll a fluorescence matrix reflected only the leaf, the matrix F'_o was used as a mask in order to isolate the leaf temperature from the environment. Using equations 4.1, 4.2, and 4.3, the new temperature matrix containing only pixels representing the leaf were transformed into the stomatal conductance matrix. At each time step, five matrices were used in this study (leaf temperature or temperature difference, g_s, Φ_{PSII}, F'_v/F'_m and F'_q/F'_v). The mean and standard deviation were calculated for each matrix. The matrices were converted into images using another Python script and the Matplotlib library.

2.3.4.1. Thresholds for spatial segmentation

We used water potential at turgor loss point (Ψ_{tlp}) and the embolism vulnerability threshold at 12% losses of hydraulic conductivity (Ψ_{P12}) to threshold the difference temperature and the quantum efficiency of photosystem II, Φ_{PSII}, into three areas based on Figure 1c and Figure 3a: Active areas characterised by open stomata with an impact on transpiration and carbon uptake (low difference temperature (below 1.5°C) with a high Φ_{PSII} (above 0.5)), inactive areas characterised by close stomata resulting in minimal impact on transpiration and carbon uptake (high difference temperature (above 3.6°C) with a low Φ_{PSII} (below 0.3)) and intermediate stomatal behaviour corresponding to areas where temperature differences were between 1.5° and 3.6°C and Φ_{PSII} was between 0.3 and 0.5. Thresholds were applied through a Python script to divide the leaf surface into

three distinct areas and calculate the relative percentage of each region. This method was applied to leaf temperature, Φ_{PSII}, F_v'/F_m' and F_q'/F_v'.

2.3.4.2. Patches and intra-patches dynamics

For the same leaf, each image derived from a matrix was generated using the minimum and maximum values of the variable (temperature or Φ_{PSII}) from the global dataset of the same leaf, ensuring an accurate representation of the 'real' dynamics across the entire dataset. Each image was then stacked and aligned using ImageJ v.1.53q (Schneider *et al.* 2012) to generate an image sequence of 10 images (or 10 minutes with 1 image per minute). Each image sequence was associated with a water potential measured before the experiment using a psychrometer. This procedure allowed the reconstruction of the leaf's response during a progressive drought. From the entire reconstructed sequence, the image with the most clearly defined patches was selected. Several patches were then extracted, and for each patch the coefficient of variation (cv=sd/mean) and Shannon's entropy were calculated.

2.3.4.3. Shannon's entropy

Shannon's entropy (H) (Shannon 1947), was used as a variable derived from information theory to quantify the randomness or information content within the pixel intensity distribution of an image. It was calculated using the histogram of pixel values, treating the image as a discrete random variable with outputs corresponding to the pixel intensity levels (from 0 to 255 in an 8-bit grayscale image for exemple). Using the dedicated functions in ImageJ, the probability distribution of these outputs was estimated, the histogram of pixel values was computed and normalised, so that the relative frequency of each intensity level represents its empirical probability. The entropy reflects the spread of pixel intensities. A uniform distribution resulted in maximum entropy (maximum information content), whereas more concentrated distributions yield lower entropy (minimum information content). Image of Φ_{PSII} derived from the matrix were

converted into 8-bit grayscale image (8 bits was then the maximum entropy available for this kind of image) and Shannon's entropy calculated for each patch using equation 4.9:

$$H = -K \sum_{i=1}^{n} p_i log_2 p_i \quad (4.9)$$

, where p_i is the probability to obtain a certain frequency. K is a constant to constrain the entropy, H, between 0 and 1 and can be estimated with $K=1/log_2$(number of bins) where the number of bins was in your case 256 bins then K=0.125 (i.e. ⅛).

2.3.5. Data processing and analysis

Image processing was performed using Python scripts with classical libraries including Numpy, Maplotlib and Scikit-Image or using ImageJ v.1.53q. R script with RStudio 2022.12.0+353 (R Core Team 2020) used to produce graphs.

2.4. Results

2.4.1. Quantum efficiency of photosystem II, Φ_{PSII} and the leaf-to-air temperature difference (ΔT) as proxies of the stomatal conductance (g_s)

As expected there was a significant negative correlation (R=-0.8, p<0.001) between the temperature difference, ΔT, and the calculated stomatal conductance (using equation 4.1) (Figure 4.1a). A higher positive temperature difference (ΔT=5.9 ± 1.07°C) was observed when g_s was low (36.15 mmol m^{-2} s^{-1}), indicating warmer leaves due to reduced evaporative cooling. During stomatal opening, stomatal conductance increased and the ΔT decreased until a plateau close to ΔT=1.19 ± 0.71 °C showing the impact of transpiration by stomatal aperture on leaf temperature. The maximal stomatal conductance achieved was 1884 mmol m^{-2} s^{-1} highlighting a wide range (from 36.15 mmol m^{-2} s^{-1} to 1884 mmol m^{-2} s^{-1}) of stomatal conductance and the remarkable ability for *H. annuus* to cool leaves.

The quantum efficiency of photosystem II, Φ_{PSII}, estimated at 2% O_2, increased positively and non-linearly with increasing stomatal conductance, g_s (R= 0.61, p<0.001) (Figure 4.1b), from a minimum of 0.06 (corresponding to a g_s= 1.41 mmol m^{-2} s^{-1}) to a plateau (approximately 0.52) for g_s values from 245 mmol m^{-2} s^{-1} to 1884 mmol m^{-2} s^{-1}

(Figure 4.1b). Value of g_s between 245 mmol m^{-2} s^{-1} and 1884 mmol m^{-2} s^{-1} corresponded to the minimum of ΔT (1.19 ± 0.71 °C) and Φ_{PSII} (approximately 0.52), indicated a high efficiency for both cooling and photosynthetic electron transport.

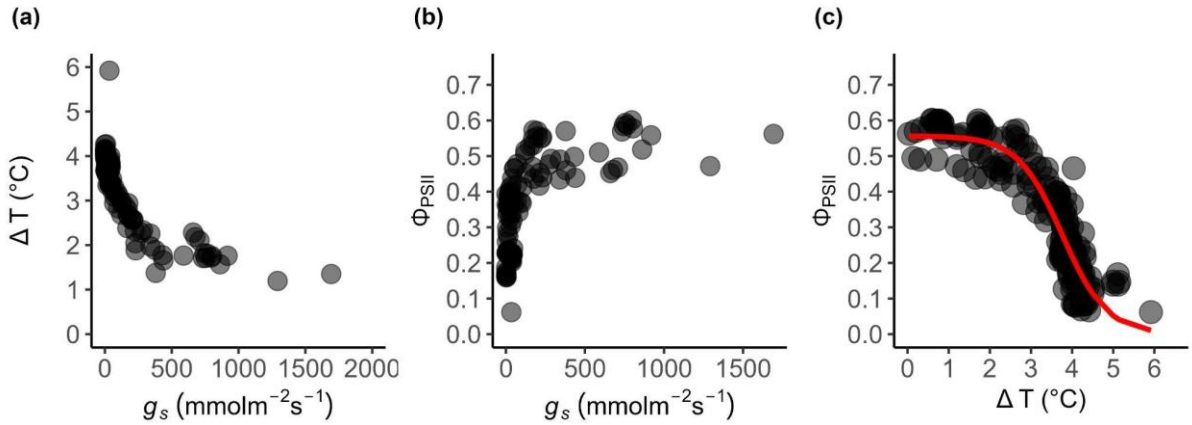

FIGURE 4.1: Stomatal impact on leaf temperature (transpiration) and quantum efficiency of photosystem II (Φ_{PSII}).
Stomatal conductance (g_s) versus (a) temperature difference, ΔT; (b) and quantum efficiency of photosystem II; (c) relationship between ΔT and quantum efficiency of photosystem II (Φ_{PSII}). The red line corresponds to a logistic model (see SI for model coefficients). Each dot represents a leaf at one time step.

There was a significant negative correlation (R=-0.88, p<0.001) between ΔT and Φ_{PSII} (Figure 4.1c) reflecting the underlying stomatal behavior. Thus, both ΔT and Φ_{PSII} provided reliable proxies for stomatal behaviour. A higher value for Φ_{PSII} corresponded to a low temperature difference, i.e. a leaf with a surface temperature close to the air temperature, indicating maximum cooling efficiency. In contrast, the lowest value of Φ_{PSII} was observed when the temperature difference was positively high, i.e. when a warm leaf had a large number of closed stomata, thereby reducing evaporative cooling and CO_2 uptake.

2.4.2. Thermal and chlorophyll fluorescence imaging tracks spatial stomatal behavior

Thermal and chlorophyll fluorescence (at 2% O_2) images (Figure 4.2) were captured simultaneously at one-minute intervals over a 10-minute period under identical environmental conditions. The sequence illustrates the spatial dynamics of a leaf during this 10-minute period at a water potential of –1.37 MPa, (between Ψ_{tlp} and Ψ_{P12}). The

sequence revealed fast changes (in the order of a minute) in the spatial heterogeneity for ΔT and Φ_{PSII}. The spatiotemporal representation of both leaf temperature (a - d) and Φ_{PSII} (a' - d') revealed a common spatiotemporal dynamic, with a notable overlap at 7 minutes (c - c'). When Φ_{PSII} was low (red, black color), the leaf temperature was high (yellow, white color) whereas when the Φ_{PSII} was higher (yellow, orange color) the leaf temperature decreased (red, black color). However, images from Φ_{PSII} offered better resolution accuracy than thermal images due to the thermal boundary layer that spread heat over the leaf.

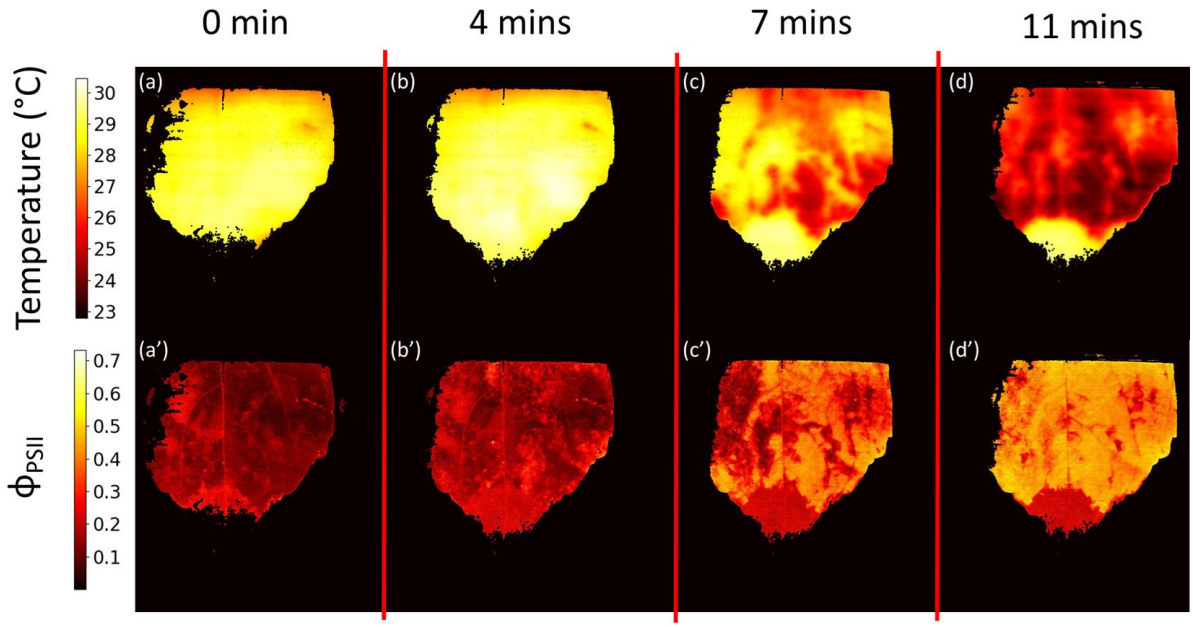

FIGURE 4.2: Spatiotemporal dynamics for the leaf temperature (a-d) and quantum efficiency of photosystem II (Φ_{PSII}).
(a'-d') for the same leaf with a water potential at -1.37 MPa. At each time step, a simultaneous image of chlorophyll fluorescence and temperature was taken.

2.4.3. Long-term spatio-temporal physiological response response at the leaf level

Both ΔT and Φ_{PSII} exhibited significant responses to increased water stress. ΔT showed a strong positive correlation with increasing water stress ($R = 0.72$, $p < 0.001$), indicating an increase in leaf temperature when the drought increased, whereas Φ_{PSII} displayed a strong negative correlation ($R = –0.75$, $p < 0.001$), reflecting a decline in quantum efficiency when drought increased (Figures 4.3a and 4.3b). For both parameters, an important shift occurred after the turgor loss point (dashed line): before this threshold, ΔT was low (less than 1°C, green dots) and Φ_{PSII} was above 0.55 (green

triangles), both with a minimal standard deviation (figure 4.3a and 4.3b) and coefficient of variation (Figure 4.3c). After the turgor loss point, the ΔT increased (orange dots) while Φ_{PSII} decreased (orange triangles) both sharply, indicating significant stomatal closure. This shift was accompanied by the development of a variability, represented by the standard deviation, in ΔT and Φ_{PSII} for each leaf. Coefficient of variation (Figure 4.3c) shows that, for both parameters, the highest variation was observed between the turgor loss point (Ψ_{tlp}) and Ψ_{P12}. When drought stress exceeded Ψ_{P12}, ΔT reached its maximum around 4°C (red dots) and Φ_{PSII} dropped to around 0.2 (red triangles) and variability returned to low levels, similar to those observed before the turgor loss point.

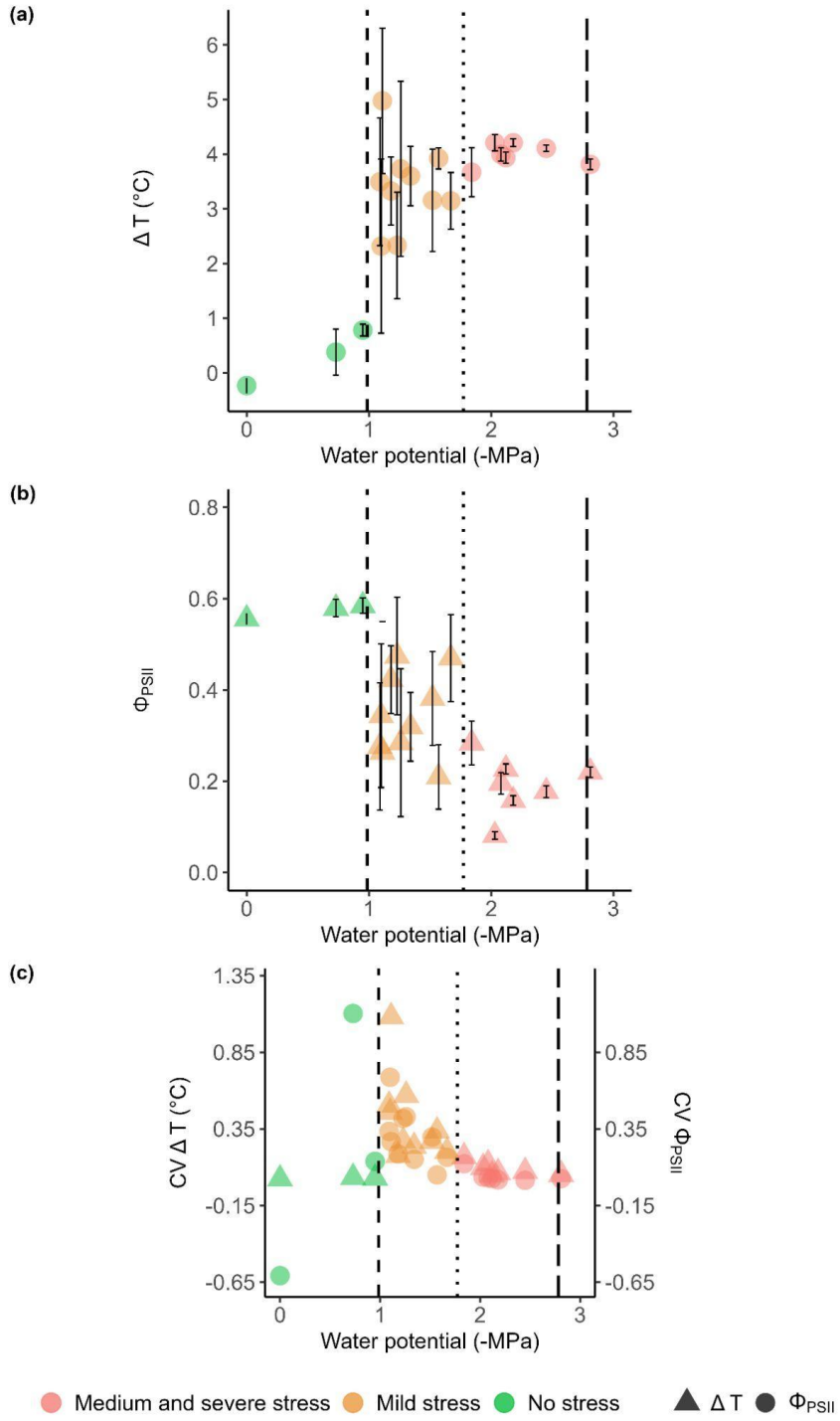

FIGURE 4.3: (a) Leaf to air temperature difference (ΔT), (b) quantum efficiency of photosystem II (Φ_{PSII}) and (c) coefficient of variation for the ΔT (dots) and the quantum efficiency of photosystem II (triangle) as a function of water potential.
Each dot or triangle represents a leaf average over a time sequence of 10 minutes and error bars represent the standard deviation. Colours represent drought stress classes (No stress [0, Ψ_{tlp}]: green dots, Mild stress [Ψ_{tlp}, Ψ_{P12}]: orange dots and Medium and severe stress [Ψ_{P12}, -Inf]: red dots). The water potential at turgor loss point, (Ψ_{tlp}; dashed line), the water potential inducing 12% losses of hydraulic conductivity in the stem, (Ψ_{12}; dotted line) and the water potential inducing 50% losses of hydraulic conductivity in the stem (Ψ_{P50}; long dashed line) are indicated. The negative value for the coefficient of variation at 0 Mpa is due to sensitivity to small changes (the mean approached zero, -0.23 ± 0.14 °C so the coefficient of variation became sensitive to this value).

The proportion of leaf surface with open stomata (blue area) decreased after the turgor loss point (-0.75 MPa<Ψ_{tlp}), as reflected in both the temperature difference (ΔT; Figure 4.4a) and the quantum efficiency of photosystem II (Φ_{PSII}; Figure 4.4b), reaching a minimum at Ψ = –2.25 MPa (Ψ_{P12}<Ψ<Ψ_{P50}). At the same time, the proportion of the leaf surface with closed stomata increased reaching a maximum at Ψ=-2.25 MPa (Ψ<Ψ_{P50}). The proportion of leaf area exhibiting spatial heterogeneity (mixture of areas with open and closed stomata (green area)) reached its maximum for ΔT and Φ_{PSII} between Ψ = –1.25 MPa and –1.75 MPa (Ψ_{tlp} < Ψ < Ψ_{P12}).

Breakdown of Φ_{PSII} into F_v'/F_m' and F_q'/F_v' made it possible to analyse the impact of water stress on mechanisms underlying the decrease in the efficiency of photosystem II. The level of photochemical quenching of photosystem II, F_q'/F_v', (Figure 4.4c) showed a maximal proportion of open stomata (close to 100% of the leaf surface) up to the turgor loss point. Beyond this threshold, an almost linear decrease in F_q'/F_v' was observed as drought intensity increased until a minimal value close to 0% at -2.25 MPa (<Ψ_{P50}). At the same time, the proportion of the leaf with closed stomata increased with a maximum proportion at Ψ=-2.25 MPa. F_q'/F_v' followed the same pattern as ΔT (Figure 4.4a) and quantum efficiency Φ_{PSII} (Figure 4.4b), as drought intensifies. After the turgor loss point (Ψ<-0.75 MPa), the proportion of leaf area exhibiting spatial heterogeneity (green area) had a maximum proportion between Ψ=-1.25 MPa and Ψ=-1.75 MPa (Ψ_{tlp}<Ψ<Ψ_{P12}).

The maximum efficiency of photosystem II in the light, F_v'/F_m' (Figure 4.4d) was remarkably stable with a high proportion of open stomata over a large part of the leaf until a severe drought (-2.25 MPa<Ψ_{P50}), indicating that changes to photosynthetic efficiency were not driven by increasing in energy dissipation in the antenna but down stream sink photosynthetic processes.

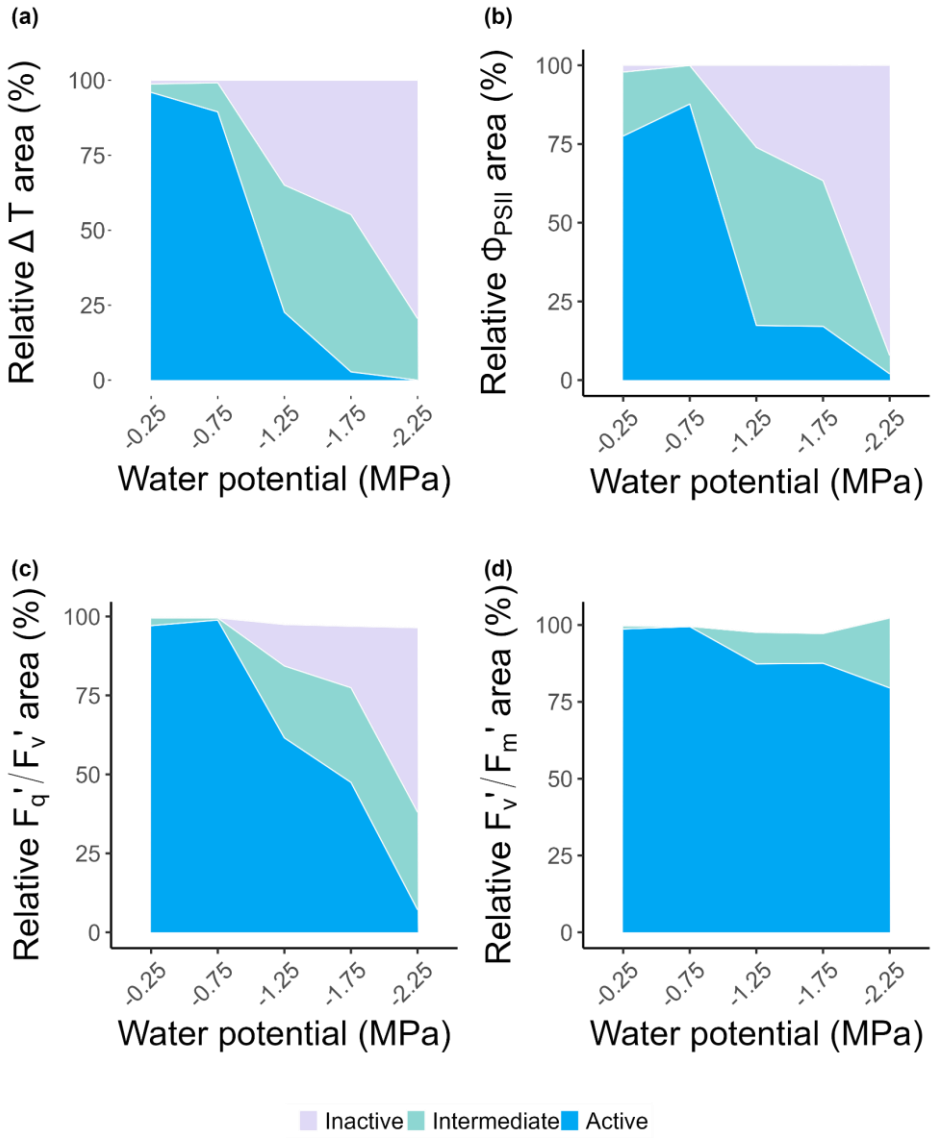

FIGURE 4.4: Relative spatial dynamic for transpiration and photosynthesis parameters along a drought sequence.
(a) Leaf to air temperature difference (ΔT); (b) quantum efficiency of photosystem II (Φ_{PSII}); (c) F'_q/F'_v, the level of photochemical quenching of photosystem II and (d) F'_v/F'_m, the maximum efficiency of photosystem II. Colours represent stomata status (Active area with open stomata: blue area, Intermediate area with both open and closed stomata: green-blue area and Inactive area with close stomata: purple area).

The spatiotemporal response of ΔT and Φ_{PSII} during drought sequence formed by assembling images taken at different water potentials of the same leaf, highlighted that the standard deviation observed in Figure 4.3 was the result of a spatial heterogeneity in stomatal response e.i. stomatal patchiness, particularly for Φ_{PSII} (Figure 4.5b). Before the turgor loss point, patchiness was not observed due to the homogeneity in the Φ_{PSII} values (Figure 4.5b). After the turgor loss point, patchiness in Φ_{PSII} was observed, with a patchwork of values ranging from high values (yellow/orange) to lower values (red, black), showing areas with open and closed stomata driven by stomatal dynamics. Patches were

not uniform in size but had sharped geometric patterns, each patch being affected by the vein network and Bundle Sheath Extension (BSE) (*H. annuus* being a heterobaric species). As water stress increased, Φ_{PSII} patch size declined with patches fragmentating into smaller patches close to Ψ_{P12} at Ψ=-1.57 MPa. Patchiness were visible at least until Ψ=-2.08MPa ($\Psi_{P12}<\Psi<\Psi_{P50}$) on this leaf.

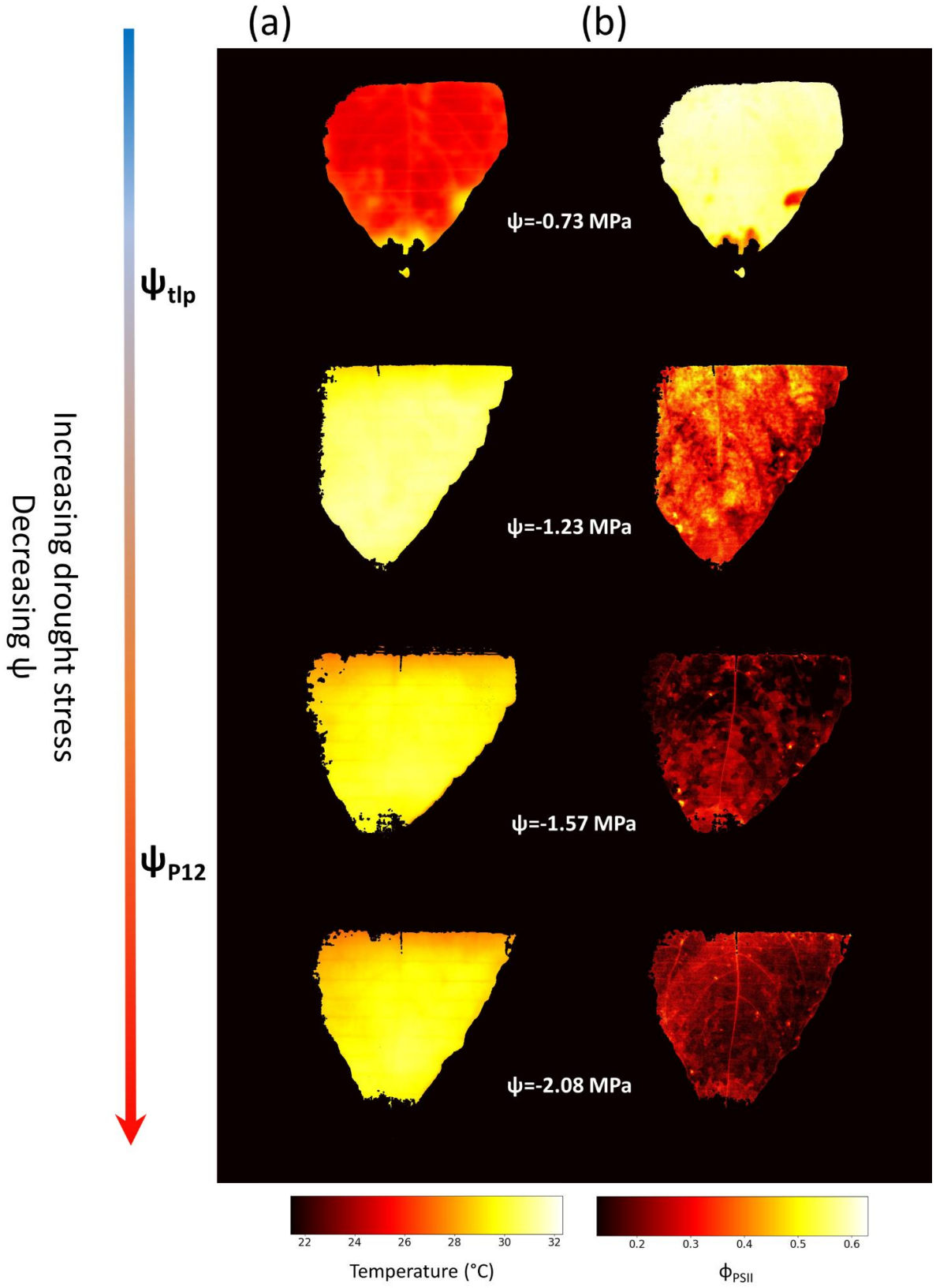

FIGURE 4.5: Difference in spatial long-term dynamics along a drought sequence for (a) the leaf temperature (°C) and (b) the quantum efficiency of photosystem II (Φ_{PSII}).
Each image corresponds to the fifth image of the same leaf taken at different water potential along a drought sequence. The vertical arrow corresponds to the drought stress progression. Ψ_{tlp} and Ψ_{P12} corresponds to the water potential at turgor loss point and the water potentials inducing 12% losses of conductance in the stem, respectively.

2.4.4. Long-term spatiotemporal biological response at patchiness scale

Whilst figure 4.5 illustrated the spatial dynamics in ΔT and Φ_{PSII} at the whole-leaf level during the drought sequence, Figure 4.6 depicted in the same leaf the spatiotemporal dynamics of Φ_{PSII} at the patch level. Each curve represented the distribution of the Φ_{PSII} inside each patch along the drought sequence.

At -0.73 MPa (before Ψ_{tlp}) and -2.08 MPa (after Ψ_{P12}), the patch' distribution was unimodal for each patch with no difference between patches (inter-patch) with a value at 0.552 ± 0.001 and 0.174 ± 0.001, respectively, whereas between these thresholds, the patch' distribution was heterogeneous with a bimodal distribution. This bimodal distribution shifted the primary peak of Φ_{PSII} from around 0.5 at -1.23 MPa to a new dominant peak with a lower Φ_{PSII} value of approximately 0.2 at -1.57 MPa. The transition state which can be defined as the shift from one uniform state over the leaf (either with stomata fully open or fully closed) to another, characterised by a change between the two conditions, was the same for each patch.

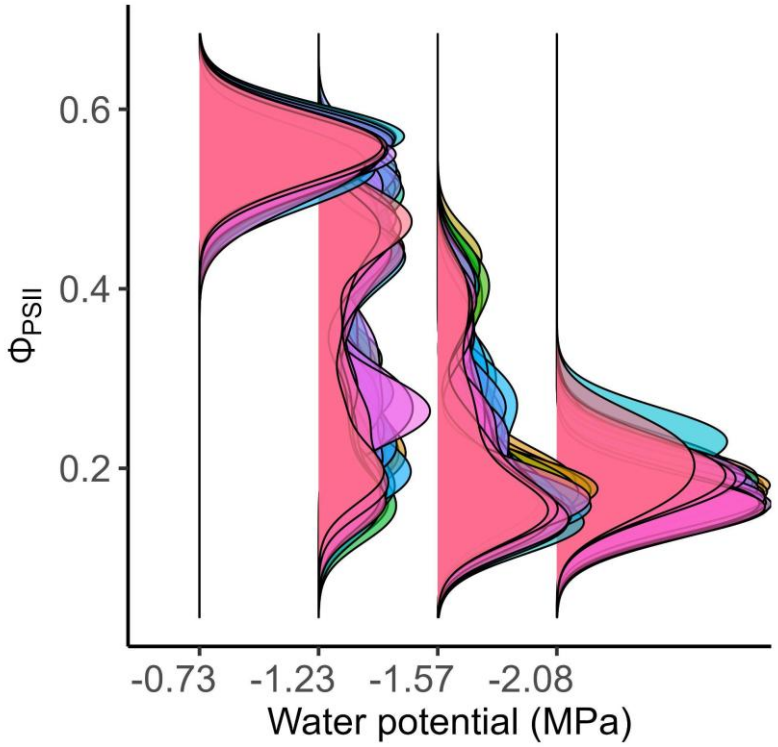

FIGURE 4.6: Spatial dynamic representation of 30 patches during 10 min along a drought sequence for the same leaf. Each colour and density curve represent a patch during 10 mins.

2.4.5. Short-term spatiotemporal biological response at patchiness scale

Intra patch (inside a same patch) dynamic for a leaf during 14 minutes at a given water potential (Ψ_{tlp}>-1.18 MPa>Ψ_{P12}) (Figure 4.7), revealed non-uniform stomatal behaviour with heterogeneous and localised opening. Initially, at 0 min, a central area was present with a low Φ_{PSII} value (dark red/brown colour). Φ_{PSII} was not homogeneous across the leaf, with some areas exhibiting higher Φ_{PSII} levels, leading in well-defined patchiness. At 5 mins, small patches appeared with a higher Φ_{PSII} (yellow colour), suggesting a stomatal opening. These smaller patches fragmented the main central dark area into a patchwork of tiny patches, adding heterogeneity to this area. The transition state occurred rapidly inside the patches and spread over the leaf within just two minutes (between 5 and 7 minutes), as value and spatial extent of Φ_{PSII} reached their maximum after 10 minutes. Each patch did not change uniformly (at the same rate during the opening process), but rather consisted of a set of internal responses represented by micro-patches or unit patches.

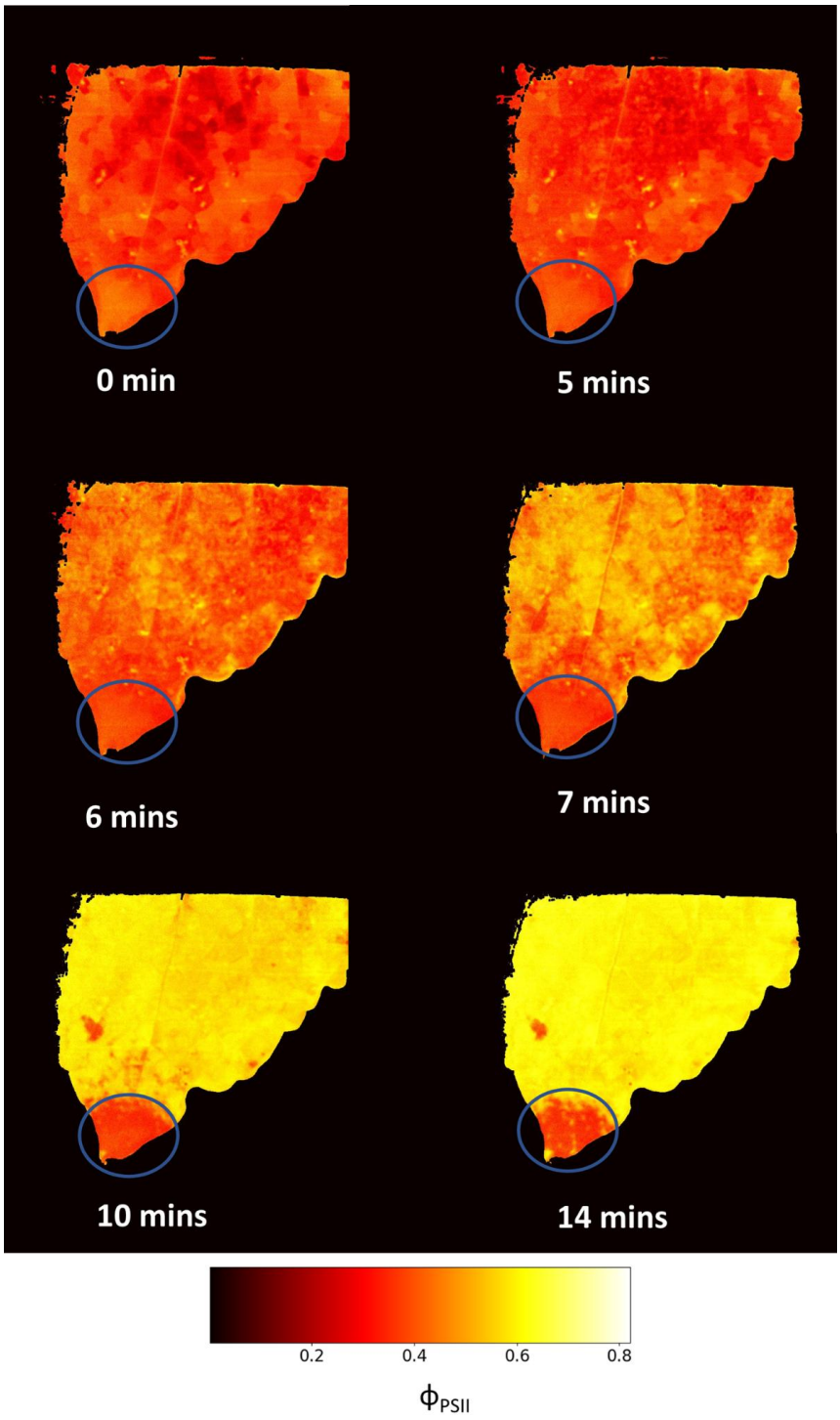

FIGURE 4.7: Leaf short-term spatiotemporal dynamic for the quantum efficiency of photosystem II (Φ_{PSII}) during 14 mins for leaf water potential at Ψ= -1.18 MPa ($\Psi_{tlp}<\Psi<\Psi_{P12}$).
The blue circle represents the position of the grease's patch used to estimate the dry temperature.

After 10 minutes the leaf had a homogenous maximum Φ_{PSII} (yellow) showing that stomata were open uniformly over the leaf. Nine distinct patches from the leaf shown in Figure 4.7 were selected (Figure 4.8a) to clarify the temporal changes inside each patch

during the transition state as highlighted by the coefficient of variation in the heatmap (Figure 4.8b) and the entropy (Figure 4.8c). Each patch displayed distinct temporal dynamics (Figures 4.8b and 4.8c), and between 4 and 7 minutes, there was a marked increase in the coefficient of variation (Figure 4.8b), indicating a transition from high to low Φ_{PSII} within individual patches. Entropy (Figure 4.8c) confirmed variability within individual patches (intra-patch) and among patches (inter-patch), with both sources of heterogeneity peaking during the transition phase (4–7 minutes) when information content was highest.

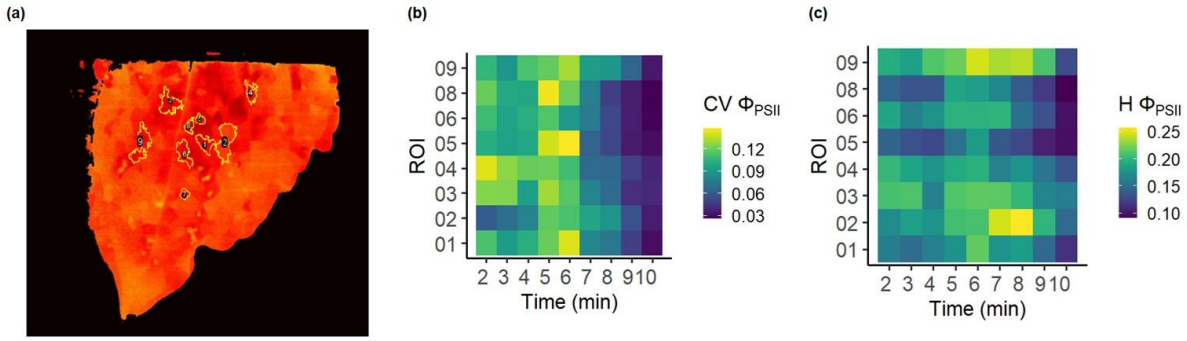

FIGURE 4.8: (a) Quantum efficiency of photosystem II at 0 min with a selection of 9 patches and heatmap of (b) coefficient of variation and (c) Shannon's entropy for each patch and for each time step during 10 minutes.
The leaf water potential was at Ψ= -1.18 MPa ($\Psi_{tlp}<\Psi<\Psi_{P12}$).

2.5. Discussion

Two independent imaging techniques, thermal and chlorophyll fluorescence under low oxygen concentration, reveal the presence and the persistence of stomatal patchiness during drought. Maximum variability in both leaf surface temperature and ΦPSII, occurs between the turgor loss point (Ψ_{tlp}) and the onset of xylem embolism, defined here as a 12% loss of stem hydraulic conductivity (Ψ_{P12}). This variability observed between these two hydraulic thresholds underscores the spatial heterogeneity, expressed as stomatal patchiness. This patchiness arises from differential stomatal responses to drought, allowing localised transpiration and carbon uptake. Notably, high values of maximum efficiency of photosystem II throughout the drought sequence indicate that decreases in the quantum efficiency are not due to structural damage but are a direct consequence of stomatal conductance decline. Combined analysis of patchiness along a long and short-term responses, revealed a spatial hierarchical pattern enabling rapid

adjustment to environmental cues and soil water scarcity. Stomatal patchiness appeared to be an important characteristic of leaves in response to drought.

2.5.1. *Long-term spatiotemporal leaf response to drought*

During drought conditions, plants must adopt a range of adaptive strategies to maintain vital physiological functions such as photosynthesis, water transport, and cellular integrity (Trueba *et al.* 2019; Gupta *et al.* 2020). One of the main strategies is the regulation of stomatal aperture (Brodribb & Holbrook 2003; Tombesi *et al.* 2015) and to a lesser degree, the cuticle biosynthesis to minimise water loss (Shepherd & Griffiths 2006; Chen *et al.* 2020) in order to protect xylem integrity and plant survival (Ziegler *et al.* 2019; Petek-Petrik *et al.* 2023). While individual stomatal closure represents the fastest response to stress by reducing aperture (Drake *et al.* 2013; Anderegg *et al.* 2015; Adams *et al.* 2017), it is not entirely effective due to stomatal leakiness (Brodribb *et al.* 2014; Kane *et al.* 2020; Machado *et al.* 2021). In contrast, stomatal patchiness, an emergent property that enables stomatal coordination (Mott & Buckley 2000; Peak *et al.* 2004; Mott & Peak 2007), represents a distinct form of stomatal response to drought, involving coordinated spatiotemporal that enhances local water-use efficiency under water stress allowing areas to maintain gas exchange and photosynthesis while other areas close to conserving (Mott *et al.* 1993). Tracking a leaf through spatiotemporal analysis during progressive drought allows not only the linkage of stomatal behavior to overall leaf water status (Buckley 2005, 2019) but also the identification of spatial changes and their implications for leaf and plant survival.

Patchiness might be the result of internal and local variability in water potential as highlighted by Jain *et al.* (2023) resulting from water unsaturation in the intercellular air spaces (Wong *et al.* 2022). Under well-watered conditions (up to Ψ_{tlp}) and after the onset of xylem embolism (after Ψ_{P12}), spatial differences in leaf surface temperature and Φ_{PSII} remain low (Figures 4.3a–b, 4.5), reflecting a uniform stomatal behaviour over the leaf. Patchiness is shaped by the vein and Bundle Sheath Extension (BSE) network in heterobaric leaves like *Helianthus annuus* and its observation is possible when there is a difference in temperature or Φ_{PSII} values between patches. Nonetheless, the patchiness pattern is already present but is not distinguishable before Ψ_{tlp} and after Ψ_{P12} due to

spatial uniformity (Figure 4.5 and 4.6). The shape of the patches does not change over the time in response to environmental cues and soil water stress.

Both short- and long-term measurements consistently reveal a uniform pattern for each patch under well-watered conditions (up to Ψ_{tlp}) and at the onset of xylem embolism at Ψ_{P12} (Figure 4.6). When water is not limiting, the initial or well-watered state, occurring before the turgor loss point (Ψ_{tlp}), corresponds to optimal physiological functioning, with parameters such as Φ_{PSII} and cooling efficiency operating near their maximum. During progressive drought, growth and photosynthetic activity decline before the onset of xylem embolism. Beyond Ψ_{P12}, when embolism begins, further losses in hydraulic conductance and cell vitality occur, marking the breakdown of the plant's remaining physiological functions (Torres-Ruiz *et al.* 2024).

Between the turgor loss point, Ψ_{tlp} and before Ψ_{P12} stomatal patchiness becomes increasingly pronounced, as indicated by increasing spatial variation in leaf surface temperature difference and Φ_{PSII} across the leaf (Figure 4.3) and a shift from a unimodal to a bimodal pattern emerges during this transition state (Figure 4.6). After Ψ_{tlp}, gradients in local water potential develop within the leaf in response to soil water stress, amplifying spatial heterogeneity across the leaf without causing significant damage to the hydraulic system (Jain *et al.*, 2023). The interval between Ψ_{tlp} and Ψ_{P12} ($\Delta\Psi_{tlp\text{-}P12}$= 0.79 MPa) allows the existence of a spatiotemporal transition state between two distinct uniform stomatal states in response to progressive soil water deficit. This internal spatial heterogeneity represents a functional trade-off strategy, whereby localised stomatal closure reduces water loss and photosynthesis while other regions sustain photosynthetic processes and water loss through an active electron transport chain and Calvin cycle (Daley *et al.* 1989; Lawson *et al.* 2002; Hofmann *et al.* 2025), thereby optimising resource use under non-optimal conditions. In this context, stomatal patchiness plays a key role, particularly between Ψ_{tlp} and Ψ_{P12}, acting as a regulatory mechanism that smooths and optimises gas exchange at the local scale (Peak *et al.* 2004). This spatial regulation balances water loss and carbon uptake, allowing plants to better cope with rapid abiotic fluctuations such as changes in VPD, light, or wind (Mott & Buckley 1998; Beyschlag & Eckstein 2001) while maintaining essential physiological processes.

The quantum efficiency of photosystem II (Φ_{PSII}) reflects the proportion of absorbed light energy that is effectively used in the photosystem II photochemistry and can therefore estimate the rate of electron transport (Murchie & Lawson 2013). Measuring chlorophyll fluorescence at 2% O_2 rather than 21% is a crucial parameter in our study, as it minimises photorespiration. For chlorophyll fluorescence imaging, photorespiration produces the same result as CO_2 fixation, as it acts as a sink for the products of the electron transport. This same result does not allow us to effectively distinguish the spatial behaviour of stomata. Inhibiting photorespiration allows us to measure only CO_2 fixation using the linear end products of electron transport and thus draw conclusions about stomatal behaviour (Murchie & Lawson 2013; Hofmann *et al.* 2025). Φ_{PSII} is the product of two other chlorophyll fluorescence parameters, the maximum photochemical efficiency of photosystem II in the light-adapted state (F_v'/F_m') (Figure 4.4d) and the operational efficiency factor (F_q'/F_v') (Figure 4.4c), which provides an indication of down stream sink strength. Breaking down Φ_{PSII} into these two parameters provides insights into the mechanisms of spatial drought-induced photosynthetic dynamics. F_v'/F_m' reflects the intrinsic capacity of Φ_{PSII} for photochemistry when all reaction centres are open, remaining consistently high and spatially uniform across leaves even under severe water stress. Consequently, stability of F_v'/F_m' at a high level indicates no irreversible damage and structural and functional integrity of the Φ_{PSII} reaction centres, and non-photochemical quenching (NPQ) remains low (Baker 2008; Murchie & Lawson 2013). In contrast, F_q'/F_v' demonstrates pronounced spatial heterogeneity and a progressive decline with drought. The emergence of leaf regions with low F_q'/F_v' values correlates with restricted CO_2 availability at Rubisco active sites, primarily from stomatal closure. Divergence between sustained F_v'/F_m' and declining F_q'/F_v' demonstrates that reduced Φ_{PSII} under drought is due to reduced Calvin cycle activity rather than direct photochemical damage or increased dissipation of excitation energy via NPQ processes. This reduced Calvin cycle activity is constrained by lower CO_2 availability imposed by the stomatal closure (Flexas *et al.* 2004; Chaves, *et al.* 2009). Our findings in *Helianthus annuus* indicate that photosystem II remains functional even under severe water stress approaching Ψ_{P50} underscoring stomatal limitation as the primary constraint on carbon assimilation during drought.

2.5.2. Multiscale dynamics of stomatal patchiness

While short- and long-term collective stomatal behaviour (Mott & Buckley 1998, 2000) is governed by leaf water potential (Figure 4.3), stomatal patchiness can be described as a hierarchical spatial pattern (Figures 4.6 and 4.7). Following (Kotliar & Wiens 1990), three distinct spatial scales of patchiness can be identified, each with significant implications for gas exchange and physiological processes during a drought sequence.

2.5.2.1. Macroscale: Leaf-level spatial heterogeneity and stomatal patchiness

At this scale, the whole leaf exhibits a distinct spatial heterogeneity, characterised by stomatal patchiness that becomes increasingly pronounced between Ψ_{tlp} and Ψ_{P12} (Figures 4.2 and 4.5). This patchiness reflects the non-uniform physiological responses of stomatal apertures across the leaf surface, driven by short- and long-term environmental cues such as declines in leaf water potential. Such spatial variability in stomatal behaviour allows different leaf regions to respond independently to water deficit optimising leaf gas exchange and water use efficiency under stress conditions (Lawson & Weyers 1999). The intrinsic spatial heterogeneity represented by stomatal patchiness can significantly affect the accuracy and interpretation of key gas exchange parameters such as the assimilation rate (A), the intercellular CO_2 concentration (C_i) and the stomatal conductance (g_s) (Buckley *et al.* 1997a; Mott & Buckley 1998). Specifically, variations in g_s and C_i across the leaf surface can lead to under- or overestimation of whole-leaf gas exchange rates if spatial variability is not accounted for, potentially leading to a reduced understanding of plant water use and photosynthetic responses and strategies to drought. Several studies have previously documented these effects, highlighting that stomatal patchiness causes deviations from the assumptions of spatial uniformity in infrared gas-exchange measurements (Mott *et al.* 1993; Buckley *et al.* 1997b; Mott & Buckley 1998). These findings emphasise the importance of integrating spatial heterogeneity into physiological measurements and modelling, particularly under environmental stress where patchiness intensifies.

2.5.2.2. Mesoscale: Dynamics and heterogeneity inside patches

This scale allows detailed analysis of the internal dynamics within each patch, revealing important patterns for understanding stomatal behaviour during environmental

cues such as reduced water soil availability (Figure 4.6). Notably, heterogeneity within patches becomes increasingly apparent after the turgor loss point (after Ψ_{tlp}), as demonstrated by the emergence of bimodal distributions of Φ_{PSII}. This shift from a unimodal to a bimodal distribution highlights asynchronous stomatal dynamic, where subgroups of stomata within the same patch diverge in behaviour, some remaining closed while others begin to open. Such asynchronous responses highlight the complexity of stomatal regulation, as not all guard cells are reacting uniformly even within a seemingly homogenous patch. Transition dynamics within patches, particularly the shift from low to high Φ_{PSII}, occurs rapidly, typically within 10-minutes (Figure 4.7). These transitions allow a rapid response to short-term environmental factors including vapour pressure deficit (VPD), fluctuations in light, wind and to intrinsic factors such as the heterogeneity of local water potential within the leaf. Moreover, the heterogeneous response of opening within and between patches can be quantitatively captured by the increases in the coefficient of variation (Figure 4.8b) and entropy (Figure 4.8c) showing that each mesoscale patch is not uniform but rather a composite of smaller-scale patches, each with distinct response. These findings emphasise that, at the mesoscale, stomatal regulation is a highly dynamic and spatially complex process.

2.5.2.3. Microscale: Influence of leaf vein network on patchiness

The microscale represents the smallest and fundamental unit of stomatal patchiness, shaped by the leaf's vein network, particularly in heterobaric species such as *Helianthus annuus*. In these species, Bundle Sheath Extension (BSE) act as physical and hydraulic barriers, compartmentalising the leaf surface into discrete sectors and thereby limiting the lateral CO_2 and H_2O diffusion (Beyschlag *et al.* 1992; Mott *et al.* 1993; Morison *et al.* 2005; Lawson & Morison 2006). The leaf vein network imposes constraints on gas diffusion and hydraulic connectivity (Lawson & Weyers 1999). The vein network effectively divides the leaf into sub-areas where stomatal function and photochemical responses can be locally coordinated yet distinct from neighbouring regions. Physiologically, microscale patchiness response can be rapid, often unfolding within minutes or even seconds, allowing quick adaptation to fluctuating microenvironmental cues. These rapid responses include synchronous stomatal aperture within these sub-areas enabling fine-tuned regulation of CO_2 influx and transpiration (Mott & Peak 2007). Importantly, understanding these unit patches and their mechanistic underpinnings

clarifies how anatomical spatial constraints shape individual and collective stomatal dynamics, ultimately affecting leaf-level gas exchange and water relations.

2.5.3. Spatial trade-off and physiological implications

Our results reveal a distinct local trade-off between carbon assimilation and transpiration at the stomata scale, as illustrated in Figure 1c. Importantly, this trade-off is neither uniform across the leaf surface nor static over time; rather, it exhibits a complex spatiotemporal pattern regulated by stomatal patchiness. This dynamic pattern emerges from the plant's capacity to coordinate the behaviour of discrete stomatal patches, enabling groups of stomata to synchronise opening and closing cycles in response to both immediate and prolonged environmental cues such as drought. Stomatal patchiness serves as a key coordinating mechanism that modulates water use efficiency across the leaf. This spatial flexibility enables plants to locally balance carbon gain and hydraulic safety, reflecting a real-time adjustment to environmental variability. During drought, patches can oscillate between states of partial opening and closure, thereby allowing leaves to maintain sufficient CO_2 uptake for photosynthesis while limiting water loss through transpiration. During drought, patches can vary between states of partial opening and closure. This characteristic allows leaves to maintain local CO_2 uptake with water loss. Complete stomatal closure over the leaf limits water loss but prevents CO_2 uptake. Conversely, if the stomata remain open or partially open, CO_2 can enter but this can cause significant and fatal water loss. Physiologically, this spatiality delays the moment to reach a fatal hydraulic and in the same time extends the capability to carbon assimilation.

2.6. Conclusion

Our findings highlight that stomatal patchiness is a feature of leaf-level drought response. Through high-resolution imaging of leaf temperature and photosystem II efficiency, stomatal patchiness emerges not only during environmental cues but also under prolonged drought. The multiscale organisation of patchiness, reflects a hierarchically coordinated response optimising local gas exchange. The breakdown of Φ_{PSII} shows that structural photochemical capacity remains intact during drought, and that reductions in efficiency are driven by stomatal limitations rather than photodamage until a mild water stress before Ψ_{P50}. Stomatal patchiness serves as a functional strategy to

optimise the trade-off between carbon uptake and water conservation at a local scale, particularly during an interval between turgor loss and Ψ_{P12} (beginning of embolism). This highlights local stomatal regulation as the primary constraint on photosynthesis under water stress for *Helianthus annuus*. The heterogeneous collective stomatal behaviour i.e. stomatal patchiness across the leaf is part of the coordinated plasticity along with the xylem and stomatal sensitivity to water deficit (Cardoso *et al.* 2018) in order to maintain physiological processes like photosynthesis.

Author contributions

GF, TL, RB contributed to the design of the study; GF performed data collection and analysis. GF, TL and RB realised the interpretation of the results; GF wrote the manuscript with help from all authors.

Conflict of interest

The authors declare no conflict of interest.

Funding

This study received financial support from the French government in the framework of the IdEX Bordeaux University "Investments for the Future" program / GPR Bordeaux Plant Sciences.TL acknowledges the following BBSRC funding BB/T0042741/1; BB/S005080/1; BB/Y000722/1 T.L. was supported by a Royal Society Leverhulme Trusts Senior Research Fellowship (SF/R1/231041).

Acknowledgements

We thank Dr Phil Davey for the technical assistance for the dual imaging experiment at the university of Essex.

2.7. References

Adams H.D., Zeppel M.J.B., Anderegg W.R.L., Hartmann H., Landhäusser S.M., Tissue D.T., … McDowell N.G. (2017) A multi-species synthesis of physiological mechanisms in drought-induced tree mortality. Nature Ecology & Evolution 1, 1285–1291.

Anderegg W.R.L., Hicke J.A., Fisher R.A., Allen C.D., Aukema J., Bentz B., … Zeppel M. (2015) Tree mortality from drought, insects, and their interactions in a changing climate. New Phytologist 208, 674–683.

Baker N.R. (2008) Chlorophyll Fluorescence: A Probe of Photosynthesis In Vivo. Annual Review of Plant Biology 59, 89–113.

Beyschlag W. & Eckstein J. (2001) Towards a causal analysis of stomatal patchiness: the role of stomatal size variability and hydrological heterogeneity. Acta Oecologica 22, 161–173.

Beyschlag W., Pfanz H. & Ryel RonaldJ. (1992) Stomatal patchiness in Mediterranean evergreen sclerophylls: Phenomenology and consequences for the interpretation of the midday depression in photosynthesis and transpiration. Planta 187.

Brodribb T.J. & Holbrook N.M. (2003) Stomatal Closure during Leaf Dehydration, Correlation with Other Leaf Physiological Traits. Plant Physiology 132, 2166–2173.

Brodribb T.J., McAdam S.A.M., Jordan G.J. & Martins S.C.V. (2014) Conifer species adapt to low-rainfall climates by following one of two divergent pathways. Proceedings of the National Academy of Sciences 111, 14489–14493.

Buckley T.N. (2005) The control of stomata by water balance. New Phytologist 168, 275–292.

Buckley T.N. (2019) How do stomata respond to water status? New Phytologist 224, 21–36.

Buckley T.N., Farquhar G.D. & Mott K.A. (1997a) Qualitative effects of patchy stomatal conductance distribution features on gas-exchange calculations. Plant, Cell and Environment 20, 867–880.

Buckley T.N., Farquhar G.D. & Mott K.A. (1997b) Qualitative effects of patchy stomatal conductance distribution features on gas-exchange calculations. Plant, Cell and Environment 20, 867–880.

Burlett R., Parise C., Capdeville G., Cochard H., Lamarque L.J., King A. & Delzon S. (2022) Measuring xylem hydraulic vulnerability for long-vessel species: an improved methodology with the flow centrifugation technique. Annals of Forest Science 79, 5.

Cardoso A.A., Brodribb T.J., Lucani C.J., DaMatta F.M. & McAdam S.A.M. (2018) Coordinated plasticity maintains hydraulic safety in sunflower leaves. Plant, Cell & Environment 41, 2567–2576.

Chaves M.M., Flexas J. & Pinheiro C. (2009) Photosynthesis under drought and salt stress: regulation mechanisms from whole plant to cell. Annals of Botany 103, 551–560.

Chen M., Zhu X., Zhang Y., Du Z., Chen X., Kong X., … Chen C. (2020) Drought stress modify cuticle of tender tea leaf and mature leaf for transpiration barrier enhancement through common and distinct modes. Scientific Reports 10, 6696.

Cochard H. (2002) A technique for measuring xylem hydraulic conductance under high negative pressures. Plant, Cell & Environment 25, 815–819.

Daley P.F., Raschke K., Ball J.T. & Berry J.A. (1989) Topography of Photosynthetic Activity of Leaves Obtained from Video Images of Chlorophyll Fluorescence. Plant Physiology 90, 1233–1238.

Dow G.J., Bergmann D.C. & Berry J.A. (2014) An integrated model of stomatal

development and leaf physiology. New Phytologist 201, 1218–1226.
Drake P.L., Froend R.H. & Franks P.J. (2013) Smaller, faster stomata: scaling of stomatal size, rate of response, and stomatal conductance. Journal of Experimental Botany 64, 495–505.
Faralli M., Mellers G., Wall S., Vialet-Chabrand S., Forget G., Galle A., … Lawson T. (2024) Exploring natural genetic diversity in a bread wheat multi-founder population: Dual imaging of photosynthesis and stomatal kinetics. Journal of Experimental Botany, erae233.
Flexas J., Bota J., Loreto F., Cornic G. & Sharkey T.D. (2004) Diffusive and Metabolic Limitations to Photosynthesis under Drought and Salinity in C 3 Plants. Plant Biology 6, 269–279.
Franks P.J. & Beerling D.J. (2009) Maximum leaf conductance driven by CO 2 effects on stomatal size and density over geologic time. Proceedings of the National Academy of Sciences 106, 10343–10347.
Gebrechorkos S.H., Sheffield J., Vicente-Serrano S.M., Funk C., Miralles D.G., Peng J., … Dadson S.J. (2025) Warming accelerates global drought severity. Nature.
Gupta A., Rico-Medina A. & Caño-Delgado A.I. (2020) The physiology of plant responses to drought. Science 368, 266–269.
Haefner J.W., Buckley T.N. & Mott K.A. (1997) A spatially explicit model of patchy stomatal responses to humidity. Plant, Cell and Environment 20, 1087–1097.
Hofmann T.A., Atkinson W., Fan M., Simkin A.J., Jindal P. & Lawson T. (2025) Impact of climate-driven changes in temperature on stomatal anatomy and physiology. Philosophical Transactions of the Royal Society B: Biological Sciences 380.
Hultgren A., Carleton T., Delgado M., Gergel D.R., Greenstone M., Houser T., … Yuan J. (2025) Impacts of climate change on global agriculture accounting for adaptation. Nature 642, 644–652.
Jain P., Huber A.E., Rockwell F.E., Sen S., Holbrook N.M. & Stroock A.D. (2023) Localized measurements of water potential reveal large loss of conductance in living tissues of maize leaves.
Jain P., Huber A.E., Rockwell F.E., Sen S., Holbrook N.M. & Stroock A.D. (2024) New approaches to dissect leaf hydraulics reveal large gradients in living tissues of tomato leaves. New Phytologist.
Jones H.G., Serraj R., Loveys B.R., Xiong L., Wheaton A. & Price A.H. (2009) Thermal infrared imaging of crop canopies for the remote diagnosis and quantification of plant responses to water stress in the field. Functional Plant Biology 36, 978.
Kamakura M., Kosugi Y., Muramatsu K. & Muraoka H. (2012a) Simulations and observations of patchy stomatal behavior in leaves of Quercus crispula, a cool-temperate deciduous broad-leaved tree species. Journal of Plant Research 125, 339–349.
Kamakura M., Kosugi Y., Takanashi S., Matsumoto K., Okumura M. & Philip E. (2011) Patchy stomatal behavior during midday depression of leaf CO2 exchange in tropical trees. Tree Physiology 31, 160–168.
Kamakura M., Kosugi Y., Takanashi S., Matsuo N., Uemura A. & Lion M. (2021) Temporal fluctuation of patchy stomatal closure in leaves of Dipterocarpus sublamellatus at upper canopy in Peninsular Malaysia over the last decade. Tropics 30, 41–51.
Kamakura M., Kosugi Y., Takanashi S., Tobita H., Uemura A. & Utsugi H. (2012b) Observation of the scale of patchy stomatal behavior in leaves of Quercus crispula using an Imaging-PAM chlorophyll fluorometer. Tree Physiology 32, 839–846.
Kamakura M., Kosugi Y., Takanashi S., Uemura A., Utsugi H. & Kassim A.R. (2015) Occurrence of stomatal patchiness and its spatial scale in leaves from various sizes of trees distributed in a South-east Asian tropical rainforest in Peninsular

Malaysia. Tree Physiology 35, 61–70.
Kane C.N., Jordan G.J., Jansen S. & McAdam S.A.M. (2020) A Permeable Cuticle, Not Open Stomata, Is the Primary Source of Water Loss From Expanding Leaves. Frontiers in Plant Science 11, 774.
Kotliar N.B. & Wiens J.A. (1990) Multiple Scales of Patchiness and Patch Structure: A Hierarchical Framework for the Study of Heterogeneity. Oikos 59, 253.
Lawson T. & Morison J. (2006) Visualising patterns of CO2 diffusion in leaves. New Phytologist 169, 641–643.
Lawson T., Oxborough K., Morison J.I.L. & Baker N.R. (2002) Responses of Photosynthetic Electron Transport in Stomatal Guard Cells and Mesophyll Cells in Intact Leaves to Light, CO2, and Humidity. Plant Physiology 128, 52–62.
Lawson T. & Weyers J. (1999) Spatial and temporal variation in gas exchange over the lower surface of Phaseolus vulgaris L. primary leaves. Journal of Experimental Botany 50, 1381–1391.
Lawson T., Weyers J. & A'Brook R. (1998) The nature of heterogeneity in the stomatal behaviour of Phaseolus vulgaris L. primary leaves. 9.
Leinonen I., Grant O.M., Tagliavia C.P.P., Chaves M.M. & Jones H.G. (2006) Estimating stomatal conductance with thermal imagery. Plant, Cell and Environment 29, 1508–1518.
Machado R., Loram-Lourenço L., Farnese F.S., Alves R.D.F.B., Sousa L.F., Silva F.G., … Menezes-Silva P.E. (2021) Where do leaf water leaks come from? Trade-offs underlying the variability in minimum conductance across tropical savanna species with contrasting growth strategies. New Phytologist 229, 1415–1430.
Marenco R.A., Siebke K., Farquhar G.D. & Ball M.C. (2006) Hydraulically based stomatal oscillations and stomatal patchiness in Gossypium hirsutum. Functional Plant Biology 33, 1103.
McAusland L., Davey P.A., Kanwal N., Baker N.R. & Lawson T. (2013) A novel system for spatial and temporal imaging of intrinsic plant water use efficiency. Journal of Experimental Botany 64, 4993–5007.
Monteith J.L. & Unsworth M.H. (2013) Principles of environmental physics: plants, animals, and the atmosphere, 4th ed. Elsevier/Academic Press, Amsterdam ; Boston.
Morison J.I.L., Gallouët E., Lawson T., Cornic G., Herbin R. & Baker N.R. (2005) Lateral Diffusion of CO2 in Leaves Is Not Sufficient to Support Photosynthesis. Plant Physiology 139, 254–266.
Mott K.A. & Buckley T.N. (1998) Stomatal heterogeneity. Journal of Experimental Botany 49, 407–417.
Mott K.A. & Buckley T.N. (2000) Patchy stomatal conductance: emergent collective behaviour of stomata. Trends in Plant Science 5, 258–262.
Mott K.A., Cardon Z.G. & Berry J.A. (1993) Asymmetric patchy stomatal closure for the two surfaces of Xanthium strumarium L. leaves at low humidity. Plant, Cell & Environment 16, 25–34.
Mott K.A. & Peak D. (2007) Stomatal Patchiness and Task-performing Networks. Annals of Botany 99, 219–226.
Murchie E.H. & Lawson T. (2013) Chlorophyll fluorescence analysis: a guide to good practice and understanding some new applications. Journal of Experimental Botany 64, 3983–3998.
Ochoa M.E., Henry C., John G.P., Medeiros C.D., Pan R., Scoffoni C., … Sack L. (2024) Pinpointing the causal influences of stomatal anatomy and behavior on minimum, operational, and maximum leaf surface conductance. Plant Physiology, kiae292.
Peak D., Hogan M.T. & Mott K.A. (2023) Stomatal patchiness and cellular computing.

Proceedings of the National Academy of Sciences 120, e2220270120.
Peak D., West J.D., Messinger S.M. & Mott K.A. (2004) Evidence for complex, collective dynamics and emergent, distributed computation in plants. Proceedings of the National Academy of Sciences 101, 918–922.
Petek-Petrik A., Petrík P., Lamarque L.J., Cochard H., Burlett R. & Delzon S. (2023) Drought survival in conifer species is related to the time required to cross the stomatal safety margin. Journal of Experimental Botany 74, 6847–6859.
Pörtner H.-O. & Roberts D.C. (2022) Climate Change 2022: Impacts, Adaptation and Vulnerability. 3068.
R Core Team (2020) R Core Team (2020) R: A Language and Environment for Statistical Computing. R Foundation for Statistical Computing, Vienna, Austria. https://www.r-project.org/.
Sack L. & Buckley T.N. (2016) The Developmental Basis of Stomatal Density and Flux. Plant Physiology 171, 2358–2363.
Sack, Pasquet-Kok & Megan Bartlett (2011) Leaf pressure-volume curve parameters.
Šantrůček J., Hronková M., Květoň J. & Sage R.F. (2003) Photosynthesis Inhibition During Gas Exchange Oscillations in ABA-Treated Helianthus annuus: Relative Role of Stomatal Patchiness and Leaf Carboxylation Capacity. Photosynthetica 41, 241–252.
Schneider C.A., Rasband W.S. & Eliceiri K.W. (2012) NIH Image to ImageJ: 25 years of image analysis. Nature Methods 9, 671–675.
Shannon C.E. (1947) A Mathematical Theory of Communication.
Shepherd T. & Griffiths D. (2006) The effects of stress on plant cuticular waxes. New Phytologist 171, 469–499.
Takanashi S., Kosugi Y., Matsuo N., Tani M. & Ohte N. (2006) Patchy stomatal behavior in broad-leaved trees grown in different habitats. Tree Physiology 26, 1565–1578.
Tombesi S., Nardini A., Frioni T., Soccolini M., Zadra C., Farinelli D., … Palliotti A. (2015) Stomatal closure is induced by hydraulic signals and maintained by ABA in drought-stressed grapevine. Scientific Reports 5, 12449.
Trueba S., Pan R., Scoffoni C., John G.P., Davis S.D. & Sack L. (2019) Thresholds for leaf damage due to dehydration: declines of hydraulic function, stomatal conductance and cellular integrity precede those for photochemistry. New Phytologist 223, 134–149.
Weyers J.D.B. & Lawson T. (1997) Heterogeneity in Stomatal Characteristics. In Advances in Botanical Research. pp. 317–352. Elsevier.
Wong S.C., Canny M.J., Holloway-Phillips M., Stuart-Williams H., Cernusak L.A., Márquez D.A. & Farquhar G.D. (2022) Humidity gradients in the air spaces of leaves. Nature Plants 8, 971–978.
Ziegler C., Coste S., Stahl C., Delzon S., Levionnois S., Cazal J., … Bonal D. (2019) Large hydraulic safety margins protect Neotropical canopy rainforest tree species against hydraulic failure during drought. Annals of Forest Science 76, 115.

2.8. Supporting Information

The following Supporting Information is available for this article:

FIGURE S4.1: Photosynthesis parameters along a drought sequence

FIGURE S4.2: Dynamic representation of quantum efficiency of photosystem II (Φ_{PSII})

FIGURE S4.3: Individual dynamic representation of quantum efficiency of photosystem II (Φ_{PSII}) for 40 patches during 10 minutes

FIGURE S4.4: Spatial dynamic representation of 30 patches for 10 minutes

FIGURE S4.5: Scheme of the experiment

FIGURE S4.6: Same leaf under the same environmental conditions except oxygen concentration in the air flow with (a) 21% and (b) 2%.

TABLE S4.1: Linear model fit results

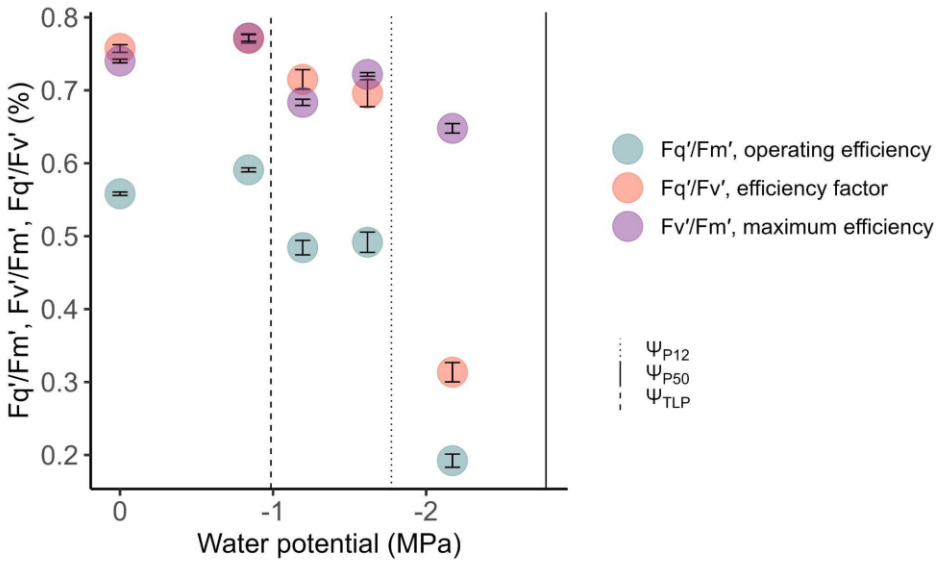

FIGURE S 4.1: Photosynthesis parameters along a drought sequence.
Blue/green dots: Φ_{PSII} or Fq'/Fm' the quantum efficiency of photosystem II, orange dots: Fq'Fv', the level of photochemical quenching of photosystem II and purple dots: Fv'Fm', the maximum efficiency of photosystem II. The water potential at turgor loss point, (Ψ_{tlp}; dashed line), the water potential inducing 12% losses of hydraulic conductivity in the stem, (Ψ_{12}; dotted line) and the water potential inducing 50% losses of hydraulic conductivity in the stem (Ψ_{P50}; solid line) are indicated.

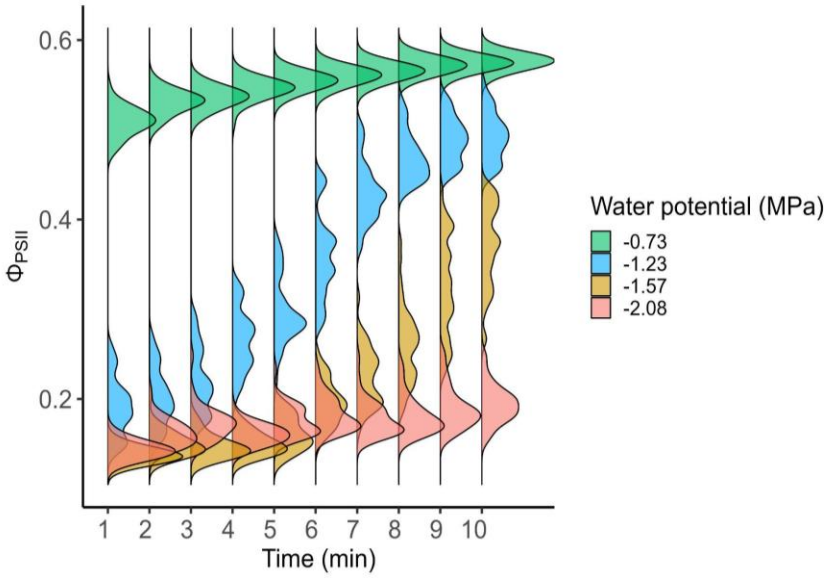

FIGURE S 4.2: Dynamic representation of quantum efficiency of photosystem II (Φ_{PSII}) during 10 minutes for the same leaf along a drought sequence.
Each density curve represents 40 patches. Colours represent the water potential of the leaf.

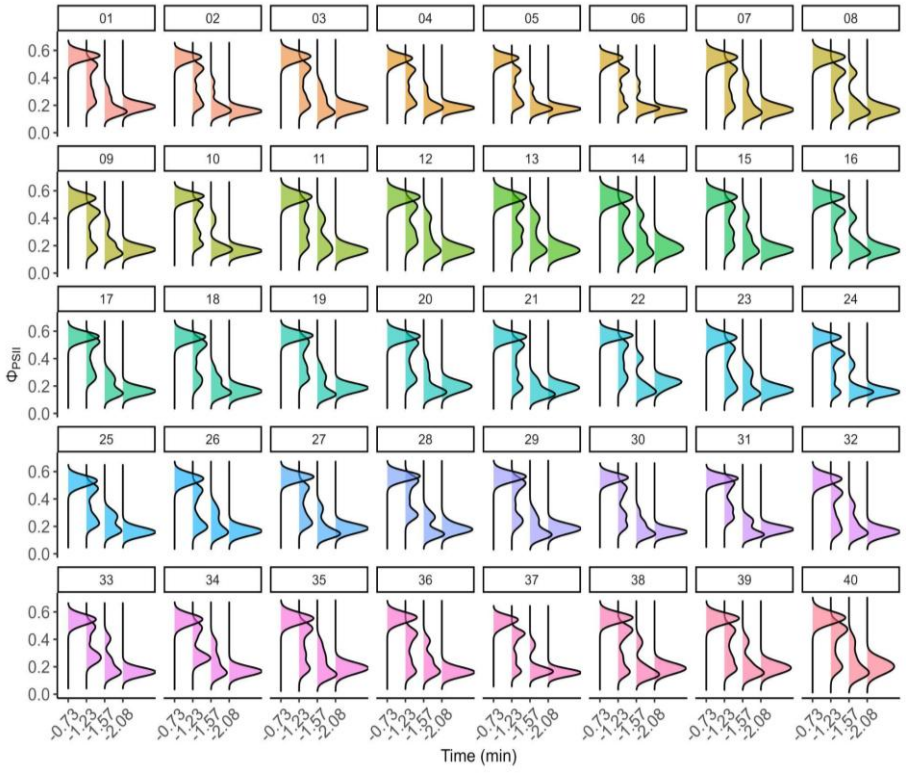

FIGURE S 4.3: Individual dynamic representation of quantum efficiency of photosystem II (Φ_{PSII}) for 40 patches during 10 minutes for the same leaf along a drought sequence.

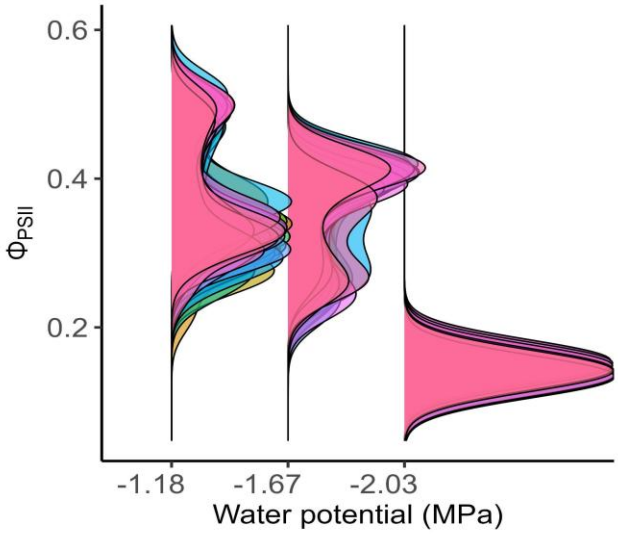

FIGURE S 4.4: Spatial dynamic representation of 30 patches for 10 minutes along a drought sequence for a leaf from a plant other than the one in Figure 6.
Each colour and density curve represent a patch during 10 mins.

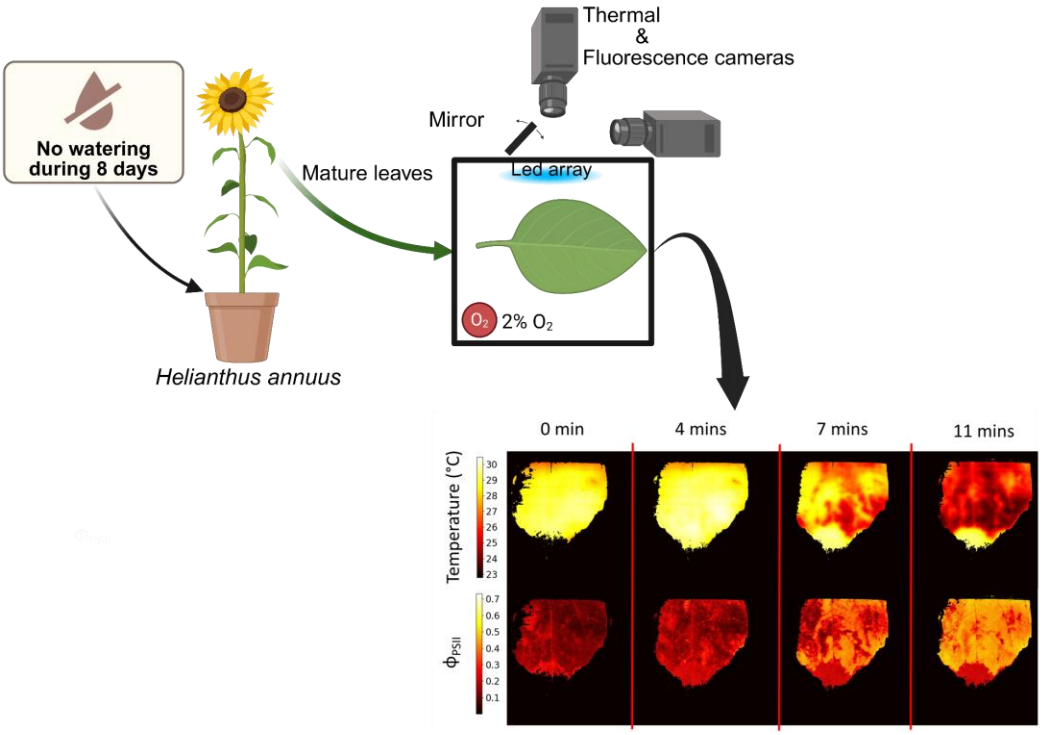

FIGURE S 4.5: Scheme of the experiment based on the system developed by (McAusland *et al.* 2013). The leaf is connected to the plant and placed into an open-box.
Oxygen is fixed at 2% to inhibit photorespiration (Murchie & Lawson 2013). Created in BioRender.com.

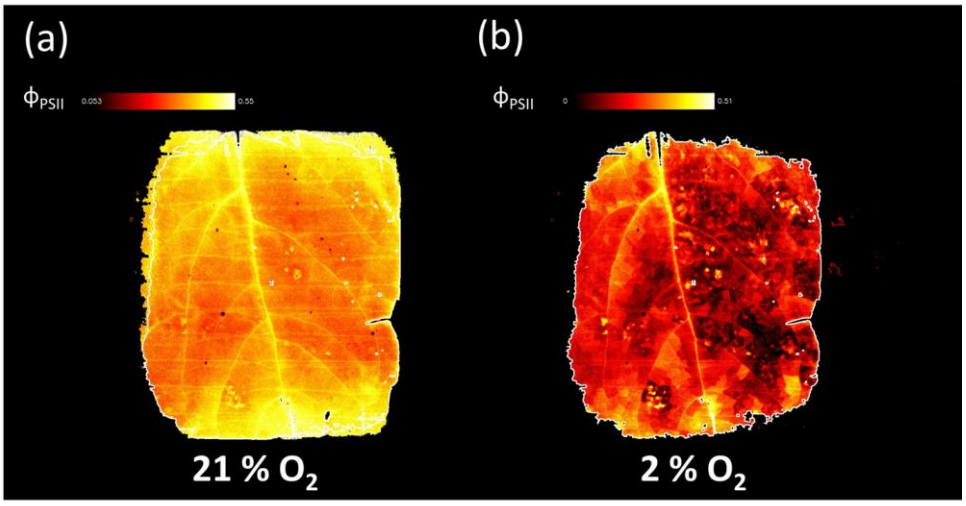

FIGURE S 4.6: Quantum efficiency of photosystem II, Φ_{PSII}, in a single leaf measured under consistent environmental conditions, with varying oxygen concentrations in the airflow: (a) 21% O_2, and (b) 2% O_2.

TABLE S 4.1: Linear model fit results

Model coefficient from figure 3

Formula: $\Phi_{PSII} = \frac{A_{sym}}{1+e^{\frac{X_{mid}-\Delta T}{S_{cal}}}}$

Estimate	Std.	Error	t value	Pr(>|t|)	
Asym	0.556611	0.008228	67.64	<2e-16	***
Xmid	3.764684	0.029727	126.64	<2e-16	***
Scal	-0.54255	0.037833	-14.34	<2e-16	***

Residual standard error: 0.05744 on 210 degrees of freedom

CHAPTER 5

Beyond stomatal closure: Leaf cuticle properties shape residual conductance during water stress

Chapter 5 Beyond stomatal closure: Leaf cuticle properties shape residual conductance during water stress

This chapter is presented in the form of a paper, entitled: "Drought-induced modification in leaf cuticle composition and their impact on minimum leaf conductance." By G. Forget, R. Burlett, M. Buridan, F. Domergue, S. Delzon and J. Joubes.
The detached leaf mass loss (DLML) measurements were conducted at BioGeCo, while the extraction of cutin and waxes was carried out at LBM, both laboratories affiliated with *the University of Bordeaux.*

1. Short introduction

Stomata represent the fastest response of leaves when exposed to stress, particularly drought. However, the cuticle, a thin layer composed of cutin polymer and waxes, also acts as an important barrier against many abiotic and biotic stresses. While drought often increases the amount of waxes and cutin in leaves, and sometimes their thickness in several species, some studies show no consistent link between waxes or cutin coverage and cuticular water permeability.

This chapter aims to study the response of the *Helianthus annuus* cuticle's response during a severe drought, depending on the leaf's age. In particular, we will separate the cuticle into its two main layers (the cutin polymer and waxes). The composition of each layer will be compared with the residual and minimum leaf conductance. Our results will show that leaves have a different residual water loss according to the age, linked to increased amounts of cutin and waxes. Interestingly, each layer exhibits a common response to drought, but not in terms of water loss.

2. Drought-*induced modification in leaf cuticle composition and their impact on minimum leaf conductance*

2.1. Abstract

During drought, the residual water loss occurs through both cuticle and incompletely closed stomata. However, the response and the relative contribution of the different layers of the cuticle, which are the cutin and waxes, to residual transpiration is not well understood. We quantified minimum leaf conductance (g_{min}) in *Helianthus annuus* using the detached leaf mass loss (DLML) method, while simultaneously assessing the cutin and waxes amount and composition on young and old leaves. Our comparative analysis highlights a significant difference in young and old leaves with a lower minimum leaf conductance associated with an increase the amount of cutin and waxes during drought in young compared to old leaves. Furthermore, in young leaves, the absence of a corresponding increase in cuticle thickness despite the increase in quantity suggests an increase in density that may alter the physicochemical properties of the cuticle. Additionally, throughout the drought sequence, on young leaves, only the cutin has a significant impact on water loss. Waxes, although responding to water stress, have no impact on water loss. This study highlights the importance of not considering the cuticle as a whole, but rather breaking it down into its main layers and studying them separately, as well as the importance of leaf age, particularly in crops such as *Helianthus annuus*.

Keywords

Drought stress, water loss, residual and minimum leaf conductance, cutin, waxes, Alkane, Alcohol.

2.2. Introduction

The leaf cuticle, a remarkable evolutionary adaptation that emerged approximately 450 million years ago, has played a pivotal role in the development and survival of terrestrial plants (Yeats & Rose 2013). This multifunctional structure serves as an interface between plant aerial organs and their environment, constituting a barrier against both biotic and abiotic stresses (Domínguez *et al.* 2017). The cuticle's primary functions include limiting water loss, maintaining structural integrity, and mitigating the effects of

excessive radiation, all of which are essential for plant survival in diverse terrestrial ecosystems (Shepherd & Griffiths 2006). The cuticle is composed of two main hydrophobic components. The cutin polymer layer with embedded polysaccharides and waxes (Yeats & Rose 2013). This structural arrangement is further enhanced by an outermost layer of epicuticular waxes (Yeats & Rose 2013). The cutin polymer is principally composed of C16 and C18 derivatives featuring hydroxy or epoxy mid-chain substitutes providing the main mechanical strength of the whole cuticle (Domínguez *et al.* 2011b; Domínguez *et al.* 2011a). Complementing this structure, cuticular waxes are overlaid on the cutin matrix and are typically a complex mixture of very-long-chain saturated aliphatic molecules and various non-acyl lipid cyclic components (Joubès & Domergue 2020).

With drought episodes increasing in both frequency and intensity across biomes (Pörtner & Roberts 2022), the leaf cuticle, as an interface, is at the forefront to cope with water scarcity in order to preserve physiological functions. The cuticle is a permeable layer allowing bidirectional water exchange with the atmosphere through a passive process driven by the water vapor diffusion gradient between the leaf interior and the surrounding air (Tredenick & Farquhar 2021; Kamtsikakis & Weder 2022). Leaf cuticle's response to drought is supported by an increase in waxes (Shepherd & Griffiths 2006) and cutin (Shellakkutti *et al.* 2022) deposition and it is often concluded that this increased helps protect plants from desiccation and enhances drought tolerance (Riederer & Schreiber 2001). This relationship between increased wax amounts and drought has been extensively documented in various plant species, including Arabidopsis (Kosma *et al.* 2009), wheat (Bi *et al.* 2017) and tea leaves (Chen *et al.* 2020). However, other studies have indicated that no consistent correlation exists between cuticular water permeability and wax coverage (Shellakkutti *et al.* 2022).

During drought, leaves continue to lose water by leaky stomata (Brodribb *et al.* 2014; Kane *et al.* 2020; Machado *et al.* 2021) and through the cuticle, a phenomenon referred to residual leaf conductance (g_{res}, mmol m^{-2} s^{-1}). Although g_{res} represents a small fraction of the stomatal conductance, it plays a crucial role in determining the time to hydraulic failure influencing plant survival under extreme water stress (Petek-Petrik *et al.* 2023). Importantly, g_{res} is not constant after the stomatal closure but varies along a drought sequence (Burlett *et al.* 2025) reflecting post-stomatal closure effects such as stomatal and cuticular leakage. Moreover, leaf age exerts a significant influence on

physiological functions, with older leaves exhibiting a loss of pigments and photosynthetic activity in sunflowers (Cabello *et al.* 2006). These changes, along with age-related declines in biochemical activity and natural weathering (Shepherd & Griffiths 2006), could result that older leaves are less effective at controlling water loss (Jordan & Brodribb 2007). To quantify g_{res}, several methods have been developed, among which the detached leaf mass loss (DLML) method is widely recognised for its simplicity and effectiveness (Kerstiens 2006; Duursma *et al.* 2019; Billon *et al.* 2020; Burlett *et al.* 2025). This method simulates severe drought conditions at leaf level and allows for reliable estimation of residual leaf conductance (Burlett *et al.* 2025). Due to the variability of the residual leaf conductance during the dehydration process, the minimum leaf conductance is determined at specific hydraulic thresholds ($g_{min\_at\_X}$) and used as a trait (Burlett *et al.* 2025).

To better understand how leaf responses to drought, it is essential to investigate cuticle layers dynamics across different developmental stages under drought conditions and to assess how cutin and waxes contribute to residual water loss. Along a water stress gradient, this study aims to: (i) estimate residual transpiration (i.e. g_{res}) between young and old leaves using the detached leaf mass loss (DLML) method; (ii) characterise the change in chemical composition of the cuticle (cutin and waxes) with increasing water stress in young and old fully expanded leaves and (iii) evaluate the influence of the cutin and dominant waxes compounds on minimum leaf conductance ($g_{min\_at\_P88}$) at the critical threshold of 88% loss of hydraulic conductivity, a point at which stomatal effects are minimised, allowing the role of the cuticle to be examined .We hypothesise that the different layers of the leaf cuticle respond to drought by accumulating compounds and therefore have an impact on water loss during severe drought. Furthermore, we hypothesise that ontogenetic variations in leaf structure affect the cuticle's response to water stress.

2.3. Materials and methods

2.3.1. Plant material

Helianthus annuus seeds were sown in plastic trays containing compost. *H. annuus* plants were placed in a glasshouse (average over the experiment period T_{amb}=24.5 ± 1.8°C and RH=65.3% ± 9.6% between 8.am and 6.pm and T_{amb}=19.3 ± 2.2°C and RH=75.4% ± 9.2% during the night) at the Grande Ferrade site (Villenave d'Ornon,

France). A growth phase of 45 days was respected before any measurements in *H. annuus* individuals to run experiments on fully expanded leaves. After the periods of growth, plants were divided into two sections, bottom leaves were considered as old leaves and top leaves were considered as young leaves (Figure S5.1). Plants were put under stress by stopping watering in groups of four individual plants.

2.3.2. Cuticular wax extraction and analysis

One hundred young and old leaves at different water potentials were excised then scanned with a scale reference in order to estimate the leaf area (A_{leaf}, m^2). Waxes were extracted by immersing the leaves in 20 mL of chloroform for 30 seconds, with 10 µg of internal standard (IS) docosane (1 mg/mL) added to the solvent. A total of 8 mL of the extract was collected in a tube and stored at 4°C until further processing. Chloroform was then completely evaporated by placing the tubes in a water bath at 40°C under air flow. The dried residue was derivatized by adding 150 µL of BSTFA + TMCS (N,O-Bis(trimethylsilyl)trifluoroacetamide with trimethylchlorosilane), followed by heating at 110°C for 15 minutes. BSTFA + TMCS was then completely evaporated under the same conditions. The resulting pellet was solubilised in 150 µL of hexane and transferred into vials. Samples were analysed with an Agilent 7890B gas chromatograph (Waldbronn, Germany) equipped with an HP-5MS column (30 m ×0.25 mm x 0.25 mm, Agilent) coupled with a flame ionization detector (FID). The initial temperature was set to 50°C for 1 min, then increased at 25°C min^{-1} to 150°C, held for 2 min at 150°C, followed by an increased at 10 °C min^{-1} to 320°C, and held for 3 min at 320°C, with helium (1.5 mL/min) as carrier gas, for a total run time of 30 min. Molecular identities were determined using an Agilent 7890A gas chromatograph equipped with a HP-5MS column and an Agilent 5975B mass spectrometer detector (70eV, mass to charge ratio 50 to 750; Waldbronn, Germany). The same GC program was used, with helium (1.5 mL/min) as carrier gas. Data collection and processing were performed using Agilent MassHunter software. The total amount of cuticular waxes was expressed per unit of leaf surface area (µg dm^{-2}). Leaf areas were determined by ImageJ v.1.53q (Schneider *et al.* 2012) before wax extraction.

2.3.3. Cutin monomer extraction and analysis

Cutin extraction was performed on the same 100 leaves already used for the wax extraction experiment by cutting six discs per leaf with a total surface of 4.71 cm^2 and incubating them in 2.5 mL of isopropanol at 85°C for 45 minutes. The samples were stored at 4°C until further processing. The isopropanol was evaporated, and the samples were sequentially washed with 3 mL of different solvent mixtures under continuous agitation (incubator wheel, speed: 40) at room temperature (RT): chloroform:methanol (C:M) 2:1 for 24 hours, C:M 1:2 for 24 hours, methanol for 24 hours, water for 2 hours, NaCl 2M for 6 hours, water for 1 hour, C:M 1:1 for 24 hours, and methanol for another 24 hours. The samples were dried at RT for 48 hours, followed by an additional 48-hour drying period in a desiccator. The dry residue (DW) was weighed. Depolymerization was performed by adding 2 mL of sulfuric acid (H_2SO_4) at 5% with 40 µg of IS (heptadecanoic acid, pentadecanol, and ω-pentadecalactone), followed by heating at 85°C for 3 hours. The reaction mixture was then extracted with 2 mL of 2.5% NaCl and 2.2 mL of methyl tert-butyl ether (MTBE), followed by centrifugation at 3300 rpm for 5 minutes. The upper phase was collected, mixed vigorously with 2 mL of Tris 100 mM/NaCl 0.9% (pH 8), and centrifuged again under the same conditions. The final upper-phase was collected and evaporated using a water bath at 40°C under air flow. The dried residue was derivatized with 150 µL of BSTFA + TMCS and heated at 110°C for 15 minutes, followed by total evaporation. The pellet was solubilized in 400 µL of hexane, transferred into vials, and analyzed by GC-MS as previously. The total amount of cutin monomers was expressed per unit of disk surface area (µg cm^{-2}).

2.3.4. Transmission electron microscopy

Leaf samples from two different leaf were collected under three distinct water potentials: well-hydrated (Ψ=-1.02 MPa; ~Ψ_{tlp}) and severely stressed (Ψ=-2.40 MPa; $\Psi_{P12}<\Psi<\Psi_{P50}$) and immediately fixed in 2.5% glutaraldehyde in 0.1 M phosphate buffer (pH 7.2) for 4 hours at 4 °C, followed by post-fixation in 1% osmium tetroxide for 2 hours at room temperature. Samples were then dehydrated through a graded ethanol series (30 min: ethanol 70%, 30 min: ethanol 100%, 2 times 20 min: Acetone) and embedded in Spurr's resin (1 h: 33% Spurr's resin + 66 % Acetone,1 h: 66% Spurr's resin + 33 % Acetone,1 h: 100% Spurr's resin and overnight 100% Spurr's resin). The resin was polymerized by incubating the embedded samples at 70 °C for 16–20 hours to ensure

complete curing. Ultra-thin sections (~70 nm) were obtained using an ultramicrotome (Leica EM UC7) and collected on copper grids. TEM imaging was performed using a FEI Tecnai G2 Spirit TWIN, operated at 120 kV to visualize the cuticle structure. Images were used to assess cuticle thickness (in µm) at 40 locations across each leaf using ImageJ v.1.53q software.

2.3.5. Hydraulic photosynthetic traits measurements

2.3.5.1. Water status measurement

We measured the leaf water potential (Ψ_{leaf}, MPa) with a pressure chamber (DG Meca, Gradigan, France) and a psychrometer (PSY1, ICT International, Armidale, NSW, Australia) directly on top leaves used for the mass loss of detached leaves method. This value of the water potential measured on the top young leaves serves as the reference leaf water potential for all other leaves on the same plant at that specific time.

2.3.5.2. *Relative water content*

Relative water content is a mass-derived important parameter that we used in the detached leaf mass loss (DLML) method for the determination of the water potential. Turgid weight (TW) of each individual leaf was measured before the water loss measurements in the climatic chamber. Weight measurements were performed with a 4-digit balance (Pioneer, Ohaus, USA). At the end of the measurement, leaves were put in an oven at 65°C for 72h and dry weight (DW) was measured. The relative water content (RWC) was then computed for each mass value (fresh mass; FW) during the dehydration process using equation 5.1:

$$RWC = 100 * \frac{FW - DW}{TW - DW} \quad (5.1)$$

2.3.5.3. Pressure-volume curve and stem embolism vulnerability

Pressure-volume curves were performed using a method adapted from Sack *et al.*, (2011) on eight leaves of *H. annuus*. Pressure-volume curves were used to determine leaf physiological traits such as the water potential (Ψ_{tlp}, MPa and RWC_{tlp}, %) at turgor loss point along with the elasticity modulus (ε) and osmotic potential at full turgor (π_0) (Table 5.1). Using ε and π_0 we estimated the water potential at any RWC during the DLML experiment based on the relative water content. Leaf water potential (Ψ_{leaf}, MPa) was

measured with a psychrometer (PSY1, ICT International, Armidale, NSW, Australia) before each measurement.

Stem vulnerability to xylem embolism was assessed on five replicates per species using the Cavitron technique (Cochard 2002; Burlett *et al.* 2022). Measurements were carried out at the platform for hydraulic traits (Caviplace, Phenobois platform, University of Bordeaux, Pessac, France). For each species a percentage loss of conductance or PLC curve was obtained and embolism vulnerability determined at thresholds Ψ_{P12}, Ψ_{P50} and Ψ_{P88} (MPa), which correspond to the xylem pressure/water potential inducing 12%, 50% and 88% losses of hydraulic conductivity, respectively.

To facilitate analysis, leaves were categorized by water potential measurements and divided into two classes using water potential at -1.5 MPa. There were leaves considered non-stressed (well-hydrated) [0; -1.5 MPa], or stressed [-1.5 MPa; -Inf].

TABLE 5.1: Leaf hydraulics variables used in this study. Mean and standard errors for each variable are provided.

Definition	Abbreviation	Unit	*H. annuus*
Relative water content	RWC	%	-
Relative water content at turgor loss point	RWC_{tlp}	%	77.98 ± 3.10
Water potentials at turgor loss point	Ψ_{tlp}	MPa	-0.98 ± 0.05
Water potentials inducing 12% losses of conductance in the stem	Ψ_{P12}	MPa	-1.77 ± 0.15
Water potentials inducing 50% losses of conductance in the stem	Ψ_{P50}	MPa	-2.78 ± 0.18
Elasticity modulus	ε	MPa	2.03 ± 0.31
Osmotic potential at full turgor	π_0	MPa	-0.74 ± 0.06

2.3.5.4. Quantum efficiency in light

Quantum efficiency in light was measured using a porometer (LI-600; LICOR, USA) and referred to the operating quantum yield of Photosystem II (PSII, unitless). This value represents the proportion of light absorbed by chlorophyll that is actually used for photochemistry under current light conditions. Quantum efficiency provided a rapid, non-destructive parameter to assess drought effects on plant photosynthetic performance and had been used to assess the leaves viability.

2.3.5.5. Residual leaf conductance (g_{res}) and estimation of residual leaf conductance at different hydraulic thresholds (g_{min})

Seventy-seven *H. annuus* leaves were cut at different water potentials with a razor blade, weighed and placed in a glass tube filled with water. The glass tube was placed in the dark for at least 12 hours into a box in order to rehydrate the leaf and close stomata avoiding the wrong way effect. We assume that the physical and chemical properties of the cuticle remain unchanged during the rehydration and the experiment, as the short time scale and use of detached leaves do not allow for the biosynthetic changes typically observed during drought. Such changes in wax coverage, thickness, or composition have been reported to occur only after 1 to 15 days following drought initiation (Chen *et al.* 2020). In this context, after the leaf excision, the cuticle composition didn't change during the experiment and corresponds to the composition at this water stress. Moreover, we assume a constant cuticular conductance estimated at Ψ_{P88} in order to have a minimal impact of stomata on water loss. After 12 hours, their petiole end was sealed with paraffin to avoid water loss. Each leaf was weighed with a 4-digit balance (Pioneer, Ohaus, USA) and scanned (v850 pro, Epson, Japan) to estimate leaf area (A_{leaf}, m^2). Leaves were then clipped to load cells inside a climatic chamber to simulate drought through desiccation (Billon *et al.*, 2020). Conditions inside the chamber were stable at 25 °C and 60% of relative humidity, with a vapour pressure deficit (VPD) of c. 1.26 kPa. We assume the leaf temperature equals the surrounding air temperature; the small temperature difference is neglected when computing the VPD. Micro load cells by Wheastone bridge board (1046_OB, Phidgets Inc., Canada) were used to measure the mass every five minutes in the chamber. During measurements, samples were placed in the dark to avoid light impacting stomatal kinetics. A custom function in R was developed for the parameterisation and treatment of raw data (*g_residual*, PHENOBOIS, University of Bordeaux; https://gitub.u-bordeaux.fr/phenobois).

The function, g_residual, calculates the residual leaf conductance as the slope of the mass data over time (equation 5.2) using the Savitsky-Golay filter to smooth the data and calculate derivatives on noisy data. The same function computes the corresponding RWC, water potential and VPD for each time step.

Residual leaf conductance g_{res} (mmol m^{-2} s^{-1}) was computed for each leaf as the water evaporation rate divided by its driving force (VPD) using equation 5.2:

$$g_{res} = \frac{dw/dt}{M_{H2O}\, A_{leaf}} \times \frac{Patm}{VPD} \quad (5.2)$$

, where dw/dt is the slope of the mass (g s^{-1}), M_{H2O} is the molecular weight of water (18.01 g mol^{-1}), P_{atm} is the atmospheric pressure in the chamber (*c*. 101.9 kPa) and VPD is the measured vapour pressure deficit of the air inside the chamber (kPa) calculated at each time step.

Leaf water potential decreases during drought, and crosses different hydraulics thresholds such as turgor loss point (Ψ_{tlp}), which coincides with the stomatal closure (Brodribb *et al.* 2003), along with Ψ_{P12}, Ψ_{P50} and Ψ_{P88}, corresponding to the water potentials inducing 12%, 50% and 88% losses of conductance, respectively. Recent research has described the variability of g_{res} across leaf dehydration, hence promoting the use of physiology-informed thresholds of water status to measure minimum (g_{min}) leaf conductance (Burlett *et al.* 2025). We estimated g_{min} at each relevant threshold described above, to establish a hydraulic trait that could facilitate interpretation and comparison between species.

2.3.6. Data processing and analysis

All data processing and analysis was carried out using R v.2022.12.0 (R Core Team 2020). To compare two groups, a Student t test was performed after checking for normality and homogeneity of variance. Non-parametric tests were used (Man Whitney test), when normality is not reached. Data are expressed as mean ± se. Linear and mixed linear models have been done using the package “stats” and “lme4” R package (Bates, Mächler, Bolker & Walker 2015). The principal component analysis (PCA) was tested using the “factoextra” R package (Kassambara & Mundt 2020). To cope with missing data (especially for the minimum leaf conductance at Ψ_{P88}, data were missing), we simulated missing values based on variables using the “missMDA” R package to run a second PCA (Josse & Husson 2016).

2.4. Results

2.4.1. Residual and minimum leaf conductance at Ψ_{P88} along drought

Continuous measurements of mass loss in 77 leaves yielded dehydration curves from which residual leaf conductance along a stress gradient could be deduced. Residual

leaf conductance declined as leaf water potential decreased during dehydration across all groups (Figure 5.1). At every hydraulic threshold, old leaves (triangles) maintained a higher minimum leaf conductance than young leaves (dots). Leaf water status before excision had an impact on the residual and minimum leaf conductance where original stressed leaves (red colour) had a lower value than well-hydrated leaves (green colour) for both old and young leaves. Before the turgor loss point, residual leaf conductance was constant for young leaves contrary to old ones where the decline started before the threshold. Between the turgor loss point and Ψ_{P50}, the slope was pronounced for each group indicating stomatal impact composed of stomatal closure dynamics and leakiness. Beyond the Ψ_{P50}, the residual leaf conductance is constant for the young leaves but continue to decrease until a stabilisation at Ψ_{P88} for the old leaves. Stomatal impact was more important for old than young leaves with residual leaf conductance always above.

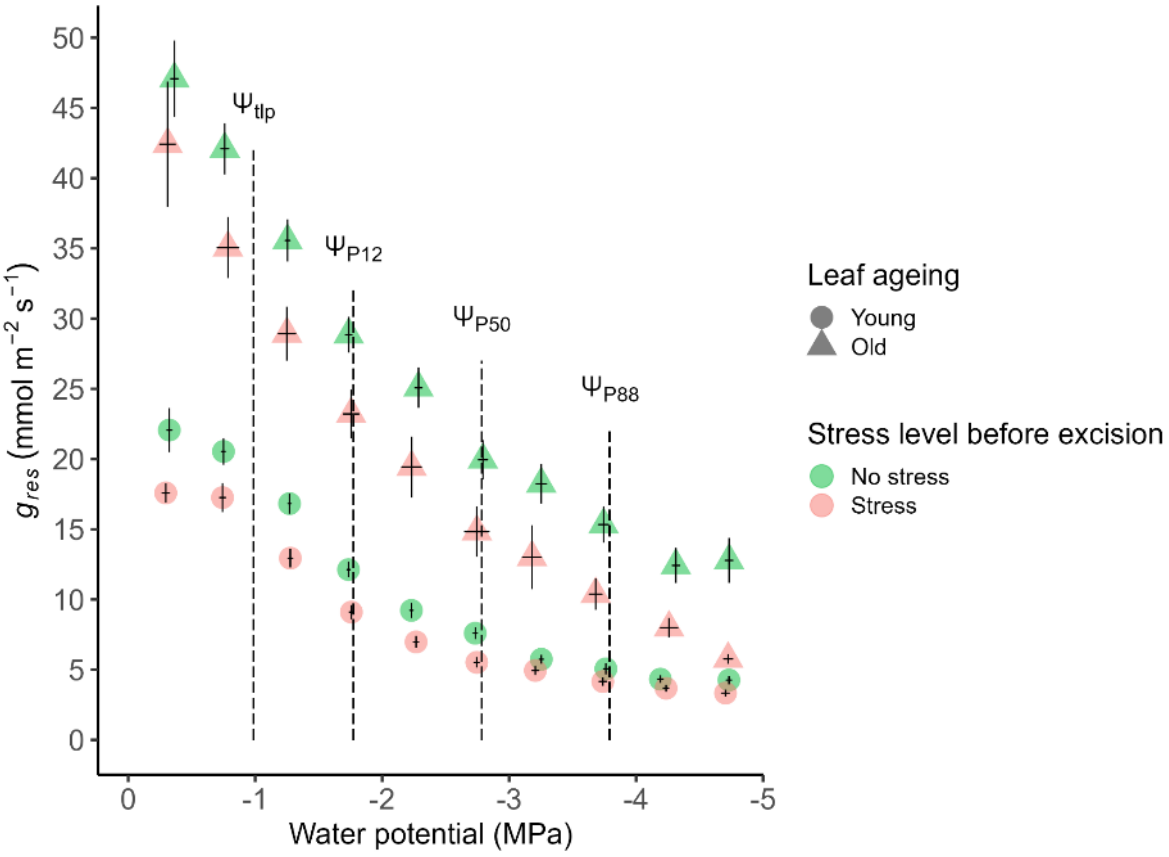

FIGURE 5.1: Residual leaf conductance dynamics along a drought sequence according to leaf ageing (dots=young leaves and triangle = old leaves) and leaf water status indicating by colour: green for well-watered leaves (water potential > –1.5 MPa) and red for drought-stressed leaves (water potential < –1.5 MPa).
Error bars for each dot represent the standard error.

We choose to use the Ψ_{P88} in order to minimise stomatal impact during dehydration (Figure 5.2). At Ψ_{P88}, minimum leaf conductance ($g_{min\_at\_P88}$) differed significantly between stressed and well-watered conditions in old leaves ($p<0.01$), whereas no significant difference was observed in young leaves (Figure 5.2). Additionally, $g_{min\_at\_P88}$, values were significantly higher in old compared to young leaves under both well-watered ($p < 0.001$) and stressed conditions ($p < 0.01$) (Figure 5.2).

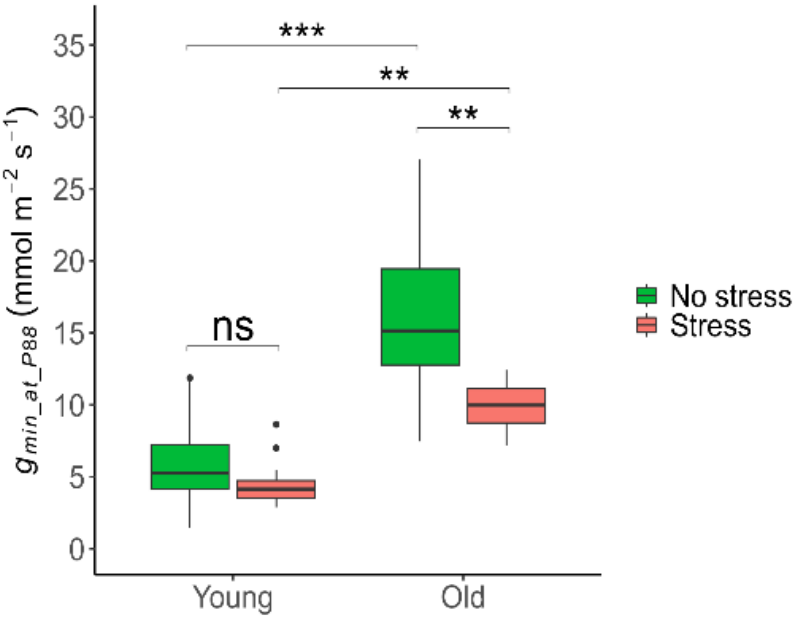

FIGURE 5.2: $g_{min\_at\_P88}$ in relation to leaf age and drought stress class.
Green boxplots indicate well-watered leaves (leaf water potential > –1.5 MPa), and red boxplots indicate drought-stressed leaves (leaf water potential < –1.5 MPa). Statistical differences were assessed using a Student's t-test (***, p<0.001; **, p<0.01; ns, p> 0.05) except when assumptions are not validated in which case the Mann-Whitney test was used.

2.4.2. Impact of water stress on cutin monomer composition according to leaf ageing

Cutin extraction revealed that cutin was a polyester primarily composed of hydroxy fatty acids, typically ω-hydroxy fatty acids with one or two additional midchain hydroxyl groups or an epoxy group. These monomers derived from saturated C16 and unsaturated C18 fatty acids. The main monomer in *H. annuus* cutin was the 10,16-dihydroxyhexadecanoic acid (10,16-diOH-C16:0); a saturated C16 ω-hydroxy fatty acid with an additional mid-chain hydroxyl group, with a proportion of between 75.1% and 81.6% depending on the level of stress and the age of the leaves (Figure S5.2). The 10,16-dihydroxyhexadecanoic acid amount differed significantly between stressed and

well-watered conditions in young leaves (p<0.01), whereas no significant difference was observed in old leaves (Figure 5.3). Moreover, the 10,16-dihydroxyhexadecanoic acid amount were significantly higher in young compared to old leaves under both well-watered ($p < 0.001$) and stressed conditions ($p < 0.001$) (Figure 5.3).

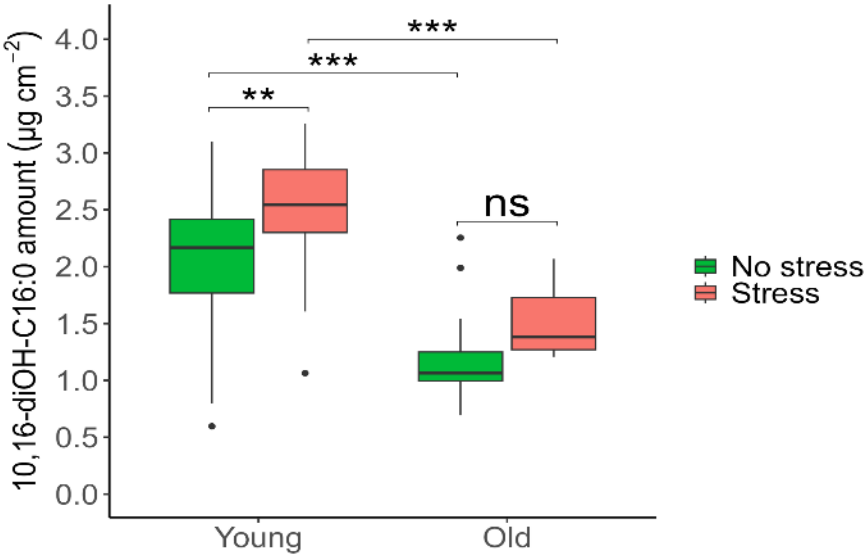

FIGURE 5.3: Amount of 10,16-dihydroxyhexadecanoic acid in relation to leaf age and drought stress class. Green boxplots indicate well-watered leaves (leaf water potential > –1.5 MPa), and red boxplots indicate drought-stressed leaves (leaf water potential < –1.5 MPa). Statistical differences were assessed using a Student's t-test (***, p<0.001; **, p<0.01; ns, p> 0.05) except when assumptions are not validated in which case the Mann-Whitney test was used.

There is a significant negative correlation between the amount of the main cutin monomer, the 10,16-dihydroxyhexadecanoic acid and the $g_{min\_at\_P88}$ for both young (R=-0.6, R^2=0.36, p<0.001) and old (R=-0.59, R^2=0.35, p<0.05) leaves (Figure 4). Water losses by the non-stomatal part was related to the amount of the 10,16-dihydroxyhexadecanoic acid.

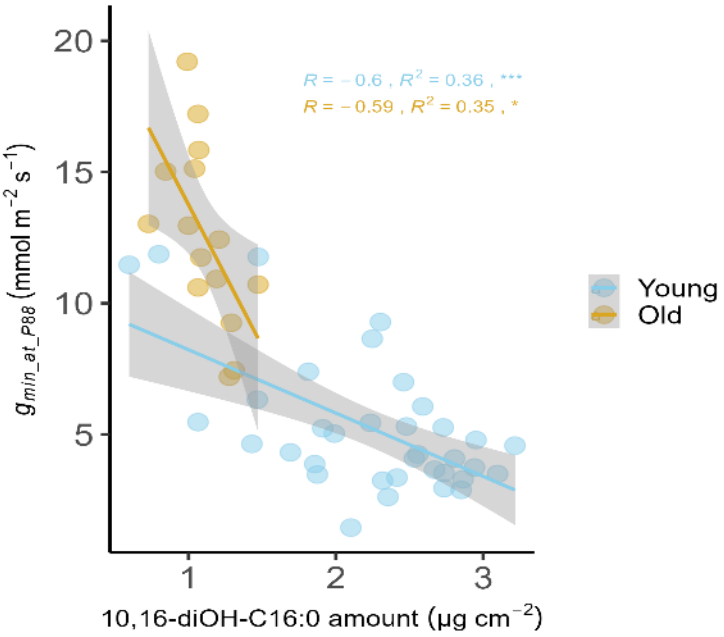

FIGURE 5.4: $g_{min\_at\_P88}$ as a function of the amount of 10,16-dihydroxyhexadecanoic acid.
Dots represent young leaves (blue colour) and old leaves (gold colour). Pearson correlation analysis with 95% confidence interval. R corresponds to the Pearson's correlation coefficient, R² to the coefficient of determination and stars to the p-value (***, p<0.001; *, p<0.05).

2.4.3. Impact of water stress on cuticular wax composition according to leaf ageing

Sunflower epicuticular waxes are mainly composed of three families of aliphatic compounds of very long chain fatty acids (VLCFAs) (C22 to C28) and their derivatives: VLC-alkanes (C25 to C31) and VLC-primary alcohols (C22 to C32) which are the main wax components (Figure S3). The heat map of Figure 5, represented the dynamic along the drought sequence for each scale compound with a distinction between the young and old leaves. In young leaves, the wax composition responded to water stress for most compounds, showing a significant positive correlation for all except C32 alcohol and C22 fatty acid. In contrast, waxes from old leaves showed no correlation with water stress (Figure 5.5).

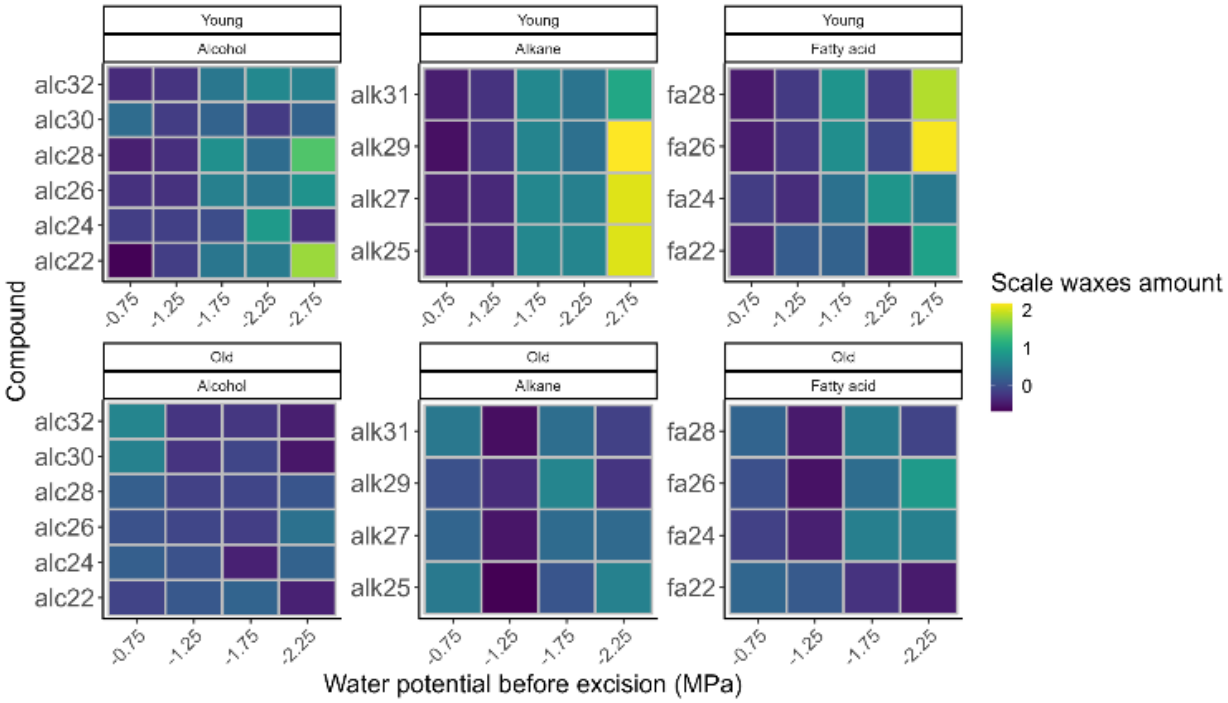

FIGURE 5.5: Heat map of cuticular wax amount by compound along a drought sequence for the young and old leaves. Cuticular waxes are scaled by 2 modalities (family compound and leaf's ageing) in order to facilitate the interpretation.

Due to the lack of correlation (Figure S5.4) for the old leaves, we focused only on young leaves to represent the relationship between the wax component family sum (represented as the sum of all compounds) versus the $g_{min\_at\_P88}$ but there was no correlation between the alkane, primary alcohol and fatty acids families versus $g_{min\_at\_P88}$ (Figure 5.6). Unlike the 10,16-dihydroxyhexadecanoic acid amount, the cuticular wax amount didn't have a correlation with the minimum leaf conductance at Ψ_{P88}.

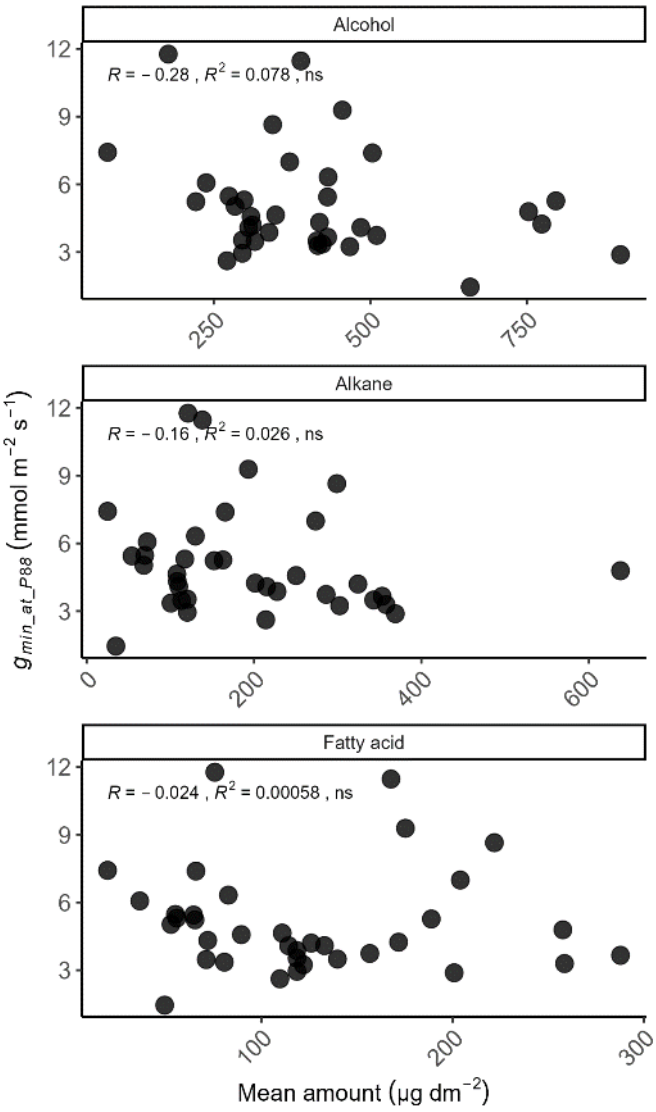

FIGURE 5.6: $g_{min\_at\_P88}$ as a function of mean amount by cuticular wax family. Dots represent young leaves. R corresponds to the Pearson's correlation coefficient, R² to the coefficient of determination and stars to the p-value (ns, p> 0.05).

2.4.4. Impact of water stress on leaf 's cuticle

A principal component analysis (Figure 5.7), revealed that water stress impacts both the amount of cutin monomers represented by the 10,16-dihydroxyhexadecanoic acid and waxes amount. However, changes in the cutin and waxes did not alter the minimum leaf conductance at Ψ_{P88} to the same extant. The first two principal components explained 64.6% of the total variance, with PC1 accounting for 39.2% and PC2 for 25.4% (Figure S5.5 and S5.6). The PCA biplot (Figure 5.7) displays clear clustering of the four experimental groups. Each group is enclosed within a 95% confidence ellipse, highlighting the distinction among treatments. Notably, young leaves with stress samples

(red crosses) are well separated along PC1, indicating strong differentiation from the other groups, particularly in relation to higher values of alkane, primary alcohol, and fatty acid amounts suggesting that stressed young leaves had more waxes than others leave especially the stressed old leaves. In contrast, old leaves under stress (brown triangles) are clearly separated along the PC2, positively correlated with the $g_{min\_at\_P88}$ and negatively with the PSII. This separation suggested that old stressed leaves had a low PSII efficiency and a high $g_{min\_at\_P88}$. Old (golden circles) and young leaves (blue squares) with no stress overlap more closely, suggesting greater similarity in their component composition. Along the drought gradient, young leaves responded with an increase in wax amount instead of old leaves.

The variable vectors indicate the contribution and direction of each trait to the principal components. Traits such as alkane, alcohol, and fatty acid amounts are positively associated with PC1 and are mostly expressed in the young with stress group. Conversely, water potential before excision and $g_{min\_at\_P88}$ are negatively associated with PC1 and are more closely related to the old leaves with no stress group. PC2 is primarily influenced by the efficiency of photosystem II, PSII efficiency, dry mass cutin, and cutin, which are more strongly associated with the young leaves with no stress group. Overall, the PCA reveals that stress treatment and leaf age both contribute to distinct physiological and biochemical trait profiles, with stress in young leaves driving the most pronounced separation along the primary axis of variation.

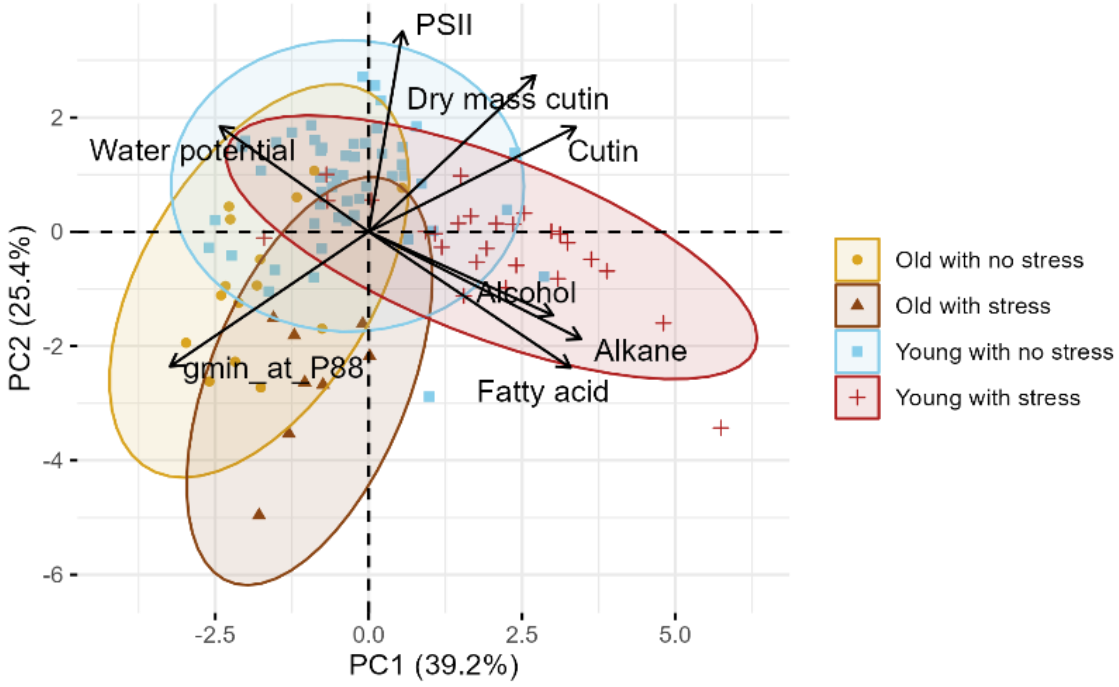

FIGURE 5.7: Principal component analysis (PCA).
PCA reveals variation in water loss and cuticle composition along a drought sequence collapse onto two axes explaining 64.6% of the variation for component traits. PC1 and PC2 correspond to 39.2% and 25.4% of the variation, respectively. Black arrows denote the contribution and direction of each variable to the principal components and correspond to the leaf water potential before excision, (MPa); $g_{min\_at\_P88}$, (mmol m^{-2} s^{-1}); dry mass cutin, (µg); 10,16-dihydroxyhexadecanoic acid amount (cutin), (µg cm^{-2}); total alkane, primary alcohol and fatty acids amount (µg dm^{-2}) and the quantum efficiency, PSII or Φ_{PSII}. Points represent individual samples (n=100), coloured and shaped by group: old leaves with no stress (golden circles), old leaves with stress (brown triangles), young leaves with no stress (blue squares), and young leaves with stress (red crosses). Ellipses indicate 95% confidence intervals for each group.

2.4.5. Impact of drought on cuticle thickness

Transmission electron microscopy (TEM) images revealed that the stressed young leaves (Ψ=-2.40 MPa) did not have a significantly thicker cuticles than unstressed leaves (Ψ=-1.02 MPa) (Figure 5.8). On average, the cuticle thickness of young unstressed leaves was 0.0770 ± 0.0024 µm whereas the thickness of young stressed leaves was 0.0738 ± 0.0015 µm. Cuticle thickness corresponded to 0.068 % and 0.120 % of the total leaf thickness in well watered and stressed leaf, respectively. This difference was due to the leaf shrinkage during drought ($p<0.001$) (Figure S5.8).

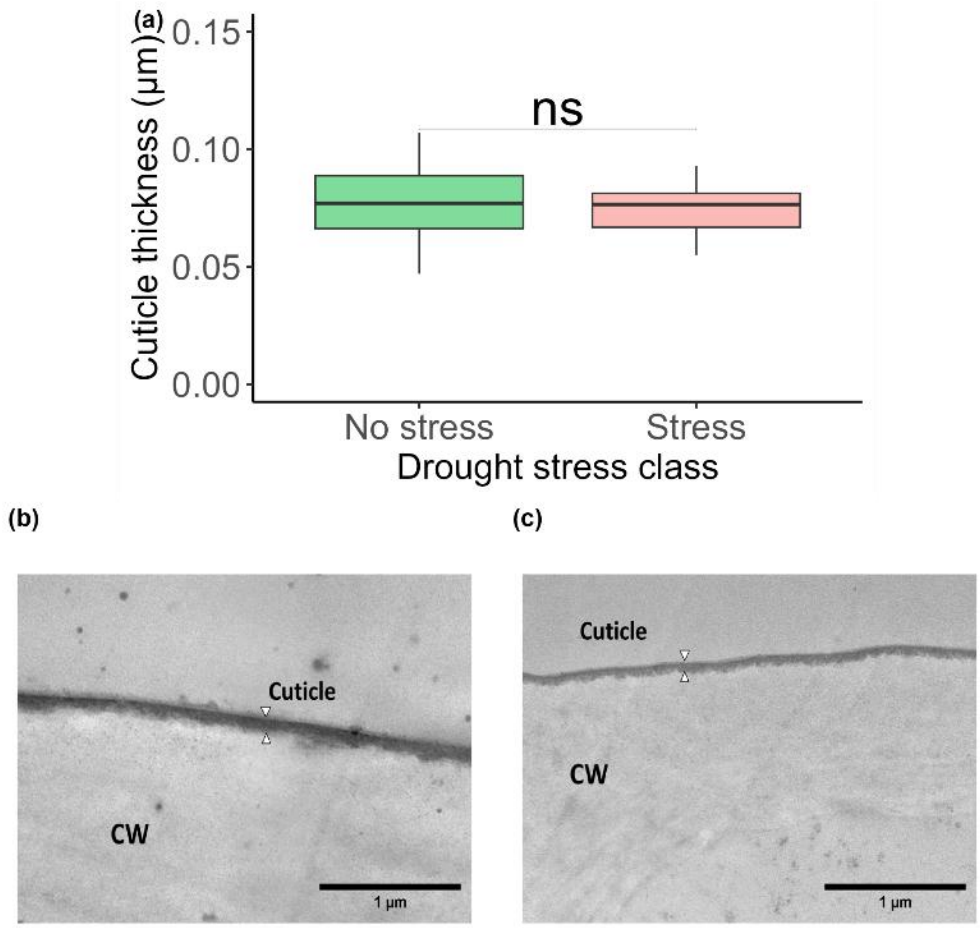

FIGURE 5.8: Cuticle thickness for young leaves in relation to drought stress class.
(a) Green boxplots indicate a well-watered leaf (Ψ= -1.02 MPa (~Ψ_{tlp}, No stress)), and red boxplots indicate a drought-stressed leaf (-2.40 MPa (Ψ_{P12}<Ψ<Ψ_{P50}, Stress)). Statistical differences were assessed using a Student t test (ns, *p*> 0.05). Images from TEM at (b) Ψ= -1.02 MPa (~Ψ_{tlp}, No stress) and (c) Ψ= -2.40 MPa (Ψ_{P12}<Ψ<Ψ_{P50}, Stress). Abbreviation: CW; Cell Wall.

2.5. Discussion

Investigating water loss after stomatal closure in crop species like *Helianthus annuus* reveals that both drought stress and leaf ageing significantly influence minimum leaf conductance, with the leaf cuticle emerging as a contributing factor. Analysis of both types of components of the cuticle, cutin and waxes, showed that their accumulation increases significantly with increasing water stress but this increase is notably confined to young fully expanded leaves. The increase in amount of the cutin and waxes layers does not have the same effect on water loss after stomatal closure, with a significant correlation between cutin monomer amount and minimum leaf conductance at Ψ_{P88} whereas there is no impact of waxes accumulation on water loss.

2.5.1. Stomatal closure efficiency and leakiness drives residual leaf conductance in young leaves during drought but what about the cuticle?

At each hydraulic threshold (Figure 5.1), young leaves exhibit significantly lower residual leaf conductance than older leaves, regardless of the level of water stress. The decrease along the water stress gradient in the residual leaf conductance for each leaf type could come from incompletely closed stomata (Machado *et al.* 2021; Burlett *et al.* 2025). The significant difference between young and old leaves can be the result of a more rapid stomatal closure in young leaves (Jordan *et al.* 1975; Reich 1984) thereby limiting leakiness without stopping it completely (Brodribb *et al.* 2014 ; Kane *et al.* 2020 ; Machado *et al.* 2021) (Figure 5.1). Furthermore, in terms of the cuticle, this difference between young and old leaves might be the result of a less healthy cuticle, thinner or with cracks generating passive leaks (Jordan & Brodribb 2007) reducing the capacities of this hydrophobic barrier. Individually, old leaves physiologically active (with a fewer efficiency of photosystem II than young leaves, Figure S5.7) may strongly alter the time to reach hydraulic failure due to their higher residual leaf conductance. However, at the plant level, this impact may not be significant, as young leaves contribute more to overall water loss due to the ratio between the number of young and old leaves. As both minimum leaf conductance and stomatal conductance change with leaf ontogeny, this variability should be considered when calculating the time to hydraulic failure (Urli *et al.* 2013; Li *et al.* 2016) or the stomatal margin retention index ($SMRI_{\Psi 50}$) (Petek-Petrik *et al.* 2023).

Studying the residual leaf conductance at a hydraulic threshold like Ψ_{P88} (Figure 5.2), minimising stomatal leakiness impact, reveals that there is no difference between water stressed and unstressed young leaves unlike to old leaves, questioning the cuticle impact during drought. Recent literature reports that there is a physiological response of the leaf cuticle by increasing compound amounts with increasing water stress (Kosma *et al.* 2009; Bi *et al.* 2017; Chen *et al.* 2020) but with contrary conclusions about which layers are involved in limiting water loss (Shellakkutti *et al.* 2022). The detached leaf mass loss (DLML) method is an accurate method to estimate the bulk residual then the minimum leaf conductance with increasing water stress but it does not allow the contribution of the cuticle to be separated from that of the stomata. To accurately estimate cuticular conductance, the detached leaf mass loss (DLML) method could be combined with the red-light method recently developed by Márquez *et al.* (2022).

2.5.2. Leaf's cuticle physiological response during drought

Studying the leaf cuticle solely under the lens of epicuticular waxes may offer an incomplete understanding of the cuticle biosynthesis under abiotic stresses such as drought. The cuticle is a multilayered structure, comprising the epi- and intracuticular waxes and the cutin polymer matrix, each of which exhibit distinct compositional changes and responses to environmental stress (Domínguez *et al.* 2011a; Heredia *et al.* 2024; Zhao *et al.* 2025). Overlooking this structural complexity risks missing critical insights into how different layers contribute to limiting water loss during drought.

2.5.2.1. Cutin monomer as the principal barrier to water loss from the leaf surface

Our findings indicate a strong association between minimum leaf conductance at Ψ_{P88} ($g_{min\_at\_P88}$) and the major cutin monomer, 10,16-dihydroxyhexadecanoic acid, the quantity of which varies with both leaf age and drought stress (Figure 5.3). In *H. annuus*, the cutin matrix responds to a drought by enhancing the amount of this cutin monomer. Statistical comparisons reveal that $g_{min\_at\_P88}$ is significantly lower in young leaves, whereas cutin content is significantly higher, regardless of stress treatments (Figures 5.2 and 5.3). These findings highlight a clear impact of the cutin matrix on water loss, indicating that the leaf age plays a role in regulating cutin properties independent of external abiotic stress such as drought. This age-dependent difference is further supported by the PCA (Figure 5.7), which reveals a strong inverse loading between $g_{min\_at\_P88}$ and 10,16-dihydroxyhexadecanoic acid amount. The direction of the $g_{min\_at\_P88}$ vector is opposite (strong negative correlation) to those cutin-related vectors (cutin amount and dry mass cutin), emphasising that the cutin is implicated to limited water loss in *H. annuus*. The clustering of young well-watered and young stressed leaves toward the upper left quadrant, closely aligned with higher cutin amount suggests that young leaves maintain a structurally protective cuticle, which may contribute to their lower $g_{min\_at\_P88}$. By contrast, older leaves, particularly during drought, shift away from this region and toward higher g_{min} values. Overall, these patterns strongly support that 10,16-dihydroxyhexadecanoic acid is a key component of the cuticle in *H. annuus* to limit non-stomatal water loss independently of the leaf water potential. As a complex and pivotal structure for leaf integrity, the cutin biosynthesis is influenced by genetic and

environmental factors such as biotic (pathogens) or abiotic multistress (including drought, salinity, extreme temperatures) (Yeats & Rose 2013; Zhao *et al.* 2025).

2.5.2.2. Epicuticular waxes: drought-responsive but do not limit water loss

Epicuticular waxes are altered by water stress (Figure 5) such as the cutin polymer and their accumulation with increasing water stress is not linked to a significant reduction in $g_{min\_at\_P88}$ (Figure 6 and 7), which is consistent with prior studies (Zeisler-Diehl *et al.* 2018; Grünhofer *et al.* 2022; Grünhofer *et al.* 2024; Shellakkutti *et al.* 2022). Highlighting the age-dependent response shows that wax biosynthesis is not uniform along the plant's life cycle. Older leaves, at an advanced stage of senescence, exhibit a reduced capacity to accumulate waxes, associated with a lower regulation of the MYB transcription factor (Seo *et al.* 2011), as a consequence of decreased ABA levels (McAdam *et al.* 2022). Like for the cutin polymer, the plant during drought sequence tries to privilege leaves with high physiological impact and limit biosynthesis in senescence leaves (Munné-Bosch & Alegre 2004).

Although epicuticular waxes do not appear to limit water loss directly, their functional role as an external barrier during drought must be sought elsewhere. The Principal Composant Analysis completes informations where vectors representing major epicuticular wax family are oriented orthogonally to the g_{min} vector. This indicates a lack of association between wax amount and minimum leaf conductance, reinforcing the conclusion that waxes do not directly influence water loss after stomatal closure. The accumulation of epicuticular waxes in young leaves under drought conditions (Figure 5.5 and 5.7) likely represents an adaptive strategy to increase surface reflectance, thereby protecting tissues from harmful radiation. Specifically, these waxes might help to mitigate the impact of short-wavelength ultraviolet radiation including UV-B (280–315 nm) and UV-A (315–400 nm) as well as thermal radiation, particularly in the near-infrared (700–1400 nm) and shortwave radiation (1400–2500 nm) regions. This reflectance-based protection may reduce both photodamage and leaf overheating (Shepherd & Griffiths 2006; Lewandowska *et al.* 2020; Grünhofer *et al.* 2024), contributing to extended physiological processes. Recent study on thermal infrared reflectance in the 8–14 µm range (longwaves radiation) for different species such as sunflower (Fabre *et al.* 2011; Xu *et al.* 2023) shows that when the leaf water content decreases, reflectance for this range increases. Longwave radiation is typically emitted by surrounding objects and can be absorbed by leaves. From an energy point of view, increasing reflectance across a broad range of wavelengths can reduce energy absorption, thereby facilitating leaf cooling.

Even though the amount of cutin and waxes increases with increasing water stress, TEM microscopy shows that the overall thickness of the cuticle does not change significantly. This therefore implies a change in the density of the cuticle in Helianthus annuus. A change in density can affect the physicochemical properties of the cuticular layers, thereby altering mechanical stiffness (Onoda *et al.* 2012) and potentially helping to improve the response to severe drought, for example through improved wave reflectance and water retention.

2.6. Conclusion

This study provides new insights into how the cuticle of *Helianthus annuus* is involved in limiting water loss during severe drought. Our results demonstrate that residual leaf conductance decreases progressively with increasing water stress, with dynamics strongly influenced by both leaf age and water stress level. Our findings highlight the pivotal role of the cuticle, in particular the cutin layer in limiting water loss during drought. Young, fully expanded leaves invest in their cuticle by increasing both cutin and wax deposition, whereas older leaves show a non-significant investment. This ontogenic suggests a strategic prioritisation of resources in leaves that contribute more effectively to maintaining plant physiology under stress. Importantly, our findings disentangle the functional roles of different cuticle layers. Both cutin and wax amounts increased in young leaves under drought, but their impacts on water loss are not the same. Cutin deposition during drought was associated with a lower minimum leaf conductance at Ψ_{P88}, highlighting its functional role in limiting water loss under severe stress. In contrast, wax deposition during drought did not limit water loss, suggesting alternative protective roles such as thermal regulation or defense against biotic stressors. Together, these results indicate that in *H. annuus*, investment in leaves during drought is not uniform and depends in particular on age, and that investment in the different cuticular layers contributes to the leaf's response during drought with complementary functions. The cutin monomer participates directly to limit water loss whereas waxes likely serve complementary functions in order to preserve and extend leaf physiology.

Author contributions

GF, JJ and RB, contributed to the design of the experiment; GF, JJ, FD and RB performed data collection and GF realised the analysis and the interpretation of the results with the help from all authors. MB prepared the samples for microscopy and imaging. GF wrote the manuscript with help from all authors.

Conflict of interest

The authors declare no conflict of interest.

Funding

This study received financial support from the French government in the framework of the IdEX Bordeaux University "Investments for the Future" program / GPR Bordeaux Plant Sciences.

Acknowledgements

We would like to thank the Phenobois platform team and particularly Gaëlle Capdeville who realised xylem embolism resistance experiments. We thank LBM's scientists (Terezinha Robbe, Sarah Bernardo, Stephanie Pascal and Claire Brehelin) for their help during the experiment. Lipid analyses were carried out at the Metabolome facility of Bordeaux (https://cgfb.u-bordeaux.fr/). The Bordeaux Metabolome-Lipidome Facility-MetaboHUB is supported by a grant from ANR (no. ANR–11–INBS–0010).

2.7. References

Bates D., Mächler M., Bolker B. & Walker S. (2015) Fitting Linear Mixed-Effects Models Using lme4. Journal of Statistical Software 67.

Bi H., Kovalchuk N., Langridge P., Tricker P.J., Lopato S. & Borisjuk N. (2017) The impact of drought on wheat leaf cuticle properties. BMC Plant Biology 17, 85.

Billon L.M., Blackman C.J., Cochard H., Badel E., Hitmi A., Cartailler J., … Torres-Ruiz J.M. (2020) The DroughtBox: A new tool for phenotyping residual branch conductance and its temperature dependence during drought. Plant, Cell & Environment 43, 1584–1594.

Brodribb T.J., Holbrook N.M., Edwards E.J. & Gutiérrez M.V. (2003) Relations between stomatal closure, leaf turgor and xylem vulnerability in eight tropical dry forest trees. Plant, Cell & Environment 26, 443–450.

Brodribb T.J., McAdam S.A.M., Jordan G.J. & Martins S.C.V. (2014) Conifer species adapt to low-rainfall climates by following one of two divergent pathways. Proceedings of the National Academy of Sciences 111, 14489–14493.

Burlett R., Parise C., Capdeville G., Cochard H., Lamarque L.J., King A. & Delzon S. (2022) Measuring xylem hydraulic vulnerability for long-vessel species: an improved methodology with the flow centrifugation technique. Annals of Forest Science 79, 5.

Burlett R., Trueba S., Bouteiller X.P., Forget G., Torres-Ruiz M., Martin-StPaul N.K., … Delzon S. (2025) Minimum leaf conductance during drought: unravelling its variability and impact on plant survival. New Phytologist.

Cabello P., Agüera E. & De La Haba P. (2006) Metabolic changes during natural ageing in sunflower (Helianthus annuus) leaves: expression and activity of glutamine synthetase isoforms are regulated differently during senescence. Physiologia Plantarum 128, 175–185.

Chen M., Zhu X., Zhang Y., Du Z., Chen X., Kong X., … Chen C. (2020) Drought stress modify cuticle of tender tea leaf and mature leaf for transpiration barrier enhancement through common and distinct modes. Scientific Reports 10, 6696.

Cochard H. (2002) A technique for measuring xylem hydraulic conductance under high negative pressures. Plant, Cell & Environment 25, 815–819.

Domínguez E., Cuartero J. & Heredia A. (2011a) An overview on plant cuticle biomechanics. Plant Science 181, 77–84.

Domínguez E., Heredia-Guerrero J.A. & Heredia A. (2011b) The biophysical design of plant cuticles: an overview. New Phytologist 189, 938–949.

Domínguez E., Heredia-Guerrero J.A. & Heredia A. (2017) The plant cuticle: old challenges, new perspectives. Journal of Experimental Botany 68, 5251–5255.

Duursma R.A., Blackman C.J., Lopéz R., Martin-StPaul N.K., Cochard H. & Medlyn B.E. (2019) On the minimum leaf conductance: its role in models of plant water use, and ecological and environmental controls. New Phytologist 221, 693–705.

Fabre S., Lesaignoux A., Olioso A. & Briottet X. (2011) Influence of Water Content on Spectral Reflectance of Leaves in the 3–15- $\mu\hbox{m}$ Domain. IEEE Geoscience and Remote Sensing Letters 8, 143–147.

Grünhofer P., Herzig L., Sent S., Zeisler-Diehl V.V. & Schreiber L. (2022) Increased cuticular wax deposition does not change residual foliar transpiration. Plant, Cell & Environment 45, 1157–1171.

Grünhofer P., Herzig L., Zhang Q., Vitt S., Stöcker T., Malkowsky Y., … Schreiber L. (2024) Changes in wax composition but not amount enhance cuticular transpiration. Plant, Cell & Environment 47, 91–105.

Heredia A., Benítez J.J., González Moreno A. & Domínguez E. (2024) Revisiting plant

cuticle biophysics. New Phytologist, nph.20009.
Jordan G.J. & Brodribb T.J. (2007) Incontinence in aging leaves: deteriorating water relations with leaf age in Agastachys odorata (Proteaceae), a shrub with very long-lived leaves. Functional Plant Biology 34, 918.
Jordan W.R., Brown K.W. & Thomas J.C. (1975) Leaf Age as a Determinant in Stomatal Control of Water Loss from Cotton during Water Stress. Plant Physiology 56, 595–599.
Josse J. & Husson F. (2016) missMDA : A Package for Handling Missing Values in Multivariate Data Analysis. Journal of Statistical Software 70.
Joubès J. & Domergue F. (2020) Biosynthesis of the Plant Cuticle. In Hydrocarbons, Oils and Lipids: Diversity, Origin, Chemistry and Fate. (ed H. Wilkes), pp. 139–157. Springer International Publishing, Cham.
Kamtsikakis A. & Weder C. (2022) Asymmetric Mass Transport through Dense Heterogeneous Polymer Membranes: Fundamental Principles, Lessons from Nature, and Artificial Systems. Macromolecular Rapid Communications 43, 2100654.
Kane C.N., Jordan G.J., Jansen S. & McAdam S.A.M. (2020) A Permeable Cuticle, Not Open Stomata, Is the Primary Source of Water Loss From Expanding Leaves. Frontiers in Plant Science 11, 774.
Kassambara A. & Mundt F. (2020) Factoextra: Extract and Visualize the Results of Multivariate Data Analyses. R Package 542 Version 1.0.7.
Kerstiens G. (2006) Water transport in plant cuticles: an update. Journal of Experimental Botany 57, 2493–2499.
Kosma D.K., Bourdenx B., Bernard A., Parsons E.P., Lü S., Joubès J. & Jenks M.A. (2009) The Impact of Water Deficiency on Leaf Cuticle Lipids of Arabidopsis. Plant Physiology 151, 1918–1929.
Lewandowska M., Keyl A. & Feussner I. (2020) Wax biosynthesis in response to danger: its regulation upon abiotic and biotic stress. New Phytologist 227, 698–713.
Li S., Feifel M., Karimi Z., Schuldt B., Choat B. & Jansen S. (2016) Leaf gas exchange performance and the lethal water potential of five European species during drought. Tree Physiology, tpv117.
Machado R., Loram-Lourenço L., Farnese F.S., Alves R.D.F.B., Sousa L.F., Silva F.G., … Menezes-Silva P.E. (2021) Where do leaf water leaks come from? Trade-offs underlying the variability in minimum conductance across tropical savanna species with contrasting growth strategies. New Phytologist 229, 1415–1430.
Márquez D.A., Stuart-Williams H., Farquhar G.D. & Busch F.A. (2022) Cuticular conductance of adaxial and abaxial leaf surfaces and its relation to minimum leaf surface conductance. New Phytologist 233, 156–168.
McAdam S.A.M., Kane C.N., Mercado Reyes J.A., Cardoso A.A. & Brodribb T.J. (2022) An abrupt increase in foliage ABA levels on incipient leaf death occurs across vascular plants. Plant Biology 24, 1262–1271.
Munné-Bosch S. & Alegre L. (2004) Die and let live: leaf senescence contributes to plant survival under drought stress. Functional Plant Biology 31, 203.
Onoda Y., Richards L. & Westoby M. (2012) The importance of leaf cuticle for carbon economy and mechanical strength. New Phytologist 196, 441–447.
Petek-Petrik A., Petrík P., Lamarque L.J., Cochard H., Burlett R. & Delzon S. (2023) Drought survival in conifer species is related to the time required to cross the stomatal safety margin. Journal of Experimental Botany 74, 6847–6859.
Pörtner H.-O. & Roberts D.C. (2022) Climate Change 2022: Impacts, Adaptation and Vulnerability. 3068.
R Core Team (2020) R Core Team (2020) R: A Language and Environment for Statistical

Computing. R Foundation for Statistical Computing, Vienna, Austria. https://www.r-project.org/.
Reich P.B. (1984) Loss of Stomatal Function in Ageing Hybrid Poplar Leaves. Annals of Botany 53, 691–698.
Riederer M. & Schreiber L. (2001) Protecting against water loss: analysis of the barrier properties of plant cuticles. Journal of Experimental Botany 52, 2023–2032.
Sack, Pasquet-Kok & Megan Bartlett (2011) Leaf pressure-volume curve parameters.
Schneider C.A., Rasband W.S. & Eliceiri K.W. (2012) NIH Image to ImageJ: 25 years of image analysis. Nature Methods 9, 671–675.
Seo P.J., Lee S.B., Suh M.C., Park M.-J., Go Y.S. & Park C.-M. (2011) The MYB96 Transcription Factor Regulates Cuticular Wax Biosynthesis under Drought Conditions in Arabidopsis. The Plant Cell 23, 1138–1152.
Shellakkutti N., Thangamani P.D., Suresh K., Baales J., Zeisler-Diehl V., Klaus A., … Kreszies T. (2022) Cuticular transpiration is not affected by enhanced wax and cutin amounts in response to osmotic stress in barley. Physiologia Plantarum 174.
Shepherd T. & Griffiths D. (2006) The effects of stress on plant cuticular waxes. New Phytologist 171, 469–499.
Tredenick E.C. & Farquhar G.D. (2021) Publisher Correction: Dynamics of moisture diffusion and adsorption in plant cuticles including the role of cellulose. Nature Communications 12, 5830.
Urli M., Porte A.J., Cochard H., Guengant Y., Burlett R. & Delzon S. (2013) Xylem embolism threshold for catastrophic hydraulic failure in angiosperm trees. Tree Physiology 33, 672–683.
Xu K., Yang W. & Ye H. (2023) Thermal infrared reflectance characteristics of natural leaves in 8–14 μm region: Mechanistic modeling and relationships with leaf water content. Remote Sensing of Environment 294, 113631.
Yeats T.H. & Rose J.K.C. (2013) The Formation and Function of Plant Cuticles. Plant Physiology 163, 5–20.
Zeisler-Diehl V., Müller Y. & Schreiber L. (2018) Epicuticular wax on leaf cuticles does not establish the transpiration barrier, which is essentially formed by intracuticular wax. Journal of Plant Physiology 227, 66–74.
Zhao P., Li Q., Lei Y., Zou J. & Li Q. (2025) Adaptation of cuticle metabolism to abiotic stress in plants. Crop and Environment 4, 38–44.

2.8. Supporting Information

The following Supporting Information is available for this article:

FIGURE S5.1: Experimental design

FIGURE S5.2: Cutin compound proportion according to leaf's ageing and water stress level

FIGURE S5.3: Boxplot of the main waxes found in *H. annuus* for young and old leaves

FIGURE S5.4: Correlation plot for (a) young and (b) old leaves versus the water potential

FIGURE S5.5: Principal component analysis (PCA) and variable importance

FIGURE S5.6: Broken stick model to determine the number of axis for the PCA analysis

FIGURE S5.7: Boxplot of efficiency of photosystem II, Φ_{PSII}, for young and old leaves versus water stress class

FIGURE S5.8: Leaf thickness versus drought stress class

TABLE S5.1: Linear model fit results

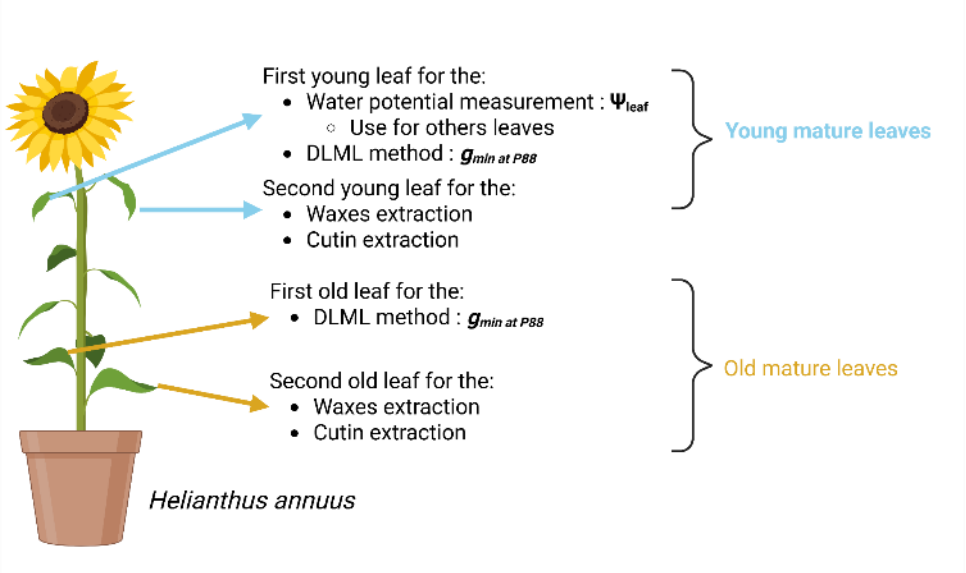

FIGURE S 5.1: Experimental design.
The experiment consists of collecting paired leaves from the top (young leaf) and bottom (old leaf) in order to simultaneously measure, with the same water potential, the minimum leaf conductance and the composition of the cuticle (cutin and waxes). Created in BioRender.com.

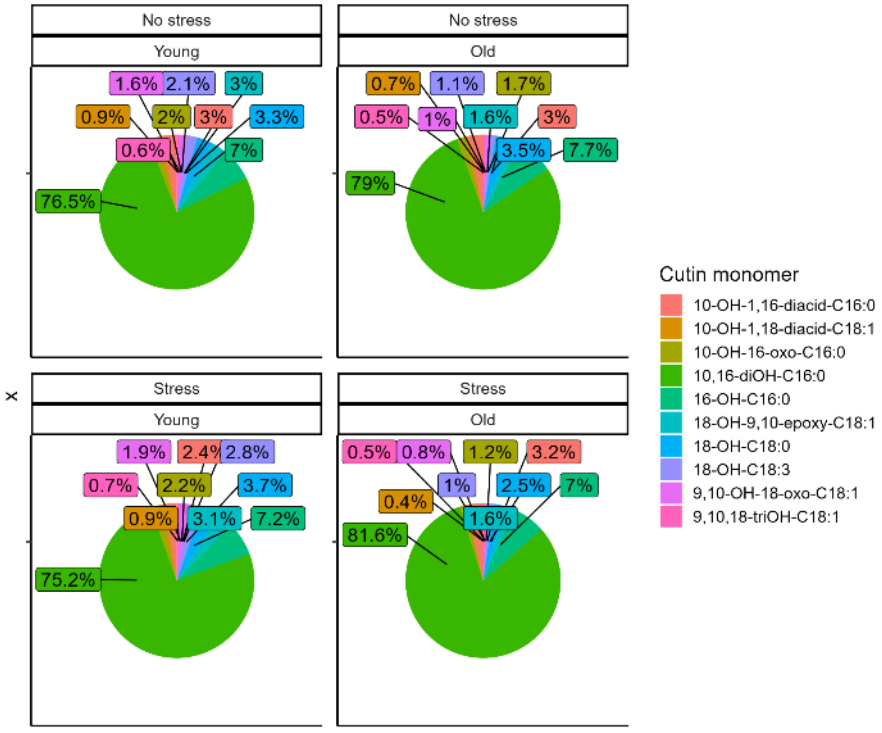

FIGURE S 5.2: Cutin compound proportion according to leaf's ageing and water stress level.
Abbreviation: 10,16-diOH-C16:0: Acid 10,16-dihydroxy-hexadécanoïque; 10-OH-16-oxo-C16:0: Acid 10-hydroxy-16-oxo-hexadécanoïque; 10-OH-1,16-diacid-C16:0: Acid 10-hydroxy-hexadécanedioïque; 16-OH-C16:0: Acid 16-hydroxyhexadécanoïque; 10-OH-1,18-diacid-C18:1: Acid 10-hydroxy-9-octadécénedioïque; 9,10-OH-18-oxo-C18:1 Acid 18-oxo-di-hydroxy-9-octadécénoïque; 18-OH-C18:1: Acid 18-hydroxy-9-octadécénoïque; 18-OH-C18:3: Acid 18-hydroxy-9,12,15-octadécatriénoïque; 18-OH-9,10-epoxy-C18:1: Acid 18-hydroxy-epoxyoctadécanoïque; 9,10,18-triOH-C18:1: Acid tri-hydroxy-octadécanoïque

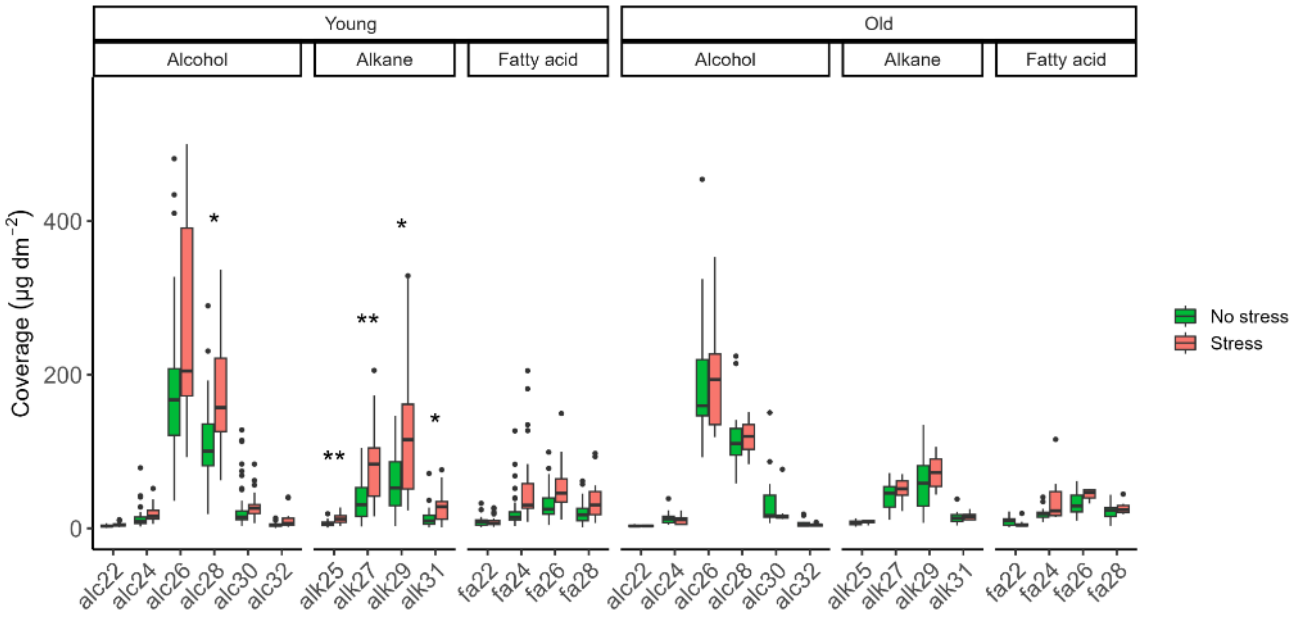

FIGURE S 5.3: Boxplot of the main waxes found in *H. annuus* for young and old leaves.
Green boxplots indicate well-watered leaves (leaf water potential > –1.5 MPa), and red boxplots indicate drought-stressed leaves (leaf water potential < –1.5 MPa). Statistical differences were assessed using a Student's t-test (***, p<0.001; **, p<0.01; *, p<0.05; ns, p> 0.05) except when assumptions are not validated in which case the Mann-Whitney test was used.

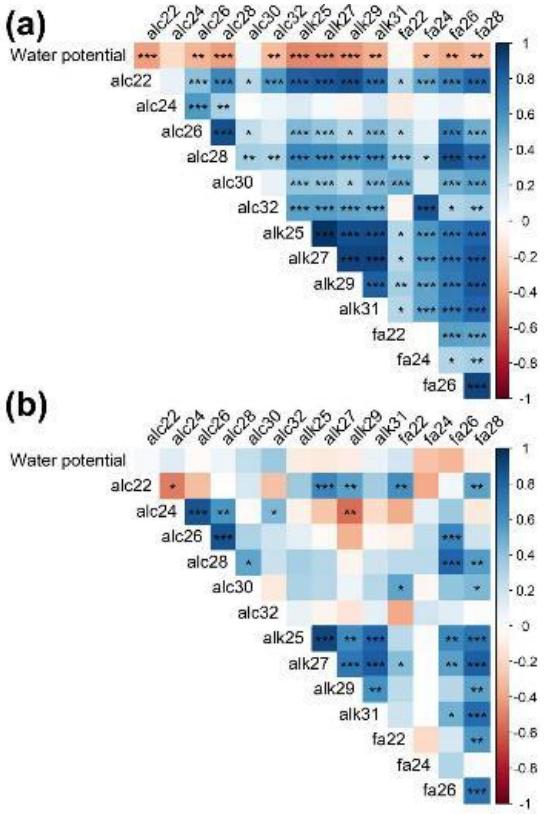

FIGURE S 5.4: Correlation plot for (a) young and (b) old leaves versus the water potential.
Color corresponds to the correlation direction. Colors correspond to the magnitude of Person correlation coefficients, while asterisks correspond to the statistical significance of the results (***, p<0.001; **, p<0.01; *, p<0.05; -, p> 0.05).

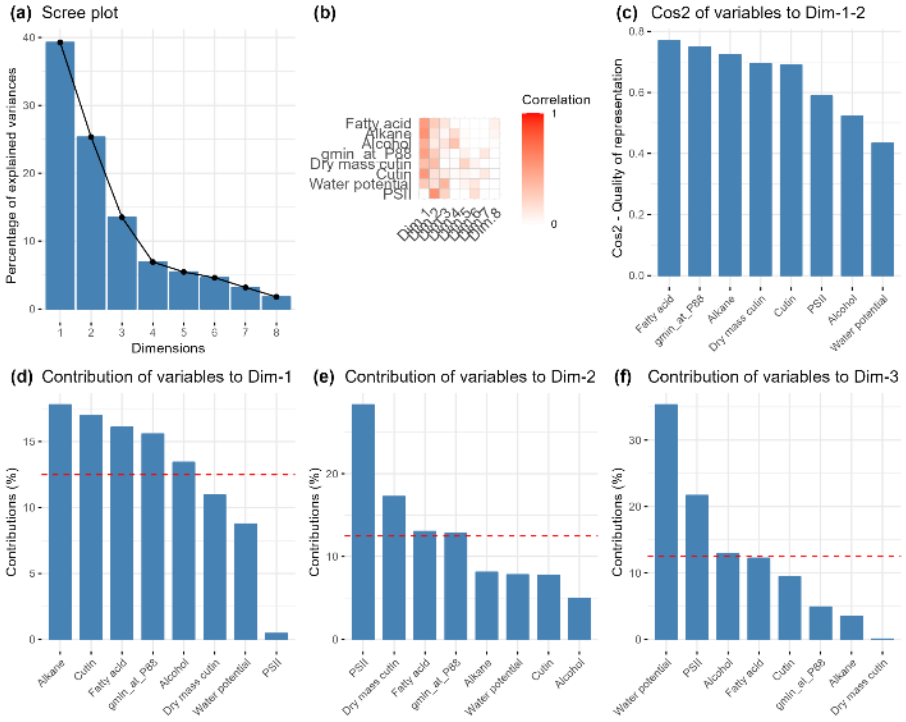

FIGURE S 5.5: Principal component analysis (PCA) and variable importance.
(a) Scree plot of eigenvalues showing the percentage of variance explained by the first eight principal components. (b) Correlation heatmap between variables used in the PCA. (c) Variable correlation plot showing the squared cosines of the variables with the first two principal components, indicating how well each variable is represented. Contribution of individual variables to the first three principal components: (d) PC1, (e) PC2, and (f) PC3). The red dashed line indicates the expected average contribution if all variables contributed equally.

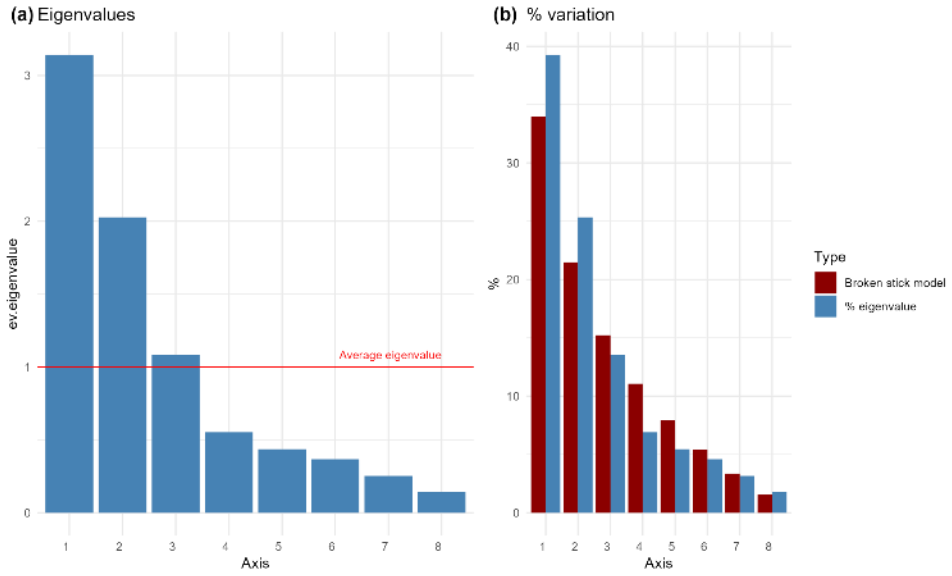

FIGURE S 5.6: Broken stick model to determine the number of axis for the PCA analysis.

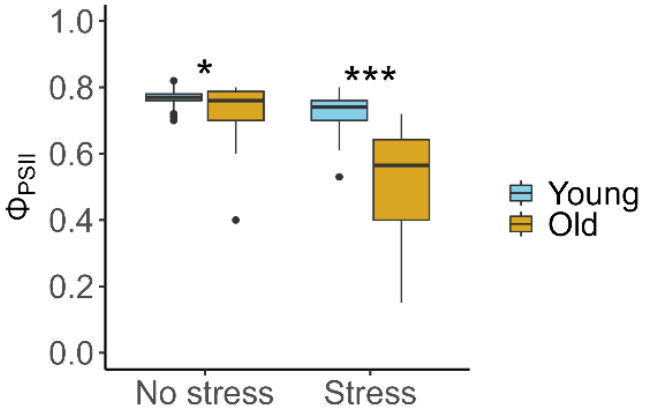

FIGURE S 5.7: Boxplot of efficiency of photosystem II, Φ_{PSII}, for young and old leaves versus water stress class.
Statistical differences were assessed using a Student's t-test (***, p<0.001; *, p<0.05) except when assumptions are not validated in which case the Mann-Whitney test was used.

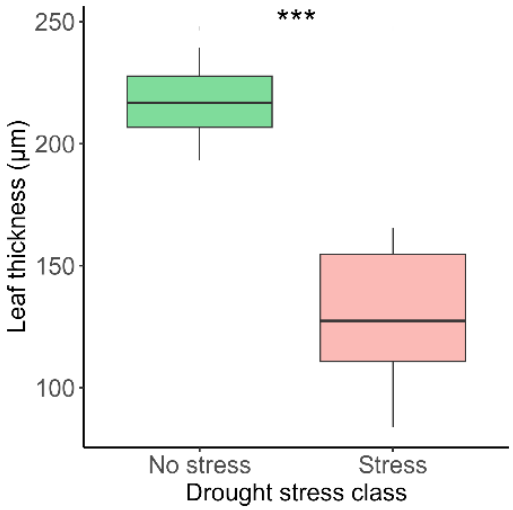

FIGURE S 5.8: Leaf thickness versus drought stress class.
Green boxplots indicate a well-watered leaf (Ψ= -1.02 MPa (~Ψ_{tlp}, No stress)), and red boxplots indicate a drought-stressed leaf (-2.40 MPa (Ψ_{P12}<Ψ<Ψ_{P50}, Stress)). Statistical differences were assessed using a Student t test (***, p<0.001). Images were used to assess leaf thickness (in µm) at 15 locations across each leaf using ImageJ v.1.53q software.

TABLE S 5.1: linear model fit results
Call:

lm(formula = g_{res} ~ WP * Stress_level * Level, data = data)

Stress_level: Well-watered or stressed leaves

Level: Young or old leaves

Coefficients:

	Estimate	Std.	Error	t value	Pr(>|t|)
(Intercept)	21.6598	0.4677	46.31	2.00E-16	***
WP	4.5081	0.1814	24.845	2.00E-16	***
stress_levelStress	-4.5265	0.7814	-5.793	8.83E-09	***
LevelOld	23.7846	0.9249	25.715	2.00E-16	***
WP:Stress_levelStressed	-0.954	0.3031	-3.148	0.00169	**
WP:LevelOld	3.532	0.3631	9.728	2.00E-16	***
Stress_levelStressed:LevelOld	-2.1533	2.2167	-0.971	0.33154	ns
WP:Stress_levelStressed:LevelOld	0.6142	0.8134	0.755	0.45036	ns

Signif. Codes: 0 ‘***’ 0.001 ‘**’ 0.01 ‘*’ 0.05 ‘.’ 0.1 ‘ ’ 1

Residual standard error: 5.658 on 1205 degrees of freedom

Multiple R-squared: 0.728, Adjusted R-squared: 0.7265

F-statistic: 460.8 on 7 and 1205 DF, p-value: < 2.2e-16

CHAPTER 6

General conclusion and perspectives

Chapter 6 General conclusion and perspectives

Water loss during a severe drought, even if it is a low flow, can rapidly compromise the physiological functions and survival of the plant. As soil moisture declines and atmospheric demand increases, plants must rely on mechanisms such as stomatal closure to limit dehydration. However, even after stomatal closure, residual water loss through the cuticle and incompletely closed stomata persists, contributing to continued water loss. Uncontrolled, this ongoing water loss can lead to loss of hydraulic conductivity, hydraulic failure and ultimately cellular damages and mortality (Trueba *et al.* 2019). Minimum leaf conductance, g_{min}, composed of two components: stomatal (through incompletely closed or leaky stomata) and cuticular conductance is a major hydraulic trait for understanding plant responses to drought and estimating the time to consume the stomatal safety margin (Petek-Petrik *et al.* 2023) and the time to hydraulic failure (Urli *et al.* 2013; Li *et al.* 2016). In a recent study, we showed that this trait exhibits important variability intra- and interspecific in vascular plants and shows only a weak phylogenetic signal resulting from convergent evolution (Trueba et al, 2025, in revision). Nevertheless, deciduous and annual species tend to exhibit higher g_{min} values than evergreen species highlighting an annual/seasonal water loss conservation. Furthermore, g_{min} is correlated with climatic variables such as mean annual temperature and annual precipitation, indicating its adaptive role in minimising water loss under water-limited conditions (Trueba et al, 2025, in revision).

We emphasised that after stomatal closure, the minimal leaf conductance, g_{min}, is not constant as drought increases but decreases as dehydration inside the leaf progresses and the leaf's water availability decreases (Burlett *et al.* 2025). That decline can be attributed to the stomatal closure dynamics until a residual leakiness and to the cuticle response with a change in amounts of wax and cutin. We showed that the two components (incompletely closed stomata and cuticle) of g_{min} contribute independently and differentially to limiting water loss during drought (chapter 3 and 5). Their distinct dynamics are relevant in the context of plant responses to drought, making them essential for research in plant drought resistance and water-use strategies. Neglecting these dynamic behaviors can lead, as we highlighted in chapter 3 and 5, to inaccurate estimates of time to hydraulic failure in drought forecasting models, resulting in either over- or underestimation of plant survival times under extreme drought.

1. Alone, we go faster, together we go further

1.1. Incomplete stomatal closure and leakiness

During progressive dehydration, stomatal closure is rarely complete and 100% hermetic (Brodribb *et al.* 2014; Kane *et al.* 2020; Machado *et al.* 2021). Incomplete closure results in a leak, allowing residual water loss even after the point at which stomata are functionally considered closed. My research has pointed out for the first time that this leakiness observed in two contrasted species (a crop, *Helianthus annuus* and a tree, *Liriodendron tulipifera*) is present along a drought sequence and persists until Ψ_{P50}, which represents a critical threshold for survival probability (chapter 3). Using independent methods such as the infiltration method, we demonstrated that this leakiness varies between the two studied species and is influenced by their capacity for stomatal closure. Although both species exhibit stomatal leakiness, it is limited and constant for the *Liriodendron tulipifera* due to rapid stomatal closure before the turgor loss point. In contrast, *Helianthus annuus* tends to maintain stomatal opening and therefore leakiness for longer during the drought sequence (chapter 3). Potential explanations for this leakage could be the inability of guard cells to fully close due to structural limitations, insufficient turgor from surrounding epidermal cells, or structural limitations. Nonetheless, this leakiness is a crucial component of the minimal leaf conductance. However, numerous fundamental questions remain open: How should stomatal leakiness be precisely defined? After the post-stomatal closure or the Ψ_{gs90} which represents the loss of 90% of stomatal conductance or after? Perhaps this leakage is simply due to a slower closing dynamic after a certain point. At what hydraulic thresholds do leaks begin and cease to be a controlled process? To highlight stomatal leakiness, we used the infiltration method. Could variations in infiltration pressure influence the occurrence or severity of leakage visualisation ?

It is essential to answer these questions to refine our understanding on stomatal leakiness impacting plant survival. To achieve this, infiltration experiments should be done with complementary approaches, such as the detached leaf mass loss (DLML) method, across different species and clades.

1.2. Stomatal patchiness as an emergent behaviour

Leakiness is examined as an isolated phenomenon, yet during dehydration it frequently co-occurs with stomatal patchiness, a spatially heterogeneous pattern of

stomatal aperture across the leaf. We shed light on stomatal patchiness significance as a collective stomatal response to drought (chapter 3 and 4). Easily observed using thermal and chlorophyll fluorescence imaging, we demonstrate that this emergent stomatal behaviour provides flexibility in the leaf response to environmental cues and especially at the onset of drought. This spatial heterogeneity enables specific leaf regions to sustain and prolong carbon assimilation while minimising water loss, thereby postponing complete metabolic shutdown and hydraulic failure (chapter 4). Such spatial trade-offs illustrate the complexity of drought adaptation and leaf response where water conservation and physiological processes must be balanced (Hatfield & Dold 2019; Machado *et al.* 2021).

To better understand spatial heterogeneity of water loss during drought, it is essential to understand the pathways taken by water in liquid or vapour form outside the xylem. It is important to look not at the leaf as a whole, but locally and, above all, with a spatio-temporal point of view, analysing the local behaviour of the water potential inside the leaf and the stomatal patchiness at the surface.

1.3. Temporal dynamics and thresholds of stomatal patchiness

Using for the first-time chlorophyll fluorescence imaging along a drought sequence, we highlighted in *Helianthus annuus* that the maximum of spatial variability for the stomatal behaviour is between the bulk water potential at turgor loss point (Ψ_{tlp}) and Ψ_{P12}. This interval between Ψ_{tlp}, considered as the stomatal closure and Ψ_{P12} representing the early stages of xylem embolism can be considered from a spatial perspective for the leaf as a buffer zone allowing local stomatal behaviour thus stomatal patchiness. Above Ψ_{tlp}, leaves achieve maximal uniform cooling efficiency and carbon assimilation over the leaf, as water is not a limiting factor. Below Ψ_{P12}, patchiness diminishes due to water scarcity and only residual stomatal leaks remain. On a hot day, for instance, high evaporative demand causes a drop in bulk leaf water potential. While overall water potential can fluctuate within the range of Ψ_{tlp} to Ψ_{P12}, substantial variation exists across different leaf regions. Relying solely on bulk water potential to trigger or delay complete stomatal closure can result in carbon starvation or conversely, excessive water loss. Allowing local regulation enables optimisation of this trade-off, even when the global bulk water potential falls below the turgor loss point and approaches Ψ_{P12}.

1.4. Hierarchical organisation and modelling perspectives

Stomatal patchiness is not exclusive to drought conditions; it can be present even in well-watered plants but is less detectable due to uniform water potential across the leaf (chapter 4). Another feature that we highlighted, is the hierarchical spatial organisation of stomatal patchiness (chapter 4). Indeed, using a long- and short-timescale, we demonstrated that patchiness can be decomposed into three scales, microscale (shaped by the vein network), mesoscale (a group of patchiness) and macroscale (whole leaf level). This structure may enable plants to optimise leaf response to environmental variations and stresses across both diurnal and seasonal timescales. We recommend including stomatal patchiness into plants' hydraulic model in order to better predict residual water loss and thereby hydraulic failure.

Spatial heterogeneity has the potential to significantly improve predictions of drought response (chapter 3 and 4). Key research questions remain regarding the role of local water potential gradients over the leaf, pathway outside the xylem, vein and bundle sheath extensions architecture, and stomatal density in controlling the initiation, spread, and persistence of patchiness (Buckley *et al.* 2011; Jain *et al.* 2023, 2024; Buckley & Sack 2024).

Ultimately, while the proverb *"alone we go faster, together we go further"* reflects the collective dynamics of stomata, in a biological context like patchiness, represent adaptive compromises that extend survival under water limitation, but only up to a yet to be determined threshold.

1.5. A jacket to limit water loss and heating

While stomatal patchiness and more broadly stomatal behaviour represent rapid responses to drought or environmental cues, unfolding over minutes to hours, the cuticular response is markedly slower, developing progressively along the drought sequence (chapter 5). The third leaf's response to drought is often associated with a change in the cuticle in terms of composition, quantity or thickness. However, the relationship between the cuticle response and reduced water loss is not straightforward, with studies reporting contradictory results (Zeisler-Diehl *et al.* 2018; Grünhofer *et al.* 2022; Grünhofer *et al.* 2024; Shellakkutti *et al.* 2022). The cuticle, composed primarily of a cutin matrix impregnated with and overlaid by waxes serves multiple functional roles: it acts as a protective barrier against non-stomatal water loss, provides defence against

pests, fungi, ultraviolet and thermal radiation, contributes to structural support, and facilitates leaf surface cleaning.

We conducted a simultaneous study on the cutin matrix and waxes layer along a drought sequence using the detached leaf mass loss (DLML) method with lipid extractions by GC-FID and GC-MS to disentangle their dynamics and impact on water loss. Our results showed for *Helianthus annuus* that both layers have a response to drought by increasing compound amount but only the cutin is significantly correlated with water loss (chapter 5). Epicuticular waxes, which form a thin layer on the top at the leaf surface, are not correlated with water loss, however their significant increases during drought suggests another protective role (chapter 5). Finally, we showed using TEM images that the thickness of the cuticle does not increase during drought, but that its density changes due to the increase in amount (chapter 5). This change in cuticle density affects water loss and may also influence its mechanical integrity, as well as its thermal and optical properties.

This raises several unresolved questions: How does cuticle composition change during drought across developmental stages and among species? My study focused on one crop, *Helianthus annuus*. How does the cuticle respond to drought in evergreen and deciduous trees? What are the specific contributions of polysaccharides and aqueous pores to water transport under water deficit? Present in the cuticle, polysaccharides came from the cell wall and are known to facilitate water transport. How does drought-driven modification of cuticle reflectance influence leaf temperature by altering radiation absorption? If the leaf increases the reflectance of long and short waves, the cooling demand is limited thus when the water availability inside the leaf is low, insulating could be a good solution to delay leaf failure. Which molecular pathways and genes regulate cuticle's response under drought stress, and how are these processes coordinated with other protective responses? Finally, from a functional ecology perspective, the post-drought phase invites an additional question: what becomes of this "blanket" once soil water availability returns, does it persist as a legacy of stress or undergo active remodelling to restore pre-drought properties?

1.6. Conclusion

Overall, this thesis deepens the understanding and interpretation of the main factors contributing to residual water loss under severe drought conditions. More specifically, this research demonstrates that stomatal leakiness is a persistent component of residual water loss throughout the drought sequence. Concomitantly, the different layers of the cuticle responses to drought, enhancing that leaf's cuticle acts as a multi protective barrier not only against water loss. Moreover, this thesis emphasises that stomatal patchiness as a key leaf-level response to drought, highlighting how localised variations in stomatal behavior extend and modulate physiological processes across the leaf surface. Finally, it is important to consider stomatal leakiness and cuticle responses, as well as a spatial and local approach in models to predict drought-related mortality.

2. Harnessing interdisciplinary approaches in plant science

Whatever the type of drought, this abiotic stress remains one of the most harmful stress affecting both ecosystems and agricultural productivity. In the context of climate change, drought events are expected to increase in frequency, intensity, and unpredictability, presenting profound challenges for plant survival, crop yield and ecosystem resilience. Drought stress impacts not only the water transport of plants, disrupting the soil–plant–atmosphere continuum, but also leads to cascading effects on key physiological processes such as photosynthesis (Torres-Ruiz *et al.* 2024). To fully grasp the complexity of plant responses to drought, an interdisciplinary approach is required. By focusing on the leaf and integrating ecophysiology, plant physiology, biochemistry, physics and modelling in this PhD project, a multi-scale spatio-temporal understanding of leaf response to drought is beginning to emerge. Furthermore, the highly ambitious goal of using numerous high-level techniques specific to each field (Micro-CT, thermal and chlorophyll fluorescence imaging, mass spectroscopy, transmission electron microscopy (TEM), cavitron, infiltration and infrared gas analysers) throughout this PhD project enabled us to go further and deeper into the understanding of phenomena involved during drought. Interdisciplinarity widens the window through which we observe and interpret plant responses not only during a drought but during a multistress. It enables us to move beyond isolated mechanisms and instead construct complex in the sense of a complex system, systems-level understanding of plant stress response.

3. Multifactorial stress analysis, a necessity to better understand plant response to drought

Understanding how plants globally respond to drought requires a shift from studying single stress factors such as water or heat stress to a multifactorial stress, as plants in natural environments are subjected to co-occurring abiotic stresses (Zandalinas & Mittler 2022). Plant responses to combined stresses cannot be reliably predicted by simply extrapolating from responses to each stress applied in isolation and then added (Zandalinas & Mittler 2022). This non-additive nature of stress responses arises from complex regulatory networks that integrate multiple signaling pathways, often involving trade-offs and re-prioritisation of metabolic resources and physiological processes that would remain hidden in single-stress analyses (Sato *et al.* 2024; Jiang *et al.* 2025). For instance, stress signaling, such as abscisic acid (ABA) and reactive oxygen species (ROS) operate differently under combined drought and heat stress, leading to unique response profiles shaped by the severity, duration, and sequence of stress exposure (Sato *et al.* 2024). The importance of this approach is underscored by recent findings on the dynamics of minimum leaf conductance (g_{min}) during and after heat stress. Fernandes *et al.* (2025) demonstrated that heat stress alone can significantly alter g_{min}. The study showed that g_{min} increased during heat exposure and remained elevated even after stress cessation, suggesting a persistent vulnerability to water loss during post-stress recovery. This altered g_{min} behavior may be particularly harmful when combined with drought, as it could amplify dehydration under limited soil moisture conditions. Moreover, plant responses to combinational stresses are not only dominated by the most severe stressor but are also shaped by the order in which stresses occur (Jiang *et al.* 2025). Sequential stress exposure can trigger physiological memory or priming effects, whereby prior exposure, even to mild stress, modifies subsequent responses. Mitchell *et al.* (2025) found that leaf drought and heat tolerance traits are often integrated across species from different temperate biomes, indicating a coordinated strategy of stress resilience that is both trait-specific and environment-dependent. Such findings underscore the importance of studying stress combinations to better predict plant survival and function under future climate scenarios.

General bibliography

Adams H.D., Zeppel M.J.B., Anderegg W.R.L., Hartmann H., Landhäusser S.M., Tissue D.T., … McDowell N.G. (2017) A multi-species synthesis of physiological mechanisms in drought-induced tree mortality. Nature Ecology & Evolution 1, 1285–1291.

Allen C.D., Breshears D.D. & McDowell N.G. (2015) On underestimation of global vulnerability to tree mortality and forest die-off from hotter drought in the Anthropocene. Ecosphere 6, art129.

Anderegg W.R.L., Klein T., Bartlett M., Sack L., Pellegrini A.F.A., Choat B. & Jansen S. (2016) Meta-analysis reveals that hydraulic traits explain cross-species patterns of drought-induced tree mortality across the globe. Proceedings of the National Academy of Sciences 113, 5024–5029.

Arend M., Link R.M., Patthey R., Hoch G., Schuldt B. & Kahmen A. (2021) Rapid hydraulic collapse as cause of drought-induced mortality in conifers. Proceedings of the National Academy of Sciences 118, e2025251118.

Arya G.C., Sarkar S., Manasherova E., Aharoni A. & Cohen H. (2021) The Plant Cuticle: An Ancient Guardian Barrier Set Against Long-Standing Rivals. Frontiers in Plant Science 12, 663165.

Batsale M., Bahammou D., Fouillen L., Mongrand S., Joubès J. & Domergue F. (2021) Biosynthesis and Functions of Very-Long-Chain Fatty Acids in the Responses of Plants to Abiotic and Biotic Stresses. Cells 10, 1284.

Beyschlag W. & Eckstein J. (2001) Towards a causal analysis of stomatal patchiness: the role of stomatal size variability and hydrological heterogeneity. Acta Oecologica 22, 161–173.

Beyschlag W., Pfanz H. & Ryel RonaldJ. (1992) Stomatal patchiness in Mediterranean evergreen sclerophylls: Phenomenology and consequences for the interpretation of the midday depression in photosynthesis and transpiration. Planta 187.

Bhanot V., Fadanavis S.V. & Panwar J. (2021) Revisiting the architecture, biosynthesis and functional aspects of the plant cuticle: There is more scope. Environmental and Experimental Botany 183, 104364.

Billon L.M., Blackman C.J., Cochard H., Badel E., Hitmi A., Cartailler J., … Torres-Ruiz J.M. (2020) The DroughtBox: A new tool for phenotyping residual branch conductance and its temperature dependence during drought. Plant, Cell & Environment 43, 1584–1594.

Boisseaux M., Nemetschek D., Baraloto C., Burban B., Casado-Garcia A., Cazal J., … Stahl C. (2025) Shifting trait coordination along a soil-moisture-nutrient gradient in tropical forests. Functional Ecology 39, 21–37.

Brisson N., Gate P., Gouache D., Charmet G., Oury F.-X. & Huard F. (2010) Why are wheat yields stagnating in Europe? A comprehensive data analysis for France. Field Crops Research 119, 201–212.

Brodribb, McAdam & Field (2009) Evolution of stomatal responsiveness to CO2 and optimization of water-use efficiency.

Brodribb T.J. (2009) Xylem hydraulic physiology: The functional backbone of terrestrial plant productivity. Plant Science 177, 245–251.

Brodribb T.J., Holbrook N.M., Edwards E.J. & Gutiérrez M.V. (2003) Relations between stomatal closure, leaf turgor and xylem vulnerability in eight tropical dry forest trees. Plant, Cell & Environment 26, 443–450.

Brodribb T.J., McAdam S.A.M., Jordan G.J. & Martins S.C.V. (2014) Conifer species adapt to low-rainfall climates by following one of two divergent pathways. Proceedings of the National Academy of Sciences 111, 14489–14493.

Buckley T.N. (2005) The control of stomata by water balance. New Phytologist 168, 275–292.
Buckley T.N. (2019) How do stomata respond to water status? New Phytologist 224, 21–36.
Buckley T.N., Farquhar G.D. & Mott K.A. (1997) Qualitative effects of patchy stomatal conductance distribution features on gas-exchange calculations. Plant, Cell and Environment 20, 867–880.
Buckley T.N. & Sack L. (2024) Resolving micro-scale water potential gradients within leaves. Journal of Plant Hydraulics.
Buckley T.N., Sack L. & Gilbert M.E. (2011) The Role of Bundle Sheath Extensions and Life Form in Stomatal Responses to Leaf Water Status. Plant Physiology 156, 962–973.
Bueno A., Alfarhan A., Arand K., Burghardt M., Deininger A.-C., Hedrich R., … Riederer M. (2019) Effects of temperature on the cuticular transpiration barrier of two desert plants with water-spender and water-saver strategies. Journal of Experimental Botany 70, 1613–1625.
Burlett R., Parise C., Capdeville G., Cochard H., Lamarque L.J., King A. & Delzon S. (2022) Measuring xylem hydraulic vulnerability for long-vessel species: an improved methodology with the flow centrifugation technique. Annals of Forest Science 79, 5.
Burlett R., Trueba S., Bouteiller X.P., Forget G., Torres-Ruiz M., Martin-StPaul N.K., … Delzon S. (2025) Minimum leaf conductance during drought: unravelling its variability and impact on plant survival. New Phytologist.
Cardon Z.G., Mott K.A. & Berry J.A. (1994) Dynamics of patchy stomatal movements, and their contribution to steady-state and oscillating stomatal conductance calculated using gas-exchange techniques. Plant, Cell and Environment 17, 995–1007.
Chamel A., Pineri M. & Escoubes M. (1991) Quantitative determination of water sorption by plant cuticles. Plant, Cell and Environment 14, 87–95.
Chater C.C.C., Caine R.S., Fleming A.J. & Gray J.E. (2017) Origins and Evolution of Stomatal Development. Plant Physiology 174, 624–638.
Chaves M.M., Flexas J. & Pinheiro C. (2009) Photosynthesis under drought and salt stress: regulation mechanisms from whole plant to cell. Annals of Botany 103, 551–560.
Choat B., Brodribb T.J., Brodersen C.R., Duursma R.A., López R. & Medlyn B.E. (2018) Triggers of tree mortality under drought. Nature 558, 531–539.
Choat B., Jansen S., Brodribb T.J., Cochard H., Delzon S., Bhaskar R., … Zanne A.E. (2012) Global convergence in the vulnerability of forests to drought. Nature 491, 752–755.
Christian J.I., Basara J.B., Hunt E.D., Otkin J.A., Furtado J.C., Mishra V., … Randall R.M. (2021) Global distribution, trends, and drivers of flash drought occurrence. Nature Communications 12.
Christian J.I., Hobbins M., Hoell A., Otkin J.A., Ford T.W., Cravens A.E., … Mishra V. (2024) Flash drought: A state of the science review. WIREs Water 11.
Clark J.W., Harris B.J., Hetherington A.J., Hurtado-Castano N., Brench R.A., Casson S., … Hetherington A.M. (2022) The origin and evolution of stomata. Current Biology 32, R539–R553.
Cochard H. (2002) A technique for measuring xylem hydraulic conductance under high negative pressures. Plant, Cell & Environment 25, 815–819.
Cochard H., Pimont F., Ruffault J. & Martin-StPaul N. (2020) SurEau .c : a mechanistic model of plant water relations under extreme drought. Plant Biology.

Cook B.I., Mankin J.S. & Anchukaitis K.J. (2018) Climate Change and Drought: From Past to Future. Current Climate Change Reports 4, 164–179.
Domínguez E., Heredia-Guerrero J.A. & Heredia A. (2011) The biophysical design of plant cuticles: an overview. New Phytologist 189, 938–949.
Donoghue P.C.J., Harrison C.J., Paps J. & Schneider H. (2021) The evolutionary emergence of land plants. Current Biology 31, R1281–R1298.
Drake P.L., Froend R.H. & Franks P.J. (2013a) Smaller, faster stomata: scaling of stomatal size, rate of response, and stomatal conductance. Journal of Experimental Botany 64, 495–505.
Drake P.L., Froend R.H. & Franks P.J. (2013b) Smaller, faster stomata: scaling of stomatal size, rate of response, and stomatal conductance. Journal of Experimental Botany 64, 495–505.
Duursma R.A., Blackman C.J., Lopéz R., Martin-StPaul N.K., Cochard H. & Medlyn B.E. (2019) On the minimum leaf conductance: its role in models of plant water use, and ecological and environmental controls. New Phytologist 221, 693–705.
Engineer C.B., Hashimoto-Sugimoto M., Negi J., Israelsson-Nordström M., Azoulay-Shemer T., Rappel W.-J., … Schroeder J.I. (2016) CO2 Sensing and CO2 Regulation of Stomatal Conductance: Advances and Open Questions. Trends in Plant Science 21, 16–30.
Fabre S., Lesaignoux A., Olioso A. & Briottet X. (2011) Influence of Water Content on Spectral Reflectance of Leaves in the 3–15- $\mu\hbox{m}$ Domain. IEEE Geoscience and Remote Sensing Letters 8, 143–147.
Fernandes V.D.A.B., Farnese F.S., Arantes B.R., Fontineles Da Silva M.L., Silva F.G., Torres-Ruiz J.M., … Menezes-Silva P.E. (2025) Leaf minimum conductance dynamics during and after heat stress: Implications for plant survival under hotter droughts. Plant Physiology 197, kiaf026.
Fernández V., Bahamonde H.A., Javier Peguero-Pina J., Gil-Pelegrín E., Sancho-Knapik D., Gil L., … Eichert T. (2017) Physico-chemical properties of plant cuticles and their functional and ecological significance. Journal of Experimental Botany 68, 5293–5306.
Flexas J. (2009) Photosynthesis limitations during water stress acclimation and recovery in the drought-adapted Vitis hybrid Richter-110 (V. berlandieri·V. rupestris).
Flexas J., Escalona J.M. & Medrano H. (1999) Water stress induces different levels of photosynthesis and electron transport rate regulation in grapevines. Plant, Cell & Environment 22, 39–48.
Foyer C., Wang A. & Shi K. (2025) CO2 signalling in plants. Philosophical Transactions of the Royal Society B: Biological Sciences 380, 20240247.
Franks P.J. & Beerling D.J. (2009) Maximum leaf conductance driven by CO 2 effects on stomatal size and density over geologic time. Proceedings of the National Academy of Sciences 106, 10343–10347.
Freedman H., AghaKouchak A., Rigden A.J., Hoek A.V.D. & Tomlinson B. (2025) Disparities in the impact of drought on agriculture across countries. Scientific Reports 15, 13465.
Gebrechorkos S.H., Sheffield J., Vicente-Serrano S.M., Funk C., Miralles D.G., Peng J., … Dadson S.J. (2025) Warming accelerates global drought severity. Nature.
Golding A.J. & Johnson G.N. (2004) Down-regulation of linear and activation of cyclic electron transport during drought. Planta 218, 682–682.
Grossiord C., Buckley T.N., Cernusak L.A., Novick K.A., Poulter B., Siegwolf R.T.W., … McDowell N.G. (2020) Plant responses to rising vapor pressure deficit. New Phytologist 226, 1550–1566.
Grünhofer P., Herzig L., Sent S., Zeisler-Diehl V.V. & Schreiber L. (2022) Increased

cuticular wax deposition does not change residual foliar transpiration. Plant, Cell & Environment 45, 1157–1171.
Grünhofer P., Herzig L., Zhang Q., Vitt S., Stöcker T., Malkowsky Y., … Schreiber L. (2024) Changes in wax composition but not amount enhance cuticular transpiration. Plant, Cell & Environment 47, 91–105.
Gu L., Schumacher D.L., Fischer E.M., Slater L.J., Yin J., Sippel S., … Knutti R. (2025) Flash drought impacts on global ecosystems amplified by extreme heat. Nature Geoscience.
Hammond W.M., Williams A.P., Abatzoglou J.T., Adams H.D., Klein T., López R., … Allen C.D. (2022) Global field observations of tree die-off reveal hotter-drought fingerprint for Earth's forests. Nature Communications 13, 1761.
Harris B.J., Harrison C.J., Hetherington A.M. & Williams T.A. (2020) Phylogenomic Evidence for the Monophyly of Bryophytes and the Reductive Evolution of Stomata. Current Biology 30, 2001-2012.e2.
Hatfield J.L. & Dold C. (2019) Water-Use Efficiency: Advances and Challenges in a Changing Climate. Frontiers in Plant Science 10, 103.
Heredia-Guerrero J.A., Guzman-Puyol S., Benítez J.J., Athanassiou A., Heredia A. & Domínguez E. (2018) Plant cuticle under global change: Biophysical implications. Global Change Biology 24, 2749–2751.
Hultgren A., Carleton T., Delgado M., Gergel D.R., Greenstone M., Houser T., … Yuan J. (2025) Impacts of climate change on global agriculture accounting for adaptation. Nature 642, 644–652.
IPCC (2023) Climate Change 2021 – The Physical Science Basis: Working Group I Contribution to the Sixth Assessment Report of the Intergovernmental Panel on Climate Change, 1st ed. Cambridge University Press.
Jain P., Huber A.E., Rockwell F.E., Sen S., Holbrook N.M. & Stroock A.D. (2023) Localized measurements of water potential reveal large loss of conductance in living tissues of maize leaves.
Jain P., Huber A.E., Rockwell F.E., Sen S., Holbrook N.M. & Stroock A.D. (2024) New approaches to dissect leaf hydraulics reveal large gradients in living tissues of tomato leaves. New Phytologist.
Jiang Z., Van Zanten M. & Sasidharan R. (2025) Mechanisms of plant acclimation to multiple abiotic stresses. Communications Biology 8.
Joubès J. & Domergue F. (2020) Biosynthesis of the Plant Cuticle. In Hydrocarbons, Oils and Lipids: Diversity, Origin, Chemistry and Fate. (ed H. Wilkes), pp. 139–157. Springer International Publishing, Cham.
Kamakura M., Kosugi Y., Muramatsu K. & Muraoka H. (2012a) Simulations and observations of patchy stomatal behavior in leaves of Quercus crispula, a cool-temperate deciduous broad-leaved tree species. Journal of Plant Research 125, 339–349.
Kamakura M., Kosugi Y., Takanashi S., Matsumoto K., Okumura M. & Philip E. (2011) Patchy stomatal behavior during midday depression of leaf CO2 exchange in tropical trees. Tree Physiology 31, 160–168.
Kamakura M., Kosugi Y., Takanashi S., Tobita H., Uemura A. & Utsugi H. (2012b) Observation of the scale of patchy stomatal behavior in leaves of Quercus crispula using an Imaging-PAM chlorophyll fluorometer. Tree Physiology 32, 839–846.
Kamakura M., Kosugi Y., Takanashi S., Uemura A., Utsugi H. & Kassim A.R. (2015) Occurrence of stomatal patchiness and its spatial scale in leaves from various sizes of trees distributed in a South-east Asian tropical rainforest in Peninsular Malaysia. Tree Physiology 35, 61–70.
Kane C.N., Jordan G.J., Jansen S. & McAdam S.A.M. (2020) A Permeable Cuticle, Not

Open Stomata, Is the Primary Source of Water Loss From Expanding Leaves. Frontiers in Plant Science 11, 774.
Kerstiens G. (2006) Water transport in plant cuticles: an update. Journal of Experimental Botany 57, 2493–2499.
Kong L., Liu Y., Zhi P., Wang X., Xu B., Gong Z. & Chang C. (2020) Origins and Evolution of Cuticle Biosynthetic Machinery in Land Plants. Plant Physiology 184, 1998–2010.
Kosma D.K., Bourdenx B., Bernard A., Parsons E.P., Lü S., Joubès J. & Jenks M.A. (2009) The Impact of Water Deficiency on Leaf Cuticle Lipids of Arabidopsis. Plant Physiology 151, 1918–1929.
Lawson T. & Matthews J. (2020a) Guard Cell Metabolism and Stomatal Function. Annual Review of Plant Biology 71, 273–302.
Lawson T. & Matthews J. (2020b) Guard Cell Metabolism and Stomatal Function. Annual Review of Plant Biology 71, 273–302.
Lawson T. & Vialet-Chabrand S. (2019) Speedy stomata, photosynthesis and plant water use efficiency. New Phytologist 221, 93–98.
Lawson T., Weyers J. & A'Brook R. (1998) The nature of heterogeneity in the stomatal behaviour of Phaseolus vulgaris L. primary leaves. 9.
Lee S.B. & Suh M.C. (2022) Regulatory mechanisms underlying cuticular wax biosynthesis. Journal of Experimental Botany 73, 2799–2816.
Lewandowska M., Keyl A. & Feussner I. (2020) Wax biosynthesis in response to danger: its regulation upon abiotic and biotic stress. New Phytologist 227, 698–713.
Li S., Feifel M., Karimi Z., Schuldt B., Choat B. & Jansen S. (2016) Leaf gas exchange performance and the lethal water potential of five European species during drought. Tree Physiology, tpv117.
Liang J., Krauss K.W., Finnigan J., Stuart-Williams H., Farquhar G.D. & Ball M.C. (2023a) Linking water use efficiency with water use strategy from leaves to communities. New Phytologist, nph.19308.
Liang X., Wang D., Ye Q., Zhang J., Liu M., Liu H., … Ellsworth D.S. (2023b) Stomatal responses of terrestrial plants to global change. Nature Communications 14, 2188.
Liu L., Wang X. & Chang C. (2022) Toward a smart skin: Harnessing cuticle biosynthesis for crop adaptation to drought, salinity, temperature, and ultraviolet stress. Frontiers in Plant Science 13, 961829.
Machado R., Loram-Lourenço L., Farnese F.S., Alves R.D.F.B., Sousa L.F., Silva F.G., … Menezes-Silva P.E. (2021) Where do leaf water leaks come from? Trade-offs underlying the variability in minimum conductance across tropical savanna species with contrasting growth strategies. New Phytologist 229, 1415–1430.
Manandhar A., Rimer I.M., Soares Pereira T., Pichaco J., Rockwell F.E. & McAdam S.A.M. (2024) Dynamic soil hydraulic resistance regulates stomata. New Phytologist 244, 147–158.
Mantova M., Herbette S., Cochard H. & Torres-Ruiz J.M. (2022) Hydraulic failure and tree mortality: from correlation to causation. Trends in Plant Science 27, 335–345.
Marenco R.A., Siebke K., Farquhar G.D. & Ball M.C. (2006) Hydraulically based stomatal oscillations and stomatal patchiness in Gossypium hirsutum. Functional Plant Biology 33, 1103.
Martin-StPaul N., Delzon S. & Cochard H. (2017) Plant resistance to drought depends on timely stomatal closure. Ecology Letters 20, 1437–1447.
McAdam S.A.M. & Brodribb T.J. (2012) Stomatal innovation and the rise of seed plants. Ecology Letters 15, 1–8.
McAdam S.A.M. & Brodribb T.J. (2015) The Evolution of Mechanisms Driving the Stomatal Response to Vapor Pressure Deficit. Plant Physiology 167, 833–843.

McAusland L., Davey P.A., Kanwal N., Baker N.R. & Lawson T. (2013) A novel system for spatial and temporal imaging of intrinsic plant water use efficiency. Journal of Experimental Botany 64, 4993–5007.
McDowell N. (2022) Mechanisms of woody-plant mortality under rising drought, CO2 and vapour pressure deficit.
McDowell N.G. & Allen C.D. (2015) Darcy's law predicts widespread forest mortality under climate warming. Nature Climate Change 5, 669–672.
Medrano H. (2002) Regulation of Photosynthesis of C3 Plants in Response to Progressive Drought: Stomatal Conductance as a Reference Parameter. Annals of Botany 89, 895–905.
Meinzer F.C., Johnson D.M., Lachenbruch B., McCulloh K.A. & Woodruff D.R. (2009) Xylem hydraulic safety margins in woody plants: coordination of stomatal control of xylem tension with hydraulic capacitance. Functional Ecology 23, 922–930.
Mirasole F.M., Nastasi S.P., Cubero-Font P. & De Angeli A. (2023) Vacuolar control of stomatal opening revealed by 3D imaging of the guard cells. Scientific Reports 13, 7647.
Mitchell D., Schönbeck L., Shah S. & Santiago L.S. (2025) Leaf drought and heat tolerance are integrated across three temperate biome types. Scientific Reports 15, 12201.
Morris J.L., Puttick M.N., Clark J.W., Edwards D., Kenrick P., Pressel S., … Donoghue P.C.J. (2018) The timescale of early land plant evolution. Proceedings of the National Academy of Sciences 115.
Mott K.A. & Buckley T.N. (1998) Stomatal heterogeneity. Journal of Experimental Botany 49, 407–417.
Mott K.A. & Buckley T.N. (2000) Patchy stomatal conductance: emergent collective behaviour of stomata. Trends in Plant Science 5, 258–262.
Mott K.A., Cardon Z.G. & Berry J.A. (1993) Asymmetric patchy stomatal closure for the two surfaces of Xanthium strumarium L. leaves at low humidity. Plant, Cell & Environment 16, 25–34.
Mott K.A. & Peak D. (2007) Stomatal Patchiness and Task-performing Networks. Annals of Botany 99, 219–226.
Muller (2023) Detailed in-situ leaf energy budget permits the assessment of leaf aerodynamic resistance as a key to enhance nonevaporative cooling under drought.
Murchie E.H. & Lawson T. (2013) Chlorophyll fluorescence analysis: a guide to good practice and understanding some new applications. Journal of Experimental Botany 64, 3983–3998.
Nobel (2009) Physicochemical and Environmental Plant Physiology.
Ochoa M.E., Henry C., John G.P., Medeiros C.D., Pan R., Scoffoni C., … Sack L. (2024) Pinpointing the causal influences of stomatal anatomy and behavior on minimum, operational, and maximum leaf surface conductance. Plant Physiology, kiae292.
Oren R., Sperry J.S., Katul G.G., Pataki D.E., Ewers B.E., Phillips N. & Schäfer K.V.R. (1999) Survey and synthesis of intra- and interspecific variation in stomatal sensitivity to vapour pressure deficit. Plant, Cell & Environment 22, 1515–1526.
Otkin J.A., Svoboda M., Hunt E.D., Ford T.W., Anderson M.C., Hain C. & Basara J.B. (2018) Flash Droughts: A Review and Assessment of the Challenges Imposed by Rapid-Onset Droughts in the United States. Bulletin of the American Meteorological Society 99, 911–919.
Peak D., Hogan M.T. & Mott K.A. (2023) Stomatal patchiness and cellular computing. Proceedings of the National Academy of Sciences 120, e2220270120.
Peak D., West J.D., Messinger S.M. & Mott K.A. (2004) Evidence for complex, collective

dynamics and emergent, distributed computation in plants. Proceedings of the National Academy of Sciences 101, 918–922.
Petek-Petrik A., Petrík P., Lamarque L.J., Cochard H., Burlett R. & Delzon S. (2023) Drought survival in conifer species is related to the time required to cross the stomatal safety margin. Journal of Experimental Botany 74, 6847–6859.
Pinheiro C. & Chaves M.M. (2011) Photosynthesis and drought: can we make metabolic connections from available data? Journal of Experimental Botany 62, 869–882.
Qing Y., Wang S., Yang Z.-L., Gentine P., Zhang B. & Alexander J. (2023) Accelerated soil drying linked to increasing evaporative demand in wet regions. npj Climate and Atmospheric Science 6, 205.
Resco De Dios V., Chowdhury F.I., Granda E., Yao Y. & Tissue D.T. (2019) Assessing the potential functions of nocturnal stomatal conductance in C 3 and C 4 plants. New Phytologist 223, 1696–1706.
Resco De Dios V., Loik M.E., Smith R., Aspinwall M.J. & Tissue D.T. (2016) Genetic variation in circadian regulation of nocturnal stomatal conductance enhances carbon assimilation and growth. Plant, Cell & Environment 39, 3–11.
Ruffault J., Pimont F., Cochard H., Dupuy J.-L. & Martin-StPaul N. (2022) SurEau-Ecos v2.0: a trait-based plant hydraulics model for simulations of plant water status and drought-induced mortality at the ecosystem level. Geoscientific Model Development 15, 5593–5626.
Sato H., Mizoi J., Shinozaki K. & Yamaguchi-Shinozaki K. (2024) Complex plant responses to drought and heat stress under climate change. The Plant Journal 117, 1873–1892.
Schell V., Kervroëdan L., Corso D., N'do D.Y., Faucon M. & Delzon S. (2025) Greater Resistance to Drought-Induced Embolism Is Linked to Higher Yield Maintenance in Soybean. Plant, Cell & Environment, pce.15538.
Schreiber L. (2005) Polar Paths of Diffusion across Plant Cuticles: New Evidence for an Old Hypothesis. Annals of Botany 95, 1069–1073.
Schuster A.-C., Burghardt M. & Riederer M. (2017) The ecophysiology of leaf cuticular transpiration: are cuticular water permeabilities adapted to ecological conditions? Journal of Experimental Botany 68, 5271–5279.
Scoffoni C., Vuong C., Diep S., Cochard H. & Sack L. (2014) Leaf Shrinkage with Dehydration: Coordination with Hydraulic Vulnerability and Drought Tolerance. Plant Physiology 164, 1772–1788.
Seale M. (2020) The Fat of the Land: Cuticle Formation in Terrestrial Plants. Plant Physiology 184, 1622–1624.
Seidl R., Thom D., Kautz M., Martin-Benito D., Peltoniemi M., Vacchiano G., … Reyer C.P.O. (2017) Forest disturbances under climate change. Nature Climate Change 7, 395–402.
Shellakkutti N., Thangamani P.D., Suresh K., Baales J., Zeisler-Diehl V., Klaus A., … Kreszies T. (2022) Cuticular transpiration is not affected by enhanced wax and cutin amounts in response to osmotic stress in barley. Physiologia Plantarum 174.
Shepherd T. & Griffiths D. (2006) The effects of stress on plant cuticular waxes. New Phytologist 171, 469–499.
Slot M., Nardwattanawong T., Hernández G.G., Bueno A., Riederer M. & Winter K. (2021) Large differences in leaf cuticle conductance and its temperature response among 24 tropical tree species from across a rainfall gradient. New Phytologist 232, 1618–1631.
Sussmilch F.C., Roelfsema M.R.G. & Hedrich R. (2019) On the origins of osmotically driven stomatal movements. New Phytologist 222, 84–90.
Taiz L., Zeiger E., Moller I.M. & Murphy A. (2015) Plant Physiology and Development,

Sixth Edition. 888.
Tombesi S., Nardini A., Frioni T., Soccolini M., Zadra C., Farinelli D., … Palliotti A. (2015) Stomatal closure is induced by hydraulic signals and maintained by ABA in drought-stressed grapevine. Scientific Reports 5, 12449.
Torres-Ruiz J.M., Cochard H., Delzon S., Boivin T., Burlett R., Cailleret M., … Martin-StPaul N.K. (2024) Plant hydraulics at the heart of plant, crops and ecosystem functions in the face of climate change. New Phytologist 241, 984–999.
Tredenick E.C. & Farquhar G.D. (2021) Dynamics of moisture diffusion and adsorption in plant cuticles including the role of cellulose. Nature Communications 12, 5042.
Trueba S., Pan R., Scoffoni C., John G.P., Davis S.D. & Sack L. (2019) Thresholds for leaf damage due to dehydration: declines of hydraulic function, stomatal conductance and cellular integrity precede those for photochemistry. New Phytologist 223, 134–149.
Urli M., Porte A.J., Cochard H., Guengant Y., Burlett R. & Delzon S. (2013) Xylem embolism threshold for catastrophic hydraulic failure in angiosperm trees. Tree Physiology 33, 672–683.
Vesala T., Sevanto S., Grönholm T., Salmon Y., Nikinmaa E., Hari P. & Hölttä T. (2017) Effect of Leaf Water Potential on Internal Humidity and CO2 Dissolution: Reverse Transpiration and Improved Water Use Efficiency under Negative Pressure. Frontiers in Plant Science 8.
Vialet-Chabrand S.R.M., Matthews J.S.A., McAusland L., Blatt M.R., Griffiths H. & Lawson T. (2017) Temporal Dynamics of Stomatal Behavior: Modeling and Implications for Photosynthesis and Water Use. Plant Physiology 174, 603–613.
Wang X., Du T., Huang J., Peng S. & Xiong D. (2018) Leaf hydraulic vulnerability triggers the decline in stomatal and mesophyll conductance during drought in rice. Journal of Experimental Botany 69, 4033–4045.
Wingler A., Quick W.P., Bungard R.A., Bailey K.J., Lea P.J. & Leegood R.C. (1999) The role of photorespiration during drought stress: an analysis utilizing barley mutants with reduced activities of photorespiratory enzymes. Plant, Cell & Environment 22, 361–373.
Yang, Brodribb & Bi (2021) Evolution of stomatal closure to optimize water-use efficiency in response to dehydration.
Ye W., Dong J. & Kinoshita T. (2022) Editorial: Stomatal Biology and Beyond. Frontiers in Plant Science 13, 848811.
Yeats T.H., Huang W., Chatterjee S., Viart H.M., Clausen M.H., Stark R.E. & Rose J.K.C. (2014) T omato C utin D eficient 1 (CD 1) and putative orthologs comprise an ancient family of cutin synthase-like (CUS) proteins that are conserved among land plants. The Plant Journal 77, 667–675.
Yeats T.H. & Rose J.K.C. (2013) The Formation and Function of Plant Cuticles. Plant Physiology 163, 5–20.
Zandalinas S.I. & Mittler R. (2022) Plant responses to multifactorial stress combination. New Phytologist 234, 1161–1167.
Zeisler-Diehl V., Müller Y. & Schreiber L. (2018) Epicuticular wax on leaf cuticles does not establish the transpiration barrier, which is essentially formed by intracuticular wax. Journal of Plant Physiology 227, 66–74.

A. Appendix

A.1. An R package to facilitate the accuracy and the reliability of residual and minimal leaf conductance

Residual leaf conductance (g_{res} ; mmol m^{-2} s^{-1}) by the detached leaf mass loss (DLML) method based on the *DroughtBox* system developed by Billon *et al.*, 2020 is one of the most common and accurate protocols to estimate water loss simulating extreme drought. We used the same system described in Burlett *et al.* 2025. The system can simultaneously manage 24 samples and in order to improve the speed and reliability of data processing, a set of functions grouped together in a R package (CuticleR) is currently being developed.

A.1.1. Input data

Two input files are used, one containing leaf mass recorded at each time step with air temperature and relative humidity and the second containing a list of metadata such as leaf area and dry weight used as a constant to estimate residual leaf conductance, water potential and relative water constant.

A.1.2. The residual leaf conductance estimation

The main function (*g_residual)* developed for the parameterisation and treatment of raw data is already available on the Phenobois github (https://gitub.u-bordeaux.fr/phenobois). That main function, *g_residual*, calculates the residual leaf conductance as the slope of the mass data over time (equation A1.1) using the Savitsky-Golay filter to smooth the data and calculate derivatives on noisy data. The Savitzky-Golay filter is a smoothing technique that fits a low-degree polynomial to a moving window of data using least squares regression, allowing it to reduce noise while preserving important features like shifts and peaks. Commonly used in time series, it is particularly useful for maintaining signal shape during smoothing or derivative estimation like the residual leaf conductance as a derivative of the mass. Key parameters include the window size and polynomial order, which must be carefully chosen to balance noise reduction and feature preservation. These parameters are present as arguments of the main function.

Residual leaf conductance was computed for each leaf as the water evaporation rate divided by its driving force (VPD) using equation A1.1:

$$g_{res}(t) = \frac{dw/dt}{M_{H2O}\, A_{leaf}} \times \frac{Patm}{VPD(t)} \qquad (A1.1)$$

, where dw/dt is the slope of the mass (g s^{-1}), M_{H2O} is the molecular weight of water (18.01 g mol^{-1}), P_{atm} is the atmospheric pressure in the chamber (*c*. 101.9 kPa) and VPD is the measured vapour pressure deficit of the air inside the chamber (kPa) calculated at each time step (Teten equation) (equation A1.2).

$$VPD(t) = e_s - e_a = \left(\frac{100 - RH(t)}{100}\right)\left(613.75e^{\left(\frac{17.502 * T_{air}(t)}{240.9 + T_{air}(t)}\right)}\right) * 10^{-3} \qquad (A1.2)$$

The same function (*g_residual)* computes also the corresponding RWC (%) and the water potential (MPa) for each time step using equation A1.3 and A1.4, respectively.

$$RWC(t) = 100 * \frac{FW(t) - DW}{FW(t=0) - DW} \qquad (A1.3)$$

, where FW(t) is the mass at each time step, DW is the dry weight and FW(t=0) is the turgid weight considered as the initial mass of the leaf.

$$WP(t) = \frac{\pi_0}{\frac{RWC}{100}} + max\left(-\pi_0 - \epsilon * \left(1 - \left(\frac{RWC}{100}\right)\right), 0\right) \qquad (A1.4)$$

, where π_0 is the osmotic potential at full turgor and ϵ the elasticity modulus both estimated via the PV-curves. If these parameters are not available, *g_residual* can run avoiding to calculate the water potential.

The output file contains the g_{res} at each time step, the VPD, the RWC and if the parameters are available the water potential. The output file contains most of the variables useful for future analysis and accompanied by a validation graph for each sample. Using input files and the main function, it is possible to obtain residual leaf conductance as well as VPD, RWC and WP for a data set of 24 samples in a few seconds using the same arguments. The dehydration curve is dependent on the species so it's recommended to

adapt the arguments of the function (window size and polynomial order) to each species and each time step recording.

A.1.3. **Others function for VPD and shrinkage correction**

The main function provides a straightforward estimation of residual leaf conductance. However, during the dehydration process, the leaf undergoes significant physiological changes like tissue shrinkage, affecting the accuracy of conductance estimates based on leaf area. Shrinkage is quantified as the percentage loss in leaf area and is determined by fitting a fourth-degree polynomial to the relationship between relative area loss and relative water content (RWC) (Burlett *et al.* 2025), equation A1.5:

$$Shrinkage(t) = \frac{a + b.RWC(t) + c.RWC(t)^2 + d.RWC(t)^3 + e.RWC(t)^4}{100} \quad (A1.5)$$

Using an independent function, the residual leaf conductance can be corrected using the shrinkage function.

$$g_{res,shinkage}(t) = \frac{g_{res}(t)}{Shinkage(t)} \quad (A1.6)$$

In addition, the drop-in water potential has an impact on the water vapour pressure in the substomatal cavities, which affects the VPD between the leaf and the air (Burlett *et al.* 2025). Using a new independent function and equation A1.7 (Vesala *et al.* 2017) and A1.8, it's possible to consider the leaf dehydration in the residual leaf conductance estimate (equation A1.9):

$$\psi = \frac{RT}{V_w} log\left(\frac{e_a}{e_s}\right) \quad (A1.7)$$

$$VPD_{corr}(t) = \left(\frac{100 - RH(t)}{100}\right)\left(e_s * e^{\left(\frac{V_w}{RT}\right)\psi(t)}\right) * 10^{-3} \quad (A1.8)$$

$$g_{res,VPD}(t) = \frac{dw/dt}{M_{H2O}\, A_{leaf}} \times \frac{Patm}{VPD_{corr}(t)} \quad (A1.9)$$

Using the VPD and shrinkage correction, it's possible to combine both corrections to have a better accuracy for the residual leaf conductance (equation A1.10):

$$g_{res,VPS,shinkage}(t) = \frac{g_{res,VPD}(t)}{Shinkage(t)} \qquad (A1.10)$$

At the end, we have four estimations of the residual leaf conductance with shrinkage and VPD correction ($g_{res}(t), g_{res,VPD}(t), g_{res,shinkage}(t)\ and\ g_{res,VPD,shinkage}(t)$.

All these variables come from different functions and are independent.

A recent study made by Fernandes *et al.* (2025) highlighted the impact of high temperature on the leaf minimum conductance estimates reinforcing the need to combine abiotic stress into a multifactorial stress analysis. Taking this "thermal leaky legacy" into account as a correction factor like the shrinkage and VPD is the next step in improving the accuracy of the estimates of the residual leaf conductance that are so important for predicting plant mortality.

A.1.4. Estimation of the minimal leaf conductance (g_{min_at}) using hydraulics traits

Leaf water potential decreases during drought, and crosses different hydraulics thresholds such as turgor loss point (Ψ_{tlp}), which coincides with the stomatal closure (Brodribb *et al.* 2003), along with Ψ_{P12}, Ψ_{P50} and Ψ_{P88}, corresponding to the water potentials inducing 12%, 50% and 88% losses of conductance, respectively. Using a new independent function, the water potential and the corrected or not residual leaf conductance, we can estimate g_{min_at} at each relevant threshold described above, to establish a hydraulic trait that could facilitate interpretation and comparison between species.

Using hydraulic thresholds assumes they are known, but this information is not always available. One approach to estimate minimum leaf conductance involves using continuous RWC measurements to calculate the rate of water loss within the RWC range of 80% to 50%. Such boundaries were set as previous research suggests that these are close to the points of stomatal closure and irreversible dehydration, respectively (Martin-

StPaul *et al.* 2017; Trueba *et al.* 2019). A new function allows us to select the RWC boundaries (such as 80% and 50%) and estimate the minimum leaf conductance as a mean ± sd between these boundaries.

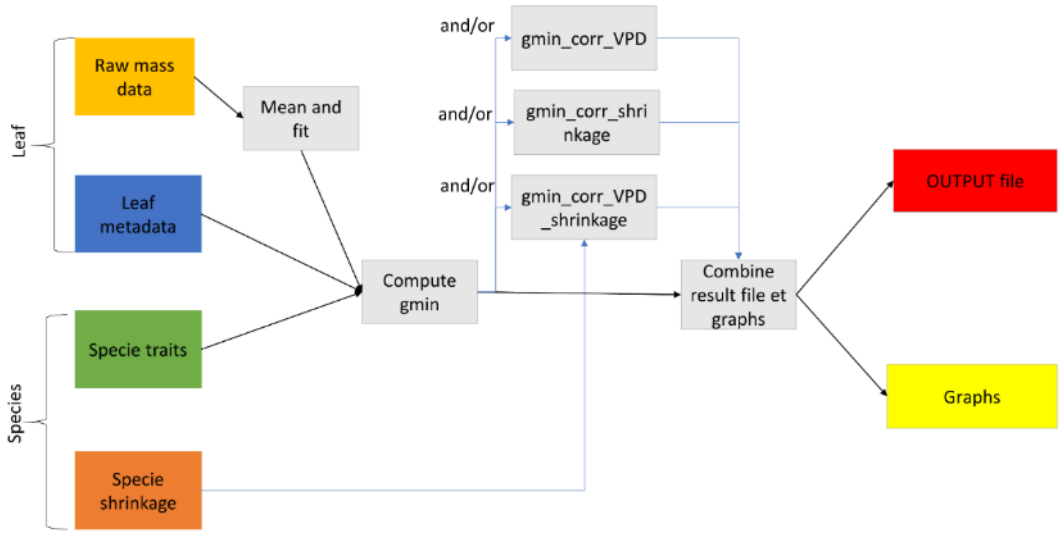

FIGURE A.1:Framework of the CuticleR package

A.2. A set of Python scripts for image processing from FluorImager software

A.2.1. The FluorImager software

The FluorImager software (McAusland *et al.* 2013) records at the same time a set of variables with an image from the thermal and the chlorophyll fluorescence camera already described in chapter 3 and 4. Here, it's a description of the workflow from the software to the figure.

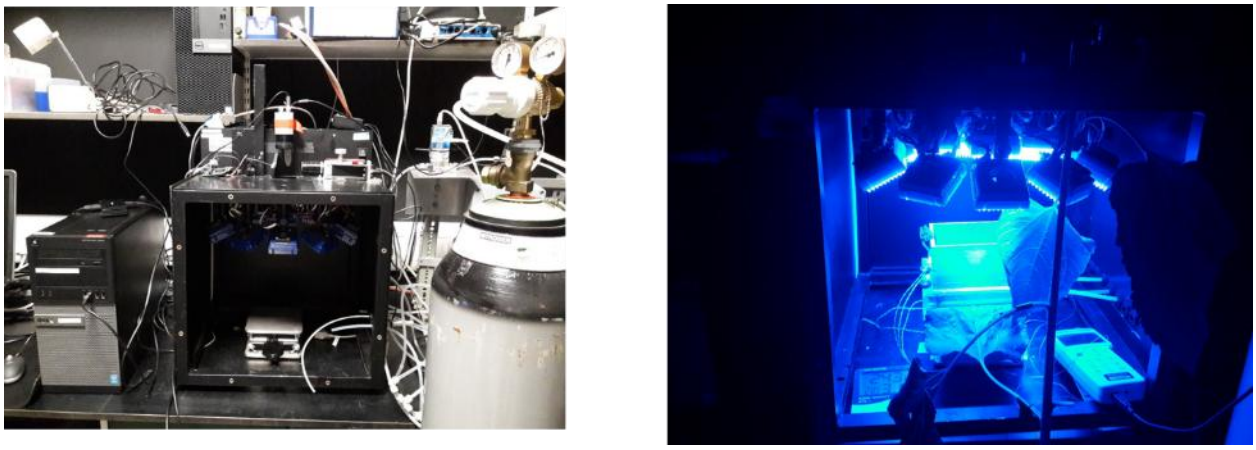

FIGURE A.2: FluorImager system

The FluorImager software written in c++ produces two zip files containing a YAML file. A YAML file is a plain-text file that stores data in a structured, human-readable format. It uses indentation to represent hierarchy, making it easy to read and write. The software was designed to capture leaf responses to temporal changes in environmental factors such as light, CO_2, humidity, and wind. At each configured time step, the software records data in paired zip files.

The first YAML file contains the thermal images, along with environmental variables specified in the initial configuration (such as PPFD and the thermal boundary layer, g_b), as well as air temperature (T_{air}) and relative humidity (RH) recorded by a temperature sensor connected to an Arduino, and the corresponding time stamps. A ROI corresponding to the leaf temperature reference (dry reference used to estimate the stomatal conductance) is recorded as a vector with 4 coordinates (x_1, y_1, x_2, y_2). The thermal image is a 2D opencv-matrix where each value corresponds to a temperature. The second YAML file stores the chlorophyll fluorescence parameters matrices (F_m, F'_m,

F_o, F') in the same dimensions and format as the thermal image. It also includes a time stamp and the corresponding thermal image filename, linking the two datasets.

A.2.2. **Python's function**

Several Python's functions have been developed and grouped in one script available on the repository: https://gitub.u-bordeaux.fr/guforget/thermal-and-fluorescence-images-analysis.

A first Python function (*gz_extract*) read all zip files in the same folder and extracted the YAML files into a new folder. YAMLs must be transformed to be correctly parsed in a python script. Two functions have been dedicated to this transformation (*opencv_matrix* and *get_loader*).

The next function (*extract_data_store_file*) (Figure A3) is the core of the process. Chlorophyl fluorescence and thermal data were extracted and processed from YAML files in the specified directory. For each fluorescence file, relevant metadata (time, PPFD, and associated temperature file) were saved, and PSII efficiency variables (Φ_{PSII}, F_v'/F_m' and F_q'/F_v') were calculated using raw parameters (F_m, F_m', F_o, F'), with NaN values replaced by zero, and stored as text files. Corresponding temperature files were parsed to extract time, air temperature, relative humidity, boundary layer conductance, and reference ROI with temperature values appropriately scaled, and the data were saved in both pickle and text formats. The reference ROI was saved separately to facilitate subsequent analyses.

```
FUNCTION extract_data_store_file(file_dir):
   FOR each file IN file_dir:
      TRY:
         PRINT "opened file {file}"
         IF "Fluo" IN file:
            # --- Process Fluorescence YAML ---
            PARSE YAML file
            EXTRACT time, PPFD, TempFile
            SAVE [time, PPFD, TempFile] TO pickle
            # Compute PSII efficiency metrics
            COMPUTE FqpFmp, FqpFvp, FvpFmp (replace NaN
with 0)
            SAVE metrics TO text files
            # --- Process Temperature YAML ---
            PARSE TempFile YAML
            EXTRACT time, Tair_raw, RH_raw, gb, RefROI, Temp
            SAVE [time, Tair_raw, RH_raw, gb] TO pickle
            SAVE Temp TO text file
            # Save RefROI
            SAVE RefROI TO "RefROI.txt"
      EXCEPT any error:
         PRINT "error opening file {file}"
         CONTINUE
END FUNCTION
```

FIGURE.A.3: Pseudo-code of the function extract_data_store_file

Using the data stored in a designated folder, metrics can be computed via a loop-based function (Figure A4). The thermal image captures both the leaf and its surrounding environment, while the fluorescence image represents only the leaf (background set to zero). Therefore, the F_o' fluorescence image is used as a mask to isolate the leaf in the thermal image. Metrics (mean, standard deviation, etc.) for the entire leaf are then calculated and saved to a CSV file.

```
# Initialize results dataframe
CREATE df_results with columns:
["time","therm","VPD","Temp min","Temp max","Temp
mean","Temp sd",
                        "Tair","Tdry","RH","fluo",
                        "FqpFmp min","FqpFmp
max","FqpFmp mean","FqpFmp sd"]
FOR each file IN natsorted(file_dir):
   IF file is a fluorescence YAML:
      LOAD FqpFmp from corresponding text file, replace
negative values with 0
      LOAD time, PPFD, TempFile from pickle
      LOAD temperature and environmental data from
TempFile
      CREATE mask for non-zero FqpFmp
      APPLY mask to Temp
      # Compute min, max, mean, sd
      CALCULATE min, max, mean, sd for masked Temp
      CALCULATE min, max, mean, sd for FqpFmp
      # Append results to dataframe
      ADD row to df_results with all values
# Save results
SAVE df_results TO csv
```

FIGURE.A.4: Loop to estimates metrics for each leaf

To create images from the matrix in the text files the *imshow* function is used from the Matplotlib library. It's possible to change the color gradient, the minimum and maximum value.

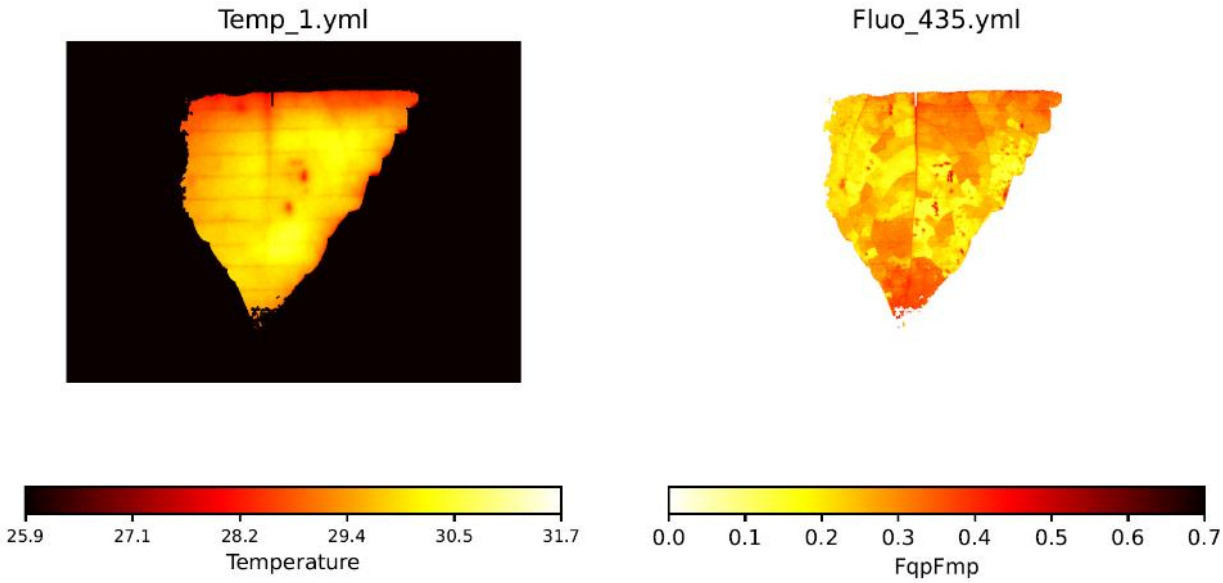

FIGURE.A.5: Thermal and Φ_{PSII} images of the same leaf at WP=-1.34 MPa using the Matplotlib library.

Several functions were developed to analyse the data from both text and image files, including ridgeline plots, image sequences, transects, and scatter plots.

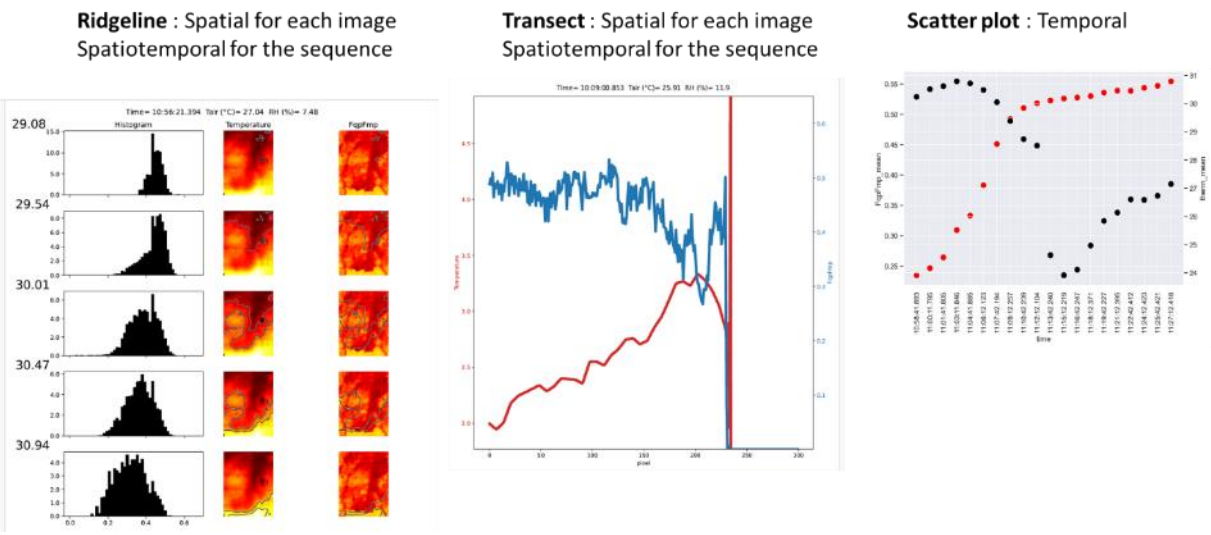

FIGURE.A.6: Example of data analysis using Python functions.

A.3. Stomatal dynamics as the key driver of nocturnal and residual leaf conductance: implications for determining minimum leaf conductance

A.3.1. Abstract

Stomata remain open in darkness in *Helianthus annuus*, resulting in elevated g_{dark} values persisting beyond the turgor loss point and even after the onset of xylem embolism (Ψ_{P12}). This sustained nocturnal conductance plays a critical role in plant water balance and survival as drought progresses. In contrast, residual leaf conductance (g_{res}) remains low and stable throughout the drought sequence, representing minimal water loss independent of stomatal control. Infrared gas exchange provides a rapid and reliable approach for estimating nocturnal leaf conductance (g_{dark}) and residual leaf conductance (g_{res}) during drought.

Determining the moment at which stomatal dynamics have a negligible influence on g_{res} is key for accurately defining g_{min}, composed solely of the cuticular and stomatal leakiness fraction. Here, we show that parameters related to leaf mass and leaf surface temperature provide interesting and easy parameters for the determination of this moment. Combining these intrinsic parameters improves the precision of estimating g_{min} from residual leaf conductance.

Keywords:

Drought stress, stomatal closure, nocturnal, residual and minimum leaf conductance, relative water content, moisture ratio, leaf temperature

A.3.2. Introduction

Leaf transpiration results from the combined diffusion of water vapor through two pathways: the stomata, which actively regulate their aperture in response to both environmental and internal cues (Oren *et al.* 1999; Buckley 2005, 2019 219; McAdam & Brodribb 2015; McDowell & Allen 2015; Tombesi *et al.* 2015; Grossiord *et al.* 2020) and the cuticle, which provides a passive pathway driven by the humidity gradient between inside and outside of the leaf (Kerstiens 1996; Schreiber *et al.* 2021). Stomata are microscopic pores, or ostioles, surrounded by a pair of guard cells on aerial part of land

plant and particularly on leaves, appeared before the divergence of bryophytes (mosses) and tracheophytes (vascular plants) (Morris *et al.* 2018; Donoghue *et al.* 2021; Clark *et al.* 2022) nonetheless after the cuticle where the apparition is dated approximately 500 Ma ago (Kong *et al.* 2020).

The overall rate of leaf water loss is determined by the stomatal (g_s, mmol m^{-2} s^{-1}) and cuticular (g_{cuti}, mmol m^{-2} s^{-1}) conductances, respectively associated with a boundary layer (Márquez *et al.* 2021). In well-watered plants, it rises during daylight as stomata open in response to light allowing CO_2 uptake for photosynthesis reflecting an active water use strategy. In darkness or under stressed conditions such as soil water scarcity, stomata close, leading to lower water loss. Contrary to the expectation that stomata remain closed in the absence of light, studies consistently demonstrate substantial water loss during the night and not only via the cuticle (Caird *et al.* 2007). Defined as the nocturnal leaf conductance (g_{dark}), water loss during the night has been documented across a wide range of plant functional types, including both C_3 species (like *Helianthus annuus*) and C_4 species (Snyder 2003; Caird *et al.* 2007; Howard & Donovan 2007; Neumann *et al.* 2014; Resco De Dios *et al.* 2019a). The functional significance of nocturnal water loss remains debated especially during drought. Proposed explanations include facilitation of nutrient uptake, maintenance of hydraulic integrity, and contributions to processes such as hydraulic redistribution (Neumann *et al.* 2014; Coupel-Ledru *et al.* 2016; Resco De Dios *et al.* 2019b). Recent theoretical work has further suggested that nighttime stomatal behavior may reflect an optimisation strategy, balancing the costs of water loss against potential benefits for carbon gain and hydraulic function (Wang *et al.* 2021). Nocturnal leaf conductance reflects minimal stomatal activity in the absence of light, providing insight into the baseline water loss occurring with no light. Although stomatal aperture is generally reduced at night, the absolute minimum level of stomatal activity is strongly constrained by water availability, particularly under soil water scarcity. Stomatal closure follows a non-steady dynamic attributable to stomatal activity (Buckley 2005; Powles *et al.* 2006; Drake *et al.* 2013) that leads to the minimal stomatal activity where only stomatal leakiness and cuticle water loss is present. This water loss rate, referred to as residual leaf conductance (g_{res}) represents a critical flux, leading the plant to death if the drought persists. Together, nocturnal and residual leaf conductance represent a significant part of plant water regulation, with important implications for plant physiology and survival under varying environmental conditions.

Based on the definition of an ecological trait (Violle *et al.* 2007), the residual and nocturnal leaf conductance can not be considered as a trait due to their dynamic nature over time and the impossibility to measure as stable, heritable characteristics allowing comparison and prediction. Nevertheless, unlike nocturnal leaf conductance, a trait related to drought tolerance based on residual leaf conductance has been described. Expressed as the minimum leaf conductance (g_{min}), this trait estimates at physiological or water status boundaries (Burlett *et al.* 2025), is relevant for comparing species' drought tolerance and for predicting the time taken for a plant to reach a lethal hydraulic failure (Cochard at al. 2020; Ruffault *et al.* 2022; Petek-Petrik *et al.* 2023).

Understanding how these conductances vary under water stress is therefore crucial for understanding water use strategies and improving predictions of plant survival, since they influence the rate of dehydration. Infrared gas analyzers (IRGA) provide a powerful tool to estimate simultaneously on the same leaf the nocturnal and residual leaf conductance under controlled conditions such as drought. By combining measurements along a drought sequence, it is possible to track the dynamics of these conductances and to infer the stomatal impact on overall water loss. However, infrared gas analysers do not allow cuticular conductance to be distinguished from stomatal conductance. Furthermore, these devices do not provide information on the leaf's water status to estimate the minimum leaf conductance. To evaluate this contribution of the cuticular fraction, it is crucial to determine the moment at which stomatal dynamics influence is minimal. Monitoring variations in the rate of water loss during dehydration thus makes it possible to detect changes in stomatal dynamics using the detached leaf mass loss (DLML) method, which allows real-time estimation of residual leaf conductance throughout dehydration, with the associated leaf's water status based on mass and 'intrinsic' parameters.

Using an infrared gas analyzer (IRGA) and the detached leaf mass loss (DLML) method, we recorded the nocturnal leaf conductance (g_{dark}) and residual leaf conductance (g_{res}) on leaves to: (i) highlight the stomatal dynamics in both conductance throughout drought sequence. We hypothesise that the discrepancy for g_{dark} and g_{res} is mainly due to stomatal closure dynamics and (ii) pinpoint, using "intrinsec" leaf parameters, the moment when stomatal dynamics ceased, hypothesising that the change in diffusion rate related to stomatal dynamics can be determined. Determining when stomatal dynamics are at their lowest is a physical approach that allows us to distinguish the minimum water

loss due solely to stomatal leakiness and the cuticle which is essential for determining the minimum leaf conductance.

A.3.3. **Material and methods**

A.3.3.1. Plant material

For the determination of the nocturnal and residual leaf conductance using infrared gas analyser, *Helianthus annuus* seeds were sown in plastic trays containing compost and germinated in a growth cabinet (Reftech BV, Sassenheim, the Netherlands). After germination, seedlings (one per pot) were transplanted into 1.5 liters pots containing compost and transferred to a temperature-controlled glasshouse at the University of Essex (average temperature was maintained at 21.8 ± 0.9 °C with RH between 40% and 55% depending on biomass in the glasshouse), supplementary sodium vapour lights (8am until 8pm) provided 400 (µmol s^{-1} m^{-2}) at the plant height).

For the detached leaf mass loss (DLML) method, *Helianthus annuus* seeds were sown into 3 liters pots containing compost. Plants grown in a 9 m² climatic chamber (Strader, France) at the University of Bordeaux where the climatic and light parameters were set to 25°C; 80% RH; Photon Flux Density c. 700 µmol m^{-2} s^{-1}.

Plants were grown for 45 days before measurements were taken on the youngest fully expanded leaf on *H. annuus* plants. After the plants reached leaf maturity but before flowering, groups of four individuals were put under water stress by stopping watering. This procedure was repeated four times, creating sets of plants with different levels of stress.

A.3.3.2. Hydraulic trait measurements: Pressure-volume curve and stem embolism vulnerability

Pressure-volume curves were performed using a method adapted from Sack *et al.*, (2011) on eight leaves of *H. annuus*. Pressure-volume curves were used to determine leaf physiological traits such as the water potential (Ψ_{tlp}, MPa) at turgor loss point along with the elasticity modulus (ε) and osmotic potential at full turgor (π_0) (Table A.1). Using ε and π_0 we estimated the water potential at any RWC during the DLML experiment based on the relative water content. Leaf water potential (Ψ_{leaf}, MPa) was measured with a psychrometer (PSY1, ICT International, Armidale, NSW, Australia) before each measurement.

Stem vulnerability to xylem embolism was assessed on five *H. annuus* stems using the Cavitron technique (Cochard 2002; Burlett *et al.* 2022). Measurements were carried out at the platform for hydraulic traits (Caviplace, Phenobois platform, University of Bordeaux, Pessac, France). A percentage loss of conductance or PLC curve was obtained and embolism vulnerability determined at thresholds Ψ_{P12}, Ψ_{P50} and Ψ_{P88} (MPa), which correspond to the xylem pressure/water potential inducing 12%, 50% and 88% losses of hydraulic conductivity, respectively.

To facilitate analysis, leaves were categorised by water potential measurements and divided into three classes using water potential at turgor loss point (Ψ_{tlp}) and embolism vulnerability threshold at 50% losses of hydraulic conductivity (Ψ_{P50}). There were well-hydrated leaves considered with no stress [0 ; Ψ_{tlp}], with mild stress [Ψ_{tlp} ; Ψ_{P50}] and with a severe stress [Ψ_{P50} ; -Inf].

A.3.3.3. Gas exchange measurement

Plants were kept in the dark for 1 hour prior to measurements in the same room as the infrared gas analyzer, with ambient conditions of ~23 °C and 40–50% relative humidity. Gas exchange measurements were conducted using a LI-COR 6800 (LICOR, USA) with the following environmental settings: flow rate 1000 µmol s^{-1}, CO_2 concentration 400 µmol mol^{-1}, fan speed 10,000 rpm, and no light. Temperature and relative humidity inside the chamber matched room conditions. Measurements were performed on 39 fully developed leaves. Each leaf was placed in the chamber and leaf conductance (g_s) was recorded after stabilization. The leaf petiole was then excised with a razor blade and air-dried on a clothesline in the same room. After 4–5 hours of drying, the leaf was returned to the chamber under identical conditions, and the leaf conductance (g_s) was recorded. Mean nocturnal (g_{dark_mean}) and residual (g_{res_mean}) leaf conductance correspond to the mean during stabilisation of the leaf conductance (g_s) before and after a period of drying, respectively. Some leaves were not removed from the chamber after the excision and the complete dynamics was recorded (Figure A7).

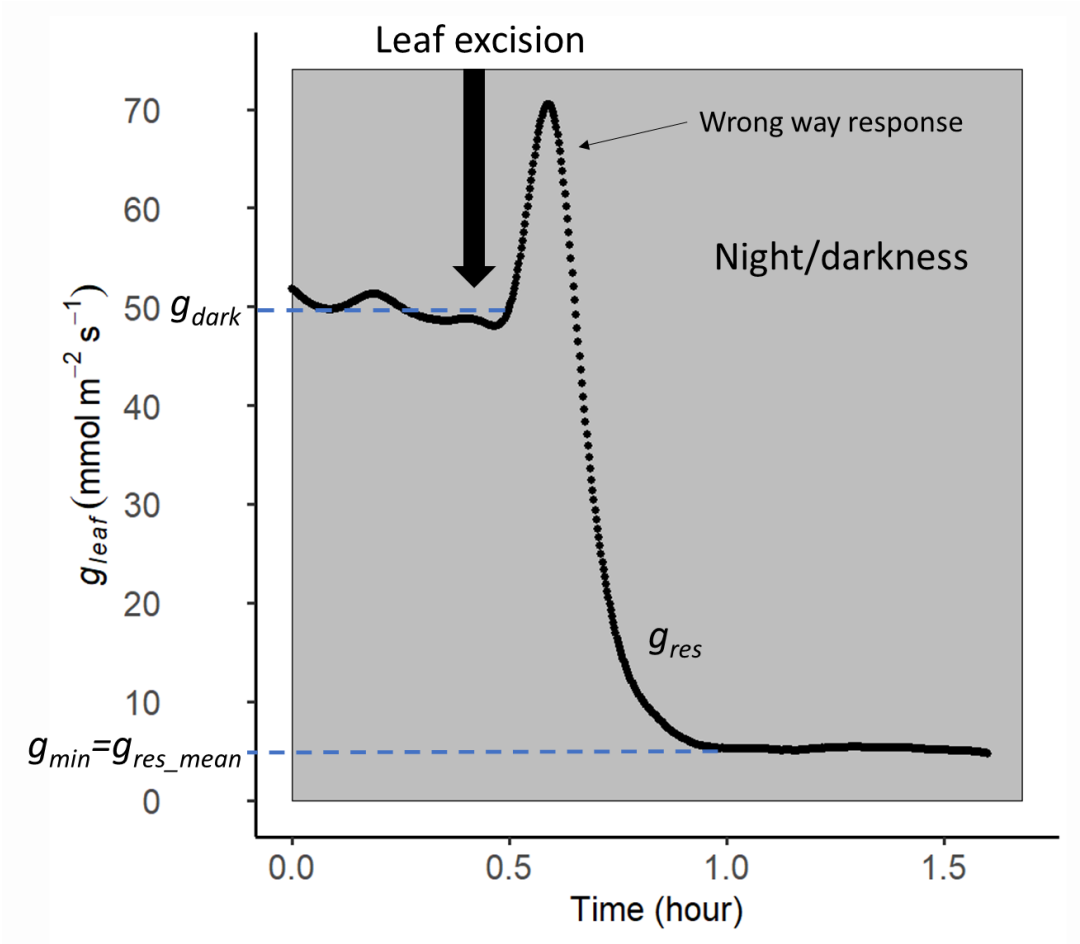

FIGURE.A.7: Scheme of leaf conductance in darkness after leaf excision.
The nocturnal leaf conductance (g_{dark}) corresponds to the stabilisation in the dark of the leaf conductance. The residual leaf conductance (g_{res}) corresponds to the leaf dehydration after the leaf excision and the minimum leaf conductance (g_{min}) is here the stabilisation of the g_{res} and corresponds to the water loss after stomatal closure.

A.3.3.4. Residual leaf conductance (g_{res}) using the detached leaf mass loss (DLML) method and determination of the stomatal closure

Residual leaf conductance (g_{res}) of detached leaves were estimated using the *DroughtBox* (Billon *et al.*, 2020) based on the detached leaf mass loss (DLML) method. Leaves were cut with a razor blade and the petiole sealed with paraffin to avoid water loss. Each leaf was weighed with a 4-digit balance (Pioneer,Ohaus, USA) and scanned (v850 pro, Epson, Japan) to estimate the projected leaf area (A_{leaf}, m²). Leaves were then clipped to load cells inside a climatic chamber to simulate drought through desiccation. Conditions inside the chamber were kept stable at 25°C and 60% of relative humidity, with a vapour pressure deficit (VPD) of c. 1.26 kPa. Micro load cells by Wheastone bridge board (1046_OB, Phidgets Inc., Canada) were used to record the mass every five minutes in the chamber. During measurements, samples were placed in the dark to avoid

light impacting stomatal kinetics. A detailed description of the system and setup is provided in (Burlett *et al.* 2025). A custom function in R was developed for the parameterisation and treatment of raw data (g_residual, PHENOBOIS, University of Bordeaux; https://gitub.u-bordeaux.fr/phenobois). The main function, g_residual, calculates the residual leaf conductance as the slope of the mass data over time (equation A3.1) using the Savitsky-Golay filter to smooth the data and calculate derivatives on noisy data. Residual leaf conductance, g_{res} (mmol m^{-2} s^{-1}), was computed for each leaf as the water evaporation rate divided by its driving force (VPD) using equation A3.1:

$$g_{res} = \frac{dw/dt}{M_{H2O}\, A_{leaf}} \times \frac{Patm}{VPD} \qquad (A3.1)$$

, where dw/dt is the slope of the mass (g s^{-1}), M_{H2O} is the molecular weight of water (18.01 g mol^{-1}), Patm is the atmospheric pressure in the chamber (c. 101.9 kPa) and VPD is the measured vapour pressure deficit of the air inside the chamber (kPa) calculated at each time step.

A.3.3.4.1. Relative water content

Relative water content (RWC) is a mass-derived parameter following the mass loss rate. It was composed of the Turgid weight (TW, g) of each individual leaf and was measured before the water loss measurements in the climatic chamber. Weight measurements were performed with a 4-digit balance (Pioneer, Ohaus, USA). At the end of the measurement, leaves were put in an oven at 65°C for 72h and dry weight (DW, g) was measured. The relative water content (RWC, %) was then computed for each mass value (fresh mass; FW, g) during the dehydration process using equation A3.2:

$$RWC = 100 * \frac{FW - DW}{TW - DW} \qquad (A3.2)$$

A.3.3.4.2. Drying curve parameters

The *DroughtBox* can be considered as a drying box. Leaves are placed in a chamber where the air flow, temperature and relative humidity are controlled and water (free and bond) evaporation is recorded by energy transfer. The main goal of the drying process is to reduce the water content of materials such as fruit, wood or leaves to a

desired level in order to prevent microbial and fungal development while preserving structural, biochemical, or physiological integrity as needed for the specific purpose. The moisture content (M_t, kg) and the moisture ratio (MR,%) were two main parameters used and were defined as:

$$M_t = \frac{(m_t - m_d)}{m_d} \qquad (A3.3)$$

$$MR = \frac{(M_t - M_e)}{(M_o - M_e)} \qquad (A3.4)$$

, where M_t was the moisture content at time *t*, m_t was the mass at time *t*, m_d was the mass of the completely dried sample. M_0 was the initial moisture content, and M_e is the equilibrium moisture content. The value of M_e was equal to the moisture content at the end of drying, at which the sample weight becomes constant with the drying time (Cai *et al.* 2023). Fick's second law of diffusion was used to describe the drying process and describes how the moisture ratio changes over time and space.

$$\frac{\partial MR}{\partial t} = \nabla(D_{eff} \nabla MR) \qquad (A3.5)$$

Effective moisture diffusivity (D_{eff}) was the key drying parameter that represents the conductive term of all moisture transfer mechanisms. A solution of the equation A3.5 is :

$$MR = \left(\frac{8}{\pi^2}\right) \sum_{n=0}^{\infty} \frac{1}{(2n+1)^2} exp\left(-\frac{(2n+1)^2 \pi^2 D_{eff}}{4L^2} t\right) \qquad (A3.6)$$

,where n was a positive integer, *t* was the drying time (s) and L was the half thickness of the sample (m). This equation can be simplified by taking the first term (n=0). Using the logarithm properties, the equation is now linear and easy to interpret by plotting it versus time.

$$ln(MR) = ln\left(\frac{8}{\pi^2}\right) - \left(\frac{\pi^2 D_{eff}}{4L^2} t\right) \qquad (A3.7)$$

A change in the slope represented by the effective moisture diffusivity can be detected, indicating a change in the way the leaf loses water. The shift in the slope was performed using the RMSE method.

A.3.3.4.3. Leaf surface temperature

By adding a non-contact infrared temperature sensor (MLX90615, Melexis Belgium) positioned in front of a leaf in the *DroughtBox* and connected to an Arduino (Figure S A1), we recorded the leaf surface temperature (T_{leaf}) during the dehydration process where the mass loss is recorded every five minutes. Using the ambient temperature (T_{air}) recorded at every time step, we estimated the leaf-to-air surface temperature difference between the leaf and air temperature, $\Delta T = T_{leaf} - T_{air}$. A change in the curve can be detected, indicating a change in leaf cooling. The change in the curve was performed using the RMSE method.

A.3.3.4.4. RMSE method to estimate the shift change in a curve

To detect shifts in the curve, such as a transition from exponential to linear dynamics, we used the RMSE to compare the goodness of fit of different models applied to separate portions of the data. By systematically testing moving points and calculating the RMSE for each model on its respective segment, the approach identifies the point where the combined error is minimised, indicating the most likely location of the shift in curve behaviour (Figure S A3). For the mass-parameter like the relative water content and the moisture ratio, the linearization produced a linear curve. The RMSE method used for the left and right part a linear model with the form $y = ax + b$. For the leaf-to-air surface temperature difference, the curve was decomposed into an exponential part $y = ae^{bt}$ and the right into a linear part $y = cx + d$.

A.3.3.5. Data processing and analysis

All data processing and analysis were carried out using RStudio 2022.12.0+353 (R Core Team 2020). To compare more than two groups, a one-way ANOVA with Tukey HSD post hoc test was performed and to compare two groups a Student-test was

performed after checking for normality and homogeneity of variance. Non-parametric tests were used, when normality was not reached.

A.3.4. **Results**

A.3.4.1. Nocturnal and residual leaf conductance along a drought sequence

In the dynamic approach, leaves were dehydrated directly within the infrared gas-exchange chamber, where stomatal conductance was continuously monitored until reaching its minimum value. In contrast, the non-dynamic approach required to remove the leaf from the chamber, allowing it to air-dry under ambient room conditions, and then placing it back into the chamber to measure stomatal conductance. Comparison of the two methods revealed no significant difference in the estimation of the mean residual leaf conductance (g_{res_mean}) ($\chi^2 = 1.64$, $p = 0.20$; Table SA3.2), which was derived from the mean of the linear part of the stomatal conductance curve (Figure S A2). Across measurements, variation in leaf water potential explained the majority of the observed variability in g_{res_mean}.

The mean nocturnal leaf conductance (g_{dark_mean}) declined progressively with increasing drought severity, showing a significant negative correlation with water status ($R = -0.62$, $R^2 = 0.39$, $p<0.001$; Figure A8a). Across the drought sequence, g_{dark_mean} decreased from 28.85 ± 5.47 mmol m^{-2} s^{-1} before Ψ_{tlp} to 5.47 ± 1.08 mmol m^{-2} s^{-1} after Ψ_{P50} (Table A1 and Figure A8b). No significant difference was calculated between g_{dark_mean} values measured before Ψ_{tlp} and between Ψ_{tlp} and Ψ_{P50}; however, both groups differed significantly with the lower g_{dark_mean} observed after Ψ_{P50} (Figure A8b). Variability was important for well-watered leaves until Ψ_{P12} and decreased to reach a minimum of variability after the Ψ_{P50} (Figure A8a and A8b).

TABLE A.1: Average and standard error, coefficient of variation, standard deviation and maximum of mean nocturnal (g_{dark_mean}) and residual (g_{res_mean}) leaf conductance.
Letters indicate significant differences across different thresholds as indicated with a one-way ANOVA with Tukey HSD post hoc test.

	Mean ± se	Coefficient of variation	sd	Maximum
unit	mmol m^{-2} s^{-1}	-	mmol m^{-2} s^{-1}	mmol m^{-2} s^{-1}
$g_{dark\_mean\_before\_tlp}$	28.85 ± 5.47^{a}	0.50	14.47	49.28
$g_{dark\_mean\_[tlp\_P50]}$	18.94 ± 2.75^{a}	0.68	12.89	51.26
$g_{dark\_mean\_after\_P50}$	5.47 ± 1.08^{b}	0.62	3.41	13.12
$g_{res\_mean\_before\_tlp}$	6.23 ± 1.07^{A}	0.45	2.82	10.49
$g_{min\_mean\_[tlp\_P50]}$	6.08 ± 0.75^{A}	0.58	3.53	15.23
$g_{min\_mean\_after\_P50}$	4.51 ± 0.59^{A}	0.41	1.86	7.68

In contrast, the mean residual leaf conductance (g_{res_mean}) showed a non-significant negative correlation with drought progression ($R = -0.32$, $R^2 = 0.099$, $p>0.05$; Figure A8a). Its variability across the drought sequence was limited, ranging from 6.23 ± 1.07 mmol m^{-2} s^{-1} before Ψ_{tlp} to 4.51 ± 0.59 mmol m^{-2} s^{-1} after Ψ_{P50} (Table A1). However, variability was higher for the [Ψ_{tlp}-Ψ_{P50}] group but no significant differences were calculated among g_{res_mean} groups (Figure A8b), suggesting that g_{res_mean} was marginally influenced by stomatal regulation unlike the nocturnal leaf conductance.

A significant difference was observed between mean nocturnal leaf conductance (g_{dark_mean}) and mean residual leaf conductance (g_{res_mean}) across all drought classes, except for the group after Ψ_{P50} (Table A2 and Figure A8b). This non-significant difference beyond Ψ_{P50} indicated that stomatal dynamics ceased i.e. stomata was maximally close at their maximum without dynamic change.

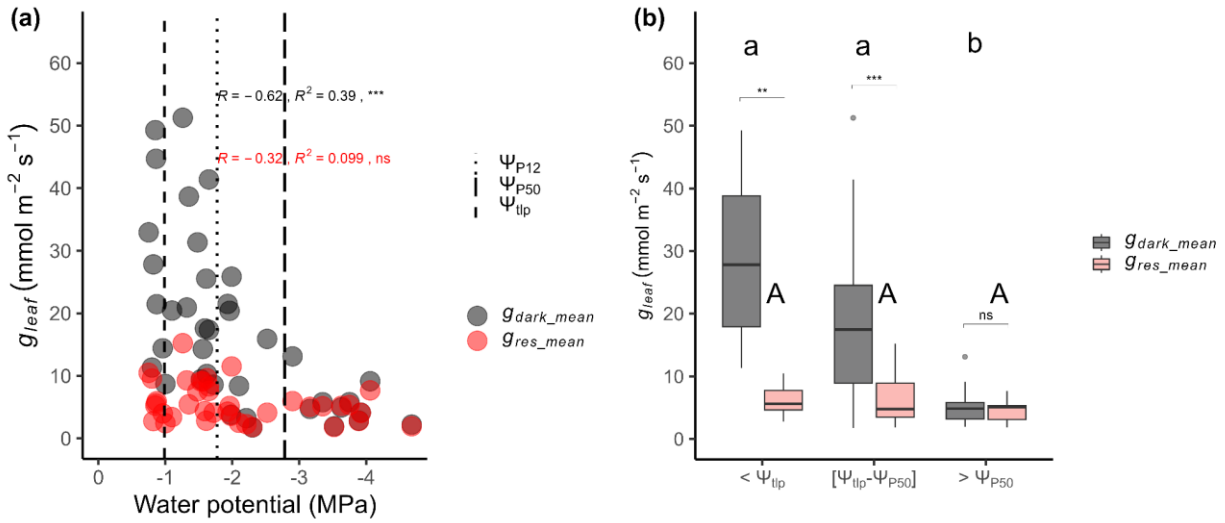

FIGURE.A.8: (a) Mean nocturnal (g_{dark_mean}, black) and residual (g_{res_mean}, red) leaf conductance along a drought sequence.
Solid red regression corresponds to the fit according to a logistic model, dashed lines represent Ψ_{tlp}, dotted line represent Ψ_{P12} and long-dashed lines represent Ψ_{P50}. R corresponds to the Peason's correlation coefficient, R^2 to the coefficient of determination and stars to the p-value (***<0.001 and ns>0.05). (b) Boxplot representations of mean nocturnal (g_{dark_mean}, black) and residual (g_{res_mean}, red) leaf conductance by drought stress class. Horizontal lines, boxes and bars show the median, quartiles and extreme values, respectively. Letters indicate significant differences across different drought stress class with a one-way ANOVA with Tukey HSD post hoc test, stars indicate differences between mean nocturnal (g_{dark_mean}, black) and residual (g_{res_mean}, red) leaf conductance inside drought stress class using a Student's t test (***, p<0.001; **, p<0.01, *, p<0.05, ns, p> 0.05).

TABLE A.2: Student's t test results for comparison between g_{dark_mean} and g_{res_mean} at each group.

	group	group	n1	n2	statistic	df	p	
Before Ψ_{tlp}	g_{dark_mean}	g_{res_mean}	7	7	4.06	12	1.58E-03	**
Between Ψ_{tlp} and Ψ_{P50}	g_{dark_mean}	g_{res_mean}	22	22	4.51	42	5.09E-05	***
After Ψ_{P50}	g_{dark_mean}	g_{res_mean}	10	10	0.783	18	4.44E-01	ns

A.3.4.2. Estimating the moment where residual leaf conductance has limited stomatal contribution using "intrinsec" parameter

Residual leaf conductance (g_{res}) decreased nonlinearly with decreasing relative water content (log(RWC)) (Figure A9a). At high water content (less negative log(RWC)), g_{res} was maximal, but as the leaf dehydrated, g_{res} declined steeply and approached near-zero values. A similar nonlinear pattern was observed between g_{res} and leaf–air temperature difference (ΔT) (Figure A9b). g_{res} was highest when ΔT was negative, indicating a maximal cooling and declined sharply as ΔT became less negative (Figure

A9b). Minimal value for the g_{res}, was reached when ΔT was above 0°C suggesting that there is no longer any cooling. The relationship between ΔT and log(RWC) was also nonlinear, with ΔT decreasing (i.e., leaves becoming warmer) as relative water content declined (less negative log(RWC)) (Figure A9c). This relationship reflects reduced cooling efficiency or transpiration as leaves lose water.

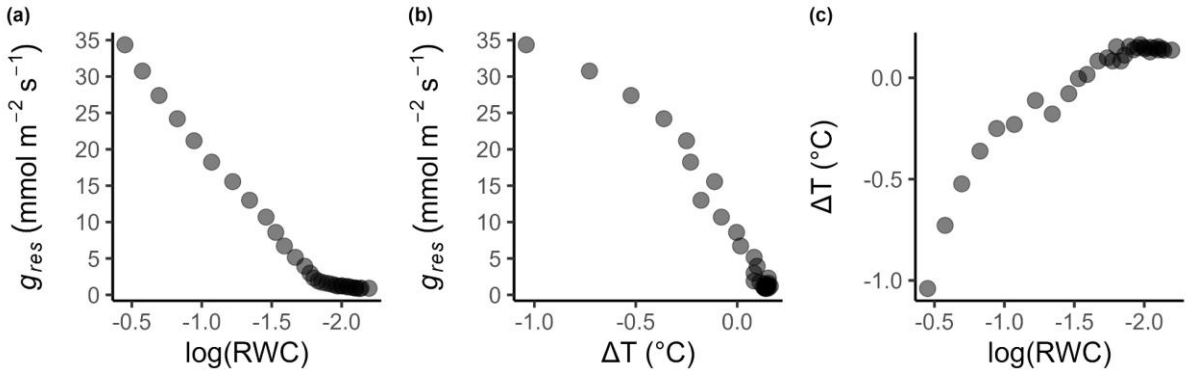

FIGURE A.9: Relationship between (a) the residual leaf conductance (g_{res}) versus the linearization of the RWC, (b) the residual leaf conductance (g_{res}) versus leaf-to-air surface temperature difference and (c) leaf-to-air surface temperature difference versus the linearization of the RWC.

The linearisation of the relative water content and the moisture ratio using the logarithm function showed a shift in the linear curve by a change in the slope. This change indicated that the diffusion rate changed over time passing from an exponential form to a linear one (Figure A9 and Figure S A4). The leaf-to-air surface temperature difference declined in an exponential manner during the dehydration process, until stabilising at a constant value above 0°C, which corresponded to a minimal impact of stomata leading to a leaf warmer than the air (Figure A10 and Figure S A4). The moment when stomatal dynamics ceased differed depending on whether it was deduced from measurements based on leaf mass or leaf surface temperature (Figure A10 and Figure S A4). Using the RMSE method, the leaf temperature difference indicated a shift after 4.5 hours of desiccation. It was 0.5 hour before the estimation using the logarithm of the relative water content and the moisture ratio, respectively (Figure A10 and Figure S A4, Table A3). The residual leaf conductance (g_{res}) associated with each time was $g_{res\_temperature}$ = 10.68 mmol m^{-2} s^{-1}, g_{res_lnRWC} = 6.81 mmol m^{-2} s^{-1} and g_{res_lnMR} = 6.81 mmol m^{-2} s^{-1}.

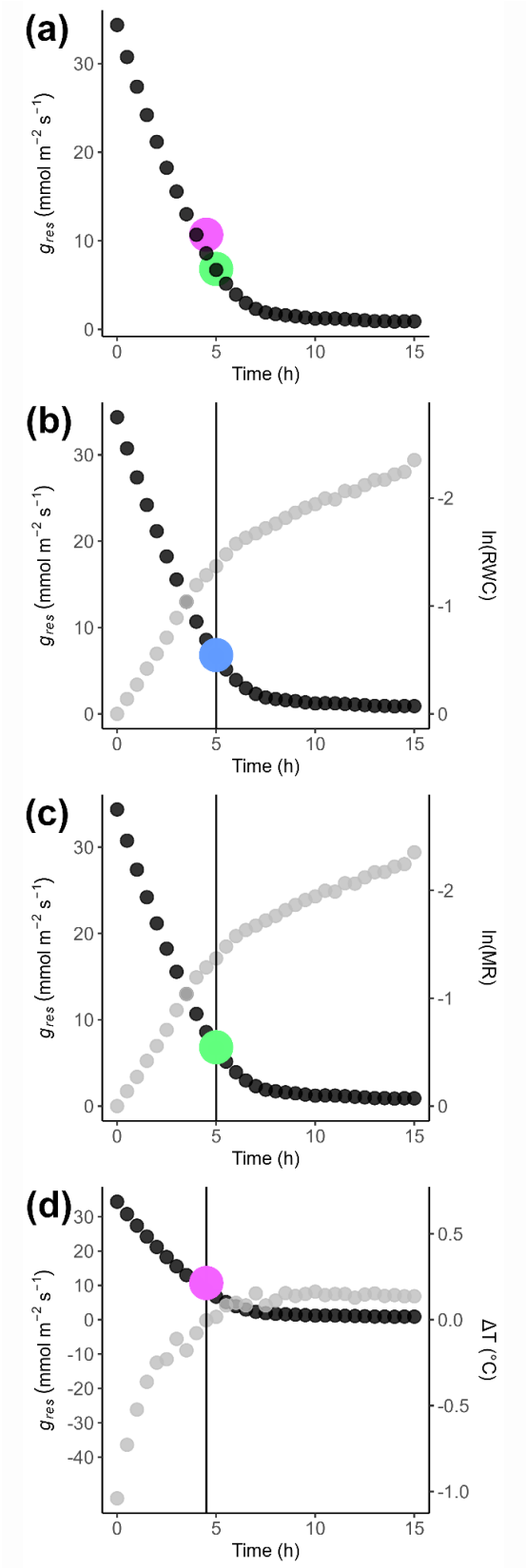

FIGURE A.10: (a) residual leaf conductance (black curve) versus Time (b), linearization of the RWC (grey curve), (b), linearization of the MR (grey curve) and (d), leaf-to-air surface temperature difference (grey curve) (c) versus time.
Blue, green and purple dots correspond to the moment change for each parameter using the RMSE method from a developed R function. Example from *Helianthus annuus* leaf.

TABLE A.3: Estimated Time and residual leaf conductance where stomatal dynamics ceased

	Estimated time (hours)	g_{res} associated (mmol m^{-2} s^{-1})
Leaf temperature	4.5	10.68
ln (RWC)	5.0	6.81
ln (MR)	5.0	6.81

A.3.5. **Discussion**

Stomatal dynamics is the main driver in nocturnal and residual leaf conductance variability until severe drought conditions, Ψ_{P50}. After this threshold, stomatal dynamic impact is negligible leading to the same low and constant nocturnal and residual leaf conductance. The shift between an active to a passive stomatal dynamic can be determined using the leaf mass and surface temperature parameters, each method given a different timing with a different biological significance.

A.3.5.1. Drought impact on nocturnal leaf conductance

Although the mechanisms driving nocturnal water loss remain incompletely understood, the persistence of relatively high nocturnal leaf conductance during drought, even beyond the turgor loss point (Ψ_{tlp}), indicates that nocturnal stomatal opening is a non-negligible component of daily plant water balance. This sustained high nocturnal leaf conductance under conditions of continuous declining soil water availability suggests that nocturnal stomatal behaviour, rather than being a passive leakage (Resco De Dios *et al.* 2019b), may represent an active regulatory process (Wang *et al.* 2021) and might influence drought responses in *Helianthus annuus* especially time to hydraulic failure.

Up to Ψ_{P50}, the g_{dark} is significantly different compare to the average g_{res} and cannot be considered as a residual or minimal leaf conductance demonstrating the crucial role played by stomata and the obligation to distinguish both g_{dark} and g_{res}. Before the turgor loss point, the mean nocturnal leaf conductance is 4.63 times higher than the mean residual leaf conductance, and it remains 3.11 times higher between Ψ_{tlp} and Ψ_{P50}, indicating a substantial contribution to nocturnal water loss during drought progression. If the residual leaf conductance is variable during dehydration as shown by Burlett *et al.* (2025), the nocturnal leaf conductance is also variable and decreases during drought impacting water loss during drought sequence. The stomatal margin retention index ($SMRI_{\Psi P50}$) (Petek-Petrik *et al.* 2023) which quantifies the speed required to consume the

stomatal safety margin (SSM) defined as the difference between water potential at 90% stomatal closure (Ψ_{gs90}) and Ψ_{P50} (Creek *et al.* 2020) could be impacted by the impact of the nocturnal leaf conductance in particular if the minimum leaf conductance is significantly different to the nocturnal leaf conductance. Incorporating nocturnal stomatal dynamics into soil–plant–atmosphere models is essential, particularly in drought-induced mortality models, to accurately consider the physiological contribution of this conductance. Similar to how minimum leaf conductance is used as a hydraulic trait derived from residual leaf conductance, a trait can be defined based on nocturnal leaf conductance and integrated into these models (Resco De Dios *et al.* 2019b). For consistency and comparability, this trait must be evaluated under standardised protocols with clearly defined reference points, for instance, at a specific water potential such as pre-dawn Ψ_{pre_dawn} when real-time water status measurements are unavailable, or alternatively at thresholds like the turgor loss point (Ψ_{tlp}) or the water potential at 50% loss of conductivity (Ψ_{P50}). Because nocturnal leaf conductance varies substantially depending on the chosen water potential boundaries, incorporating these dynamic values into models could significantly enhance estimation of time to hydraulic failure.

The mean residual leaf conductance (5.70 ± 0.49 mmol m^{-2} s^{-1}) corresponds to the final and constant section of the residual leaf conductance (g_{res}) (Figure A3.2a and A3.2b). However, this value is lower than this estimate using the detached leaf mass loss (DLML) method ($g_{min\_at\_\Psi P88}$ = 10.5 ± 2.14 mmol m^{-2} s^{-1}) determined in chapter 3. Unlike the DLML method, infrared gas exchange measurements do not account for or estimate leaf water status, and our protocol does not include reassessing water potential, it is therefore impossible to determine the leaf water status at which g_{res} is measured. The stability of the mean residual leaf conductance at the end of the curve indicates that this method captures the final residual water loss, independent of stomatal dynamics. It reflects only the cuticular component together with stomatal leakiness. However, at such low conductance levels, measurement noise increases substantially, which reduces overall accuracy. Consequently, fine variations in cuticular permeability or stomatal leakiness cannot be reliably resolved with this approach. Nevertheless, the use of an infrared gas analyser makes it possible to estimate a kind of minimum leaf conductance (g_{min}) based on the average of the flat part of the residual leaf conductance, but the protocol needs to be improved by adding the measurement of the water status of the leaves during drying.

A.3.5.2. Defining the transition point of residual leaf conductance with limited stomatal influence

Leaf cooling occurs through the combined effects of radiation, sensible heat, and latent heat (Jones & Rotenberg 2001). Heat from long and short waves can be lost by re-emitting to the surroundings using leaf radiative properties (Jones & Rotenberg 2001). Sensible heat is transferred from the leaf to the air through conduction and convection, with wind enhancing this process. The last way to cool a leaf comes from latent heat, where water evaporates from the leaf surface during transpiration, absorbing energy thus lowering leaf temperature. Together, these mechanisms help leaves maintain a favourable temperature for photosynthesis. Under field conditions, the contribution of each type of cooling changes according to environmental cues like incoming solar radiation and wind for the radiative and convection cooling respectively. Regarding latent heat, that contribution is highly related to the stomatal dynamic given the leaf surface temperature, a well-known proxy to estimate that dynamic (Jones 1999, 2002). Evaporative cooling through stomata is an active cooling, while radiative and sensible heat loss represent passive cooling driven by the leaf's inherent physical properties and environmental cues. In the *DroughtBox*, environmental conditions remained constant during leaf dehydration, keeping radiative cooling and sensible heat loss steady with slight variation. Latent heat loss, however, changed in response to stomatal closure and water availability inside the leaf. As the leaf dehydrates, the leaf-to-air surface temperature difference gradually decreases until it stabilises, indicating minimal stomatal impact and an equilibrium between the leaf with its environment inside the box. Transient cooling is a first-order differential equation, which is the form of Newton's law of cooling (Monteith & Unsworth 2013). The solution of this equation is an exponential-like form. The transition from an exponential curve to a plateau marked the moment when stomata reached their minimum opening and influence in leaf cooling. The shift determined by the RMSE method is estimated at g_{res}=10.68 mmol m^{-2} s^{-1} in our study. The $g_{res\_temperature}$ value is closed to the value estimated at Ψ_{88} (10.5 ± 2.14 mmol m^{-2} s^{-1}) in a previous study (chapter 3) but twice as high as the estimates obtained using the infrared gas analyser (5.70 ± 0.49 mmol m^{-2} s^{-1}). The difference may be due to a numerical resolution problem with the determination of the exponential and linear parts using the RMSE method. The elbow of the exponential curve is not easily detected by the RMSE method.

Although different in the calculation and interpretation; the relative water content (RWC) compares the leaf water content to its maximum capacity (the turgid weight)

whereas the moisture ratio (MR) compares this water content to its initial value at the start of the experiment, these mass-based parameters have the same dynamic clearly highlighted by their linearization. Linearization of mass parameters such as RWC and MR shows a change in slope during dehydration at the same time. This change indicates a change in the diffusion rate and can be attributed to stomatal activity during closure. Shift values close to these estimated with the infrared gas exchanger (5.70 ± 0.49 mmol m^{-2} s^{-1}) suggest that these shifts capture the moment where the residual leaf conductance corresponds only to the cuticle and stomatal leakiness, and can therefore be termed minimum leaf conductance.

The difference between the shift produced by the leaf-to-air surface temperature difference and the mass parameter can be attributed to lower accuracy of the infrared leaf temperature sensor. The difference may be due to a variation in sensible or radiative losses resulting from a change in thermal and radiative properties (thermal heat capacity, emissivity) and therefore in heat transfer coefficients during dehydration. Nevertheless, the temperature difference between the leaf surface and the air indicates a point at which stomatal impact begins to become less dominant, suggesting that the estimated minimal leaf conductance (g_{min}) before this shift (10.68 mmol m^{-2} s^{-1}) contains a too high stomatal fraction. On the contrary, the shift given by the mass parameters suggests a minimum value for the same g_{min}. As the leaf-to-air surface temperature difference and the mass-parameter are a first-order differential equation, using the time constant (τ; s) which is a fundamental parameter that characterises the speed at which a process approaches equilibrium could be an easier solution. After one time constant, the leaf-to-air temperature difference will have decreased by about 63%. After two- and three-time constants (t=2τ, t=3τ), more than 86% and 95% of the difference will be reached, respectively, corresponding to the equilibrium thus the minimal impact of stomata.

A.3.6. **Conclusion**

Measurements with infrared gas exchange provide a rapid and reliable method for estimating both nocturnal leaf conductance (g_{dark}) and residual leaf conductance (g_{res}) during drought. In *Helianthus annuus*, stomata remain open during the night or a darkness period, resulting in high nocturnal leaf conductance even at the onset of xylem embolism (after Ψ_{P12}). This persistent high nocturnal leaf conductance, particularly beyond the point of turgor loss, may play an important role in plant survival as drought intensifies. Clarifying

the physiological significance of nocturnal leaf conductance, particularly under drought conditions, is crucial, as it may substantially influence plant water balance and survival during severe drought. It is important to determine g_{dark} as a trait in order to introduce it into the soil-plant-atmosphere model. By contrast, g_{res_mean} remains low and stable throughout the drought sequence, reflecting only minimal water loss independent of stomatal dynamics. An understanding of stomatal dynamics, and in particular the determination of when these dynamics reach a minimal impact, can be done using parameters related to leaf mass and surface temperature. The combination of these 'intrinsic' parameters can help improve the timing at which the g_{min} as a trait can be estimated from residual leaf conductance.

Author contribution

GF, RB contributed to the design of the study; GF performed data collection and analysis. GF and RB realised the interpretation of the results; GF wrote the manuscript with help from all authors.

Conflict of interest

The authors declare no conflict of interest.

Funding

This study received financial support from the French government in the framework of the IdEX Bordeaux University "Investments for the Future" program / GPR Bordeaux Plant Sciences. TL acknowledges the following BBSRC funding BB/T0042741/1; BB/S005080/1; BB/Y000722/1 T.L. was supported by a Royal Society Leverhulme Trusts Senior Research Fellowship (SF/R1/231041).

Acknowlegement

We would like to thank the Phenobois platform team. We thank Dr Phil Davey for the technical assistance for the Li-COR experiment at the university of Essex. We would like to thank the Phenobois platform team and particularly Gaëlle Capdeville who conducted xylem embolism resistance experiments.

A.3.7. **References**

Billon L.M., Blackman C.J., Cochard H., Badel E., Hitmi A., Cartailler J., … Torres-Ruiz J.M. (2020) The DroughtBox: A new tool for phenotyping residual branch conductance and its temperature dependence during drought. Plant, Cell & Environment 43, 1584–1594.

Buckley T.N. (2005) The control of stomata by water balance. New Phytologist 168, 275–292.

Buckley T.N. (2019) How do stomata respond to water status? New Phytologist 224, 21–36.

Burlett R., Parise C., Capdeville G., Cochard H., Lamarque L.J., King A. & Delzon S. (2022) Measuring xylem hydraulic vulnerability for long-vessel species: an improved methodology with the flow centrifugation technique. Annals of Forest Science 79, 5.

Burlett R., Trueba S., Bouteiller X.P., Forget G., Torres-Ruiz M., Martin-StPaul N.K., … Delzon S. (2025) Minimum leaf conductance during drought: unravelling its variability and impact on plant survival. New Phytologist.

Cai J., Zhu L., Wei Q., Huang D., Luo M. & Tang X. (2023) Drying Kinetics of a Single Biomass Particle Using Fick's Second Law of Diffusion. Processes 11, 984.

Caird M.A., Richards J.H. & Donovan L.A. (2007) Nighttime Stomatal Conductance and Transpiration in C3 and C4 Plants. Plant Physiology 143, 4–10.

Clark J.W., Harris B.J., Hetherington A.J., Hurtado-Castano N., Brench R.A., Casson S., … Hetherington A.M. (2022) The origin and evolution of stomata. Current Biology 32, R539–R553.

Cochard H. (2002) A technique for measuring xylem hydraulic conductance under high negative pressures. Plant, Cell & Environment 25, 815–819.

Cochard H., Pimont F., Ruffault J. & Martin-StPaul N. (2020) SurEau .c : a mechanistic model of plant water relations under extreme drought. Plant Biology.

Coupel-Ledru A., Lebon E., Christophe A., Gallo A., Gago P., Pantin F., … Simonneau T. (2016) Reduced nighttime transpiration is a relevant breeding target for high water-use efficiency in grapevine. Proceedings of the National Academy of Sciences 113, 8963–8968.

Creek D., Lamarque L.J., Torres-Ruiz J.M., Parise C., Burlett R., Tissue D.T. & Delzon S. (2020) Xylem embolism in leaves does not occur with open stomata: evidence from direct observations using the optical visualization technique. Journal of Experimental Botany 71, 1151–1159.

Donoghue P.C.J., Harrison C.J., Paps J. & Schneider H. (2021) The evolutionary emergence of land plants. Current Biology 31, R1281–R1298.

Drake P.L., Froend R.H. & Franks P.J. (2013) Smaller, faster stomata: scaling of stomatal size, rate of response, and stomatal conductance. Journal of Experimental Botany 64, 495–505.

Grossiord C., Buckley T.N., Cernusak L.A., Novick K.A., Poulter B., Siegwolf R.T.W., … McDowell N.G. (2020) Plant responses to rising vapor pressure deficit. New Phytologist 226, 1550–1566.

Howard A.R. & Donovan L.A. (2007) Helianthus Nighttime Conductance and

Transpiration Respond to Soil Water But Not Nutrient Availability. Plant Physiology 143, 145–155.

Jones H.G. (1999) Use of thermography for quantitative studies of spatial and temporal variation of stomatal conductance over leaf surfaces. Plant, Cell & Environment 22, 1043–1055.

Jones H.G. (2002) Use of infrared thermography for monitoring stomatal closure in the field: application to grapevine. Journal of Experimental Botany 53, 2249–2260.

Jones H.G. & Rotenberg E. (2001) Energy, Radiation and Temperature Regulation in Plants. In Encyclopedia of Life Sciences, 1st ed. Wiley.

Kerstiens G. (1996) Cuticular water permeability and its physiological significance. Journal of Experimental Botany 47, 1813–1832.

Kong L., Liu Y., Zhi P., Wang X., Xu B., Gong Z. & Chang C. (2020) Origins and Evolution of Cuticle Biosynthetic Machinery in Land Plants. Plant Physiology 184, 1998–2010.

L. Schreiber, T. Kirsch, & Markus Riederer (1996) Diffusion through cuticles: principles and models.

Márquez D.A., Stuart-Williams H. & Farquhar G.D. (2021) An improved theory for calculating leaf gas exchange more precisely accounting for small fluxes. Nature Plants 7, 317–326.

McAdam S.A.M. & Brodribb T.J. (2015) The Evolution of Mechanisms Driving the Stomatal Response to Vapor Pressure Deficit. Plant Physiology 167, 833–843.

McDowell N.G. & Allen C.D. (2015) Darcy's law predicts widespread forest mortality under climate warming. Nature Climate Change 5, 669–672.

Monteith J.L. & Unsworth M.H. (2013) Principles of environmental physics: plants, animals, and the atmosphere, 4th ed. Elsevier/Academic Press, Amsterdam ; Boston.

Morris J.L., Puttick M.N., Clark J.W., Edwards D., Kenrick P., Pressel S., … Donoghue P.C.J. (2018) The timescale of early land plant evolution. Proceedings of the National Academy of Sciences 115.

Neumann R.B., Cardon Z.G., Teshera-Levye J., Rockwell F.E., Zwieniecki M.A. & Holbrook N.M. (2014) Modelled hydraulic redistribution by sunflower (H elianthus annuus L .) matches observed data only after including night-time transpiration. Plant, Cell & Environment 37, 899–910.

Oren R., Sperry J.S., Katul G.G., Pataki D.E., Ewers B.E., Phillips N. & Schäfer K.V.R. (1999) Survey and synthesis of intra- and interspecific variation in stomatal sensitivity to vapour pressure deficit. Plant, Cell & Environment 22, 1515–1526.

Petek-Petrik A., Petrík P., Lamarque L.J., Cochard H., Burlett R. & Delzon S. (2023) Drought survival in conifer species is related to the time required to cross the stomatal safety margin. Journal of Experimental Botany 74, 6847–6859.

Powles J.E., Buckley T.N., Nicotra A.B. & Farquhar G.D. (2006) Dynamics of stomatal water relations following leaf excision. Plant, Cell and Environment 29, 981–992.

R Core Team (2020) R Core Team (2020) R: A Language and Environment for Statistical Computing. R Foundation for Statistical Computing, Vienna, Austria. https://www.r-project.org/.

Resco De Dios V., Chowdhury F.I., Granda E., Yao Y. & Tissue D.T. (2019a) Assessing the potential functions of nocturnal stomatal conductance in C 3 and C 4 plants. New Phytologist 223, 1696–1706.

Resco De Dios V., Chowdhury F.I., Granda E., Yao Y. & Tissue D.T. (2019b) Assessing the potential functions of nocturnal stomatal conductance in C3 and C4 plants. New Phytologist 223, 1696–1706.

Ruffault J., Pimont F., Cochard H., Dupuy J.-L. & Martin-StPaul N. (2022) SurEau-Ecos v2.0: a trait-based plant hydraulics model for simulations of plant water status and drought-induced mortality at the ecosystem level. Geoscientific Model Development 15, 5593–5626.

Sack, Pasquet-Kok & Megan Bartlett (2011) Leaf pressure-volume curve parameters.

Snyder K.A. (2003) Night-time conductance in C3 and C4 species: do plants lose water at night? Journal of Experimental Botany 54, 861–865.

Tombesi S., Nardini A., Frioni T., Soccolini M., Zadra C., Farinelli D., … Palliotti A. (2015) Stomatal closure is induced by hydraulic signals and maintained by ABA in drought-stressed grapevine. Scientific Reports 5, 12449.

Tredenick E.C. & Farquhar G.D. (2021) Dynamics of moisture diffusion and adsorption in plant cuticles including the role of cellulose. Nature Communications 12, 5042.

Violle C., Navas M.-L., Vile D., Kazakou E., Fortunel C., Hummel I. & Garnier E. (2007) Let the concept of trait be functional! Oikos 116, 882–892.

Wang Y., Anderegg W.R.L., Venturas M.D., Trugman A.T., Yu K. & Frankenberg C. (2021) Optimization theory explains nighttime stomatal responses. New Phytologist 230, 1550–1561.

A.3.8. **Supporting information**

TABLE SA3.1: Leaf hydraulics variables used in this study

FIGURE SA3.1: Illustration of the experimental setup

FIGURE SA3.3: Result of the RMSE method after the linearisation of the RWC

FIGURE SA3.4: Result of the RMSE method for determining the minimum leaf conductance

TABLE SA3.2: Linear mixed model result

TABLE S A.1: Leaf hydraulics variables used in this study. Mean and standard errors for each variable are provided.

Definition	Abbreviation	Unit	*H. annuus*
Water potentials at turgor loss point	Ψ_{tlp}	MPa	-0.98 ± 0.05
Water potentials inducing 12% losses of conductance in the stem	Ψ_{P12}	MPa	-1.77 ± 0.15
Water potentials inducing 50% losses of conductance in the stem	Ψ_{P50}	MPa	-2.78 ± 0.18
Elasticity modulus	ε	MPa	2.03 ± 0.31
Osmotic potential at full turgor	π_0	MPa	-0.74 ± 0.06

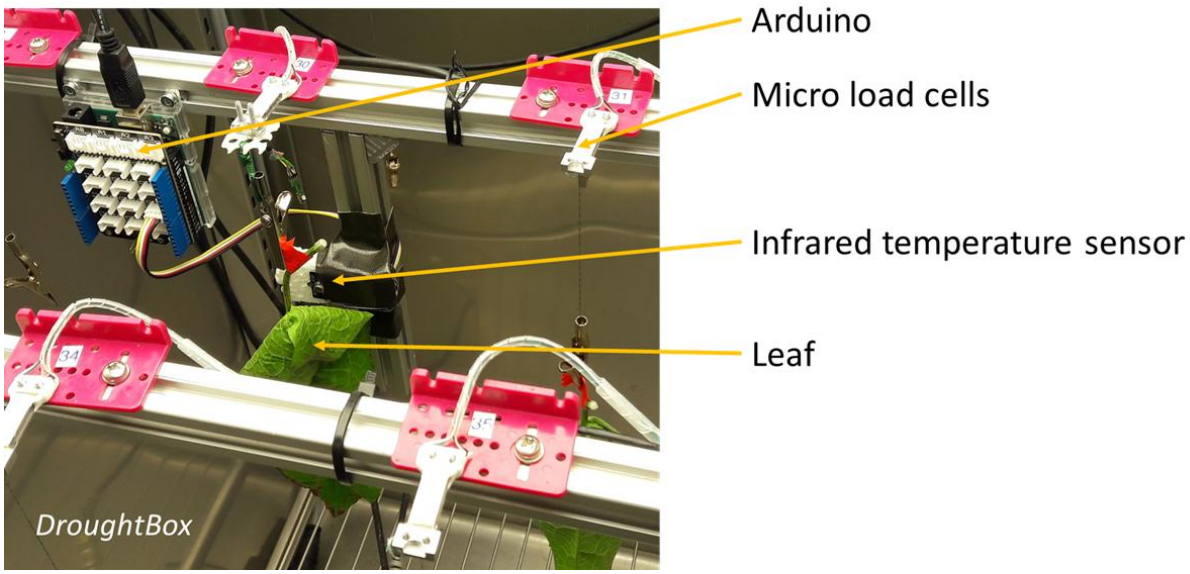

FIGURE S A.1: Illustration of the experimental setup for the detached leaf mass loss (DLML) method and the leaf temperature.

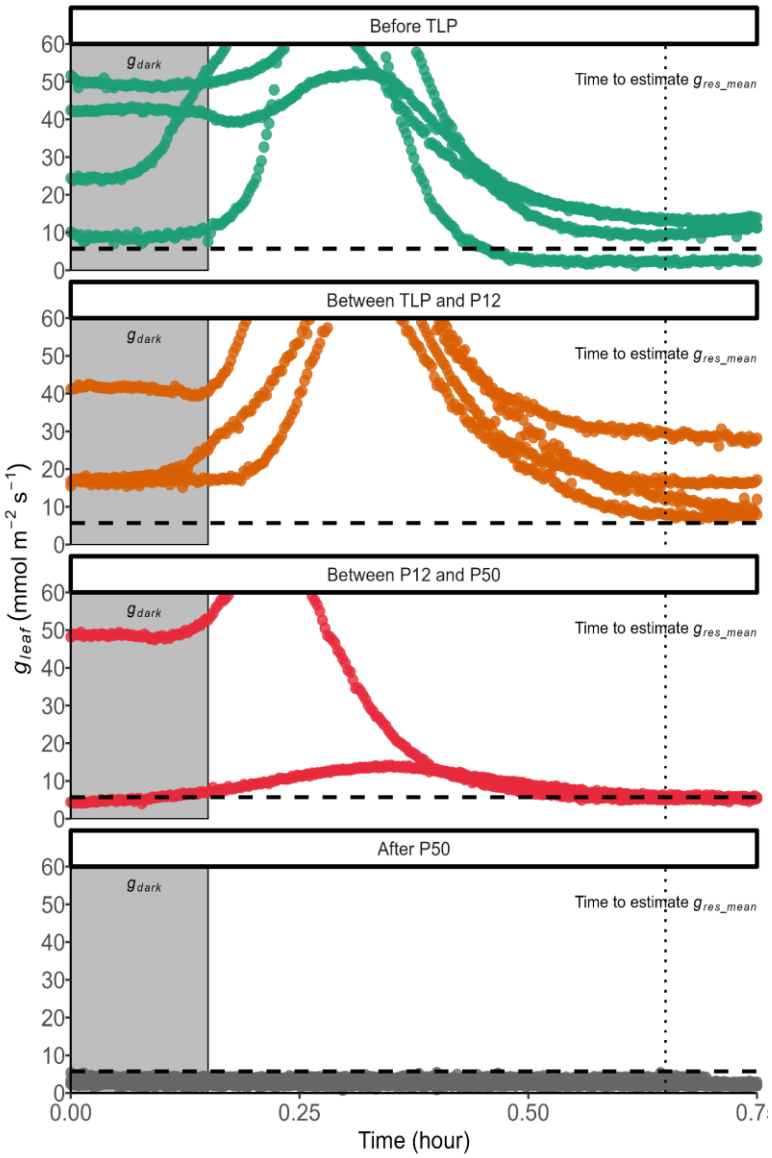

FIGURE S A.2: Leaf conductance dynamics before and after the leaf excision over a selection of leaves in each drought stress class.
Value inside the box corresponds to the drought stress class. The peak corresponds to the wrong-way response of Iwanoff's effect due to the leaf excision. Nocturnal (g_{dark}) and residual (g_{res}) leaf conductance correspond to the g_{leaf} before and after the peak, respectively. Time to estimate g_{res_mean} (vertical dotted line) is the approximative time where it's possible to estimate the g_{res_mean}, e.i. the g_{min}. The grey area corresponds to the zone where g_{dark} is estimated. The horizontal dashed line corresponds to the average value of g_{res_mean}.

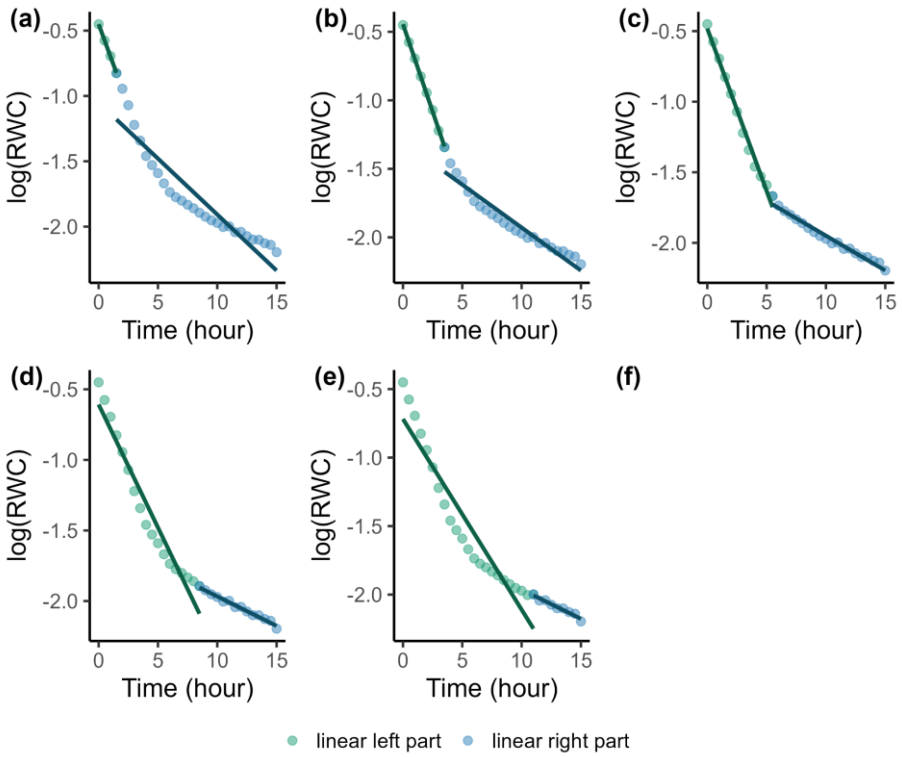

FIGURE S A.3: Result of the RMSE method after the linearisation of the RWC.
The linearisation of an exponential-like curve product produces a linear curve. The left and right part is fitted with a linear equation then the RMSE between the data and the fitted data for each part is estimated and the difference is calculated. This procedure is repeated using a moving data selection (a-f). The minimum value of the RMSE difference corresponds to the shift of the curve (c).

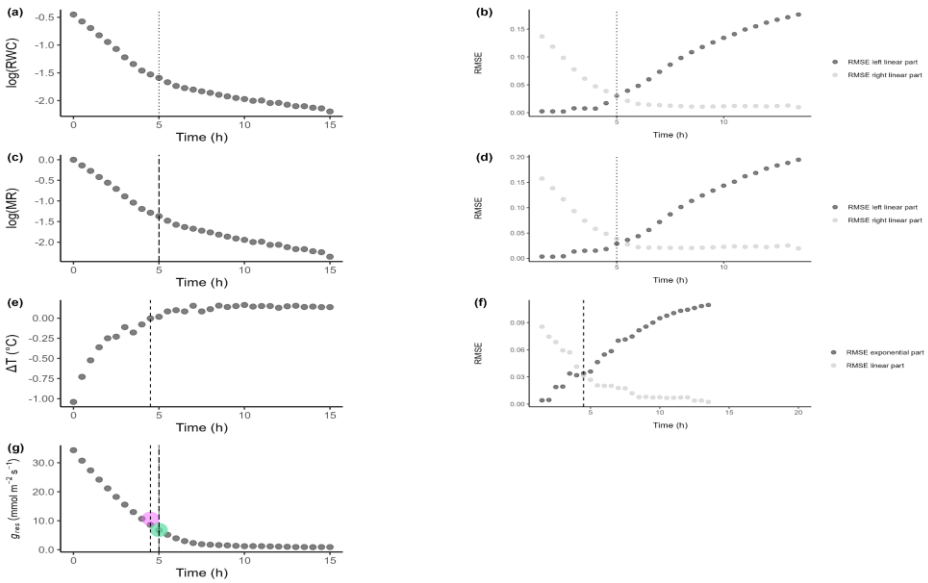

FIGURE S A.4: Result of the RMSE method for determining when stomatal dynamics ceases on residual leaf conductance (g_{res}).
(a) The linearation of the RWC versus Time, the vertical dotted line corresponds to the moment of the shift curve determined with the RMSE method (b). (c) The linearation of the MR versus Time, the vertical longdashed line corresponds to the moment of the shift curve determined with the RMSE method (d). (e) leaf-to-air surface temperature difference versus Time, the vertical dashed line corresponds to the moment of the shift curve determined with the RMSE method (f).
TABLE S A.2: Linear mixed model fit by REML

Formula: g_{res_mean} ~ Dynamique + (1 | WP)

Analysis of Deviance Table (Type III Wald chisquare tests)

Response: g_{res_mean}

	Chisq	Df	Pr(>Chisq)	
(Intercept)	109.8255	1	<2e-16	***
Dynamique	1.6358	1	0.2009	

Linear model

lm(formula = g_{res_mean} ~ WP, data = data)

Coefficients:

	Estimate	Std. Error	t value	Pr(>|t|)	
(Intercept)	7.5343	1.0224	7.369	9.18e-09	***
WP	0.8901	0.4406	2.020	0.0506	.

Analysis of Deviance Table (Type III Wald chisquare tests)

Response: g_{res_mean}

	Chisq	Df	Pr(>Chisq)	
(Intercept)	54.3079	1	1.714e-13	***
WP	4.0819	1	0.04334	*

A.4. 2025 Society for Experimental Biology (SEB) annual conference poster

Importance of stomatal patchiness in the physiological response to water stress

Guillaume Forget[1,2,@], *Régis Burlett*[1], *Jérôme Joubes*[2], *Sylvain Delzon*[1], *Tracy Lawson*[3,4]

[1]INRAE, UMR BIOGECO, Université de Bordeaux, Pessac, 33615, France, [2]CNRS, UMR LBM, Université de Bordeaux, 33140 Villenave d'Ornon, France, [3]School of Life Sciences, University of Essex, Colchester CO4 3SQ, UK,[4]Departement of Plant Biology & Institute for Genomic Biology, School of Integrative, Biology, College of Liberal Arts and Sciences, University of Illinois at Urbana-Champaign; 1402 Inst for Genomic Biology, 1206 W Gregory Dr | M/C 195, Urbana, IL 61801.

INTRODUCTION

Stomatal patchiness: Refers to the phenomenon where groups of stomata behave differently from adjacent groups, resulting in spatially heterogeneous patterns[1] of stomatal opening and closing across a leaf.

Stomatal patchiness can be triggered by a wide range of environmental cues like light, relative humidity or CO_2 changes and water status inside the leaf.

We investigated the presence and the role of stomatal patchiness in *Helianthus annuus* (Sunflower) during drought by using thermal and fluorescence imaging to capture stomatal closure and to assess its effects on gas exchange.
We hypothesised that stomatal patchiness is a critical response to drought at leaf level, optimising leaf gas exchange over time.

METHODS

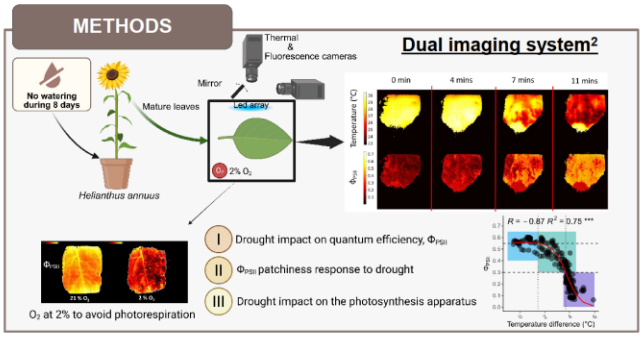

RESULTS

I Drought impact on quantum efficiency, Φ_{PSII}

- After the turgor loss point (Ψ_{tlp}), spatial variability in Φ_{PSII} values reveals stomatal patchiness due to heterogeneity in water potential causing **uneven** stomatal closure.
- **For heterobaric species,** patch shaped by vein network and bundle sheath extensions.

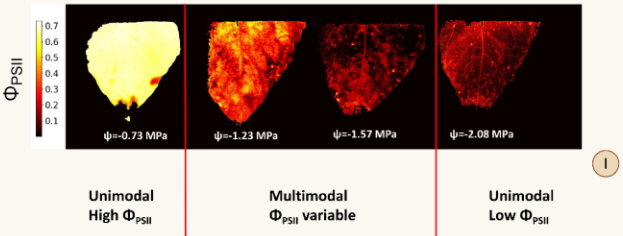

II Φ_{PSII} patchiness response to drought

- Unimodal: Before Ψ_{tlp} **and after** Ψ_{P12},distributions of Φ_{PSII} values present a single clear peak.
  - Indicates that most leaf areas have similar values, reflecting uniform photosynthetic efficiency across the tissue.
- Multimodal: Between Ψ_{tlp} and Ψ_{P12} distributions show multiple peaks indicating that regions of the leaf are behaving differently.
  - Some areas maintain high Φ_{PSII}, while others drop, reflecting patchiness and spatial variability in photosynthetic performance.

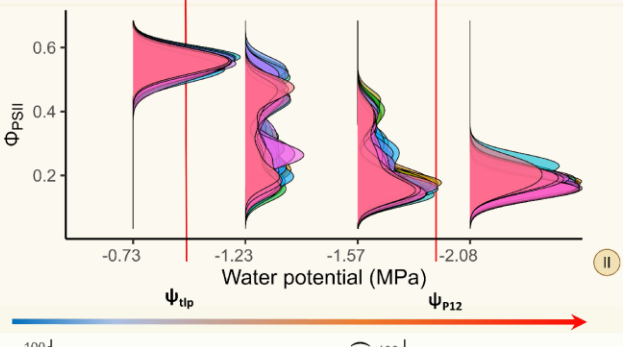

III Drought impact on the photosynthesis apparatus

- Φ_{PSII} spatial decline without structural damage:
  - Operating efficiency (Φ_{PSII}) declines rapidly and becomes patchy with increasing drought.
    - Loss of photosynthetic function across the leaf.
  - Maximum efficiency remains stable; no structural damage of PSII even until mild stress (< Ψ_{P50})
    - Stomatal closure is the main contributor to the photosynthetic efficiency loss

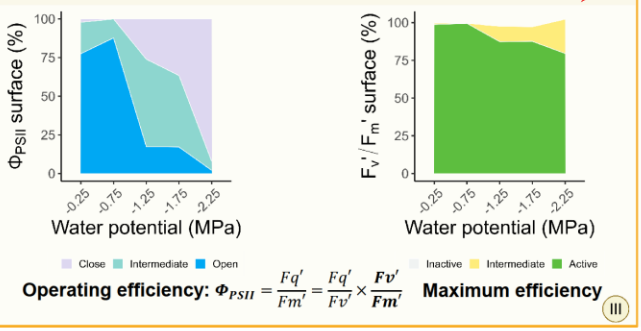

CONCLUSION

- Stomatal patchiness is as a spatiotemporal feature of drought response in *Helianthus annuus* with physiological implications for gas exchange.
- Spatial heterogeneity of stomatal behavior across the leaf surface enhances capacity to maintain and extend physiological function under variable environmental conditions.
- Stomatal patchiness might be a strategy to balance carbon assimilation and water conservation under mild drought.
- The findings emphasise the need to integrate spatial heterogeneity into models of plant water relations under drought.

References
[1]Mott, Keith A, and Thomas N Buckley. 'Patchy Stomatal Conductance: Emergent Collective Behaviour of Stomata'. Trends in Plant Science 5, no. 6 (June 2000): 258–62. https://doi.org/10.1016/S1360-1385(00)01648-4.
[2]McAusland, L., P. A. Davey, N. Kanwal, N. R. Baker, and T. Lawson. 'A Novel System for Spatial and Temporal Imaging of Intrinsic Plant Water Use Efficiency'. *Journal of Experimental Botany* 64, no. 16 (November 2013): 4993–5007. https://doi.org/10.1093/jxb/ert288.

Correspondence: **guillaume.forget@u-bordeaux.fr**
Created with BioRender.com

A.5. Minimum leaf conductance during drought: unravelling its variability and impact on plant survival

New Phytologist

Research

Minimum leaf conductance during drought: unravelling its variability and impact on plant survival

Régis Burlett[1]*, Santiago Trueba[1,2]*, Xavier Paul Bouteiller[1], Guillaume Forget[1], José M. Torres-Ruiz[3], Nicolas K. Martin-StPaul[4], Camille Parise[1], Hervé Cochard[5] and Sylvain Delzon[1]

[1]INRAE, UMR BIOGECO, Université de Bordeaux, Pessac, 33615, France; [2]AMAP, Université de Montpellier, CIRAD, CNRS, INRAE, IRD, Montpellier, 34398, France; [3]Instituto de Recursos Naturales y Agrobiología de Sevilla (IRNAS), Consejo Superior de Investigaciones Científicas (CSIC), Seville, 41012, Spain; [4]INRAE, UEFP, Avignon, 84914, France; [5]INRAE, PIAF, Université Clermont Auvergne, Clermont-Ferrand, 63000, France

Author for correspondence:
Régis Burlett
Email: regis.burlett@u-bordeaux.fr

Received: *7 October 2024*
Accepted: *15 February 2025*

New Phytologist (2025)
doi: 10.1111/nph.70052

Key words: cuticular conductance, drought stress, relative water content, stomatal closure, turgor loss point, water potential.

Summary

- Leaf water loss after stomatal closure is key to understanding the effects of prolonged drought on vegetation. It is therefore important to accurately quantify such water losses to improve physiology-based models of drought-induced plant mortality.
- We measured water loss of detached leaves continuously during dehydration in nine woody angiosperm species. We computed minimum leaf conductance (g_{min}) at different water potential thresholds along a sequence of physiological function losses, spanning from turgor loss point to hydraulic failure. A mechanistic model evaluated the impact of different g_{min} estimations on the time to hydraulic failure (THF).
- Residual conductance is not steady and decreases continuously at varying rates across species during the entire dehydration process, even after correcting for leaf shrinkage and vapor pressure deficit shifts. Different estimations of g_{min} had a significant impact on the THF predicted by the model, especially for drought-resistant species.
- We demonstrate that residual conductance is variable during dehydration, and thus, it is important to use physiological or water status boundaries for its estimation in order to determine distinct g_{min} values of water loss. We describe an accurate, repeatable and open-source methodology to estimate g_{min}. Such methodology could enhance models of plant mortality under drought.

Introduction

In the last few decades, a large number of studies have brought to light the particular threat of drought and increasing temperatures on plant survival (Allen & Breshears, 1998; Carnicer *et al.*, 2011; Brodribb *et al.*, 2019; Hammond *et al.*, 2022). One of the main consequences of increasing environmental drought stress is a negative impact on the hydraulic function of plants (Choat *et al.*, 2012; Arend *et al.*, 2021). Indeed, during prolonged drought, dehydration causes large water potential differences between soil and leaves, which can result in hydraulic dysfunction due to embolism formation in the xylem conduits. Such hydraulic failures, induced by sharp drops in water potential, can be avoided through stomatal closure (Creek *et al.*, 2020), which plays a major role in plant survival under drought (Martin-StPaul *et al.*, 2017). Despite stomatal closure being a key reaction to reduce significant plant water losses, water is still lost through imperfectly closed stomata and the leaf cuticle. This process can be quantified by the minimum leaf conductance (g_{min}) (Duursma *et al.*, 2018). Although the rates of whole-plant water conductance are greatly diminished, g_{min} can be sufficient to deplete the plant water reserves during stress. Therefore, under prolonged drought, continued water loss via g_{min} can lead to catastrophic hydraulic failure and substantial tissue dehydration that contribute to organ and plant death (Urli *et al.*, 2013; Mantova *et al.*, 2023; Petek-Petrik *et al.*, 2023). Consequently, g_{min} has been highlighted as an important trait in predicting whole-plant transpiration and water status under severe stress (Barnard & Bauerle, 2013; Kala *et al.*, 2016). More recently, g_{min} has been advanced as a key trait to predict the time taken by a plant to reach hydraulic failure (THF) and subsequent mortality during drought (Cochard *et al.*, 2021; Ruffault *et al.*, 2022a; Petek-Petrik *et al.*, 2023) and to predict other current hazards to vegetation such as wildfire incidence (Ruffault *et al.*, 2022b; Torres-Ruiz *et al.*, 2024).

Synthetic studies gathering g_{min} data showed that estimations of residual transpiration in the literature come from a wide

*These authors contributed equally to this work.

variety of experimental techniques (Kerstiens, 1996; Duursma *et al.*, 2018). While cuticular conductance on isolated cuticles has been measured since early studies (Stålfelt, 1956; Schönherr & Mérida, 1981; Pearcy *et al.*, 1989), only a few protocols to measure g_{min} on a full leaf have been tested. Generally, measurement protocols rely on evaluating water loss through balance-based mass estimations over time and selecting the slope of the relationship between mass and time after the point of stomatal closure, assuming that water losses through the cuticle are steady as the leaf dehydrates (Sack & Scoffoni, 2010) or through water vapor conductance measurements using custom gas exchange systems (Boyer *et al.*, 1997; Márquez *et al.*, 2022). Automated devices have recently been developed in order to provide continuous measurements of water loss during dehydration under constant environmental conditions (Billon *et al.*, 2020). Yet, to date, no study has estimated potential shifts in leaf water conductance during the entire desiccation process. Furthermore, intrinsic factors can provoke shifts in water conductance estimations. Among these factors, leaf shrinkage or leaf rolling during dehydration can significantly impact the estimation of leaf hydraulic traits (Scoffoni *et al.*, 2014); hence, variations in leaf area need to be considered in conductance calculations. Additionally, water potential decline during leaf dehydration can also slightly influence conductance rates by affecting the water vapor pressure (vapor pressure deficit, VPD) inside the leaf and therefore the driving force for transpiration between the leaf and the atmosphere (Nobel, 2009).

Using a dynamic approach to estimate residual water losses during the entire dehydration process, and including phenomena that are often neglected in leaf conductance estimations, such as leaf shrinkage and water potential-induced VPD changes, this study aimed to assess the dynamics of residual leaf water conductance during dehydration. By measuring its variability during dehydration, this work also aimed to strictly distinguish residual conductance (g_{res}) as a dynamic water loss during dehydration after stomatal closure, and g_{min} as conductance values bounded by physiology-informed boundaries. We therefore capture variable residual conductance by measuring g_{min} at specific thresholds. Because of the key role of g_{min} in the depletion of the last vital water reserves of the plant after stomatal closure, there is a need to use repeatable and reliable protocols for its estimation. Here, we describe a complete methodology to investigate g_{min} based on continuous measurements of relative water content (RWC) over time. Moreover, we use water status- and physiology-based thresholds to determine g_{min}. We provide detailed information on the device and open-source software used to analyze data. By applying this new technique to a selection of nine species with various phenologies, water use strategies, and resistances to drought, we will (i) test the hypothesis that residual conductance after stomatal closure varies along a gradient of declining water potential and RWC, (ii) assess how this variation affects the estimation of g_{min} at physiologically relevant thresholds distributed along a temporal sequence, and (iii) investigate how the range of g_{min} estimated along this drought physiological time sequence can influence model outcomes of plant survival under drought stress.

Materials and Methods

Plant material and species selection

We selected nine woody angiosperm species with different phenologies (five deciduous and four evergreen) and resistances to drought (Table 1). Six- to 7-yr-old saplings with heights of *c.* 2 m were obtained from local nurseries and planted in 30 l pots with a fertilized substrate. Plants were placed in a climate-controlled glasshouse in March 2019 (before leaf expansion) and kept irrigated to field capacity during the whole experiment. In September 2019, five sampling campaigns were performed on well-watered plants during the morning. Mature leaves, located at the top of the trees, were cut at the base of the petiole. This cut end was immediately placed in a water-filled reservoir, and the leaves were left to rehydrate for at least 8 h in the dark in a coolbox with vapor-saturated air using previously established rehydration protocols (Trueba *et al.*, 2019).

Measurements of water loss and relative water content

Water loss measurements of detached leaves were performed with a custom setup using similar data acquisition hardware to the *droughtbox* device (Billon *et al.*, 2020). Weight loss was monitored by continuous logging of micro-load cells using a Wheatstone bridge board (1046_OB; Phidgets Inc., Calgary, AB, Canada). Our setup consisted of 24 load cells, with a range of 0–100 g (3139_0; Phidgets Inc.) enclosed in a commercially available 1200 l growing chamber (Fitoclima 1200, Aralab, Portugal). Temperature and relative humidity (RH) in the chamber were set to 25°C and 60%, respectively, resulting in an air VPD of *c.* 1.26 kPa. During measurements, samples were illuminated from the top and the bottom with a photon flux density of 400 µmol m^{-2} s^{-1}. The base of the petiole was covered in paraffin wax before entering the chamber to prevent direct desiccation from the cut end. Samples were automatically weighed every 5 min. Custom software (Cuticular v1, University of Bordeaux) was developed to handle data acquisition, calibration, and metadata management. More details of the measurement system are available in Supporting Information Methods S1.

The measuring system designed in this study provided a resolution of the load cell acquisition system of 0.001 g with a typical instant standard deviation of 0.033 g (5 min average). The relatively big difference between resolution and standard deviation is mostly explained by the movement of the samples caused by the ventilation in the chamber. The measured signal-to-noise ratio is typically 77 at 2 g and 260 at 8 g. The long-term temperature drift remained below 0.03°C d^{-1}, and the long-term RH drift was below 0.08% d^{-1}. Further information on data acquisition and system performance is available in Methods S1.

Turgid weight (TW) and area (A_{leaf}) of each individual leaf were measured before the water loss measurements in the climatic chamber. Weight measurements were performed with a 4-digit balance (Pioneer, Ohaus, USA). Leaf area was obtained from images taken with a calibrated flatbed scanner (v850 pro; Epson,

Table 1 List of the nine species studied including physiological variables.

Species	Family	Phenology	Species code	π_0 (MPa)	ε MPa	RWC_TLP (%)	RWC_P_{12} (%)	RWC_P_{50} (%)	RWC_P_{88} (%)	Succulence (g m^{-2})	Symplast fraction (%)	Hydraulic safety margin (MPa)
Fraxinus excelsior L.	Oleaceae	Deciduous	FREX	−1.56	10.93	83.9	28.7	25.2	22.5	105.1 ± 2.1	76.6 ± 1.8	−5.47
Liriodendron tulipifera L.	Magnoliacea	Deciduous	LITU	−1.41	10.95	84.2	72.8	67.1	62.2	139.1 ± 4.3	61.4 ± 3.1	−0.85
Magnolia grandiflora L.	Magnoliacea	Evergreen	MAGR	−1.37	7.63	78.2	53.6	48.3	44	228.6 ± 1.4	75.8 ± 2.6	−1.75
Olea europaea L.	Oleaceae	Evergreen	OLEU	−2.11	12.65	83.4	38.7	36.8	35.1	238.0 ± 2.5	83.9 ± 4.3	−3.91
Prunus avium L.	Rosaceae	Deciduous	PRAV	−1.90	12.05	83.0	51.8	42.2	35.6	117.1 ± 0.8	65.5 ± 2.5	−3.43
Prunus laurocerasus L.	Rosaceae	Evergreen	PRLA	−1.65	14.02	87.0	40.0	33.1	28.2	231.1 ± 1.7	50.6 ± 3.2	−4.21
Quercus ilex L.	Fagaceae	Evergreen	QUIL	−1.93	8.16	73.4	37.7	27.1	21.2	198.6 ± 5.5	73.2 ± 1.4	−7.20
Quercus robur L.	Fagaceae	Deciduous	QURO	−1.72	11.27	81.6	43.0	36.2	31.3	124.1 ± 1.6	80.4 ± 2.9	−3.77
Vitis vinifera L.	Vitaceae	Deciduous	VIVI	−1.29	7.73	79.0	63.6	58.7	54.5	126.3 ± 3.8	74.4 ± 2.1	−1.08

π_0, osmotic potential at full turgor; ε, modulus of elasticity; RWC_TLP, relative water content at turgor loss point; RWC_P_{12}, relative water content at 12% loss of hydraulic conductivity; RWC_P_{50}, relative water content at 50% loss of hydraulic conductivity; RWC_P_{88}, relative water content at 88% loss of hydraulic conductivity. Physiological variables used as inputs for the SurEau model and units for each variable are included. Reported error values are SE.

Suwa, Japan) and analyzed with dedicated software (Winfolia, Regent Inst., Canada). At the end of the measurement, leaves were placed in an oven at 65°C for 72 h, and dry weight (DW) was measured. The RWC was then computed for each mass value (fresh mass; FW) during the dehydration process using Eqn 1:

$$\mathrm{RWC} = 100 \times \frac{\mathrm{FW}-\mathrm{DW}}{\mathrm{TW}-\mathrm{DW}} \qquad \text{Eqn 1}$$

Computation of minimum and residual leaf conductance

Minimum and residual conductance were computed for each leaf as the water evaporation rate divided by its driving force (VPD), using Eqn 2:

$$g_{\min} = \frac{\mathrm{d}w/\mathrm{d}t}{M_{H_2O} \times A_{leaf}} \times \frac{P_{atm}}{\mathrm{VPD}} \qquad \text{Eqn 2}$$

where $\mathrm{d}w/\mathrm{d}t$ is the first derivative of the curve of the hourly mean of weight (in g) as a function of time (in s), M_{H_2O} is the molecular weight of water (18.01 g mol^{-1}), A_{leaf} is the projected leaf area of the sample (in m^2), P_{atm} is the atmospheric pressure in the chamber (*c.* 101.9 kPa), and VPD is the vapor pressure deficit between the substomatal cavity and the air inside the chamber (in kPa). To compute minimum conductance in a reproducible and efficient manner, console-based software was developed in Python (*gminComputation*, University of Bordeaux) and also implemented as an R script (*g_Residual*, University of Bordeaux). Both software are available in the repository: https://gitub.u-bordeaux.fr/phenobois. The computation pipeline automatically performs a finite impulse response smoothing filter, using the Savitzky–Golay method. This method uses polynomial model fitting to determine the averaged mass and computes the derivative within a given time frame to estimate the conductance every hour or within a set of given ranges of RWC. For all the dehydration curves in this study, we applied a centered 120 min filter and used a third-order polynomial to fit each curve (Methods S1).

Measurements of hydraulic traits from pressure–volume curves

For each species, the water potentials of the leaves during the conductance measurements were estimated from the relationship between RWC and water potential obtained from pressure–volume (PV) curves (Tyree & Hammel, 1972). PV curves were performed on a set of 7–12 leaves collected in the evening on well-watered potted plants and left to rehydrate overnight in the dark. The next day, the leaves were weighed just before water potential was measured with a pressure chamber (Precis 2000, Gradignan, France). Samples were then left to dehydrate at room conditions, and the measurements were repeated 10–20 times until water potential dropped significantly below the turgor loss point (TLP). Elasticity modulus (ε) and osmotic potential at full turgor (π_0) were determined using a standard protocol (Sack *et al.*, 2010). Results of the parameters extracted from the PV curves for each species are available in Table 1. Additionally, the Hydraulic stomatal Safety Margin (HSM) for each species was computed, using the definition from Delzon & Cochard (2014), as the difference between the water potential inducing stomatal closure ($P_{close} = P_{TLP}$, defined as the value of water potential at TLP) and the water potential inducing a lethal level of embolism ($P_{lethal} = P_{88}$, defined as the value inducing 88% of embolism in the stem). HSM values for each species are available in Table 1.

Leaf shrinkage measurements

For each species, seven leaves of different sizes were placed on a flatbed scanner (v850 pro, Epson, Japan), with the lid slightly ajar to allow for potential leaf rolling. A custom automation script (autoIT) was used to launch the image acquisition and record time-coded images every 15 min. Individual leaf areas were obtained for each image in the stack with the 'batch mode' of image analysis software (Winfolia, Regent Inst., Canada). For each leaf, the weight was measured regularly with a precision balance (Pioneer, Ohaus, USA) and RWC estimated following the previously described protocol (Eqn 1) until RWC reached 30%,

assuming that below this threshold leaves lose rehydration capacities and present irreversible damage to the photochemical apparatus (Trueba *et al.*, 2019). The percentage of shrinkage was determined for each species by fitting a 4-degree polynomial on the relation of the percentage of area loss as a function of RWC (Table S1). This polynomial has been used, for each RWC level, to sequentially correct the leaf area values used in the g_{min} computation.

Leaf to air vapor pressure deficit correction

As leaves dehydrate, the water potential decreases, which impacts the water vapor pressure (P_{wv}) in the substomatal cavities, thereby affecting the VPD between leaf and air ($VPD_{leaftoair}$). While negligible for hydrated leaves, this phenomenon needs to be taken into account for the computation of conductance during more intense dehydration. If we assume that the air in the intercellular air space of the mesophyll is in equilibrium with the liquid water at the surface of the mesophyll cells, we can determine the water potential of the water vapor in the gas phase (Ψwv) of the air in the substomatal cavities (Nobel, 2009; Vesala *et al.*, 2017) using Eqn 3:

$$\psi_{wv} = \frac{RT}{V_w} \log_e \frac{P_{wv_{inleaf}}}{P^*_{wv}} \quad \text{Eqn 3}$$

where ψ_{wv} is the water potential of the water vapor, V_w is the molar volume of water ($18 \times 10^{-6}\ m^3\ mol^{-1}$), R is the universal gas constant, T is the interfacial temperature (K), P_{wv} is the water vapor pressure, and P^*_{wv} is the water vapor pressure at saturation. In this study, the interfacial temperature is assumed to be in equilibrium with air temperature, as the cooling effect of transpiration is negligible (below 0.2°C) in the conditions of the measurement. From this equation, we can estimate $VPD_{leaf\text{-}to\text{-}air}$ using Eqn 4:

$$\begin{aligned} VPD_{leaftoair} &= P_{wv_{inleaf}} - P_{wv_{inair}} \\ &= \left(P^*_{wm} \times \exp\left(\frac{V_w}{RT}\psi_{wv}\right)\right) - P_{wv_{inair}} \end{aligned} \quad \text{Eqn 4}$$

For all conductance estimations in this study, this value of VPD corrected for water potential ($VPD_{leaftoair}$) was used instead of the air VPD as defined in Eqn 2, unless specified otherwise.

Different approaches to determine the range of g_{min} measurements

Under the assumption that residual conductance is variable, we need to consider which value has to be used for comparing species and how this variation can be taken into account in the parameterization of the models. For that, we assessed four different exploratory methods to determine g_{min}, extracting slope values at different ranges of the mass–RWC relation in the curves of dehydrating leaves: (1) A first physiology-based approach consisted of the calculation of g_{min} using the slope (dw/dt) at RWC_{TLP}, under the hypothesis that TLP is a close *proxy* of stomatal closure (Brodribb & Holbrook, 2003). (2) A second approach consisted in calculating g_{min} using the slope at the major points along stem vulnerability to embolism curves, previously established with the cavitron technique (Cochard, 2002; Burlett *et al.*, 2022). For all those points, we used stem vulnerability, rather than leaf, curves because they are more commonly available. The threshold values we used correspond to the water potentials inducing 12%, 50%, and 88% losses of conductance in the stem (respectively P_{12}, P_{50}, and P_{88}) under the rationale that hydraulic failure occurs around those water status levels (Sperry *et al.*, 1988), between P_{12} (beginning of embolism) and P_{88} (the threshold inducing mortality). Moreover, estimating g_{min} at different thresholds of hydraulic failure was also a way to control for the lack of stomatal activity, since it has been shown that stomatal closure occurs well before embolism initiation (Lamarque *et al.*, 2018; Creek *et al.*, 2020). In order to estimate the RWC corresponding to these points (respectively RWC_P_{12}, RWC_P_{50}, and RWC_P_{88}), we used the relationship between RWC and water potential obtained from the PV curves. (3) A third approach to estimate g_{min} was by extracting the slope between the thresholds of RWC inducing stomatal closure (*c.* 80%) and the loss of rehydration capacity (*c.* 50%) based on a previous study (Trueba *et al.*, 2019). Such boundaries were also established under the assumption that a water potential of −4 MPa represents a boundary of absolute stomatal closure (Martin-StPaul *et al.*, 2017), which is concomitant to *c.* 80% RWC according to PV curves performed in this study. This approach was implemented in order to use conservative boundaries that could be applied *a priori* across plant species without preexisting physiological assessments. The values of g_{min} obtained using the previously described methods were compared in order to assess their potential dissimilarities. (4) A fourth approach consisted in estimating g_{min} in 10% ranges from 100% to 0% RWC. These ranges were used to estimate conductance dynamically, including corrections for leaf shrinkage and leaf-to-air VPD. Such an approach allowed us to understand at which stages of dehydration shrinkage and VPD variation had a major impact on residual conductance.

Determination of time to hydraulic failure with various g_{min} values

Time to hydraulic failure (THF) is often defined as the time required by a plant to reach a RWC value corresponding to a loss of 88% of hydraulic conductance (RWC_{P88}). This level of water stress has been previously shown to correspond to a threshold inducing plant mortality in angiosperm species (Urli *et al.*, 2013; Li *et al.*, 2016). For each species, RWC_{P88} has been estimated using PV relationships and vulnerability curves. The time to reach this 88% threshold (THF_observed) was then directly measured for each individual detached leaf inside the *droughtbox*, during the dehydration experiment. This measurement was used as a reference.

Additionally, the model SurEau (Cochard *et al.*, 2021) has been used to estimate, at the leaf level, THF using different values of g_{min} computed with the different thresholds previously described. Namely: THF_TLP, THF_P_{12}, THF_P_{50}, THF_P_{88}, and

THF_RWC$_{80\text{-}50}$. An additional approach taking into account the continuous variability of g_{min} has also been implemented in the model (THF_variable). The dynamics of g_{min} was estimated using a segmented linear model in the equation $g_{min} = f(RWC)$. In short, the variation of g_{min} was assumed constant before stomatal closure (i.e. between RWC$_{100\%}$ and RWC_TLP) and decreased linearly after stomatal closure. In practice, the slope of the function between RWC_TLP and RWC$_{30\%}$ was used to estimate g_{min}. Coefficients of the linear fit for each species can be found in Table S1. In all simulations, model computation was performed with the following hypotheses: (1) leaves remain connected to the stem throughout the dry down, and (2) hydraulic vulnerability curves are similar for leaves and stems.

SurEau model parameterization

Simulations of THF were performed for each species using averaged values of each leaf-related trait. These values can be found in Tables 1 and S1. The degree of succulence was estimated by the ratio of fresh weight to leaf area (Delf, 1912) on a set of at least 10 hydrated leaves. The symplastic water fraction (SWF) was estimated from the PV curve (Koide *et al.*, 2000) with Eqn 5:

$$\frac{1}{\psi} = a * (100 - \mathrm{RWC}) + b \qquad \text{Eqn 5}$$

where ψ is the water potential (in MPa), RWC is the relative water content (in kg kg^{-1}), and a and b are the slope and intercept of the linear part of the PV curve (RWC < 80%), respectively. In short, we extrapolated the PV curve function to estimate the RWC deficit at a low water potential, which gives a direct estimation of the SWF. The apoplastic water fraction was defined as 100 − SWF.

Statistical analyses

Assumptions of residual homogeneity and normality were tested before analyses. Correlation analyses were used to assess relationships between PV curve parameters and g_{min} values estimated with different physiological thresholds. A model explaining the variance of percent leaf area, including the interaction RWC × species, was also performed to assess whether RWC had an effect on leaf shrinkage across all species. Bivariate linear regressions were used to estimate relationships between modelled and measured THF. Similarly, linear models were used to assess the prediction of safety margins from the THF. All analyses were considered significant at $\alpha = 0.05$. All statistical analyses, data treatment, and graphics were performed using R v.4.3.2 (R Core Team, 2022).

Results

Leaf mass decline and shrinkage during dehydration

Continuous measurements of mass loss using 5 min intervals provided extensive dehydration curves (Fig. S1). Most of the species showed exponential declines in RWC over time, starting with a steep decrease, followed by a gradual slope flattening (Fig. 1). Species showed overall declines in projected leaf area during dehydration (Fig. 2). Species varied significantly in their shrinkage under dehydration (one-way ANOVA; $P \leq 0.001$; Table S1). Although the onset of leaf shrinkage started early during dehydration in some species, more significant leaf area reductions were observed after RWC_TLP, the RWC at turgor loss (Fig. 2). Across species, *Magnolia grandiflora* had the least shrinkable leaves, decreasing only by 3% on average across the dehydration process, while *Olea europaea* showed the strongest decline in projected leaf area, with a 37% reduction across the entire RWC decline, mostly because of a strong curling occurring after 50% of RWC. A model explaining leaf shrinkage variance, including the RWC interval × species interaction, showed that species explained shrinkage variations better than RWC, when considered at similar RWC intervals (Table S2), implying that a larger fraction of the leaf shrinkage variation, at a given RWC, was explained by attributable differences in leaf structure across species.

Dynamics of residual conductance during leaf dehydration

Continuous measurements of leaf water conductance over declining RWC showed that residual conductance varied greatly during dehydration (Fig. 3). For every species, such conductance declines were mostly driven by a decline in dw/dt, and these declines persisted even after g_{min} values were corrected for leaf shrinkage and leaf-to-air VPD (Fig. 3). None of these corrections showed significant differences with raw g_{min} estimations ($P > 0.6$ for each pairwise comparison). Leaf water conductance variations persisted after the TLP, which was assumed here to correspond to the point of stomatal closure. Between the point of stomatal closure (RWC_TLP) and the point of desiccation (defined previously as the point at which RWC reaches 30%), we observed a linear decrease of g_{min} as RWC decreased (Fig. 3). The slope of this decline in g_{min} varied by almost an order of magnitude between the studied species, ranging from 0.007 g h^{-1} for *O. europaea* to 0.083 g h^{-1} for *Liriodendron tulipifera*. At very low RWC values, below the desiccation point, the decrease is typically more pronounced and can reach near-zero values of g_{min}, when leaves dried below RWC 10% (Fig. 3).

Estimation of residual conductance along a dehydration time sequence

PV curve parameters (Table 1) were used to convert RWC thresholds into water potential (Ψ) values, obtaining the dynamics of a declining Ψ over time (Fig. S2). Converted Ψ values were used to estimate g_{min} at different dehydration levels, namely g_{min}_TLP, g_{min}_RWC$_{80\text{–}50}$, g_{min}_P$_{12}$, g_{min}_P$_{50}$, and g_{min}_P$_{88}$ (Table 2). Across the studied species, the absolute values of the different thresholded g_{min} estimations varied by more than an order of magnitude (Table 2; Fig. S3). However, for every species the magnitude of g_{min} based on these different thresholds followed the same order. The highest conductance was observed

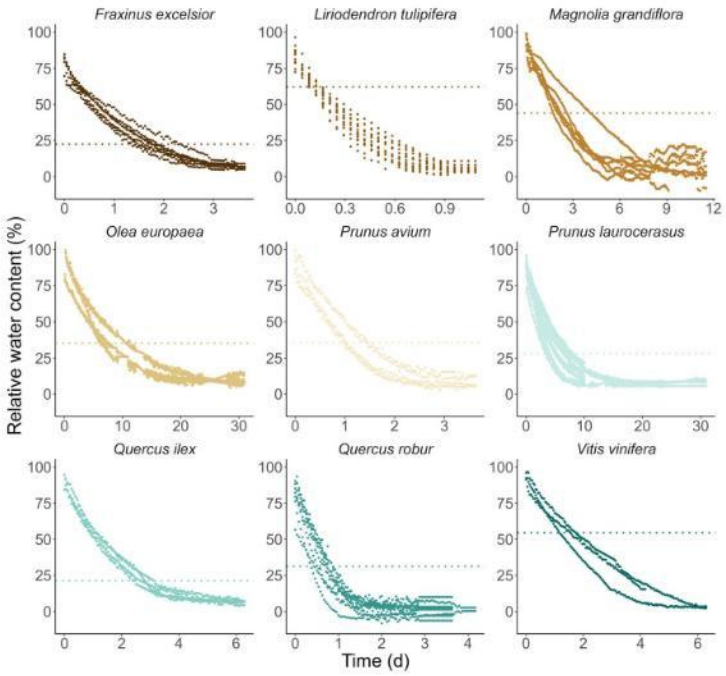

Fig. 1 Change in leaf relative water content (RWC) over elapsed time for each individual sample used in this study. Dashed horizontal lines represent the RWC at which the species reach P_{88}, the water content equivalent to the water potential inducing an 88% loss in hydraulic conductance. The apparent low initial RWC values for some samples result from a 120-min running mean filter to smooth the raw data.

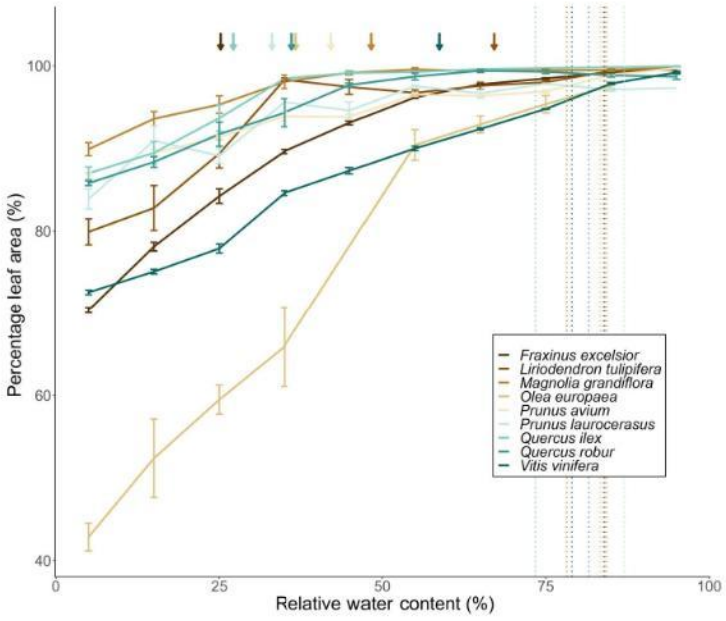

Fig. 2 Percentage of leaf area as a function of relative water content for the nine studied species. The projected leaf area, relative to the leaf area of a fully hydrated turgid leaf, declines with relative water content (RWC). Error bars indicate species mean values and SE for leaf area along segments of 10% RWC. Vertical dotted lines indicate turgor loss point (RWC_{TLP}), and arrows indicate RWC at P_{50} (RWC_P_{50}) for each species.

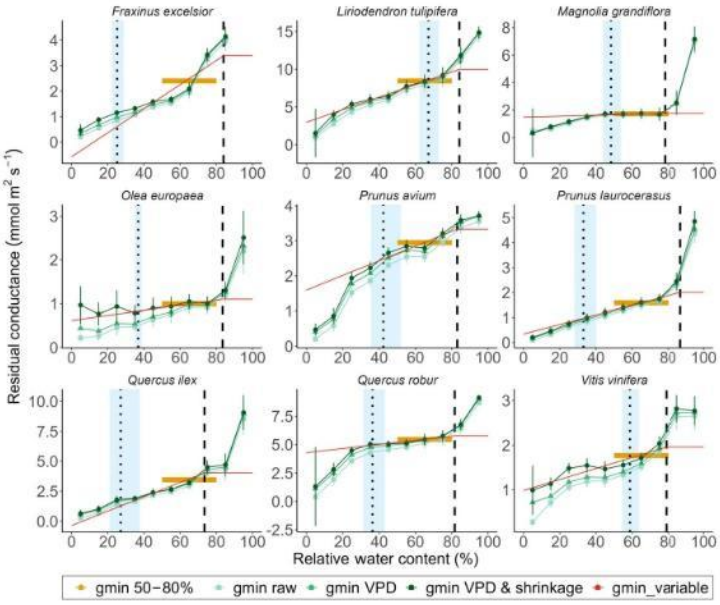

Fig. 3 Changes in residual conductance under declining relative water content. Species means of g_{min} values computed for each range of relative water content (RWC) with no correction (green square), with correction for vapor pressure deficit (VPD) only (green triangle), with correction for VPD & shrinkage (green circle). A detailed description of both corrections is provided in the Materials and Methods section. Orange bars represent the mean value of g_{min} between 50% and 80% RWC. Red lines represent the fitted values of g_{min} used as input for the dynamic computation of 'g_{min}_variable' in the SurEau model. Vertical dashed lines indicate RWC_TLP, and vertical dotted lines indicate RWC_P50. Blue shaded boxes indicate the ranges between P_{12} and P_{88}. Error bars indicate SE. Note the *y*-axis is defined differently for each species.

before TLP when leaves were not stressed. Then, the residual conductance decreased in sequence, with the g_{min} values estimated at TLP always higher than those measured between 50% and 80% of RWC, which were always higher than the estimation at different hydraulic dysfunction thresholds (Fig. S3). We found a significant effect of g_{min} computation method when considering all species ($P = 5.852e\text{-}07$).

Leaf minimum conductance at TLP showed the highest estimations with a mean value across all species of 3.78 ± 0.90 mmol m^{-2} s^{-1} (mean ± SE). As expected, given the decline in g_{min} values over leaf dehydration, g_{min} values thresholded at water statuses inducing P_{12}, P_{50}, and P_{88} declined sequentially across species with average values of 2.79 ± 0.893, 2.57 ± 0.87, and 2.42 ± 0.84 mmol m^{-2} s^{-1}, respectively. Estimates of g_{min} using the range 80–50% RWC provided a mean value of 3.25 ± 0.78 mmol m^{-2} s^{-1}, which was closer to the g_{min} values estimated at P_{12}, and both estimations were closely correlated to each other ($r = 0.97$; $P \leq 0.001$). Indeed, despite showing differences in g_{min} absolute values, all g_{min} estimates using different physiological and RWC thresholds were significantly correlated with each other (Table S3). Across species, we observed a positive correlation ($r = 0.87$; $P \leq 0.005$) between the modulus of elasticity (ε) and RWC_TLP. Yet, PV-curve parameters were not correlated with different g_{min} estimates (Table S3).

Impact of g_{min} on the time to hydraulic failure

The measured THF, defined as time to reach RWC_P_{88}, of detached leaves varied from 0.12 ± 0.01 d in *L. tulipifera* to 8.52 ± 1.86 d in *O. europaea* (Fig. 4). The deciduous species systematically showed shorter THF than the evergreen species (Fig. 4). The results from SurEau models showed that taking into account different ways to estimate g_{min} values leads to variations in THF for a given species (Table 2). The largest differences between extreme values (i.e. between g_{min}_P88 and g_{min}_TLP) for a given species range from 0.06 d for *L. tulipifera* to 6.01 d for *Fraxinus excelsior* (Fig. 5).

We found a close relationship between the modelled vs measured THF (Fig. 6a). Estimations based on fixed g_{min} values tend to show a bigger scatter than estimations based on a variable g_{min}. Root mean square error (RMSE) analysis shows that using a variable g_{min} provides an overall better agreement between modelled and measured THF (Fig. 6b). The modelled THF using the range 80–50% RWC or the fixed g_{min}_P_{12} value also provided a relatively small RMSE (< 1) compared to THF estimations based on either g_{min}_TLP or g_{min}_P_{50}.

Discussion

Leaf minimum water conductance, previously interchangeably referred to as residual conductance, is a hydraulic trait that is becoming increasingly central to studies of drought resistance and drought-induced mortality. Until this study, the methodology for estimating this trait assumed that leaf minimum conductance remained constant for a given sample along dehydration. We estimated leaf water loss along a temporal sequence of drought stress, and demonstrated that residual conductance (g_{res}) varies during the dehydration process and therefore cannot be considered a constant trait. Given the continuous variation of g_{res} during dehydration, we propose to use physiologically informed

Table 2 Average values of leaf minimum conductance (g_{min}) and time to hydraulic failure (THF) for each species.

Species	g_{min}_RWC$_{80-50}$ (mmol m^{-2} s^{-1})	g_{min}_TLP (mmol m^{-2} s^{-1})	g_{min}_P$_{12}$ (mmol m^{-2} s^{-1})	g_{min}_P$_{50}$ (mmol m^{-2} s^{-1})	g_{min}_P$_{88}$ (mmol m^{-2} s^{-1})	THF_ RWC$_{80_50}$ (d)	THF_ TLP (d)	THF_ P$_{12}$ (d)	THF_ P$_{50}$ (d)	THF_ P$_{88}$ (d)	THF_ variable (d)	THF_ observed (d)
Fraxinus excelsior	2.40 ± 0.52	3.39 ± 0.41	0.78 ± 0.17	0.61 ± 0.2	0.48 ± 0.23	1.43	1.02	4.39	5.56	07.03	3.48	1.74 ± 0.12
Liriodendron tulipifera	8.46 ± 0.42	10.00 ± 0.75	9.05 ± 0.67	8.58 ± 0.63	8.17 ± 0.6	0.29	0.25	0.27	0.29	0.30	0.27	0.12 ± 0.01
Magnolia grandiflora	1.93 ± 0.13	2.15 ± 0.05	1.77 ± 0.04	1.69 ± 0.05	1.62 ± 0.05	2.24	1.99	2.45	2.58	2.70	2.44	2.38 ± 0.75
Olea europaea	1.06 ± 0.01	1.22 ± 0.95	0.87 ± 0.28	0.85 ± 0.32	0.84 ± 0.36	6.08	5.29	7.40	7.53	7.64	6.62	8.53 ± 0.84
Prunus avium	2.95 ± 0.18	3.34 ± 0.19	2.68 ± 0.18	2.48 ± 0.19	2.34 ± 0.2	1.09	0.97	1.20	1.29	1.37	1.20	1.18 ± 0.12
Prunus laurocerasus	1.59 ± 0.12	2.01 ± 0.12	1.11 ± 0.14	0.97 ± 0.16	0.88 ± 0.17	4.57	3.62	6.54	7.43	8.22	6.43	5.62 ± 0.48
Quercus ilex	3.46 ± 0.54	4.04 ± 0.55	1.90 ± 0.29	1.27 ± 0.25	0.91 ± 0.24	1.74	1.50	3.12	4.66	6.45	3.66	2.75 ± 0.14
Quercus robur	5.59 ± 0.14	5.93 ± 0.69	5.13 ± 0.21	4.98 ± 0.19	4.88 ± 0.22	0.57	0.54	0.62	0.64	0.65	0.61	0.58 ± 0.08
Vitis vinifera	1.77 ± 0.14	1.96 ± 0.24	1.77 ± 0.22	1.71 ± 0.21	1.66 ± 0.2	1.28	1.16	1.28	1.33	1.37	1.33	1.49 ± 0.16

'g_{min}_' denotes minimum conductance at different thresholds. 'THF_' denotes time to hydraulic failure at different thresholds. 80–50% RWC, 80% to 50% relative water content; TLP, turgor loss point; P_{12}, 12% loss of hydraulic conductivity; P_{50}, 50% loss of hydraulic conductivity; P_{88}, 88% loss of hydraulic conductivity. Reported error values are SE.

or water content-based thresholds for its estimation. Therefore, our study urges distinguishing the terms 'residual' conductance, as a dynamic water loss after stomatal closure, and 'minimum' conductance, which imply the use of established boundaries for its estimation. In this context, we estimated g_{min} at physiologically relevant thresholds distributed along a temporal sequence of drought stress and demonstrated that g_{min} estimations vary during leaf dehydration. We subsequently show that, depending on the threshold at which g_{min} is estimated, the drought survival time estimated by our model varies considerably. These results have important implications for better estimating the risk of hydraulic failure during drought and predicting the impact of climate change on species survival and distribution.

Residual conductance varies during dehydration

Residual conductance decreases continuously during the entire dehydration process. Such declines in conductance rates were observed in all the studied species. Decreases in leaf water conductance were still observed after normalizations by projected leaf area corrected for leaf shrinkage, which is a main variable for the calculation of g_{min} (see Eqn 2). An effect of shrinkage on the reduction of g_{min} could be expected since it has been shown that leaf thickness during dehydration is negatively correlated with hydraulic conductance (K_{leaf}) on 14 diverse species (Scoffoni *et al.*, 2014). However, leaf surface shrinkage seems to be less effective in driving decreases in residual conductance estimations, especially at the first stages of dehydration since leaf shrinkage was relatively limited in the range of RWC between 100% and 50%. Similarly, the investigation of the effect of VPD shifts during conductance measurements, which is considered here to be affected mainly by the drop in water potential inside the leaf, showed that even though the decrease is less pronounced after correction, it does not change the direction of the slope. Overall, corrections of leaf shrinkage and dehydration-induced leaf-to-air VPD slightly increased our residual conductance estimations. Yet, the dynamics of residual conductance decrease under declining RWC or dehydration time remained unaffected after correcting for both potential drivers. Taking into consideration the main finding that residual conductance is not steady during dehydration, we provide solutions for calculating g_{min} either at fixed values (based on RWC or physiological thresholds) or dynamically during a dehydration process. Altogether, these results demonstrate that g_{min} is not a constant hydraulic trait for a given species and varies in time during a drought event. We therefore suggest the use of physiology-based boundaries for its calculation.

The variation of leaf water conductance during dehydration observed in this study is in line with several studies that evidenced contrasted responses of leaf weight loss rates for different water stress conditions. For instance, it has been shown that drought significantly impacts the water loss rate for both young and mature tea (*Camellia sinensis*) leaves (Chen *et al.*, 2020). The process leading to this variation during a stress gradient is not fully known and needs to be further investigated. We can hypothesize that it could come from incompletely closed stomata (Machado *et al.*, 2021), driving stomatal patchiness, which is the irregular closing of

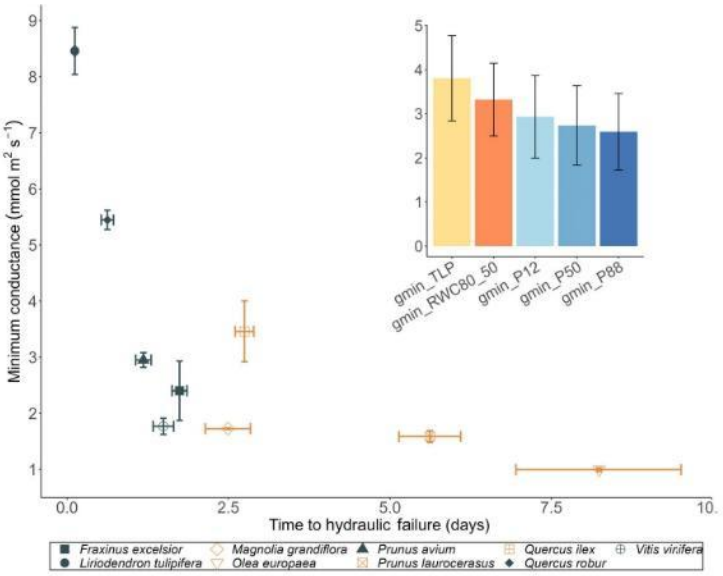

Fig. 4 Relationship between measured time to hydraulic failure (THF) and leaf minimum conductance (g_{min}) corrected for shrinkage and vapor pressure deficit variation. For each sample, g_{min} is computed for a relative water content between 50% and 80%. Error bars represent SE. Deciduous species are represented by blue symbols and evergreen species by yellow symbols. Inset represents averaged g_{min} values computed at different thresholds.

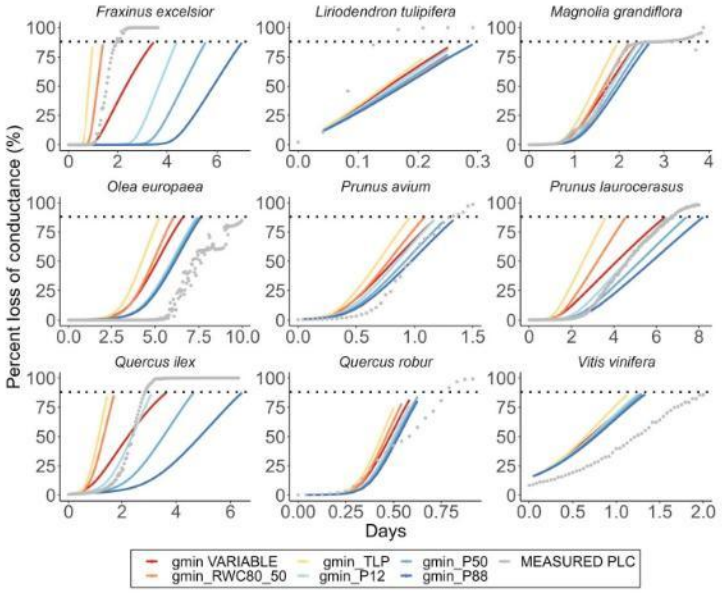

Fig. 5 Changes in modelled and measured percent loss of conductance (PLC) in relation to time. Colored lines represent model results for different types of computation of g_{min}. Gray points represent the measured value of PLC (estimated from relative water content (RWC), with the pressure–volume curve). Dashed black lines represent the value of P_{88} (defined as the threshold for the time to hydraulic failure). Note the *x*-axis is defined differently for each species.

stomata over the entire surface of the leaf (Mott & Buckley, 1998). Along with such mechanisms deriving from stomatal activity, features of the cuticular structure could also explain such variation in residual conductance. More specifically, the main effect of the cuticle on g_{min} could come from a modification of the structure by the elongation of the molecules composing the cuticle (Shepherd & Wynne Griffiths, 2006; Lewandowska *et al.*, 2020) or *de novo* cuticular wax biosynthesis (Premachandra *et al.*, 1991). In this respect, a study on *Nicotiana glauca* leaves described a strong effect of water stress on leaf permeance by the accumulation of waxes during stress

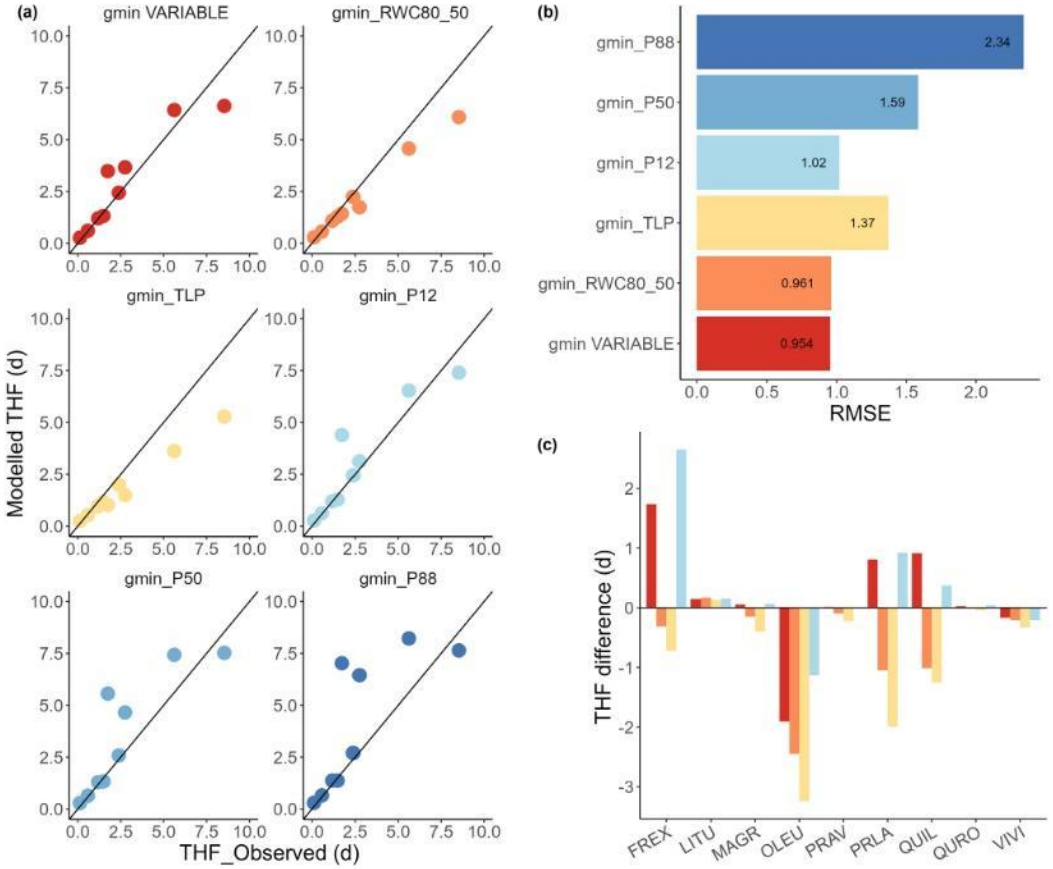

Fig. 6 Relationship between modelled and observed time to hydraulic failure using different computations of g_{min}. (a) Comparison between modeled and measured time to hydraulic failure (THF) across different g_{min} estimations. THF is defined as the time to reach P_{88}. Each point corresponds to the average of THF for each of the studied species. Black lines indicate a 1 : 1 relationship. (b) Root mean square error (RMSE) comparing the performance of the models using different g_{min} values. (c) Difference between modelled and observed THF for each species, and color codes, corresponding to different g_{min} values, are the same as in panel b. Species abbreviation codes are included in Table 1.

(Cameron *et al.*, 2006). Moreover, a recent study on *Nicotiana benthamiana* has shown effective responses to drought stress by changes in the composition and accumulation of cuticular waxes, resulting in increases in cuticular thickness (Asadyar *et al.*, 2024). However, such accumulation of waxes during stress might mostly drive seasonal changes in residual conductance and would not explain the variation observed in our study, which occurred over a much shorter time frame.

Despite the relevance of the cuticular features previously presented, several studies show a weak effect of the amount of cuticle on minimal conductance, which would suggest that the amount of cuticular waxes is not the only driver of the decline in g_{min} observed here. For example, no difference in the amount of wax has been found for *Quercus coccifera* growing in different environments (Bueno *et al.*, 2019). Additionally, a recent study found no difference in permeance for a *Populus* × *canescens* clone while the authors measured 10-fold differences in wax composition (Grünhofer *et al.*, 2022). These findings would suggest that the variation in residual conductance is substantially driven by the dynamics of stomatal closure during dehydration. Further work is, however, needed to investigate the extent of the role played by a modification of the structure or composition of the cuticle in this variation.

Impact of the variation in minimum conductance estimates on time-to-death prediction

Decreases in leaf g_{min} values are observed even at mild stress levels when leaves are still hydraulically connected to the stem (typically

between TLP and P_{50}). This variation has a direct consequence on the speed of diminution of plant water content, and therefore, a direct influence on the quality of the prediction of the THF, which is a prominent proxy of plant survival under drought, using mechanistic models based on hydraulic traits (Cochard *et al.*, 2021; Ruffault *et al.*, 2022a). The effect of a variable g_{min} on the THF estimations is, however, more or less pronounced for the different species. For instance, the modelled THF for species having the lowest resistance to embolism (i.e. the highest RWC_P_{88}), like *L. tulipifera* or *Vitis vinifera*, was less impacted by the variation in g_{min} values. Conversely, the species that show higher resistance to embolism, like *F. excelsior* or *Quercus ilex*, present large g_{min}-induced variations in modelled THF, suggesting that the variation in residual conductance could be more relevant in predicting hydraulic failure in species with a more resistant hydraulic apparatus and hence a larger safety margin (Fig. S4). Given the importance of g_{min} on the pace to cross the safety margin (Petek-Petrik *et al.*, 2023), a variable residual conductance could be more relevant in species with wider margins, where the speed of water loss would be more relevant to reaching hydraulic failure.

Even though the simulations in this study are based on several simplifying assumptions and on a limited set of traits, the absolute values of the modelled THF showed overall good agreement with the observed THF, which is the time to reach water contents inducing P_{88} directly measured during the dehydration experiment. One of the main simplifying assumptions we made in the model parametrization is that the vulnerability to cavitation is similar between leaf and stem. However, we know that many plants differ from this assumption and exhibit hydraulic vulnerability segmentation between their organs. For instance, several studies reported significant segmentation for species closely related to our selection of species. Leaves are slightly more vulnerable to cavitation (typically below 1 MPa) for most species; for example, segmentation of −0.67 MPa is reported for *Quercus douglasii* (Skelton *et al.*, 2019), *c.* −0.8 MPa for *V. vinifera* (Hochberg *et al.*, 2016), *c.* −0.8 MPa for *Juglans regia* (Tyree *et al.*, 1993), −0.9 MPa for *Fraxinus mandshurica* (Song *et al.*, 2022), and between −0.73 MPa (Li *et al.*, 2020) and −0.91 MPa (Rodriguez-Dominguez *et al.*, 2018) for *O. europaea*.

Despite the previously observed trend, where leaves are more sensitive to drought than stems, some species included in our study have shown the opposite pattern, with more drought-resistant leaves. For instance, in *L. tulipifera*, two different studies have reported that leaves are more resistant than stems with leaf-to-stem segmentations of +0.47 MPa (Li *et al.*, 2020) and +0.68 MPa (Guan *et al.*, 2022). Additionally, *Prunus avium* and *Quercus robur* also have positive leaf-to-stem hydraulic vulnerability segmentations of +1.84 MPa and +0.31 MPa, respectively (Guan *et al.*, 2022). Such a positive leaf-to-stem hydraulic vulnerability segmentation might explain why our model output overestimated the THF for these species (Fig. 5). Even at the level of the single organ, the estimation of THF is the result of several parameters, among which residual conductance and its temporal variation can play a major role. Leaves might however be disconnected before significant stem cavitation (RWC_P_{50}). This implies that only the variation of g_{min} above this point of disconnection is relevant to estimate time-to-death at the plant level. Given that some species studied here showed a positive leaf-to-stem vulnerability segmentation, the use of stem P_{50} as a reference threshold for minimum conductance could be interesting, despite belonging to a different organ, since it informs residual water losses that occur at earlier stages of drought-induced hydraulic dysfunction.

Toward a standardized methodology to estimate g_{min}

The data acquisition system and the linked computation pipeline described in this study provided an accurate, versatile, cheap, and time-efficient methodology to compute g_{min}, even for a large number of samples. Using a standardized averaging procedure, like the one implemented in this pipeline, combined with data oversampling permits a good fit of the raw data even if the signal is noisy (e.g. due to movement of the sample caused by ventilation). We show that accounting for tissue shrinkage and the water-potential-induced changes in VPD during drought has only a minor effect on the calculation of residual conductance, particularly within the RWC range where leaves remain hydraulically connected to the stem.

Our approach, which dynamically investigates the contributions of all the aspects involved in g_{min} computation, describes more accurately the phenomenon occurring *in vivo* during dehydration and demonstrates its impact on the output of models considering hydraulic traits. However, this approach is not solely based on the measurement of mass loss during dehydration. A prior knowledge of several other traits, such as PV curves and vulnerability curve parameters, is required. It remains important, however, to have a reproducible method to compute a g_{min} value representative of a sample along a dehydration threshold even when physiological data are not available. In such cases, RWC can be used as a convenient metric to specify relevant thresholds for conductance estimations. If physiological or RWC thresholds are specified, then g_{min} values could be considered as a measurable and more stable trait. For instance, the use of a range between stomatal closure and leaf disconnection provides an estimation that integrates over the whole dehydration range. These thresholds are typically close to RWC of 80% and 50%, respectively, and we show that such a range produces a good estimation of THF as compared to the observed values during the experiment. We therefore encourage using the minimum conductance estimated between those values ($g_{min}\_RWC_{80\_50}$) as a relevant trait when comparing species or genotypes over the entire course of dehydration, and without preliminary knowledge of other physiological traits. Other thresholds might be relevant for different types of studies. We would recommend that, for future reports of g_{min}, researchers make available both the threshold (or range of RWC) used for the computation and the raw data used to compute g_{min} so that future studies could harmonize computations if needed. The methodology presented in this study is a step toward a unified framework for studying residual water losses and minimum conductance values for many organs, such as leaves, branches, roots, and flowers.

Acknowledgements

The authors wish to thank Anne-Isabelle Gravel and Gaëlle Capdeville for their help in the glasshouse and in the laboratory and Annabel Porte for thoughtful advice. All measurements were performed at the PHENOBOIS platform. This study received financial support from the French government in the framework of the IdEX Bordeaux University 'Investments for the Future' program/GPR Bordeaux Plant Sciences. Financial support was also received from the French National Research Agency (ANR) in the frame of the Investments for the future Program, within the Cluster of Excellence COTE(ANR-10-LABX-0045), project LEAFSHED.

Competing interests

None declared.

Author contributions

RB, ST, SD, HC, JMT-R and NKM-SP contributed to the design of the study and the interpretation of the results; RB and ST performed data collection and analysis; HC carried out the simulations.; CP performed pressure–volume curves and provided help in the glasshouse; GF and XPB wrote the software for the computation of g_{min}; RB wrote the data acquisition software; RB, ST and SD wrote the manuscript with help from all authors.

ORCID

Xavier Paul Bouteiller https://orcid.org/0000-0001-8621-383X
Régis Burlett https://orcid.org/0000-0001-8289-5757
Hervé Cochard https://orcid.org/0000-0002-2727-7072
Sylvain Delzon https://orcid.org/0000-0003-3442-1711
Guillaume Forget https://orcid.org/0009-0000-4778-3194
Nicolas K. Martin-StPaul https://orcid.org/0000-0001-7574-0108
Camille Parise https://orcid.org/0000-0001-5222-4928
José M. Torres-Ruiz https://orcid.org/0000-0003-1367-7056
Santiago Trueba https://orcid.org/0000-0001-8218-957X

Data availability

Codes developed for data acquisition (software 'cuticular' for Windows) and computation of raw residual conductance (project 'gminComputation' is developed as a console version in python, and 'g_Residual' is a script written in R language) are available in the following public Gitlab repository: https://gitub.u-bordeaux.fr/phenobois. Data specifically used for this manuscript are available on the dataverse https://recherche.data.gouv.fr; doi: 10.57745/S11KRP.

References

Allen CD, Breshears DD. 1998. Drought-induced shift of a forest–woodland ecotone: Rapid landscape response to climate variation. *Proceedings of the National Academy of Sciences, USA* **95**: 14839–14842.

Arend M, Link RM, Patthey R, Hoch G, Schuldt B, Kahmen A. 2021. Rapid hydraulic collapse as cause of drought-induced mortality in conifers. *Proceedings of the National Academy of Sciences, USA* **118**: e2025251118.

Asadyar L, de Felippes FF, Bally J, Blackman CJ, An J, Sussmilch FC, Moghaddam L, Williams B, Blanksby SJ, Brodribb TJ *et al.* 2024. Evidence for within-species transition between drought response strategies in *Nicotiana benthamiana*. *New Phytologist* **244**: 464–476.

Barnard DM, Bauerle WL. 2013. The implications of minimum stomatal conductance on modeling water flux in forest canopies. *Journal of Geophysical Research: Biogeosciences* **118**: 1322–1333.

Billon LM, Blackman CJ, Cochard H, Badel E, Hitmi A, Cartailler J, Souchal R, Torres-Ruiz JM. 2020. The DroughtBox: a new tool for phenotyping residual branch conductance and its temperature dependence during drought. *Plant, Cell & Environment* **43**: 1584–1594.

Boyer JS, Wong SC, Farquhar GD. 1997. CO_2 and water vapor exchange across leaf cuticle (epidermis) at various water potentials. *Plant Physiology* **114**: 185–191.

Brodribb TJ, Cochard H, Dominguez CR. 2019. Measuring the pulse of trees; using the vascular system to predict tree mortality in the 21st century. *Conservation Physiology* **7**: 1–7.

Brodribb TJ, Holbrook NM. 2003. Changes in leaf hydraulic conductance during leaf shedding in seasonally dry tropical forest. *New Phytologist* **158**: 295–303.

Bueno A, Sancho-Knapik D, Gil-Pelegrín E, Leide J, Peguero-Pina JJ, Burghardt M, Riederer M. 2019. Cuticular wax coverage and its transpiration barrier properties in *Quercus coccifera* L. leaves: does the environment matter? *Tree Physiology* **40**: 827–840.

Burlett R, Parise C, Capdeville G, Cochard H, Lamarque LJ, King A, Delzon S. 2022. Measuring xylem hydraulic vulnerability for long-vessel species: an improved methodology with the flow centrifugation technique. *Annals of Forest Science* **79**: 5.

Cameron KD, Teece MA, Smart LB. 2006. Increased accumulation of cuticular wax and expression of lipid transfer protein in response to periodic drying events in leaves of tree tobacco. *Plant Physiology* **140**: 176–183.

Carnicer J, Coll M, Ninyerola M, Pons X, Sánchez G, Peñuelas J. 2011. Widespread crown condition decline, food web disruption, and amplified tree mortality with increased climate change-type drought. *Proceedings of the National Academy of Sciences, USA* **108**: 1474–1478.

Chen M, Zhu X, Zhang Y, Du Z, Chen X, Kong X, Sun W, Chen C. 2020. Drought stress modify cuticle of tender tea leaf and mature leaf for transpiration barrier enhancement through common and distinct modes. *Scientific Reports* **10**: 1–12.

Choat B, Jansen S, Brodribb TJ, Cochard H, Delzon S, Bhaskar R, Bucci SJ, Feild TS, Gleason SM, Hacke UG. 2012. Global convergence in the vulnerability of forests to drought. *Nature* **491**: 752–755.

Cochard H. 2002. A technique for measuring xylem hydraulic conductance under high negative pressures. *Plant, Cell & Environment* **25**: 815–819.

Cochard H, Pimont F, Ruffault J, Martin-StPaul N. 2021. SurEau: a mechanistic model of plant water relations under extreme drought. *Annals of Forest Science* **78**: 55.

Creek D, Lamarque LJ, Torres-Ruiz JM, Parise C, Burlett R, Tissue DT, Delzon S. 2020. Xylem embolism in leaves does not occur with open stomata: evidence from direct observations using the optical visualization technique. *Journal of Experimental Botany* **71**: 1151–1159.

Delf EM. 1912. Transpiration in succulent plants. *Annals of Botany* **26**: 409–442.

Delzon S, Cochard H. 2014. Recent advances in tree hydraulics highlight the ecological significance of the hydraulic safety margin. *New Phytologist* **203**: 355–358.

Duursma RA, Blackman CJ, Lopéz R, Martin-StPaul NK, Cochard H, Medlyn BE. 2018. On the minimum leaf conductance: its role in models of plant water use, and ecological and environmental controls. *New Phytologist* **221**: 693–705.

Grünhofer P, Herzig L, Sent S, Zeisler-Diehl VV, Schreiber L. 2022. Increased cuticular wax deposition does not change residual foliar transpiration. *Plant, Cell & Environment* **45**: 1157–1171.

Guan X, Werner J, Cao K-F, Pereira L, Kaack L, McAdam SAM, Jansen S. 2022. Stem and leaf xylem of angiosperm trees experiences minimal embolism in temperate forests during two consecutive summers with moderate drought. *Plant Biology* **24**: 1208–1223.

Hammond WM, Williams AP, Abatzoglou JT, Adams HD, Klein T, López R, Sáenz-Romero C, Hartmann H, Breshears DD, Allen CD. 2022. Global field

observations of tree die-off reveal hotter-drought fingerprint for Earth's forests. *Nature Communications* **13**: 1761.

Hochberg U, Albuquerque C, Rachmilevitch S, Cochard H, David-Schwartz R, Brodersen CR, McElrone A, Windt CW. 2016. Grapevine petioles are more sensitive to drought induced embolism than stems: evidence from *in vivo* MRI and microcomputed tomography observations of hydraulic vulnerability segmentation. *Plant, Cell & Environment* **39**: 1886–1894.

Kala J, De Kauwe MG, Pitman AJ, Medlyn BE, Wang Y-P, Lorenz R, Perkins-Kirkpatrick SE. 2016. Impact of the representation of stomatal conductance on model projections of heatwave intensity. *Scientific Reports* **6**: 23418.

Kerstiens G. 1996. Signalling across the divide: a wider perspective of cuticular structure-function relationships. *Trends in Plant Science* **1**: 125–129.

Koide RT, Robichaux RH, Morse SR, Smith CM. 2000. Plant water status, hydraulic resistance and capacitance. In: Pearcy RW, Ehleringer JR, Mooney HA, Rundel PW, eds. *Plant physiological ecology: field methods and instrumentation*. Dordrecht, the Netherlands: Springer Netherlands, 161–183.

Lamarque LJ, Corso D, Torres-Ruiz JM, Badel E, Brodribb TJ, Burlett R, Charrier G, Choat B, Cochard H, Gambetta GA *et al.* 2018. An inconvenient truth about xylem resistance to embolism in the model species for refilling *Laurus nobilis* L. *Annals of Forest Science* **75**: 88.

Lewandowska M, Keyl A, Feussner I. 2020. Wax biosynthesis in response to danger: its regulation upon abiotic and biotic stress. *New Phytologist* **227**: 698–713.

Li S, Feifel M, Karimi Z, Schuldt B, Choat B, Jansen S. 2016. Leaf gas exchange performance and the lethal water potential of five European species during drought. *Tree Physiology* **36**: 179–192.

Li X, Delzon S, Torres-Ruiz J, Badel E, Burlett R, Cochard H, Jansen S, King A, Lamarque LJ, Lenoir N *et al.* 2020. Lack of vulnerability segmentation in four angiosperm tree species: evidence from direct X-ray microtomography observation. *Annals of Forest Science* **77**: 1–12.

Machado R, Loram-Lourenço L, Farnese FS, Alves RDFB, de Sousa LF, Silva FG, Filho SCV, Torres-Ruiz JM, Cochard H, Menezes-Silva PE. 2021. Where do leaf water leaks come from? Trade-offs underlying the variability in minimum conductance across tropical savanna species with contrasting growth strategies. *New Phytologist* **229**: 1415–1430.

Mantova M, Cochard H, Burlett R, Delzon S, King A, Rodriguez-Dominguez CM, Ahmed MA, Trueba S, Torres-Ruiz JM. 2023. On the path from xylem hydraulic failure to downstream cell death. *New Phytologist* **237**: 793–806.

Márquez DA, Stuart-Williams H, Farquhar GD, Busch FA. 2022. Cuticular conductance of adaxial and abaxial leaf surfaces and its relation to minimum leaf surface conductance. *New Phytologist* **233**: 156–168.

Martin-StPaul N, Delzon S, Cochard H. 2017. Plant resistance to drought depends on timely stomatal closure. *Ecology Letters* **20**: 1437–1447.

Mott KA, Buckley TN. 1998. Stomatal heterogeneity. *Journal of Experimental Botany* **49**: 407–417.

Nobel PS. 2009. Chapter 2 – water. In: Nobel PS, ed. *Physicochemical and environmental plant physiology*. San Diego, CA, USA: Academic Press, 44–99.

Pearcy RW, Schulze E-D, Zimmermann R. 1989. Measurement of transpiration and leaf conductance. In: Pearcy RW, Ehleringer JR, Mooney HA, Rundel PW, eds. *Plant physiological ecology: field methods and instrumentation*. Dordrecht, the Netherlands: Springer Netherlands, 137–160.

Petek-Petrik A, Petrík P, Lamarque LJ, Cochard H, Burlett R, Delzon S. 2023. Drought survival in conifer species is related to the time required to cross the stomatal safety margin. *Journal of Experimental Botany* **74**: 6847–6859.

Premachandra GS, Saneoka H, Kanaya M, Ogata S. 1991. Cell membrane stability and leaf surface wax content as affected by increasing water deficits in maize. *Journal of Experimental Botany* **42**: 167–171.

R Core Team. 2022. *R: a language and environment for statistical computing*. Vienna, Austria: R Foundation for Statistical Computing.

Rodriguez-Dominguez CM, Carins Murphy MR, Lucani C, Brodribb TJ. 2018. Mapping xylem failure in disparate organs of whole plants reveals extreme resistance in olive roots. *New Phytologist* **218**: 1025–1035.

Ruffault J, Pimont F, Cochard H, Dupuy J-L, Martin-StPaul N. 2022a. SurEau-Ecos v.2.0: a trait-based plant hydraulics model for simulations of plant water status and drought-induced mortality at the ecosystem level. *Geoscientific Model Development* **15**: 5593–5626.

Ruffault J, Pimont F, Dupuy JL. 2022b. SurEau-Ecos-FMC: mechanistic modelling of fuel moisture content (FMC) at leaf and canopy scale under extreme drought. *Journal of Advances in Forest Fire Research* **4**: 1318–1322.

Sack L, Pasquet-Kok J, Bartlett M. 2010. *Leaf pressure–volume curve parameters protocol*. PROMETHEUS Wiki.

Sack L, Scoffoni C. 2010. Minimum epidermal conductance (gmin, a.k.a. cuticular conductance). PROMETHEUS Wiki.

Schönherr J, Mérida T. 1981. Water permeability of plant cuticular membranes: the effects of humidity and temperature on the permeability of non-isolated cuticles of onion bulb scales. *Plant, Cell & Environment* **4**: 349–354.

Scoffoni C, Vuong C, Diep S, Cochard H, Sack L. 2014. Leaf shrinkage with dehydration: coordination with hydraulic vulnerability and drought tolerance. *Plant Physiology* **164**: 1772–1788.

Shepherd T, Wynne Griffiths D. 2006. The effects of stress on plant cuticular waxes. *New Phytologist* **171**: 469–499.

Skelton RP, Anderegg LDL, Papper P, Reich E, Dawson TE, Kling M, Thompson SE, Díaz J, Ackerly DD. 2019. No local adaptation in leaf or stem xylem vulnerability to embolism, but consistent vulnerability segmentation in a North American oak. *New Phytologist* **223**: 1296–1306.

Song J, Trueba S, Yin X-H, Cao K-F, Brodribb TJ, Hao G-Y. 2022. Hydraulic vulnerability segmentation in compound-leaved trees: evidence from an embolism visualization technique. *Plant Physiology* **189**: 204–214.

Sperry JS, Donnelly JR, Tyree MT. 1988. A method for measuring hydraulic conductivity and embolism in xylem. *Plant, Cell & Environment* **11**: 35–40.

Stålfelt MG. 1956. Die cuticuläre transpiration. In: Adriani MJ, ed. *Pflanze und Wasser/water relations of plants. Handbuch der Pflanzenphysiologie/encyclopedia of plant physiology*. Berlin, Heidelberg, Germany: Springer.

Torres-Ruiz JM, Cochard H, Delzon S, Boivin T, Burlett R, Cailleret M, Corso D, Delmas CEL, Caceres M, Diaz-Espejo A *et al.* 2024. Plant hydraulics at the heart of plant, crops and ecosystem functions in the face of climate change. *New Phytologist* **241**: 984–999.

Trueba S, Pan R, Scoffoni C, John GP, Davis SD, Sack L. 2019. Thresholds for leaf damage due to dehydration: declines of hydraulic function, stomatal conductance and cellular integrity precede those for photochemistry. *New Phytologist* **223**: 134–149.

Tyree MT, Cochard H, Cruiziat P, Sinclair B, Ameglio T. 1993. Drought-induced leaf shedding in walnut: evidence for vulnerability segmentation. *Plant, Cell & Environment* **16**: 879–882.

Tyree MT, Hammel HT. 1972. The measurement of the turgor pressure and the water relations of plants by the pressure-bomb technique. *Journal of Experimental Botany* **23**: 267–282.

Urli M, Porté AJ, Cochard H, Guengant Y, Burlett R, Delzon S. 2013. Xylem embolism threshold for catastrophic hydraulic failure in angiosperm trees. *Tree Physiology* **33**: 672–683.

Vesala T, Sevanto S, Grönholm T, Salmon Y, Nikinmaa E, Hari P, Hölttä T. 2017. Effect of leaf water potential on internal humidity and CO_2 dissolution: reverse transpiration and improved water use efficiency under negative pressure. *Frontiers in Plant Science* **8**: 54.

Supporting Information

Additional Supporting Information may be found online in the Supporting Information section at the end of the article.

Fig. S1 Changes in individual leaf mass raw values over elapsed time.

Fig. S2 Changes in mean modelled water potential values over elapsed time.

Fig. S3 Minimum conductance (g_{min}) estimations based on physiological and water content thresholds for each species.

Fig. S4 Relationship between hydraulic safety margin and the difference in time to hydraulic failure between stomatal closure and plant death.

Methods S1 Detailed description of the minimum conductance measurement setup.

Table S1 Additional physiological variables used for the parameterization of the SurEau model.

Table S2 Analysis of variance of percent leaf area as a function of 10% relative water content intervals and species.

Table S3 Coordination between pressure–volume curve parameters and different minimum conductance estimations.

Please note: Wiley is not responsible for the content or functionality of any Supporting Information supplied by the authors. Any queries (other than missing material) should be directed to the *New Phytologist* Central Office.

A.6. List of publication

A.6.1. Accepted publications

Burlett, R., Trueba, S., Bouteiller, X.P., **Forget, G.**, Torres-Ruiz, M., Martin-StPaul, N.K., Parise, C., Delzon, S., 2025. Minimum leaf conductance during drought: unravelling its variability and impact on plant survival. New Phytologist. https://doi.org/10.1111/nph.70052

Ganie, S.A., **Forget, G.**, Amaral, J., Wall, S.A., Singh, P., Kromdijk, J., Carmo-Silva, E., Lawson, T., 2025. Unravelling the Physiological and Anatomical Basis of Divergent Adaptations in Cultivated and Wild Tomatoes. Journal of Experimental Botany eraf390. https://doi.org/10.1093/jxb/eraf390

My contribution to this work included all R scripts, statistical analyses and the preparation of the figures. My work is available on this repository https://gitub.u-bordeaux.fr/guforget/lea-lost.

Faralli, M., Mellers, G., Wall, S., Vialet-Chabrand, S., **Forget, G.**, Galle, A., Van Rie, J., Gardner, K.A., Ober, E.S., Cockram, J., Lawson, T., 2024. Exploring natural genetic diversity in a bread wheat multi-founder population: Dual imaging of photosynthesis and stomatal kinetics. Journal of Experimental Botany erae233. https://doi.org/10.1093/jxb/erae233

During my international mobility at the Lawson's lab, I participated in the validation method, which consisted of determining the thermal boundary layer in order to estimate leaf conductance.

A.6.2. Publications submitted or in preparation

Forget, G., Burlett, R., Trueba, S., Lawson, T., Joubès, J., Delzon, S., 2025. Deciphering the impact of stomatal leakiness and its spatial variability within the leaf on residual water loss during severe drought. Plant, Cell & Environment but rejected the 24/10/2025.

Forget, G., Burlett, R., Joubès, J., Delzon, S., Lawson, T. 2025. Revealing stomatal patchiness under drought in sunflower plants.

Trueba, S., Burlett, R., Bouteiller, X.P., Burneau, T., **Forget, G.**, Larter, M., N'Do, D., Ziegler, C., Delzon, S., 2025. Leaf dehydration dynamics after stomatal closure in vascular plants. Submitted to Global change biology but rejected the 23/09/25.

Forget, G., Burlett, R., Buridan, M., Domergue, F., Delzon, S., Joubès, J., 2025. Drought-induced modification in leaf cuticle composition and their impact on minimum leaf conductance.

Forget, G., Burlett, R., Lawson, T., Joubès, J., Delzon, S., 2025. Stomatal dynamics as the key driver of nocturnal and residual leaf conductance: implications for determining minimum leaf conductance. In preparation.

A.6.3. Poster Communication

Forget, G., Burlett, R., Joubès, J., Delzon, S., Lawson, T. Importance of stomatal patchiness in the biological response to water stress. SEB Annual Conference Antwerp 2025, Jul 2025, Anvers, Belgium. ⟨hal-05261991⟩

List of abbreviation

ABA: Abscisic acid
ABCG transporter: ATP binding cassette transporter
ADP: Adénosine diphosphate
AED: Atmospheric evaporative demand
ATP: Adénosine triphosphate
b6f complex: cytochrome b6f complex
CD: cutin synthase
CER: Eceriferum
CoA: Co-Enzyme A
CYP: Cytochrome P450s
DCA: Dicarboxylic acid
DCR: Defective in cuticular ridge
di/triOH FA: di- and tri-hydroxy fatty acid
ER: Endoplasmic Reticulum
FA: Fatty Acid
FA: Fatty acid
FAE: Fatty Acid Elongase
FAR: Fatty Acid Reductase
Fd: Ferredoxin
GAP: Glyceraldehyde-3-phosphate
GC-FID: Gaz-Chromatography coupled with a Flame Ionization Detector
GC-MS: Gaz-Chromatography coupled with Mass Spectrometry
GPAT: Glycerol-3-phosphate acyltransferase
H: Sensible heat loss,
IPCC: Intergovernmental panel on climate change
KCR: β-Ketoacyl-CoA Reductase
KCS: β-Ketoacyl-CoA Synthase
L: Latent heat loss
LACS: Long chain acyl-coenzyme synthetase
MAH: midchain alkane hydroxylase
MYB: A class of transcription factors (MYB96, MYB94)
NADH: reduced form of Nicotinamide Adenine Dinucleotide

NADPH: reduced form of Nicotinamide Adenine Dinucleotide Phosphate

OEW: Outer cell wall

PC: Plastocyanin

PQ: Plastoquinone

PSI: Photosystem I

PSII: Photosystem II

ROS: Reactive oxygen species

RuBP: Ribulose-1,5-bisphosphate

SPAC: Soil plant atmosphere continuum

TGN: trans-Golgi Network

VLCFA: Very Long Chain Fatty Acid

VPD: Vapour pressure deficit.

WS: Wax synthase

WUE: Water use efficiency

Φs: Thermal (shortwave) radiation

ΦL: Thermal (longwave) radiation

ω-OH FA: ω-hydroxy fatty acid

List of Figures

List of Tables